

**CONCRETE SLABS REINFORCED WITH GFRP BARS**

**CENTRE FOR NEWFOUNDLAND STUDIES**

---

**TOTAL OF 10 PAGES ONLY  
MAY BE XEROXED**

**(Without Author's Permission)**

**MOHAMMAD INTIAZ RASHID**





# **Concrete Slabs Reinforced with GFRP Bars**

by



**© Mohammad Imtiaz Rashid, B. Sc. Engg. (Civil)**

**A thesis submitted to the School of Graduate  
Studies in partial fulfillment of the  
requirements for the degree of  
Master of Engineering**

**Faculty of Engineering and Applied Science  
Memorial University of Newfoundland  
June 2004**

**St. John's**

**Newfoundland**

**Canada**



Library and  
Archives Canada

Bibliothèque et  
Archives Canada

Published Heritage  
Branch

Direction du  
Patrimoine de l'édition

0-494-06607-5

395 Wellington Street  
Ottawa ON K1A 0N4  
Canada

395, rue Wellington  
Ottawa ON K1A 0N4  
Canada

*Your file* *Votre référence*

*ISBN:*

*Our file* *Notre référence*

*ISBN:*

#### NOTICE:

The author has granted a non-exclusive license allowing Library and Archives Canada to reproduce, publish, archive, preserve, conserve, communicate to the public by telecommunication or on the Internet, loan, distribute and sell theses worldwide, for commercial or non-commercial purposes, in microform, paper, electronic and/or any other formats.

The author retains copyright ownership and moral rights in this thesis. Neither the thesis nor substantial extracts from it may be printed or otherwise reproduced without the author's permission.

---

In compliance with the Canadian Privacy Act some supporting forms may have been removed from this thesis.

While these forms may be included in the document page count, their removal does not represent any loss of content from the thesis.

#### AVIS:

L'auteur a accordé une licence non exclusive permettant à la Bibliothèque et Archives Canada de reproduire, publier, archiver, sauvegarder, conserver, transmettre au public par télécommunication ou par l'Internet, prêter, distribuer et vendre des thèses partout dans le monde, à des fins commerciales ou autres, sur support microforme, papier, électronique et/ou autres formats.

L'auteur conserve la propriété du droit d'auteur et des droits moraux qui protègent cette thèse. Ni la thèse ni des extraits substantiels de celle-ci ne doivent être imprimés ou autrement reproduits sans son autorisation.

---

Conformément à la loi canadienne sur la protection de la vie privée, quelques formulaires secondaires ont été enlevés de cette thèse.

Bien que ces formulaires aient inclus dans la pagination, il n'y aura aucun contenu manquant.

  
**Canada**

## ABSTRACT

The performance of non-ferrous reinforcing material, in the form of GFRP bars, as the primary reinforcement of flat plates is investigated. In total, nine interior slab-column connections, that represent full scale specimens, were made and tested to failure at the structural laboratory of MUN. The 1900 × 1900 mm square slabs were simply supported along the four edges. The reinforcement ratio, concrete strength and effective depth were the main variables. Transverse central load was applied to the slabs through a central column stub. The load was applied in displacement control. The structural behaviour of the test specimens was investigated in terms of load-deflection relationship, crack pattern and width, deflection profile, concrete and FRP strains, failure mode and ultimate failure load. The effects of those variables on the behaviour were examined. Eight slabs were made with GFRP bars commercially known as ISOROD<sup>®</sup>. One slab was made with traditional steel bars. Two slabs were with high strength concrete, over 85 MPa. The rest of the slabs were made with normal strength concrete. Two slabs were 200 mm thick with an effective depth of 150 mm. The other slabs were 150 mm thick with an effective depth of 100 mm. All GFRP slabs were designed with over reinforced section capacity.

The test results revealed that slabs reinforced with GFRP bars exhibit higher deflection and greater crack width compared to similar slabs with traditional steel bars. The failure loads are also lower than those of slabs with traditional reinforcement. Nevertheless, the structural performance of the GFRP reinforced slabs can be improved by increasing the slab depth. High strength concrete increases the ultimate failure load but does not significantly improve the serviceability of the slabs.

The existing code formulas were examined to check their applicability in predicting the shear capacity of two-way slabs reinforced with GFRP bars. Elastic plate theory was used in an attempt to calculate the flexural capacity of such slabs. The results revealed that, with proper modifications, the equations that use a cubic root relationship for concrete strength and include the effect of the reinforcement ratio are able to predict the capacity of the slabs with reasonable accuracy.

An existing mechanical model was adopted and modified. That model had an unidentified limitation. The limitation is described and removed by modification of model geometry. Further modification is made to incorporate FRP's properties and structural behaviours and thus the model is made applicable for slabs reinforced with FRP as well as for slabs reinforced with traditional steel bars. The model results were compared to the slab test results available in literature with both steel and FRP reinforcement. The model gives a fairly good agreement between the predicted and experimental punching failure loads.

## ACKNOWLEDGEMENTS

The author would like to thank Almighty Allah for providing him with the opportunity and strength as well as showing him the way during the work on this thesis.

This thesis is completed at Memorial University of Newfoundland funded by a Discovery Grant from the Natural Sciences and Engineering Research Council of Canada. Funding in the form of graduate fellowship and graduate supplement from the Faculty of Engineering, Memorial University, is gratefully acknowledged.

The author would like to express his gratitude to his supervisor Dr. Amgad Hussein, Assistant Professor of Civil Engineering, for his financial support, keen supervision and effort during the period of the program.

Thanks are due to Dr. R Venkatesan, Associate Dean of Engineering for Graduate Studies and Research, for his understanding, encouragement and the facilities provided. Furthermore, Ms. M. Crocker, secretary of the Associate Dean's office, is acknowledged for ensuring smooth and efficient operation of the associated administrative tasks of my graduate program.

Sincere thanks are due to the technical staff who made their services available at every stage of this project, specially Messrs A. Bursey, S. Organ and T. Pike. I also express my warm appreciation to the Technical Services of Memorial University for their help when it was needed.

Special thanks to Professor Dr. Brahim Benmokrane, University of Sherbrooke, who provided the GFRP bars for this research program. Sincere gratitude is extended to the following organizations for donating the materials that were used in the current program. Mr. Doug Tipton of Concrete Products 2001 Limited, Newfoundland, donated the concrete used in preparing the specimens. St. Lawrence Cement donated the cement. Euclid Canada donated the required chemical admixtures used in producing the high strength concrete. Mr. Eric Oates of Olympic Construction helped with casting and finishing some of the test slabs. I gratefully acknowledge these persons and organization for their help and support to this research program.

Finally, I would like to express my deepest appreciation to my family members and friends, especially my father M. Harun-ur-Rashid and my mother Surieya Begum, for their support and deep understanding during the course of this study.

# Table of Contents

Page No.

Abstract.....	ii
Acknowledgements.....	iii
Table of Contents.....	iv
List of Tables.....	vii
List of Figures.....	ix
List of Abbreviations and Symbols.....	xiii
<b>Chapter 1 – Introduction.....</b>	<b>1</b>
1.1 General.....	1
1.2 Problem definition.....	3
1.3 Scope and objectives .....	5
1.4 Thesis outline.....	6
<b>Chapter 2 - Literature Review.....</b>	<b>7</b>
2.1 Introduction.....	7
2.2 FRP reinforcement.....	7
2.2.1 Properties of FRP.....	9
2.2.2 Types of FRP.....	11
2.2.3 Properties of FRP bars as reinforcing for concrete.....	11
2.3 Failure of slab column joints.....	14
2.4 Punching shear capacity of interior slab-column connections according to different codes.....	18
2.4.1 Canadian Code .....	19
2.4.2 American Concrete Institute Code .....	20
2.4.3 British Standard.....	21
2.4.4 CEB-FIP Model Code 90 .....	22
2.4.5 The Eurocode 2 .....	23
2.5 Concrete members reinforced with FRP bars .....	24
2.5.1 Earlier research .....	24
2.5.2 Design recommendations for members in bending.....	25
2.6 Previous work on two-way slabs reinforced with FRP bars.....	28
2.7 Rational studies.....	38
2.7.1 Models based on Kinnunen and Nylander model.....	38
2.7.1.1 Original model by Kinnunen and Nylander....	38
2.7.1.2 Shehata.....	39
2.7.1.3 Marzouk and Hussein .....	40

2.7.1.4	Hallgren.....	41
2.7.2	Analytical model by Menétrey.....	45
2.7.3	The Truss model.....	48
2.7.4	Bond model by Alexander and Simmonds.....	50
2.7.5	Gardner (1990).....	53
2.7.6	Strain Approach and Modified Approach.....	54
2.7.7	Elastic analysis.....	56

### **Chapter 3 - Experimental Program.....58**

3.1	Introduction.....	58
3.2	Mechanical properties of the GFRP bars used in the current program.....	58
3.3	Concrete.....	65
3.3.1	Normal strength concrete.....	66
3.3.2	High strength concrete.....	66
3.3.2.1	Cementitious materials.....	67
3.3.2.2	Aggregates.....	68
3.3.2.3	Water reducing admixture.....	69
3.3.2.4	Retarding agent.....	69
3.3.2.5	Superplasticizer.....	69
3.3.2.6	Concrete mix .....	70
3.3.2.7	Mixing procedure.....	71
3.4	Test specimens.....	72
3.5	Formwork .....	76
3.6	Test frame.....	76
3.7	Placing of a slab.....	80
3.8	Instrumentation and measurements.....	80
3.8.1	Loading system.....	80
3.8.2	Deflections.....	82
3.8.3	Strains in reinforcement (FRP bars).....	82
3.8.4	Concrete strains.....	88
3.8.5	Crack detection device.....	88
3.8.6	Data acquisition system.....	89
3.9	Casting and curing.....	89
3.10	Test procedure.....	90

### **Chapter 4 - Test Results and Discussion.....92**

4.1	Introduction.....	92
4.2	Load-deflection characteristics.....	96
4.3	Ductility and energy absorption.....	99
4.4	Concrete strains.....	101
4.5	FRP strains.....	113

4.6	Cracking characteristics.....	123
4.7	Bar force gradients.....	136
4.8	Forces in the slab reinforcement.....	140
4.9	Deflection profile.....	144
4.10	Post punching behaviour.....	145
4.11	Modes of failure.....	151
4.12	Comparison of test results with different code predictions and some other rational approaches.....	156
 <b>Chapter 5 – Proposed Mechanical Model.....</b>		<b>161</b>
5.1	Introduction.....	161
5.2	Mechanical model proposed by Hallgren (1996).....	162
5.2.1	Model geometry.....	162
5.2.2	Tangential strains.....	165
5.2.3	Depth of the tangential compression zone.....	166
5.2.4	Resulting forces on concrete in compression and steel in tension.....	168
5.2.5	Dowel force.....	170
5.2.6	Equilibrium equations.....	171
5.2.7	Failure criterion.....	171
5.3	Some aspects of Hallgren's model .....	173
5.4	Proposed model.....	177
5.4.1	Model geometry.....	178
5.4.2	Implementation of FRP properties .....	181
5.5	Solution algorithm .....	184
5.6	Verification of the proposed model.....	188
 <b>Chapter 6 - Conclusion and Recommendation.....</b>		<b>193</b>
6.1	Discussion and conclusions.....	193
6.2	Recommendations for future research.....	197
 <b>References.....</b>		<b>198</b>
 <b>Appendix A:</b> Strain gauge locations on GFRP bars.....		<b>203</b>
<b>Appendix B:</b> Estimation of the mechanical properties of concrete.....		<b>205</b>
<b>Appendix C:</b> Computer program of the proposed mechanical model.....		<b>207</b>
<b>Appendix D:</b> Slab details, test and calculated results for slabs tested by other investigations.....		<b>215</b>

## List of Tables

Table 3.1:	Mechanical properties of the GFRP bars.....	65
Table 3.2:	Mix proportions for one batch of normal strength concrete.....	66
Table 3.3:	Mix proportions for one batch of high strength concrete.....	70
Table 3.4:	Details of the test slabs.....	73
Table 4.1:	Slab details and observed ultimate loads.....	93
Table 4.2:	Slab stiffness and ultimate deflection.....	98
Table 4.3:	Ductility and energy absorption capacity.....	100
Table 4.4:	Concrete strains.....	109
Table 4.5:	FRP strains.....	115
Table 4.6:	Cracking load and crack width.....	132
Table 4.7:	Failure modes of test slabs.....	153
Table 4.8:	Comparison of test results with various code equations.....	159
Table 4.9:	Comparison of test results with the prediction of some other rational models.....	160
Table 5.1:	Comparison of proposed model with test results.....	190
Table D-1:	Slabs tested by Ospina <i>et al.</i> (2003).....	215
Table D-2:	Slabs tested by El-Ghandour <i>et al.</i> (2003).....	215
Table D-3:	Slabs tested by Matthys and Taerwe (2000).....	215
Table D-4:	Comparison of proposed model predictions and test results of slabs with FRP reinforcement.....	216

Table D-5: Circular slabs tested by Regan et al. (1993).....	217
Table D-6: Rectangular slabs tested by Tomaszewicz (1993).....	217
Table D-7: Circular normal strength concrete slabs tested by Tolf (1988).....	218
Table D-8: Rectangular slabs tested by Marzouk and Hussein (1991).....	218
Table D-9: Circular slabs tested by Hallgren (1996).....	218
Table D-10: Comparison of proposed model predictions and test results of slabs with steel reinforcement.....	219

## List of Figures

Fig. 2.1:	FRP products and cross sectional view of FRP composite.....	8
Fig. 2.2:	Typical stress-strain relationships of fibre, matrix and FRP.....	10
Fig. 2.3:	Stress-strain behaviour of steel bars and FRP reinforcing products..	12
Fig. 2.4:	Various types of flexural failure by Rankin and Long (1987).....	15
Fig. 2.5:	Punching shear failure.....	15
Fig. 2.6:	Critical section or control perimeter of punching shear failure as recommended by various codes.....	17
Fig. 2.7:	Kinnunen and Nylander's model (1960).....	42
Fig. 2.8:	Shehata's model (1985).....	43
Fig. 2.9:	Hallgren's model (1996).....	44
Fig. 2.10:	Model proposed by Menétrey (1996).....	47
Fig. 2.11:	Truss model by Alexander and Simmonds (1987).....	49
Fig. 2.12:	Bond model by Alexander and Simmonds (1992).....	52
Fig. 3.1:	GFRP bars used in the test program.....	60
Fig. 3.2:	GFRP bar specimen before and after testing.....	61
Fig. 3.3:	GFRP bar specimen in the test machine before and after testing....	62
Fig. 3.4:	Sketch of the special grips for the FRP bar tension test.....	63
Fig. 3.5:	Recorded stress-strain relationship of GFRP bar.....	64
Fig. 3.6:	Grading of aggregates.....	68
Fig. 3.7:	Conventional slab-column specimen idealization.....	74

Fig. 3.8:	Typical test slab specimen.....	75
Fig. 3.9:	Photograph of the formwork .....	77
Fig.3.10:	A schematic of test frame.....	78
Fig. 3.11:	Photograph of the test frame with a test specimen in place.....	79
Fig. 3.12:	Actuator behind the test frame.....	81
Fig. 3.13:	A 410 digital function generator, 407 controller and data acquisition system.....	83
Fig. 3.14:	Location of the LVDTs and dial gauges.....	84
Fig. 3.15:	Strain gauge locations on the reinforcement of slab GS1.....	85
Fig. 3.16:	Concrete strain gauge locations.....	87
Fig. 3.17:	Manual crack marking, crack width measurement and dial gauge reading collection at a load interval.....	91
Fig. 4.1:	Load-deflection history.....	94
Fig. 4.2:	Radial and tangential concrete strains.....	102
Fig. 4.3:	Strain level and the propagation of crack depth.....	106
Fig. 4.4:	Variation of radial and tangential concrete strain w.r.t deflection of the slab center.....	110
Fig. 4.5:	Radial and tangential FRP strains.....	116
Fig. 4.6:	FRP strains at the end of the critical bars.....	120
Fig. 4.7:	FRP strain profile in radial direction of some typical slabs.....	121
Fig. 4.8:	FRP strain profile in tangential direction of some typical slabs.....	122
Fig. 4.9:	Crack patterns of the test slabs.....	126

Fig. 4.10:	Crack width expansion of certain cracks with respect to deflection of slab center.....	133
Fig. 4.11:	Crack width of a typical FRP slab, at the time of testing, around the column periphery.....	134
Fig. 4.12:	Crack depth at the side of a test slab.....	135
Fig. 4.13:	Force gradient of some critical bars.....	137
Fig. 4.14:	Bar forces in some critical bars.....	141
Fig. 4.15:	Schematic diagram of the dial gauges and LVDT locations along a center line of the slab on tension face.....	146
Fig. 4.16:	Slab rotation versus slab central deflection.....	147
Fig. 4.17:	Deflection profiles.....	149
Fig. 4.18:	Compression side of slabs at failure.....	154
Fig. 5.1:	Model geometry [Hallgren (1996)].....	163
Fig. 5.2:	Distribution of steel and concrete tangential strains, $\epsilon_{sT}$ and $\epsilon_{cT}$ , respectively, along the radius $r$ .....	164
Fig. 5.3:	Adopted stress-strain curves for concrete and steel, respectively.....	166
Fig. 5.4:	Distribution of tangential concrete stresses, $\sigma_{cT}$ , in the compression zone, along the radius $r$ of the slab, when some part of the compression zone is yielded.....	168
Fig. 5.5:	Tangential steel stress $\sigma_{sT}$ in the flexural reinforcement, along the radius $r$ of the slab, when some steel is yielded.....	169
Fig. 5.6:	Model geometry proposed by Hallgren (1996).....	173

Fig. 5.7:	Geometry of truncated wedge for $\alpha = 22.5^\circ$ .....	175
Fig. 5.8:	Geometry of truncated wedge for $\alpha = 35^\circ$ .....	176
Fig. 5.9:	Geometry of proposed model.....	178
Fig. 5.10:	Stress-strain relation of FRP reinforcement.....	180
Fig. 5.11:	Tangential strain distribution of FRP reinforced slab segment outside the shear crack.....	181
Fig. 5.12:	Variation of the dowel force reduction factor, $\mu$ .....	184
Fig. 5.13:	Flow-chart of the algorithm of the proposed model for steel reinforced slabs.....	186
Fig. 5.14:	Flow-chart of the algorithm of the proposed model for FRP reinforced slab.....	187
Fig.5.15:	Observed ultimate load versus predicted ultimate load using the proposed model.....	191
Fig. 5.16:	Ratio between the observed ultimate load and ultimate load predicted by proposed model versus bar spacing.....	191
Fig. A1:	Reinforcement layout and strain gauge locations.....	203

# List of Abbreviations and Symbols

## Abbreviations

ACI	=	American Concrete Institute
AFRP	=	Aramid Fibre Reinforced Plastic or Polymer
BS	=	British Standard
CEB-FIP	=	Comité Euro-Internacional du Béton - Fédération Internationale de la Précontrainte
CFRP	=	Carbon Fibre Reinforced Plastic or Polymer
CSA	=	Canadian Standards Association
CS	=	Concrete Strain-gauge (i.e. strain gauge on concrete)
Dm	=	Design value with modification for lower $E_{frp}$
DPF	=	Ductile Punching Failure
EC2	=	Eurocode 2
FFC	=	Flexural Failure by Compression
FRP	=	Fibre Reinforced Plastic or Fibre-Reinforced Polymer
GFRP	=	Glass Fibre Reinforced Plastic or Polymer
ISIS	=	Intelligent Sensing for Innovative Structures
LVDT	=	Linear Variable Differential Transformer
M	=	Mean value
MC 90	=	Model Code 1990
Mm	=	Mean value with modification for lower $E_{frp}$

PPF	=	Pure Punching Failure
RCC	=	Reinforced Cement Concrete
RS	=	Reinforcement Strain-gauge (i.e. strain gauge on reinforcement)
w.r.t.	=	with respect to
2-D	=	two dimensional
3-D	=	three dimensional

### **Roman upper case letters**

$A_{bar}$	=	area of reinforcing bar being considered
$A_{FRP}$	=	actual cross sectional area of a FRP bar
$A_g$	=	gross concrete area
$A_s$	=	effective steel area crossing the perimeter of the critical section or equivalent steel area (in case of Strain Approach)
$B$	=	diameter of column
$D$	=	dowel force
$E_c$	=	modulus of elasticity of concrete
$E_{FRP}$	=	modulus of elasticity of FRP bar
$E_s$	=	modulus of elasticity of steel or FRP bar (in case of proposed model)
$F_{sd}$	=	factored concentrated force
$G_F^\alpha$	=	fracture energy for an infinitely large structure
$G_F^R$	=	fracture energy, measured according to the RILEM recommendation
$M_{cr}$	=	cracking moment

- $M_r$  = factored moment resistance or moment in radial direction
- $P$  = reaction which acts along the periphery of the circular slab as line load
- $P_{ACI}$  = punching load calculated by ACI 318-02 code recommendation
- $P_{BS}$  = punching load calculated by BS 8110-97 code recommendation
- $P_{CSA}$  = punching load calculated by CSA A23.3-94 code recommendation
- $P_{MC90}$  = punching load calculated by Model Code 1990 code recommendation
- $P_{MT}$  = punching load calculated by empirical equation proposed by Matthys and Taerwe (2000)
- $P_m$  = failure load calculated from moment
- $P_v$  = failure load calculated from summation of all vertical forces
- $R_{cT}$  = tangential concrete force
- $R_{sR}$  = steel force in radial direction
- $R_{sT}$  = steel force in tangential direction
- $S_{eff}$  = effective tributary width of the reinforcing bar (max  $6d'$ )
- $T$  = inclined compressive force passing through the truncated wedge from slab to column
- $V_U$  = factored shear force acting on the connection

### **Roman lower case letters**

- $a_v$  = the distance from the edge of the loaded area to the perimeter considered
- $b_o$  = the perimeter of the critical section
- $c$  = dimension of column face perpendicular to the bar being considered or diameter of circular slab (in case of model)

- $c_o$  = distance from the column center to the shear crack at the level of the flexural reinforcement
- $d$  = the effective depth of the slab
- $d'$  = cover of the reinforcing mat measured from center of mat to nearest surface of slab
- $d_a$  = maximum aggregate size
- $d^R$  = depth of the RILEM test beam
- $d_s$  = effective depth of reinforcing mat measured from center of mat to compression surface of slab
- $e$  = base of natural logarithm
- $f_c'$  = cylinder compressive strength of concrete
- $f_{cc}$  = cylinder compressive strength of concrete [in case of Hallgren (1996) and proposed model]
- $f_{cd}$  = design compressive strength of concrete
- $f_{ck}$  = characteristic compressive strength of concrete
- $f_{cm}$  = mean compressive strength of concrete
- $f_{ct}$  = tensile strength of concrete
- $f_{ctk}$  = characteristic tensile strength of concrete (5-percent fractile)
- $f_{ctm}$  = mean tensile strength of concrete
- $f_{cu}$  = characteristic cube concrete strength
- $f_r$  = modulus of rupture
- $f_s$  = steel yield strength [in case of model proposed by Menétrey (1996)]

- $f_s$  = stress of FRP bar or steel bar (in case of proposed model)
- $f_{su}$  = ultimate strength of FRP bar (in case of proposed model)
- $f_{sy}$  = yield stress of steel [in case of Hallgren (1996) model]
- $f_y$  = yield strength of steel
- $k_E$  = stiffness factor due to the biaxial compression in concrete
- $r$  = radius of any point from slab center (in case of model)
- $r_c$  = yield radius (yielding of concrete) measured from slab center
- $r_s$  = yield radius (yielding of steel bar) measured from slab center
- $u_l$  = control perimeter
- $u_o$  = the perimeter of the column or column capital or loaded area
- $v_c$  = ultimate punching shear strength of concrete
- $v_f$  = shear stress due to factored design loads
- $v_{max}$  = maximum shear stress at the face of column
- $v_r$  = factored shear stress resistance capacity
- $v_u$  = factored nominal shear stress at slab-column connection
- $x$  = depth of tangential compression zone (in case of Hallgren's model)
- $x_2$  = depth of tangential compression zone (in case of proposed model)
- $y$  = distance from column face to the projection of center of rotation,  $Q$ , on the bottom of slab
- $0.7x_1$  = distance from column face to the projection of center of rotation,  $Q$ , on the bottom of slab when  $\alpha > 20^\circ$

## Greek letters

- $\Delta_c$  = central deflection of slab when it changes its stiffness
- $\Delta_u$  = ultimate deflection of slab center
- $\alpha$  = angle of inclination of force  $T$
- $\alpha_c$  = a factor to calculate average stress of concrete at any point
- $\alpha_{c0}$  = factor  $\alpha_c$  at  $r = c_0$
- $\beta_c$  = the ratio of long side to short side of the column
- $\delta$  = multiplying factor to determine the angle of inclined shear crack
- $\epsilon_{cT}$  = tangential concrete strain
- $\epsilon_{cTu}$  = ultimate tangential concrete strain which is the failure strain
- $\epsilon_{cTz}$  = ultimate tensile transverse strain in Z-direction
- $\epsilon_{cy}$  = yield strain of concrete
- $\epsilon_{cu}$  = ultimate strain of concrete
- $\epsilon_s$  = strain of FRP bar or steel bar (in case of proposed model)
- $\epsilon_{sT}$  = tangential steel strain
- $\epsilon_{sT0}$  = tangential steel strain at  $r = c_0$
- $\epsilon_{sy}$  = yield strain of steel
- $\epsilon_{su}$  = ultimate strain of FRP bar (in case of proposed model)
- $\phi$  = diameter of steel bars (mechanical model) or strength reduction factor (ACI 318-02 Code) or a modification factor (Modified Approach)
- $\phi_c$  = resistance reduction factor for concrete which is 0.6

- $\gamma$  = density of concrete [ $\text{kg/m}^3$ ]  
 $\gamma_m$  = partial safety factor for the concrete strength = 1.5  
 $\lambda$  = factor to allow for low density concrete  
 $\mu$  = dowel force reduction factor  
 $\mu\epsilon$  = micro-strain  
 $\nu$  = Poisson's ratio  
 $\rho$  = reinforcement ratio  
 $\rho_f$  = reinforcement ratio of flexural reinforcement  
 $\rho_{fb}$  = balanced reinforcement ratio of flexural reinforcement  
 $\rho_x$  = reinforcement ratio in  $x$  direction  
 $\rho_y$  = reinforcement ratio in  $y$  direction  
 $\rho_b$  = balanced reinforcement ratio  
 $\sigma_{cT}$  = tangential concrete stresses in compression  
 $\sigma_{FRP}$  = actual FRP stress  
 $\sigma_{sT}$  = tangential steel stress of the flexural reinforcement along the radius  $r$   
 $\sigma_{steel}$  = equivalent steel stress  
 $\tau_{rd}$  = shear resistance of concrete  
 $\tau_{sd}$  = factored nominal shear stress  
 $\xi$  = size factor or modular ratio ( $E_{FRP} / E_s$ )

# **Chapter 1**

## **Introduction**

### **1.1 General**

Reinforced Cement Concrete (RCC) is a composite material. Any material with higher tensile strength can be provided in the tension zone of the concrete as a reinforcing material. Normally, mild steel bars are used as reinforcing material for concrete. Steel reinforcement has good bond with concrete and show yielding phenomena at a certain level of stress. It is an important property of steel. RCC design philosophy considers this property of steel in all design formulas. All concrete structures are designed as under reinforced members so that they will not exhibit catastrophic failure when a member is overstressed. Nevertheless, mild steel is highly corrosive and has heavy weight. Corrosion of steel reduces the lifetime of a structure. Repairing or rebuilding of the structure would be costly. For these reasons, engineers are looking for suitable alternatives of mild steel reinforcing bars.

Fibre Reinforced Plastic or Fibre-Reinforced Polymer (FRP) bars may be a suitable alternative of mild steel. "Fibre" or "filament" is the basic constituent of FRP. Fibres and matrix are the two major constituents of FRP. In FRP, the fibre or filament is used as the reinforcing material. Various kinds of resin are used as binder for the fibres in FRP and are also known as the matrix.

FRP products are now available in various shapes, such as FRP sheets, FRP grid (2-D and 3-D), FRP bars, pipes, tubes and other various shapes according to the needs. FRP bar is the form of FRP which is the focus of this research program. FRP bars comes in different forms such as smooth surface, sanded surface, twisted, glued surface, ribbed or indented rebar. These surface preparations are made to increase the bond capacity of FRP bars. Sanded surface GFRP bars that are commercially known as ISOROD<sup>®</sup> are used in this experimental program.

Nowadays, FRP bars are used in RCC instead of mild-steel. The cost of FRP bars is relatively higher than the traditional mild steel bars. Nevertheless, FRP bars are used in high value-added applications where corrosion is the primary concern.

More than 40% of the existing bridges in Canada were built more than 30 years ago. A significant number of these existing bridges are now in need of strengthening, rehabilitation or replacement. Canada's adverse climate and extensive use of de-icing salts have very adverse effects on the traditional concrete structures, in an exposed environment. Besides this, underground, costal and offshore structures all over the world are always affected by environmental effects. In traditional concrete structures, mild steel are used as reinforcing materials, which is very vulnerable to corrosion, and consequently concrete structures become very deteriorated. The traditional approaches of protecting steel from corrosion effects are; using large clear cover, high cement ratio in concrete, limited crack width, epoxy-coated steel reinforcing bars, etc. However, these traditional approaches may not be very effective. Maintaining, repairing and rebuilding of

the concrete structures are expensive. These huge costs could incline the owners of infrastructures toward the use of a more effective and affordable solution, such as, using FRP which is corrosion resistive, durable and easy to install. Thus, it is possible to increase the service life of infrastructure and reduce maintenance costs, although the initial building or installation cost is higher.

## **1.2 Problem definition**

The modulus of elasticity of FRP bars is lower than steel bars and it depends on its constituents. FRP bars made with carbon fibres have higher modulus of elasticity than FRP bars made with glass fibres. Carbon FRP bars could be made with a modulus of elasticity that is very close to that of steel. However, this is very costly. Generally available FRP bars have a modulus of elasticity lower than that of steel bars. This lower modulus of elasticity leads to higher strains i.e. higher deflection in loaded structures, which can exceed the acceptable serviceability limits. Another problem involved in using FRP bars as reinforcing material in concrete structures is its lower bond strength. This bond strength also depends on the surface finishing. FRP bars may have smooth surface, sanded surface, glued surface or various kinds of deformed surfaces. Depending on surface finish, its bond capacity can vary from 0.69 MPa to 23.02 MPa [Cosenza (1997)]. An FRP bar does not show any yield phenomena like steel bars; it shows elastic behaviour up to rupture.

Slab column joint is a critical part of some concrete structures. A structure may fail at the slab-column joint. This failure could either be a flexural failure or a shear failure. The

shear failure is known as punching shear failure. It is a premature sudden failure and is catastrophic in nature. Design engineers have to design a structure in such a way that the punching shear capacity is higher than the shear forces that develop. The shear stress is normally measured on an assumed failure surface (critical surface) when the structure is fully loaded with the design loads. Traditional slabs are designed for flexure so that the slabs fail, in flexure, by yielding of the reinforcement. In addition, punching shear failure must be avoided.

It is hard to determine the failure surface or critical surface for punching failure. The position and inclination of the failure surface are not very well defined. Engineers use different empirical formulae that are described in various codes to design slabs for punching shear. For example, the British code (BS 8110) assumes a critical surface at a distance  $1.5d$  ( $d$  = effective depth of slab) away from column face and also considers that the reinforcement has some effect on the punching shear capacity. The North American codes take the critical surface at a distance  $0.5d$  away from the column face and do not consider any effects for the reinforcement on the punching shear capacity. Also, these existing empirical code formulas are developed for RCC slabs with traditional mild steel bars. If FRP is used in RCC, there may be a need to revise the existing empirical formulas and to develop new rational models. Therefore, further research is needed and experimental data are required to establish applicable empirical formulas or rational models for punching shear capacity of RCC slab-column joint reinforced with FRP bars.

### **1.3 Scope and objectives**

The main objective of this experimental research program is to study the behaviour of two-way slabs reinforced with FRP bars. The second objective is to develop a rational mechanical model to calculate the punching shear capacity of such slabs.

In this investigation, two-way slabs reinforced with FRP bars are tested up to failure. The effects of the different parameters on the slab behaviour are been examined. Sand coated Glass Fibre Reinforced Polymer (GFRP) bars are used as reinforcement. The concrete strength, slab effective depth and reinforcement ratio are the main variables. The structural behaviour in terms of load-deflection relation, crack pattern and crack width, failure nature, ultimate failure load, concrete strain and FRP bars strain in radial and tangential direction is investigated.

The observed behaviour of the FRP-reinforced slabs is compared with the behaviour of slabs with traditional steel reinforcement. The ultimate punching loads are compared with the existing code recommendations. Some existing rational models are also studied to examine if they are capable of predicting the capacity of slabs reinforced with FRP reinforcement.

The scope of this study is limited to only one type of FRP reinforcement, that is, a GFRP bar which is commercially known as ISOROD<sup>®</sup>. Furthermore, only interior slabs under central load are investigated.

## **1.4 Thesis outline**

Chapter 2 contains the literature review. At the beginning of the chapter, the properties of FRP are explained. The different code recommendations that are available to predict the punching capacity of slabs with traditional steel reinforcement are presented. The research conducted on two-way slabs with FRP reinforcement is described chronologically. Finally, some mechanical models for two-way slabs, that are available in the literature, are discussed.

Chapter 3 describes the details of the experimental program. Details of the test setup, instruments used and testing procedure are presented.

Chapter 4 contains the test results and observations obtained from the experimental program. The results are described, analysed and discussed. The experiment results are compared with the different code predictions in this chapter.

In Chapter 5, an existing mechanical model was adopted and modified. In the model, the FRP properties are incorporated to make it applicable for slabs with FRP reinforcement. The proposed modified model is verified with existing test results from this experimental program as well as the test results available in the literature.

Chapter 6 contains the findings from this research program and the recommendations for further research.

# **Chapter 2**

## **Literature Review**

### **2.1 Introduction**

The focus of this research program is on punching shear of flat slabs and column connections reinforced with FRP bars. Slabs with traditional reinforcement have been the subject of numerous studies for almost a century. However, experimental work on punching shear of slabs with FRP bars is scarce. Very few experimental studies were conducted on this topic. Initially, some problems were faced by the researchers as the properties of FRP are different than traditional steel reinforcement. Also, the problem of predicting the punching capacity of the slab arose. Some researchers proposed to modify the existing code equations by introducing the properties of FRP bars into the equations. However, none of the equations are widely accepted. A literature review on the slab-column connections reinforced with FRP reinforcement is presented in this chapter.

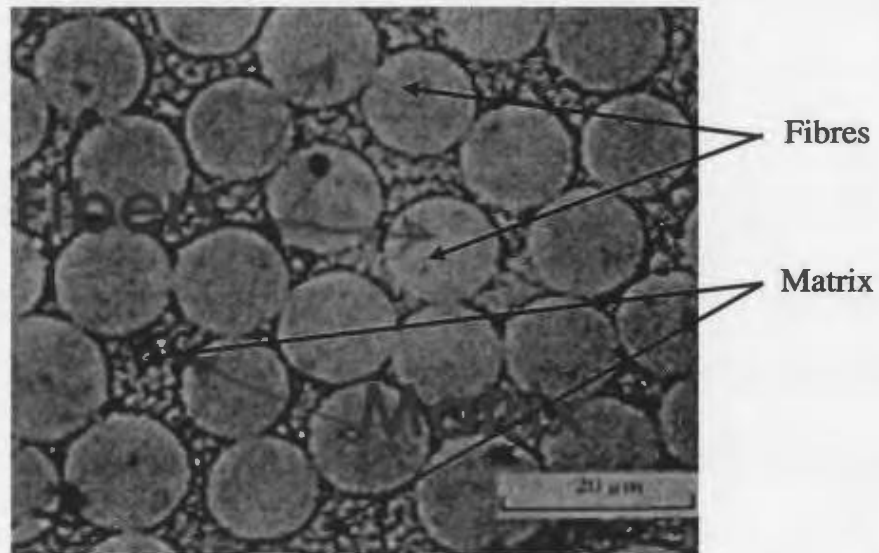
### **2.2 FRP reinforcement**

A material with a length that is at least 100 times of its diameter is known as "filament". The term "filament" is often used synonymously with "fibre". This "fibre" or "filament" is the basic constituent of Fibre Reinforced Plastic or Fibre-Reinforced Polymer (FRP). Reinforcement and matrix are the two major constituents of FRP.

A fibre or filament is used as reinforcing material and various kinds of matrix are used as binders of the fibres in FRP. Carbon, Aramid, Glass, Ceramic and other polymer fibres



**(a) Common glass and carbon fibres and FRP products used in structural engineering**



**(b) Electron micrograph of partial cross section Glass cFRP composite**

**Fig. 2.1: FRP products and cross sectional view of FRP composite [Chung (2002)]**

are used as reinforcing fibres. Polyester resin, Vinyl Ester resin, Epoxy resin, Polyimide resin and thermoplastic resins are used as Matrix. Fibres are used as reinforcement in FRP for strength, stiffness and dimensional stability.

The matrix is used to provide lateral support to the fibres and to protect the fibre from physical and chemical trauma due to the surroundings. In addition, the matrix provides some important physical characteristic to the FRP such as stiffness, strength, fracture toughness, diffusivity, thermal susceptibility etc.

Some resin additives are used to enhancing the resistance of the matrix, and thus FRP products, to flames, smoke generation, moisture, microbial degradation, oxidation, heat, chemicals, shrinkage, surface roughness and ultraviolet radiation.

### **2.2.1 Properties of FRP**

Properties of FRP can be divided in to two categories: 1) Physical properties such as mass properties, geometric properties, chemical properties, thermal properties and transport properties, etc, 2) Mechanical properties such as elastic stiffness properties, failure properties, etc. Some of the mechanical properties of FRP are:

- The longitudinal shear modulus of FRP is generally low compared with steel reinforcement.
- Failure modes of FRP can be divided into two parts, the matrix dominated failure modes and the fibre dominated failure modes. The failure strain of the fibre is less

than the failure strain of the matrix. Under tensile loading, the composite fails when the fibre reaches its failure tensile strain.

- Compressive failure properties may be significantly less than the tensile failure properties of FRP.
- Fatigue properties of FRP are good when it is loaded in the fibre direction.
- The impact properties of FRP are expected to be higher in longitudinal direction than transverse direction and shear direction.

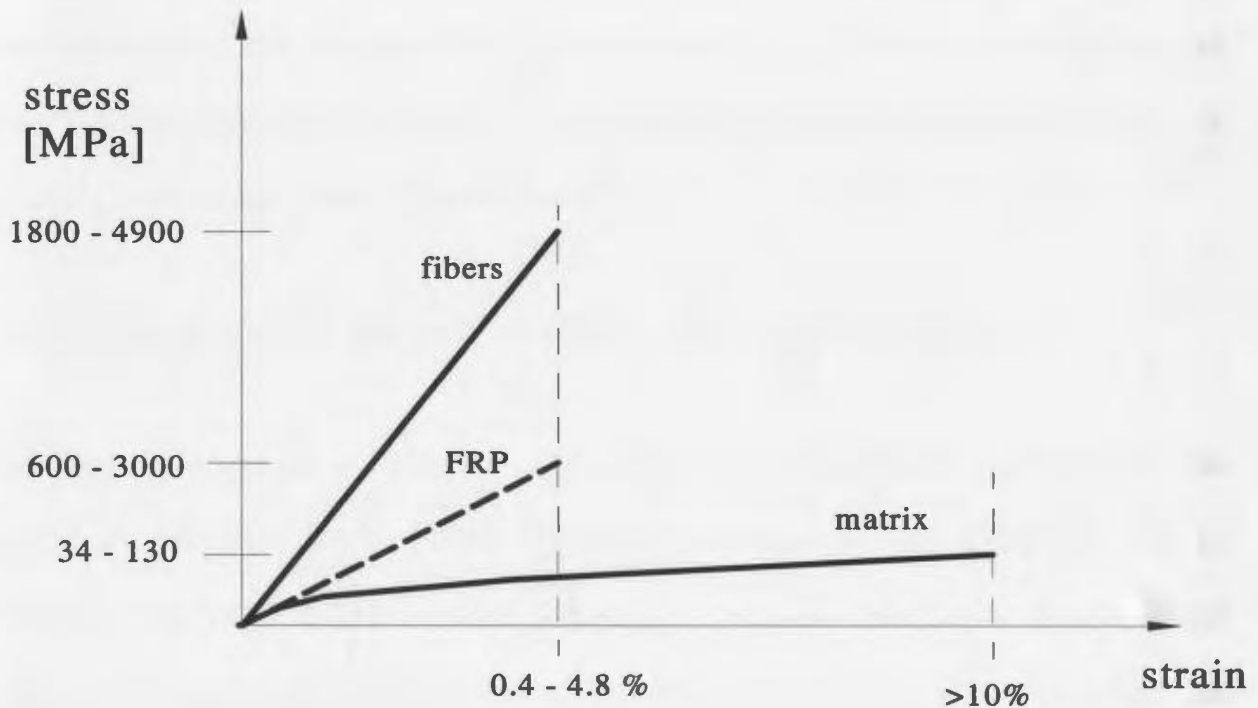


**Fig. 2.2: Typical stress-strain relationships of fibre, matrix and FRP [ISIS Canada (2001)]**

The fibres are stronger than the matrix. The strength of FRP composite depends on the strength of the fibre and matrix both. The mechanical properties of the final FRP product depend on the fibre quality, orientation, shape, volumetric ratio, adhesion to the matrix and on the manufacturing process. A qualitative stress-strain relations of fibre, matrix and FRP are depicted in Fig. 2.2.

### **2.2.2 Types of FRP**

Based on the fibre type, FRP can be classified as Glass, Carbon, Aramid and Hybrid Fibre Reinforced Polymer products. Based on the shape of the finished FRP product, FRP can be designated as FRP sheets, FRP grids (2-D and 3-D), FRP bars, pipes and tubes and other various shapes according to the different needs. FRP bars in the form of GFRP, is the main focus of the current experimental program.

### **2.2.3 Properties of FRP bars as reinforcement for concrete**

FRP bars could be used as reinforcement for reinforced concrete members instead of the traditional mild-steel reinforcement. The main advantages of such a selection are: 1) corrosion resistance, 2) high tensile strength, 3) low mechanical relaxation, 4) good toughness, 5) high fatigue resistance, 6) dimensional stability, 7) particular electrical and magnetic properties (transparent to electromagnetic emissions), and 8) light weight (specific gravity  $1.8 \times 10^{-3}$  g/mm<sup>3</sup> compared to  $2.8 \times 10^{-3}$  for the Aluminium and  $7.6 \times 10^{-3}$  for Steel).

FRP bars have some limitations compared to mild steel reinforcement. That is, the modulus of elasticity of FRP bars is lower than steel. The value of the modulus of elasticity of an FRP bar depends on its constituents. FRP bars made with carbon fibres have a higher modulus of elasticity than those made with glass fibres. Carbon FRP bars can be made with a modulus of elasticity that is almost the same as that of mild steel, but this will be very costly. Commercially available FRP bars have a modulus of elasticity that is lower than that of steel. The magnitude of the modulus of elasticity depends on the type of fibre that is being used, fibre-matrix ratio, adhesion, manufacturing process etc.

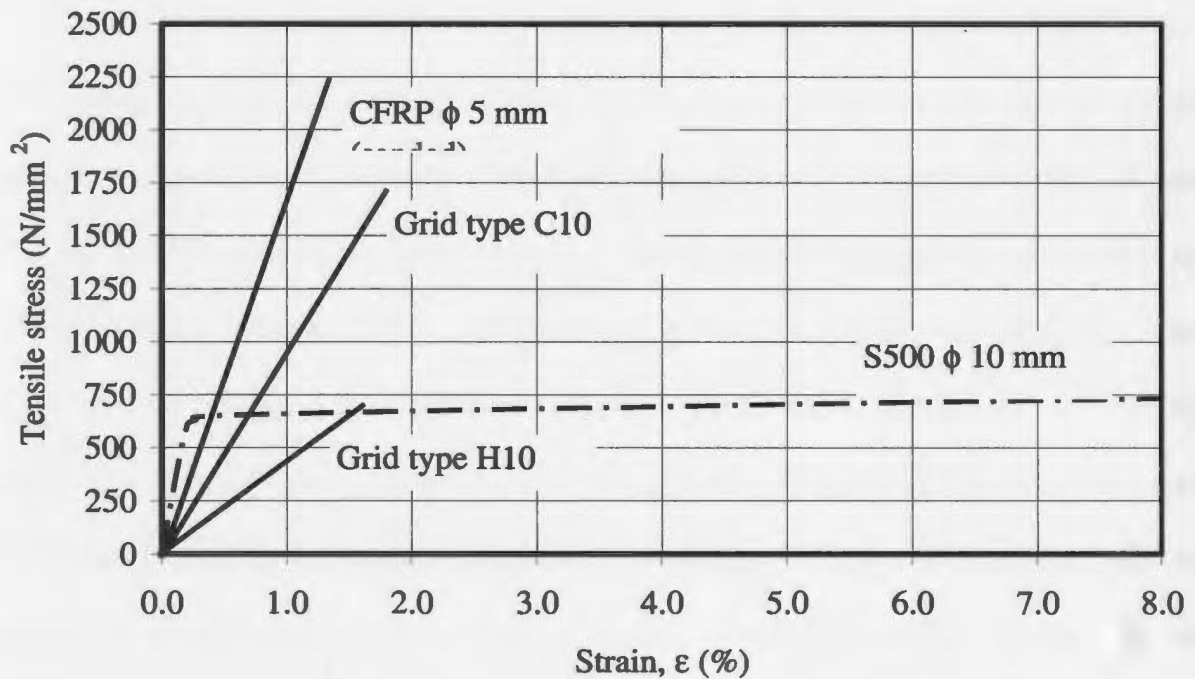


**Fig. 2.3: Stress-strain behaviour of steel bars and FRP reinforcing products [Matthys and Taerwe (2000)]**

Depending on those parameters, the modulus of elasticity can vary from 37 GPa to 43 GPa for GFRP and from 100 to 147 GPa for CFRP [ISIS Canada Corporation (2001)]. This lower modulus of elasticity leads to higher strains i.e. higher deflections and crack width in structures under load.

FRP bars do not show any yield phenomena like steel bars. They show elastic behaviours up to rupture. Thus, failure is brittle in nature. Note that all existing design philosophy and code equations in reinforced concrete design and analysis depend on the yield properties of steel reinforcement. To illustrate the different properties of FRP and steel reinforcement, typical stress-strain relations are shown in Fig. 2.3.

Another disadvantage when using the FRP bars as reinforcement for concrete structures could be the lower bond strength. The bond strength mainly depends on the surface finishing. FRP bars may be with smooth surface, sanded surface, glued surface or deformed surface (twisted, ribbed, indented and braided or braided and sanded). Other parameters that influence the bond strength are chemical bond, mechanical interlocking of FRP reinforcement and concrete, hydrostatic pressure against the FRP reinforcement due to the shrinkage of hardened concrete, swelling of FRP reinforcement due to temperature change and moisture absorption, bar diameter, position of bar (top or bottom), embedment length and shear strength of the matrix. Depending on these factors, the bond capacity of FRP bars can vary from 0.69 MPa to 23.02 MPa [Cosenza (1997)], as mentioned earlier in the previous chapter. Sand coated bars are used in the current test program. These bars have excellent bond strength. The bond strength of such bars, in

normal concrete, ranges between 11 to 15 MPa. [ISIS Canada Corporation (2001)].

In conclusion, FRP bars differ from traditional steel bars significantly. Therefore, the code provisions and design formulas available for traditional concrete structure may not be completely applicable to concrete structure reinforced with FRP bars. The existing code provisions and philosophy need to be re-examined and, if necessary, they should be revised and modified before they could be applied to concrete structures reinforced with FRP bars.

Finally, FRP bars are one kind of thermosetting material. So it is not possible to bend them to various shapes according to needs in a construction site. The bars have to be fabricated in a certain shape that could not be altered once they are manufactured.

### **2.3 Failure of slab column joints**

Failure of slab-column joints can be classified to two distinct types:

- a) Flexure mode: where failure is initiated by the yielding of the reinforcement or crushing of concrete.
- b) Shear mode: where failure is initiated by internal diagonal cracking (pure punching).

Flexural failure can be classified to three types [Rankin and Long (1987)]:

- a) Full-yielding failure (very lightly reinforced slabs).
- b) Localized compression failure (balanced or over reinforced slabs).
- c) Partial yielding failure (intermediate reinforcement).

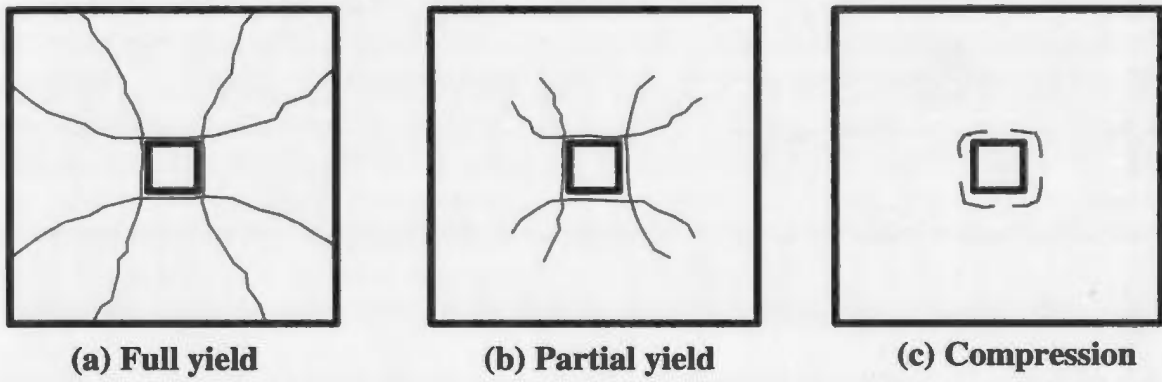


**Fig. 2.4: Various types of flexural failure by Rankin and Long (1987)**

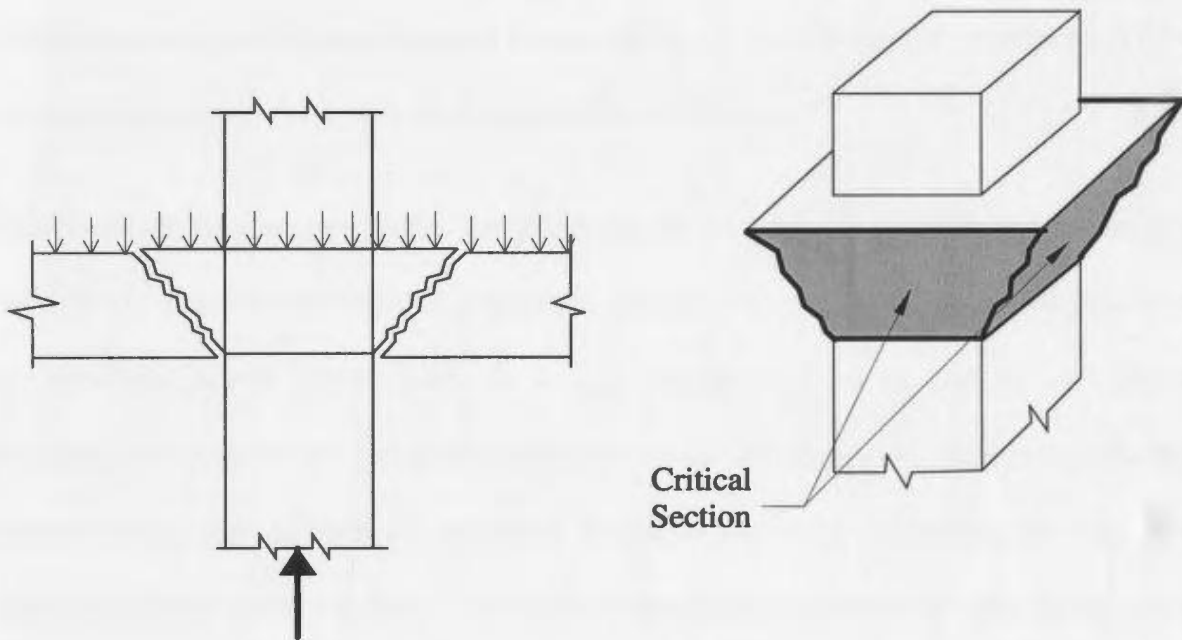


**Fig. 2.5: Punching shear failure**

If the slab is lightly reinforced, the yielding of traditional steel reinforcement spreads throughout the slab and yielding approaches the full yield pattern as shown in Fig. 2.4(a). Conversely, in highly reinforced slabs, yielding becomes more localized and the failure mode approaches that of localized compression failure of the concrete around the column face as depicted in Fig. 2.4(c). Flexural failure may occur in between these two modes i.e. yielding of reinforcement spread a certain distance from the column face but not throughout the slab. This could be designated as partial yield failure. The failure pattern for this case is illustrated in Fig. 2.4(b).

A slab may fail at the column vicinity without yielding of reinforcement or crushing of concrete. This kind of failure is initiated by diagonal tension cracking in concrete and the failure surface form a cone shape as shown in Fig. 2.5. This type of premature failure is known as punching shear failure or pure punching failure.

The shape of the punching cone, i.e. the angle of the cone, and the starting point of the cone, is not always well defined. Therefore, it is not easy to derive a formula to calculate the punching shear failure load. In design, engineers have to depend on empirical formulas to calculate the punching load. Numerous investigations have been conducted on this topic, and several of empirical formulas have been proposed for slabs with traditional steel reinforcement. However, different researchers do not agree on any unique position of the critical section for punching shear failure. Different codes have adopted different empirical formulas with different locations of the critical section. For example, British code (BS 8110) assumes a critical surface at a distance  $1.5d$  away from

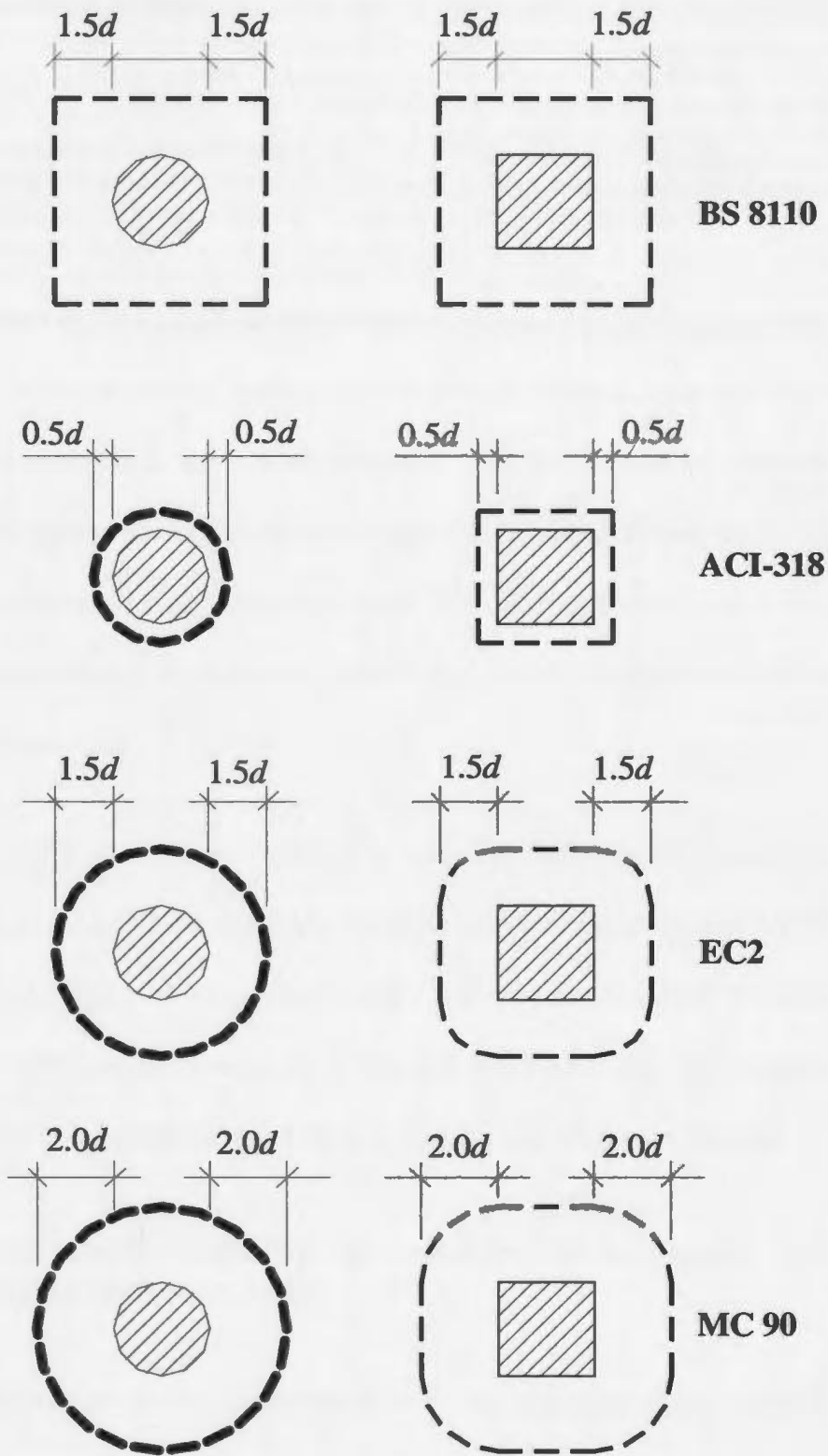


**Fig. 2.6: Critical section or control perimeter of punching shear failure as recommended by various codes**

column face, where  $d$  is the effective depth. It also assumes that the reinforcement has some effect on the punching shear capacity. The North American codes (CSA A23.3 and ACI-318) take a critical perimeter that is  $0.5d$  away from column face and they do not consider the influence of reinforcement on the punching shear capacity.

Different locations of the critical sections that are adopted by the various codes are shown in Fig. 2.6. All of these critical sections and the related formulas are developed for slabs reinforced with traditional steel reinforcement. The failure modes, discussed in this section, and the corresponding formulas (empirical or rational) are well developed for concrete slabs reinforced with traditional steel. The existing formulas and models should be examined and revised, if necessary, before they could be applied to FRP reinforced slab-column connections.

Some research work has been carried out by a number of researchers on this topic. It is very important to establish an empirical formula, mechanical or mathematical model to predict the flexural and punching failure loads. This is very essential to understand how to design such slab column systems in a safe and economic way. The research work on this topic and the outcome of such research is discussed later in this chapter.

#### **2.4 Punching shear capacity of interior slab-column connections according to different codes**

The focus of the current experimental study is on the punching shear capacity of interior slab-column connection. Such slabs are not supported on beams, have no drop panel and

no shear reinforcement. The recommendations of the different existing building codes to calculate the punching capacity are presented in this section.

### 2.4.1 Canadian Code

According to the current Canadian code CSA A23.3-94 (1994), the critical section is at a distance  $d/2$  away from the face of column and is in the same shape as the column. The punching resistance depends on the concrete strength, the column geometry and the length of the control perimeter. The well known dependence of the punching shear strength on the flexural reinforcement ratio is not considered. The design philosophy is:

$$v_f \leq v_r \quad (2.1)$$

where:  $v_f$  = factored shear stress due to factored design loads

$v_r$  = shear stress resistance capacity

The factored shear stress resistance,  $v_r$ , at the critical surface is the smallest of:

$$(a) \quad v_r = v_c = \left(1 + \frac{2}{\beta_c}\right) 0.2 \phi_c \sqrt{f'_c} \quad (2.2)$$

where  $\beta_c$  is the ratio of long side to short side of the column, concentrated load or reaction area. Parameter  $\phi_c$  is the resistance reduction factor for concrete which is 0.6 and  $v_c$  is the shear resistance of concrete.

$$(b) \quad v_r = v_c = \left(\frac{\alpha_s d}{b_0} + 0.2\right) \lambda \phi_c \sqrt{f'_c} \quad (2.3)$$

where  $\alpha_s = 4$  for interior columns, 3 for edge column and 2 for corner column.

$$(c) \quad v_r = v_c = 0.4\lambda\phi_c\sqrt{f'_c} \quad (2.4)$$

Where  $\lambda$  is 1.00 for normal density concrete, 0.85 for structural semi-low-density concrete in which all the fine aggregate is natural sand, 0.75 for structural low-density concrete in which none of the fine aggregate is natural sand. Linear interpolation may be applied based on the fraction of natural sand in the mix.

## 2.4.2 American Concrete Institute Code

The American Concrete Institute (ACI 318-02) assumes the same location of the critical section as the CSA code. The design philosophy is:

$$v_u < \phi v_c$$

where,  $v_u$  = factored nominal shear stress for slab-column connection, given by:

$$v_u = \frac{V_u}{b_o d} \quad (2.5)$$

where  $b_o$  = the perimeter of the critical section

$d$  = the effective depth of the slab

$V_u$  = factored shear force acting on the connection

$\phi$  = strength reduction factor = 0.85

$v_c$  = ultimate punching shear strength of concrete

The ultimate punching shear strength of concrete  $v_c$  should be the smallest value given by the following three equations:

$$(a) \quad v_c = \left(1 + \frac{2(4)}{\beta_c}\right) \frac{\sqrt{f'_c}}{6} \quad (2.6)$$

where  $\beta_c$  is the ratio of the long side to the short side of the column,  $\beta_c \leq 2$ .

$$(b) \quad v_c = \left( \frac{\alpha_s d}{b_o} + 2 \right) \frac{\sqrt{f'_c}}{12} \quad (2.7)$$

where,  $\alpha_s = 40$  for interior columns, 30 for edge columns, 20 for corner columns.

$$(c) \quad v_c = 0.33 \sqrt{f'_c} \quad (2.8)$$

The compressive strength,  $f'_c$ , should be  $\leq 35$  MPa for all equations in (a), (b) and (c).

### 2.4.3 British Standard

The British Standard (BS 8110-97) considers the concrete strength, the flexural reinforcement ratio and a size effect of the effective depth. According this Standard, the critical section lies  $1.5d$  from the column face. The design philosophy is that  $v \leq v_c$ . The design shear stress,  $v$ , due to a shear force,  $V$ , is calculated as:

$$v = \frac{V}{ud} \quad (2.9)$$

where  $u$  is the length of the perimeter of the critical section. The shear capacity of the critical section, which is taken the same as in one-way shear strength, is:

$$v_c = \left( \frac{1.5d}{a_v} \right) \frac{0.79}{\gamma_m} \left( \frac{100A_s}{ud} \right)^{1/3} \left( \frac{400}{d} \right)^{1/4} \left( \frac{f_{cu}}{25} \right)^{1/3} \quad (2.10)$$

where,  $a_v =$  is the distance from the edge of the loaded area to the perimeter considered

$d =$  effective depth in mm and  $(400/d) \geq 1$

$\gamma_m =$  partial safety factor for strength of material (1.25)

$A_s =$  effective steel area crossing the perimeter of the critical section,  
( $100A_s/ud$ )  $\leq$  3.0

$f_{cu} =$  characteristic cube concrete strength and should not be taken less than  
25 MPa and not greater than 40 MPa ( $f_{cu} = 1.18 f_c'$ )

In addition, the maximum shear stress,  $v_{max}$ , at the face of column should neither exceed  $0.8(f_{cu})^{1/2}$  nor 5.0 MPa, whichever is less. The value of  $v_{max}$  is given by:

$$v_{max} = 2.0 \frac{V_c}{u_o d} \quad (2.11)$$

where  $u_o$  is the perimeter of the column or column capital  $V_c$  is the characteristic punching resistance without shear reinforcement.

#### 2.4.4 CEB-FIP Model Code 90

The CEB-FIP Model Code (1990) considers the position of the critical section at a distance  $2d$  away from the loaded area or face of the column or column capital. Like the British Code, it also considers the concrete strength, reinforcement ratio and size effect.

The Design philosophy is:

$$\tau_{sd} \leq \tau_{rd} \quad (2.12)$$

$$\tau_{sd} = \frac{F_{sd}}{u_1 d} \quad (2.13)$$

$$\tau_{rd} = 0.12 \xi (100 \rho f_{ck})^{1/3} \quad (2.14)$$

where,  $\tau_{sd}$  = factored nominal shear stress

$\tau_{rd}$  = shear resistance of concrete

$F_{sd}$  = factored concentrated force

$u_l$  = control perimeter length

$\xi$  = size factor =  $1 + \sqrt{\frac{200}{d}}$  ( $d$  in mm)  $\leq 2.0$

$\rho$  = flexural reinforcement ratio =  $\sqrt{\rho_x \rho_y}$

$f_{ck}$  = characteristic compressive strength of concrete

In each direction, the reinforcement ratio should be calculated within a width equal to the side dimension of the column plus  $3d$  to either side of column.

Maximum shear capacity:

$$V_{\max} = 0.3 \left( 1 - \frac{f_{ck}}{250} \right) f_{cd} u_o d$$

where  $u_o$  = perimeter of loading area

$f_{cd}$  = design compressive strength of concrete

## 2.4.5 The Eurocode 2

In the same fashion as the British Code, the Eurocode 2 (EC2 - 1991) also considers the position of a critical section at a distance  $1.5d$  away from the face of column or loaded area. The punching shear strength of slab without shear reinforcement is given as:

$$v_{R1} = \tau_R k (12 + 40\rho) / \gamma_m \quad (2.15)$$

$$\begin{aligned} \tau_R &= 0.25 f_{ctk} = 0.25(0.7 f_{ctm}) = (0.25)(0.7)(0.30 f_{ck}^{2/3}) \\ &= 0.0525 f_{ck}^{2/3} \quad [\text{MPa}] \end{aligned} \quad (2.16)$$

$$k = 1.6 - d \geq 1.0 \quad [d \text{ in meter, } \rho \leq 0.015] \quad (2.17)$$

where,  $f_{ctk}$  = characteristic tensile strength of concrete (5-percent fractile)

$f_{ctm}$  = mean tensile strength of concrete

$f_{ck}$  = characteristic compressive strength of concrete

$\gamma_m$  = partial safety factor for the concrete strength = 1.5

$\rho$  = effective reinforcement ratio =  $\sqrt{\rho_x \rho_y}$

## 2.5 Concrete members reinforced with FRP bars

### 2.5.1 Earlier research

In 1951, Rubinsky took an initiative to investigate the applicability of fibre-glass as the main reinforcement in concrete. From the initial tests, he concluded that it is not feasible to use fibre-glass as main reinforcement in concrete instead of the steel bars due to its low modulus of elasticity. The author conducted further experiments with glass-fibre, fibre-glass cords and finally with fibre-glass rods used as tendons for prestressed beam. He found that the fibre-glass rods were better against alkali attack of the cement.

Since the early tests by Rubinsky in 1951, no major experimental work was done on non-

prestressed concrete reinforced with fibre-glass. In the meantime, the quality of commercially available fibre-glass was improved. The levels of both the ultimate tensile strength of fibre glass rods and the Young's modulus were raised.

The first well developed FRP rod was used in non-prestressed concrete by U. S. Army Corps of Engineers at the U. S. army Engineer Waterways Experiment Station, Vicksburg, Mississippi [Wines *et al.* (1966)]. Some experimental and theoretical works were conducted on concrete beams. The researchers concluded that the bars suffer from the lower modulus of elasticity and lower bond capacity. The final comment was that the bars may be good for prestressed concrete but not for reinforced concrete.

Presently the FRP bars are more developed in terms of bond capacity, modulus of elasticity and strength. From the beginning until today, numerous research works have been conducted on various types of FRP products. But most of the work concentrated on one-way flexure, that means, either on beams or on one-way slabs. Based on those works, some design guidelines and codes are now available for designing concrete members. In the next section, some design guidelines and code recommendations for members in bending are described.

### **2.5.2 Design recommendations for members in bending**

ACI Committee 440 (2001) provides guidelines for the flexural design of concrete structures reinforced with FRP. The guidelines are based on experimental studies on

rectangular flexural sections with single layer of one type of FRP bars. For different geometric sections, or different kinds of FRP in the same flexural member or for multiple layers, the recommended guidelines should be applicable but may need to be confirmed by experimental results.

Unlike traditional steel reinforcement, FRP shows elastic behaviour up to rupture. The material properties of FRP are discussed in Section 2.2. As FRP doesn't show yielding, i.e. ductile behaviour, failure of any flexural member by FRP rupture is a catastrophic one. On the other hand, concrete crushing failure mode could be marginally more desirable for flexural members reinforced with FRP bars. Members may exhibit some plastic behaviour before failure in case of concrete crushing failure.

Nevertheless, both types of failure modes (FRP rupture or concrete crushing) are accepted in the governing criteria used for the design of flexural members reinforced with FRP bars. To compensate for the lack of ductility, the flexural members should satisfy strength and serviceability criteria. In addition, the margin of safety should be higher than that used in the design of concrete members reinforced with traditional steel reinforcement.

According to ACI 440, the computation of the strength of a cross sections should be performed based on of the following assumptions:

- Strains in the concrete and the FRP reinforcement are proportional to the distance from the neutral axis.

- The maximum usable compressive strain in the concrete is assumed to be 0.003.
- The tensile strength of concrete is ignored.
- The tensile behaviour of the FRP reinforcement is linearly elastic until failure.
- Perfect bond exists between concrete and FRP reinforcement.

The strength design philosophy states that the design flexural capacity of a member must exceed the flexural demand. To ensure this, new strength reduction factor has been recommended for FRP reinforced flexural members. Equation 2.18 gives a factor of 0.70 for sections controlled by concrete crushing, 0.50 for sections controlled by FRP rupture, and provides a linear transition between the two cases. In Eq. 2.18,  $\rho_f$  is the reinforcement ratio of FRP bars in flexure and  $\rho_{fb}$  is the balanced reinforcement ratio.

$$\phi = \begin{cases} 0.50 & \text{for } \rho_f \leq \rho_{fb} \\ \frac{\rho_f}{2\rho_{fb}} & \text{for } \rho_{fb} < \rho_f < 1.4\rho_{fb} \\ 0.70 & \text{for } \rho_f \geq 1.4\rho_{fb} \end{cases} \quad (2.18)$$

If the concrete strength is higher than the specified strength, FRP can rupture instead of concrete crushing. For this reason, and to establish a transition between the two values of  $\phi$ , a section controlled by concrete crushing is defined as a section in which  $\rho_f \geq 1.4\rho_{fb}$  and a section controlled by FRP rupture is defined as one in which  $\rho_f < \rho_{fb}$ .

In Canada, CSA S806-02 (2002) is the standard for design and construction of building components with FRP. According to this CSA code, the minimum flexural reinforcement

shall be proportioned so that  $M_r > 1.5M_{cr}$ , where the cracking moment,  $M_{cr}$ , is calculated using the modulus of rupture,  $f_r$ . For slabs, the minimum area of reinforcement should be  $400E_f/A_g$  ( $\text{mm}^2$ ) in each of the two direction. This reinforcement shall be greater than  $0.0025A_g$  and shall be spaced no farther apart than four times the slab thickness or 400 mm, whichever is less. The material strength reduction factor  $\phi_c$  is 0.60 for cast in situ concrete and 0.65 for precast concrete. Material strength reduction factor for FRP is 0.7 for AFRP and 0.85 for CFRP (for prestressed reinforcement).

## **2.6 Previous work on two-way slabs reinforced with FRP bars**

Nawy and Neuwerth (1976) conducted an experimental program on beam and two-way slab specimens with fibre-glass reinforcing rods. The FRP rods used in the study were made of fibre-glass filament tendons impregnated with resin. The resin content was approximately 40%, producing rods of 1/4" nominal diameter. The beam specimens were tested in bending, i.e. as a flexural member. However, the slab specimens were the focus of the study. In particular, the flexural behaviours of two-way slabs were investigated. The two-way slabs were tested under uniform applied load. The study did not cover any concentrated load to investigate the punching resistance and behaviour of the slabs. This study is the first work on two way slabs with FRP bars available in the literature. The experimental results covered the flexural cracking characteristics of the test specimens, their deformation and their load capacity up to failure. They tested 12 slabs. The slabs had different reinforcement ratio. The author reported that the first 6 slabs with lower reinforcement ratio (0.210% to 0.384%) showed major yield line diagonal cracks. The

remaining 6 slabs with higher reinforcement ratio (0.463% to 0.769%) had orthogonal cracks dominating up to 30% to 60% of the ultimate load. The yield line diagonal cracks started to be fully developed beyond that stage.

In conclusion, the authors stated that this type of fibre-glass rods could be a potential reinforcing material for concrete. The results revealed that the ultimate strength of the fibre-glass rods could not be fully developed when used as reinforcement for concrete. This could be attributed to the low modulus of elasticity of the bars. Due to the service load limitations of the code, the rod remained at a much lower stress level than its ultimate stress. As a result, a slab can absorb any unusual excessive loads by increasing the deflection and crack width and the reinforcement would remain in an elastic state. The slab can return to its previous position after the removal of excessive load. Finally, the authors recommended two separate models to calculate the slab deflection and crack width.

Punching shear tests on slabs reinforced with non-metallic reinforcement was carried out by Ahmad *et al.* (1994). In the study, a 3-D Carbon Fibre Fabric was used as reinforcing material for the concrete slabs. This was considered to be a pilot study in this field. The experiment included six square slabs reinforced with 3-D continuous carbon fabric and two reference slabs reinforced with traditional steel reinforcement. The crack pattern, load-deflection response and ultimate load capacity were investigated. The slabs reinforced with 3-D carbon fibre showed significant non-linear behaviour before the maximum load and a deflection softening behaviour after the maximum load. This

softening was considered to be a relative measure of ductility and redistribution of stress after the maximum load. The ultimate load capacity was compared with the punching capacity predicted by ACI 318-89 and BS 8110-85 code equations. It was found that the ACI code prediction was conservative in all cases. The BS 8110 overestimated the punching capacity.

Banthia *et al.* (1995) carried out an experimental investigation on the punching shear of concrete slabs reinforced with FRP grid (NEFMAC) as flexure reinforcement. The authors tested 3 slabs with FRP reinforcement and one reference slab with traditional steel reinforcement. Among the three FRP slabs, one was made with normal strength concrete, the second with high strength concrete, and the third slab was made with fibre-reinforced normal strength concrete. Hooked-end fibres 28 mm long and 0.5 mm in diameter were used. All slabs were tested for punching by applying a concentrated load at the center. The reinforcement failed in all slabs. The steel-reinforced slab failed in a ductile mode with a cup and cone mechanism. The failure in FRP was brittle and was precipitated mainly by fibre fracture. The use of high strength concrete increased the initial stiffness somewhat and exhibited a nominal increase in total energy-absorption capacity. The use of fibre reinforcement in the concrete led to an improvement in the ultimate load-carrying capacity as well as in the overall energy-absorption capacity. The strain gauges at all locations indicated unloading prior to attaining the peak load, except in the fibre-reinforced slab. The authors compared the results with the predicted values of different code equations. It was concluded that significant changes to the code equations

may not be necessary when computing the punching shear capacity of slabs reinforced with FRP grids. It was also concluded that slabs reinforced with FRP grid absorb less energy than those reinforced with steel reinforcement. The fibre-reinforced concrete slab showed improved ultimate load carrying capacity and energy absorption.

Matthys and Taerwe (2000) carried out an extensive test program to investigate the punching shear of concrete slabs reinforced with FRP reinforcement. The investigation focused on slabs reinforced with NEFMAC grids of type C and type H. The test program included 11 slabs reinforced with FRP grids and 2 slabs reinforced with CFRP bars. The reinforcement ratio and type, slab depth, loading area, compressive strength of concrete were the main variables. One slab was made with high strength concrete. The failure mode, punching cone shape, deflection and ultimate load capacity were examined. The slabs ultimate capacities were compared with the predictions of various codes as well as the empirical expression proposed by authors which is similar to the expression given by Gardner (1990). The results were also compared to the predictions of a mechanical model for punching proposed by Hallgren (1996) and an analytical model based on numerical simulation proposed by Menétrey (1996). Most of the slabs showed a punching cone failure. The punching strength and stiffness at cracked state were less than those of steel reinforced slabs of the same flexural strength. It was also found that the design punching capacity can be safely calculated using a material capacity reduction factor and reinforcement ratio modification factor ( $E_{FRP}/E_s$ ), where  $E_{FRP}$  is the modulus of elasticity

of FRP and  $E_s$  is the modulus of elasticity of steel. The predicted design values showed sufficient safety (mean global safety factor of about 1.9-2.6).

To determine the failure criterion, the flexural strength and pure punching capacity of the slabs were calculated. As FRP reinforcement does not yield, traditional yield line analysis cannot be used to calculate the flexural capacity of an FRP-reinforced slab. Elastic analysis formulas for plates, as given in Bareš (1997), were used. FRP behaves as an elastic material up to failure but concrete does not. Slabs with FRP are a composite material and, consequently, will not behave in an elastic fashion up to failure. So this approach of calculating flexural capacity of FRP slab is an approximate one. Nevertheless, this approach can be used to give an idea about the failure mode of an FRP slab. The authors reported the ultimate test loads,  $Q_u$ , the predicted flexural capacity,  $Q_f$ , and the predicted punching capacity,  $Q_p$ . The published results indicated that a number of slabs failed well below their calculated flexural and punching capacity. This means that either method of calculating the flexural and punching capacity may not be acceptable or that the slabs may have failed for other reasons. Some slip of the flexural reinforcement was observed which depended on the bond behaviour. Some wide cracks running parallel to the reinforcement were observed. It is unclear whether this could be the reason for the lower failure loads of some slabs. However, the authors classified the failure mode as flexural or punching mode. The ratios  $Q_u/Q_f$  and  $Q_u/Q_p$ , reported in the paper, do not support the authors comment on the failure mode of some slabs. Most probably, the failure mode was classified on the basis of crack propagation pattern, inside the slab, at

the vicinity of column. This was done by inspecting the slabs that were diametrically cut through the point of loading to investigate the failure crack pattern. It seems that a more general criterion is needed to classify the different failure modes. Finally, in modifying the mechanical model proposed by Hallgren (1996), the dowel action of FRP reinforcement was completely ignored and no proper justification was provided. In addition, the punching angle was assumed constant in contrast with a variable angle assumption that was used in constructing the original model.

El-Ghandour *et al.* (2003) tested a total of eight slabs in two phases. In the first two slabs (one with CFRP and the other with GFRP reinforcement), combined shear and bond slip were found. The cracks developed directly above the flexural reinforcement as there exists a weak plane at that location. The authors assumed that it would be possible to resist this kind of bond slip failure by providing suitable FRP shear reinforcement.

Consequently, the authors used special FRP Shearband as shear reinforcement in two slabs. These slabs were identical to the previous two slabs except for the shear reinforcement. However, the reinforcement's performance was not as expected. Again, the slabs experienced bond slip of the flexural reinforcements. Both slabs failed below the expected failure loads. To prevent this bond slip, authors made two alternative decisions. The first alternative was to prevent the bond slip by reshaping the shearbands. This was achieved by minimizing the distance between the vertical legs to which flexural bars will be anchored. The other alternative was to reduce the spacing and the area of the flexural bars (to maintain the same reinforcement ratio). In the second phase, the authors

tested four slabs with closely spaced reinforcement. One of these slabs had shear reinforcement. The spacing was half of that of the previous slabs and the reinforcement ratio was 2.26 times that of the previous slab. For these slabs, punching shear failure was obtained with no sign of bond slip of the flexural bars. Finally, the authors proposed two models to predict the punching shear capacity of FRP-reinforced slabs without shear reinforcement. The models were based on the modification of an existing model.

The concrete clear cover was 25 mm which was almost 2.5 times the FRP bar diameter. However, cracks were formed directly over the bars. This could be attributed to the deformed pattern of FRP bars. Such bars may have low bond capacity. Stress concentration could have developed at certain points along the bars, which may be enough to split the concrete clear cover.

The authors claimed that the shearband provided anchorage to the flexural bars after reducing the distance between the verticals legs. Perhaps the flexural reinforcement ratio increased a little bit after providing the shear reinforcement. That's why some improved load carrying capacity was obtained. However, the slab SCS1 does not support this logic.

To avoid bond slip, reduction in spacing may not be a proper decision. In an actual slab system, the bars can be extended to provide enough development length and thus increase the anchorage capacity. To prepare the test specimen, perhaps it was better to provide mechanical anchorage to overcome the slippage problem.

As FRP is corrosion free, the clear cover in FRP slabs could be lowered. It is one of the major advantages of FRP slabs. It was found that splitting of the concrete occurred just above the flexural bars. Shear reinforcement was provided to prevent this kind of splitting. This solution may be costly. From an economic viewpoint, it is better to increase clear the cover. So research on the effect of clear cover in FRP slabs could be needed.

Therefore, providing mechanical anchorage at the end of bars could have been a better solution against bond slipping and increasing the clear cover could be an economical solution for concrete splitting.

The authors applied the strain approach, proposed by Clarke (1996), to calculate the capacity of the slabs. In the strain approach, which was combined with the BS 8110 code equation; it is assumed that the strain, and thus the force, in the FRP flexural reinforcement is roughly the same as an equivalent conventional reinforced slab. This approach always gives a lower bound solution. This could be attributed to the strain in FRP bars, which is at the time of punching shear greater than the yield strain in the equivalent steel slab.

The authors realized the above incompatibility between the actual FRP slab and the equivalent slab. Consequently, the authors proposed another approach that they designated as the 'Stress Approach'.

In the stress approach, the strain is not considered. The basic idea was that the force in the flexural reinforcement must be equal in both slabs (actual FRP slab and equivalent steel slab) regardless of the strain condition. This means that, the force in the bars of the equivalent slab is equal to yield force in magnitude. However, for FRP bars it is neither yield force (FRP has no yield) nor ultimate force. Thus, the stress in the FRP bars, at the time of punching failure, is needed to calculate this force.

The authors described a procedure to calculate the stress in the FRP flexural reinforcement at the time of punching failure. In this procedure, a correlation between applied load and applied moment at critical section needs to be established. For the author's test specimens, it was possible to establish this kind of relationship due to the support conditions of the test specimens. In general, it is not always possible to establish such a relationship as FRP slabs do not follow yield line theory.

The stress in the FRP, at the time of punching failure, is calculated using a punching shear envelope and the variation of the stress in the flexural reinforcement with the applied load. The calculated failure stress is higher than actual failure stress. This means that failure occurs at the lower stress level due to the lower stiffness of FRP bars. That's why the stress approach always gives an upper bound result.

The strain in FRP bars is obviously higher than yield strain of steel at the time of punching failure. From the observation of test results, the authors settled that the failure strain was 0.0045 in FRP bars at the time of punching shear failure. As a result, the authors proposed another approach named the 'Modified Approach'. It is a modification

of the strain approach. The basis of this approach is that the force in the FRP bars at 0.0045 strain will be equal to the force in an equivalent slab reinforcement at 0.0025 strain (yield strain). But question is why select a strain equal to 0.0045? The assumption of 0.0045 strain appear to be dubious at best.

Ospina *et al.* (2003) carried out an experimental program to investigate the punching shear behaviour of two-way concrete slabs reinforced with GFRP. Four isolated full-scale slab-column connections were tested. Two slabs were reinforced with deformed GFRP bars (C-bars), one with GFRP 2-D grid (NEFMAC) and one with traditional steel. Mechanical end anchorage was provided to prevent any premature bar slippage. All test slabs failed in punching. It was observed that the crack patterns closely matched the layout of the reinforcing bars in the tension side. The authors found that the tension-stiffening effect plays a larger role in the behaviour of GFRP reinforced slabs than in slabs with traditional steel bars. It was also concluded that the factors associated with flexure-bond affected the punching strength of the slab column connections. The authors concluded that the equation proposed by Matthys and Taerwe (2000) provided the best estimation for the punching capacity of two-way slabs.

The cracks were developed along the reinforcement of the slabs. However, the authors claimed that all slab-column joint ultimately failed by punching. This punching failure may be a secondary failure. The authors also mentioned that the tension stiffening effects in FRP reinforced slab. This is an important issue that is hard to identify for two way

slab. Further research on this subject is needed. The explanation given by authors about tension stiffening effect on their test slabs need to be further substantiated.

In conclusion, very few experimental works have been done on this topic. Very few test data are available in the literature on the punching strength of two-way slabs reinforced with FRP bars. Further studies are needed to fully understand the behaviour of such structural element to be able to provide design recommendations that are safe and economical.

## **2.7 Rational studies**

### **2.7.1 Models based on Kinnunen and Nylander model**

#### **2.7.1.1 Original model by Kinnunen and Nylander**

Kinnunen and Nylander (1960) proposed a rational mechanical model to predict the punching capacity of two-way slabs. The authors carried out an experimental investigation and theoretical study. Based on observations of a number of tests on circular slabs with central column, an idealized model was proposed for punching strength of two-way slabs. The model was based on the assumption that the slab portion outside the shear crack bounded by radial cracks, shear crack and circumference of the slab act as a rigid body and turn, under the action of the load, around a center of rotation located at the root of the shear crack. The model is illustrated in Fig. 2.7.

The punching failure criterion in the model was the collapse of the conical shell. The collapse occurred when the tangential strain on the surface of the slab, in the vicinity of the root of the shear crack, reached a characteristic failure strain. A set of empirical equations were proposed to calculate this characteristic failure strain. The punching load was calculated by assuming a dimension of the conical shell and then following a convergent iterative process to maintain force equilibrium. The values of the various parameters were determined on the basis of the test results obtained from slabs with ring reinforcement only. The authors found that the model predicted low values in the case of slabs with two way reinforcement. They suggested that the calculated value be multiplied by 1.1 to account for the effect of dowel forces and membrane forces.

#### **2.7.1.2 Shehata**

Shehata (1985) and Shehata and Regan (1989), presented a model which they claimed to be an improvement over that of Kinnunen and Nylander. In this model, the dowel forces and membrane action forces were directly calculated from the model and the original failure criteria were modified. It was assumed that the inclined shear crack had an angle of  $20^\circ$  for two-way reinforced slabs and  $30^\circ$  for ring reinforced slabs. As in the original model by Kinnunen and Nylander, the authors considered the rigid radial segments that rotate about the center of rotation. However, the center of rotation was assumed at the face of the column, at the same level of the neutral axis. In addition, a rigid wedge element bounded by the inclined crack and initial circumferential tangential crack was assumed as detached from each radial segment. The wedge rotated around the center of

rotation under the action of its own steel forces. A schematic of the model is shown in Fig. 2.8. The dowel force was calculated from the equilibrium of the wedge element considering that the wedge rotation, at failure, was equal to that of the radial segment. Finally, the unknown quantities such as the punching load, depth of neutral axis and slab rotation were calculated by iteration considering the equilibrium of forces in horizontal direction, vertical direction and equilibrium of moment. Three types of failure criteria were set. For lightly reinforced slabs, small steel forces result in a steeper angle of the inclined compression at the column face. The second kind of failure occurred in heavily reinforced slabs, where high radial strains resulted due to a higher level of the neutral axis. In slabs with moderate steel ratio, the failure is of the third type, with the tangential strains reaching the crushing value just before radial failure.

### **2.7.1.3 Marzouk and Hussein**

Marzouk and Hussein (1990) adopted a mechanical model for high strength concrete slabs which was a modification of the original Kinnunen and Nylander model including the idealization proposed by Shehata. From the experimental program, the authors found that the angle of the failure surface for high strength concrete slabs varied between  $32^\circ$  and  $38^\circ$ . The same angle ranged between  $26^\circ$  and  $30^\circ$  for normal strength concrete. Two failure criteria were set. If the yielding of tensile reinforcement spread in the whole slab, then the slab is assumed to have failed in flexure. The other criterion is reaching of the tangential concrete strain, at the column periphery, to a characteristic value of 0.0035.

The authors obtained good agreement between the test results and the results predicted by the model.

#### **2.7.1.4 Hallgren**

Hallgren (1996) proposed another mechanical model which is also a modification of the original Kinnunen and Nylander model. The modifications were based on the test results and some nonlinear finite element analysis done by the author. The main modification was focused on the failure criterion. To calculate the ultimate tangential concrete strain, a set of semi-empirical equations were recommended for the original Kinnunen and Nylander model.

The values were based on the strain measured in the tests. In the model, an attempt was made to derive the ultimate tangential concrete strain from a simple fracture mechanics model, which reflected both the brittleness of the concrete and the size effect. The depth of the compression zone in the tangential direction was calculated directly from the compatibility of strain and stress distribution across the section. The slope of the shear crack was not constant in this model; it varied with the geometry and the material properties of the slab. The model does not include slabs with shear reinforcement and unsymmetrical loading. The model is also limited to the analysis of slabs with shear-span to effective depth ratio equal to or greater than 3.5. If the shear span is shorter, the failure type is probably more similar to the shear failure of beam. The geometry of the model is shown in Fig. 2.9.



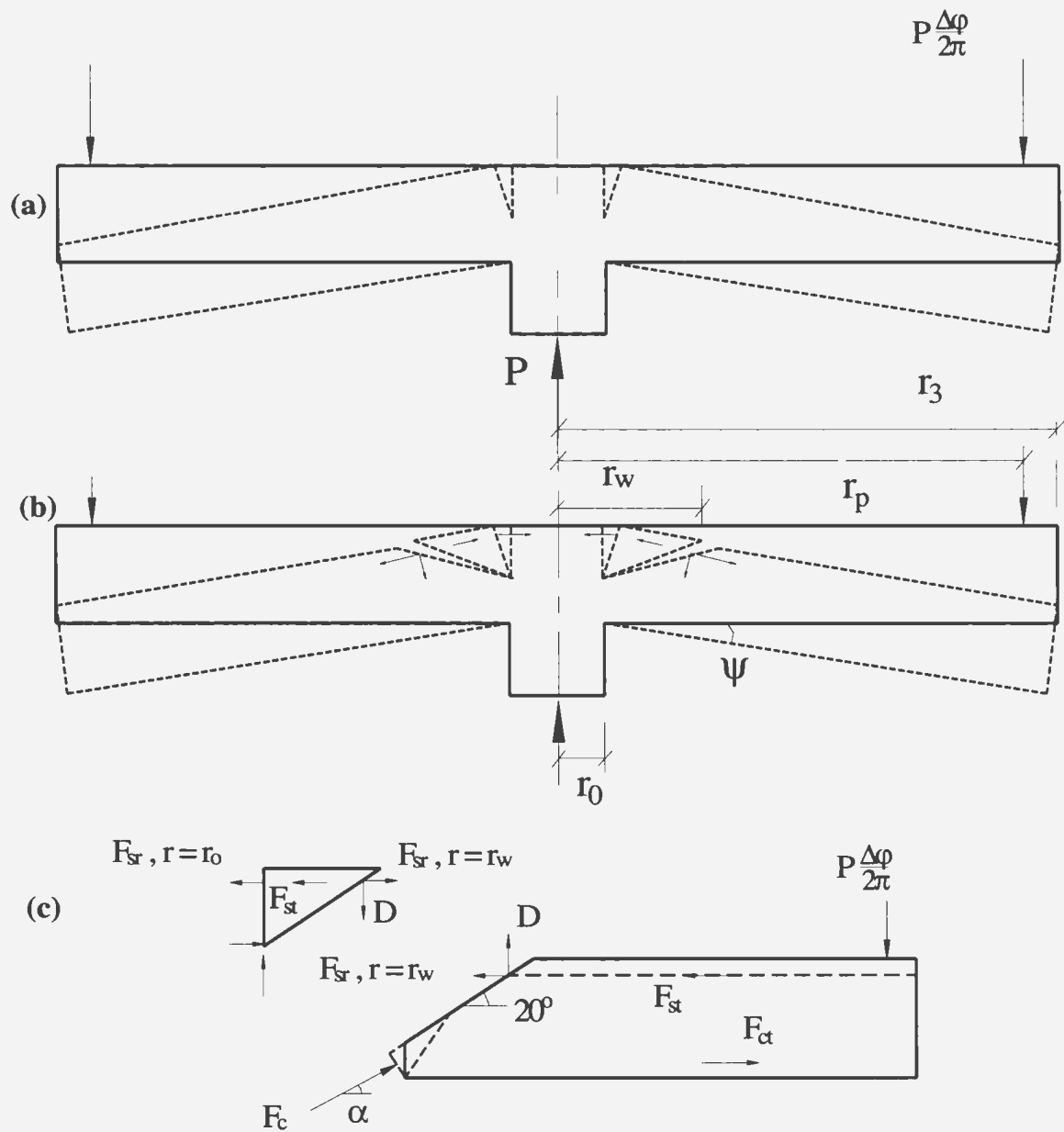


Fig. 2.8: Shehata's model (1985)

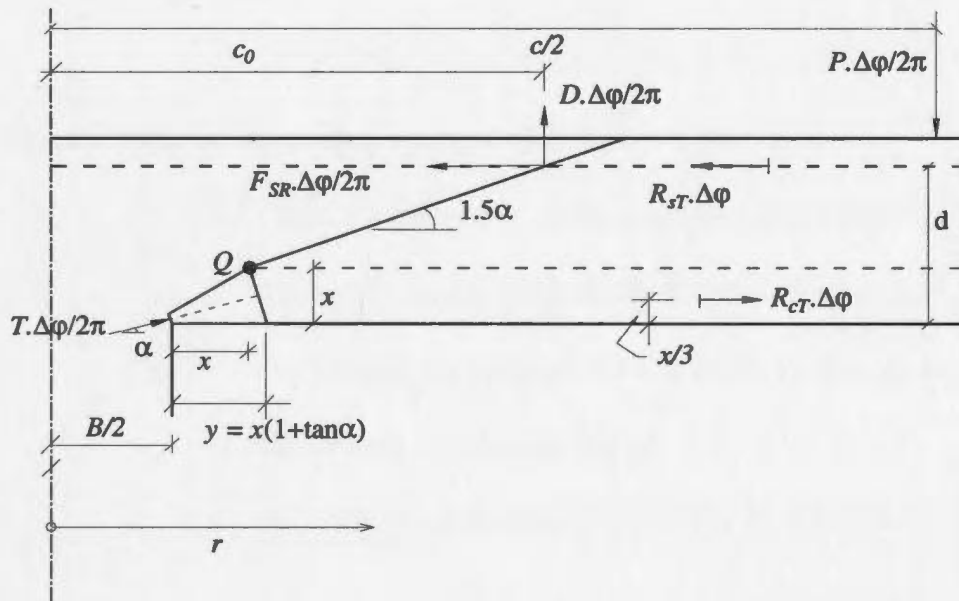
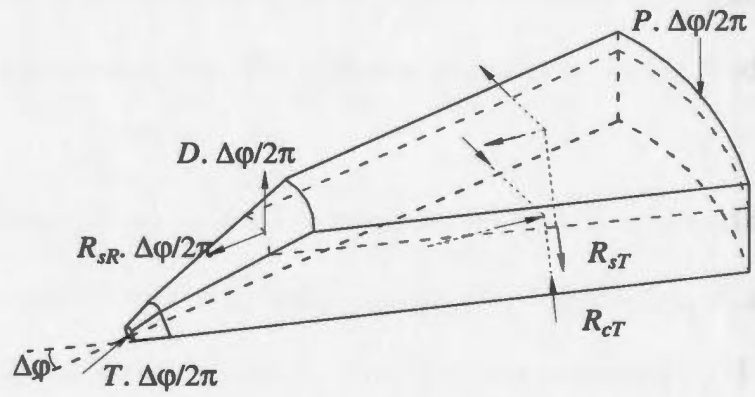
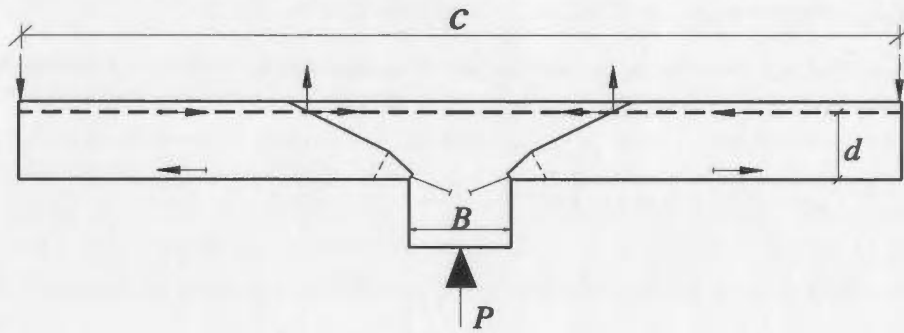


Fig. 2.9: Hallgren's model (1996)

## 2.7.2 Analytical model by Menétrey

Menétrey (1996) proposed an analytical expression to calculate the punching shear strength of a slab column connection. The analytical expression was derived from the results obtained from numerical simulation of the failure phenomenon. The basic idea of this model is that the punching failure corresponds to the failure of the concrete tie, i.e. the tie strength is equivalent to the punching strength. Therefore, the punching strength of a reinforced concrete slab is based on the integration of the tensile resistance of concrete and the reinforcement along the punching crack. The different components of the model are shown in Fig. 2.10.

The model is generalized by taking into account the reinforcement. This is achieved by simply adding to the integration of the concrete tensile stress, the contribution of all reinforcement which are crossing the punching crack. The resulting punching load is expressed as:

$$P_{pun} = P_{ct} + P_{dow} + P_{sw} + P_p \quad (2.19)$$

where,  $P_{pun}$  = punching strength of slab

$P_{ct}$  = vertical component of the concrete tensile force

$P_{dow}$  = the dowel contribution of the flexural reinforcement

$P_{sw}$  = the vertical component of the force in the studs, stirrups or bent up bars which are well-anchored

$P_p$  = the vertical component of the force in the tendons

The formulas required to calculate the above force components were presented by the author. The dowel contribution  $P_{dow}$  to the punching strength is calculated iteratively because the punching load is required to compute the tensile stress in the reinforcing bar which is necessary to calculate the dowel force component.

The author proposed that this analytical method could be adopted for design purposes also. The safety factor can be included by reducing the values of the tensile strength of concrete, the tensile strength of shear reinforcement and the stresses in the prestressing steel. Dowel forces can be neglected to make the model easier to use, as the determination of the dowel contribution is iterative and time demanding. This proposed model is one of the few models which treats different types of reinforcement (flexural, shear and prestressed reinforcement) so that its range of application covers a broad range of slabs.

The author claimed that the model results were in agreement with the test results of slabs with a wide range of variables. However, it was found that the model was very sensitive to  $d_a$  and  $d_s$ , where  $d_a$  is the maximum diameter of the coarse aggregate and  $d_s$  is the diameter of flexural reinforcement.

The author finally suggested that the analytical expression be extended for slabs with different conditions. This is achieved by taking into account the existence of holes by reducing the surface where the tensile stresses are activated, and conversely to account for stiffening by increasing such surface.

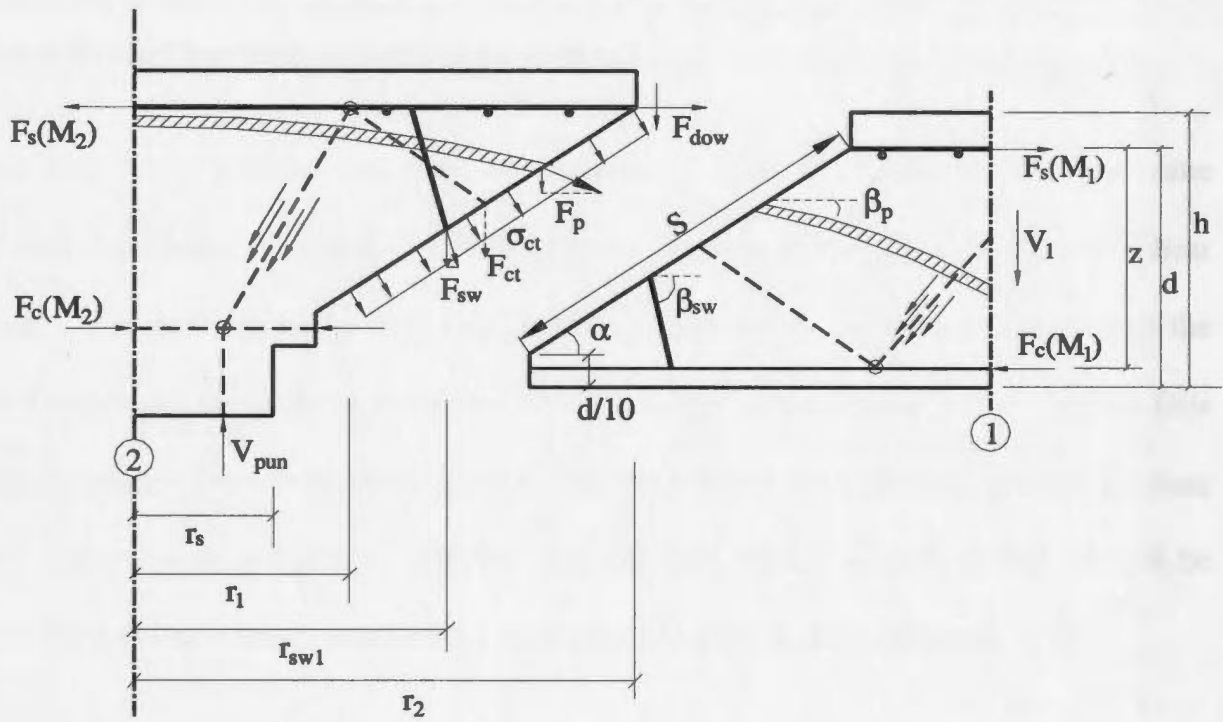


**Fig. 2.10: Model proposed by Menétrey (1996)**

### 2.7.3 The Truss model

Alexander and Simmonds (1987) proposed the Truss Model. In this model, a three dimensional space truss, composed of concrete compression struts and steel tension ties, was suggested. The reinforcing steel and concrete compression fields were broken down into individual bar-strut units as shown in Fig. 2.11.

The truss model included two types of compression struts: (1) those parallel to the plane of slab (anchoring ties) and, (2) those at some angle  $\alpha$  to the plane of the slab (shear struts). The model predicts only two possible failure modes for a shear strut; either the steel yields and the angle of shear strut  $\alpha$  reaches some critical value, or the concrete fails in compression prior to yielding of steel. This implies that the traditional concept of shear and flexure does not apply, and the two possible modes of slab failure should be classified as local connection failures as opposed to overall slab collapse.

The angle  $\alpha$  was calibrated using the test results available in literature for slabs on interior column. The value of  $\tan(\alpha)$  was calculated as the ratio of the failure load to the total area of top mat shear steel times its yield strength. Then, the value of  $\tan(\alpha)$  was plotted against a non-dimensional factor  $K$ . The following relationship was derived:

$$\tan \alpha = 1 - e^{-2.25k} \quad (\text{SI}) \quad (2.20)$$

and,

$$K = \frac{S_{eff} \cdot d' \cdot \sqrt{f_c'}}{A_{bar} \cdot f_y \cdot (c/d_s)^{0.25}} \quad (2.21)$$

where,  $S_{eff}$  = effective tributary width of the reinforcing bar (max.  $6d'$ )

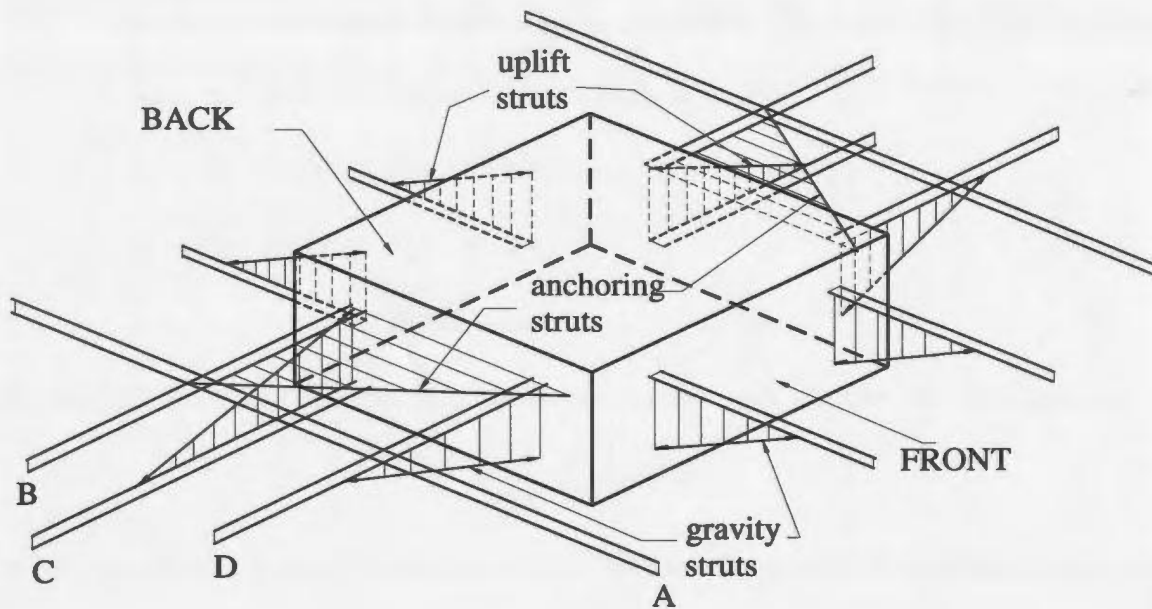


**Fig. 2.11: Truss model by Alexander and Simmonds (1987)**

- $d'$  = cover of the reinforcing mat measured from center of mat to the nearest surface of slab
- $d_s$  = effective depth of reinforcing mat measured from center of mat to compression surface of slab
- $c$  = dimension of column face perpendicular to the rebar being considered
- $A_{bar}$  = area of reinforcing bar being consider
- $f'_c$  = compressive cylinder strength of concrete
- $f_y$  = yield strength of steel
- $e$  = base of natural logarithm

In case of concentrically loaded column, the failure load,  $P_u$ , can be calculated as:

$$P_u = \sum A_{bar} f_y \tan \alpha \quad (2.22)$$

where  $A_{bar}$  is the area of flexural steel that is close enough to the column to participate in resisting shear.

It was also assumed that the concrete compression struts do not fail and therefore, their capacity need not be considered. In conclusion, Alexander and Simmonds stated that the evaluation of the angle  $\alpha$  needed further investigation, as it was based on an empirical equation.

#### **2.7.4 Bond model by Alexander and Simmonds**

The bond model proposed by Alexander and Simmonds (1992) is the result of a modification to the truss model proposed earlier by the authors. In the same fashion as the

truss model, a slab-column connection is described as an assembly of steel tension ties and concrete compression struts.

In the truss model, the compression strut was straight and inclined with a constant angle  $\alpha$ . In the bond model, the compression strut was assumed as a curved arch which was derived from strain measurements in punching tests. The model is shown in Fig. 2.12(a). The curved arches are located along the four radial strips extending from the column parallel to the reinforcement [Fig. 2.12(b)]. The curved arch has a steep slope at the face of column and moderate slope, close to zero, at the intersection of the curve and the reinforcement. The geometry of the curved arch is governed by the interaction between the arch and the adjacent quadrants of the two-way plate. The radial strips are taken in such a way that the column is separated from the slab by the radial strips and all loads reaching to the column must be carried by the radial strips. Within each strip, the shear is carried in the radial direction by the vertical component of the curved compression strut and the horizontal component of the strut is taken as constant. Therefore, the shear carried by the strut varies from a maximum at the face of the column, where the slope of the strut is larger, to a minimum, or perhaps zero, at the intersection of the strut and the reinforcing steel.

Each strip is loaded on its side-faces by the maximum one-way shear that can be carried by the adjacent gradients of the plate. The plate must maintain moment gradients perpendicular to the radial strips to deliver an internal shear to the radial strips. To maintain moment gradient, force gradient is required in the reinforcement.

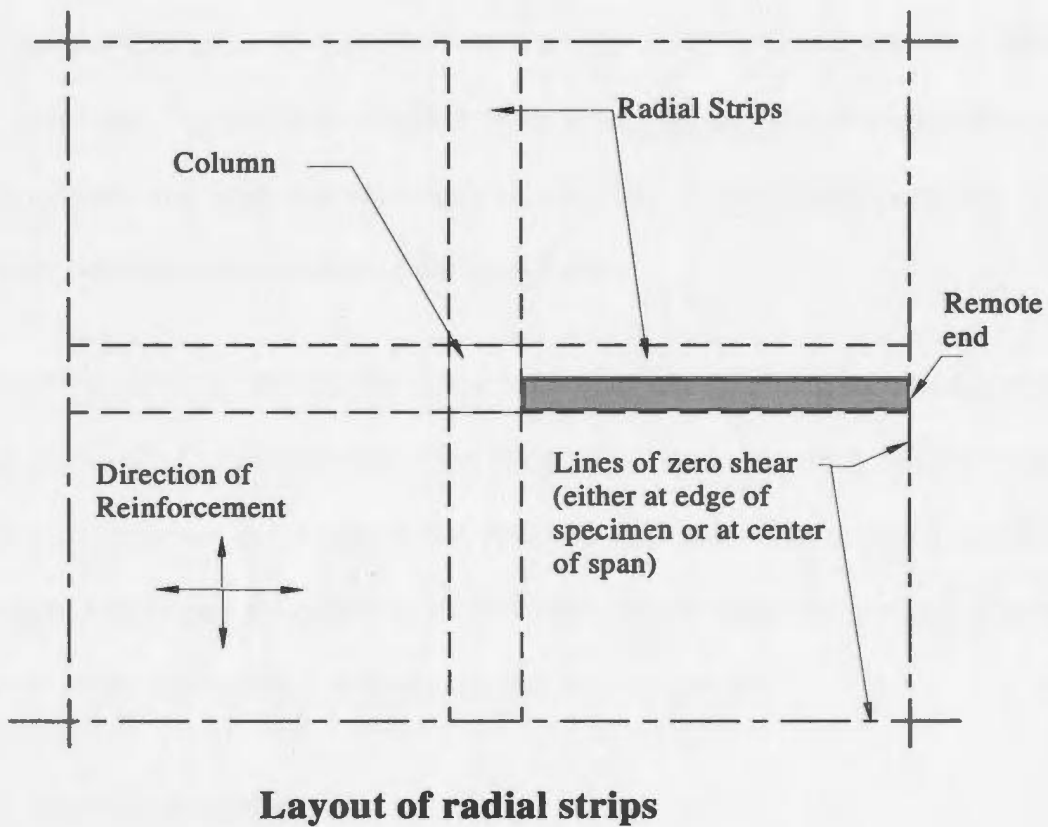
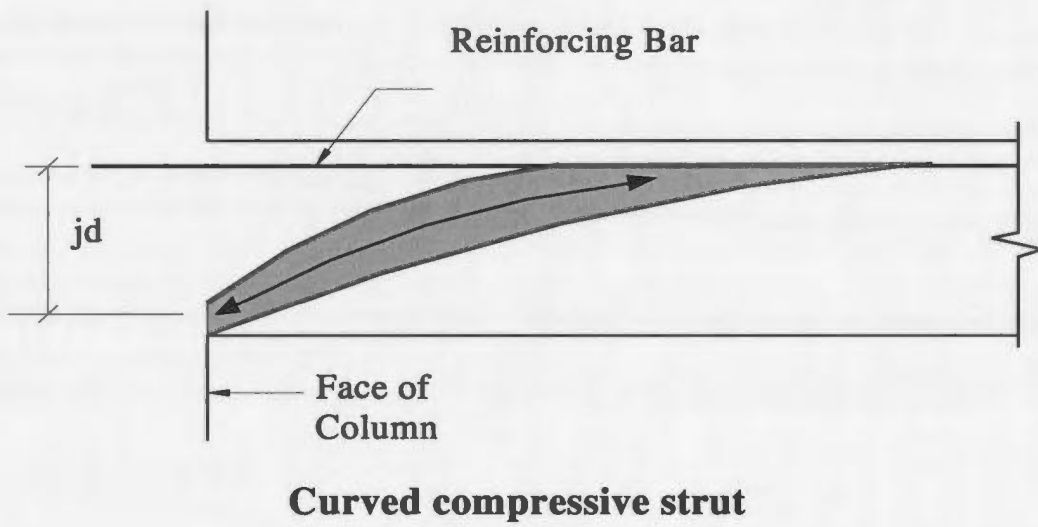


**Fig. 2.12: Bond model by Alexander and Simmonds (1992)**

Bond failure of the bars or the spreading of yielding along the length of bars poses a limitation on the force gradient in the reinforcing bars. Whatever the reason, the loss of reinforcing bar gradient in the quadrants of the plate reduce the ability of the slab to carry shear in the vicinity of the column. Therefore, all punching failure may be attributed to the loss of moment gradient regardless, whether or not; they are preceded by extensive yielding of the slab reinforcement. In the same way, they also lose the shear capacity in the vicinity of column.

Based on this theory, the authors derived the maximum loading of the radial strips and thus the punching capacity from the bond strength of the reinforcement perpendicular to the radial strips. Various code predictions for a limiting nominal one-way shear stress that can be transferred from the quadrants of the plate to the radial strips can be used to calculate the maximum loading of the radial strips.

In summary, model combines the radial arching action with the concept of a critical shear stress on a critical section (beam action shear). For brittle punching failure, bond strength of the reinforcement is the significant factor to limit the beam action shear. Finally, the authors conclude that the bond model provides a lower bound estimation of the punching capacity of the slab-column connections and it is consistent.

### **2.7.5 Gardner (1990)**

Gardner (1990) proposed an empirical equation based on his test results on normal strength concrete slabs as well as test results available in literature. The main objective of

his study was to find out the relation between the concrete strength and the punching shear strength of an interior slab. The author found out that the punching strength of slab is proportional to the cubic root of the concrete strength. This cubic root relation was also proposed by Marzouk and Hussein (1990) based on their experimental results on high strength concrete slabs. The code equations of the ACI 318-83 and CSA A23.3 84M standards use a square root relationship of the concrete strength. Gardner proposed the following equation, which is in the exact form as the BS 8110-85 code equation:

$$v_c = 0.99 \left[ \rho \cdot f_c' \right]^{1/3} \cdot \left[ (400/d)^{1/4} \right] \quad (\text{S.I. units}) \quad (2.23)$$

The shear perimeter is rectangular and is located at a distance 1.5 times the effective slab depth outside the column regardless of whether the loaded area is rectangular or circular in section. Again, this is identical to the critical section by BS 8110-85 critical perimeter.

Equation (2.23) is conservative. The average ratio of test result to calculated result is 1.42. Nevertheless, the equation satisfies the 5% percentile recommended by Eurocode 1. Matthys and Taerwe (2000) proposed a modification to this equation as follows:

$$P_u = 1.36 \frac{(100 \rho f_{cm})^{1/3}}{d^{1/4}} u_{1.5d} d \quad (2.24)$$

### 2.7.6 Strain Approach and Modified Approach

Clarke (1996) recommended the Strain Approach. According to this approach, an equivalent area of reinforcement is used in conjunction with the BS 8110-85 punching

shear equation. The equivalent reinforcement area is the actual area multiplied by the modular ratio of FRP and steel:

$$A_s = A_{FRP} (E_{FRP}/E_{steel}) \quad (2.25)$$

Where,  $A_s$  = equivalent steel area  
 $A_{FRP}$  = actual FRP area in the slab

El-Ghandor *et al.* (2003) proposed the Stress Approach. According to this approach, the strain of the flexural bars has no effect on the punching shear capacity of the slab. The modified value of the equivalent area of steel can be obtained by finding the point of intersection of the punching shear capacity curve with the flexural capacity curve. The equivalent area is calculated as follows:

$$A_s = A_{FRP} (\sigma_{FRP}/\sigma_{steel}) \quad (2.26)$$

where,  $\sigma_{steel}$  = equivalent steel stress  
 $\sigma_{FRP}$  = actual FRP stress

This Stress Approach gives an upper bound solution. The authors provided an alternative method to improve the accuracy of prediction; they proposed the Modified Approach. It is a modification of the Strain Approach where a factor  $\phi = 1.8$  was used which is nothing but a strain correction factor. Hence, the area of steel is modified by:

$$A_s = A_{FRP} (E_{FRP} / E_{steel}) (\phi) \quad (2.27)$$

The philosophy behind the Strain Approach, Stress Approach and Modified Approach and their limitations are described in details in Section 2.6.

### **2.7.7 Elastic analysis**

An FRP bar behaves elastically up to rupture. Concrete could be considered elastic at lower strain levels but after a certain strain it is not elastic. The elastic analysis method could be used to estimate the flexural capacity of slabs reinforced by FRP bars. However, this method would be an approximate one. There is no acceptable method to calculate the flexural capacity of slab with FRP, as this kind of reinforcement has no yielding property. Accordingly, the classical yield line analysis that is used for slabs with traditional mild steel reinforcement would not be applicable.

The elastic plate analysis is based on some idealized assumptions and has some limitations. The assumptions concerning the material and the shape of the plate are: 1) the material of the plate is completely elastic, 2) the material confirms the Hook's law and has the same elastic constants (modulus of elasticity, Poisson's ratio) for all loading levels, 3) the material of the plate is homogeneous and isotropic, 4) the thickness of the plate is constant, and 5) the thickness is small in comparison with the other dimensions of the plate. In reality, no material is completely elastic, isotropic and homogeneous. However, for most engineering materials, the differences in actual and 'ideal' material properties are not too great to invalidate the assumptions.

Bareš, (1971) published a book which contains tables and formulas that could be used to calculate various internal forces and deformations of plates with various shapes based on elastic theory. For a circular slab having concentric circular load at the center, the radial

moment at any location outside the loaded area can be calculated from the following equation:

$$M_r = \frac{qa^2\beta^2}{16} \left[ (1-\mu)\beta^2 \left( \frac{1}{\rho^2} - 1 \right) - 4(1+\mu) \lg \rho \right] \quad (2.28)$$

where,  $M_r$  = Moment in radial direction (t-m/m, where 1 t = 1000 kgf)

$a$  = radius of the plate

$b$  = radius of the loaded area

$q$  = load intensity (t/m<sup>2</sup>)

$\beta$  =  $b/a$  = relative size of aperture in plate

$\rho$  =  $r/a$  = relative distance of the point considered

$r$  = distance of the point considered from plate center

This equation can be used for square slabs assuming an equivalent circular slab with an equivalent circular column.

## **Chapter 3**

### **Experimental Program**

#### **3.1 Introduction**

The main objective of the experimental program is to investigate the structural behaviour of concrete slabs reinforced by GFRP bar. The test program consisted of casting, instrumenting and testing eight slabs reinforced with GFRP bar and one reference specimen reinforced with traditional steel reinforcement. The structural performance was evaluated through the slab capacity, deformations, strains and crack widths. In this chapter, the procedures used in preparing and testing the slabs are described. The test set-up and the different equipments used to measure the load, deformations, strains and crack widths are presented.

#### **3.2 Mechanical properties of the GFRP bars used in the current program**

The test specimens were reinforced with GFRP bars (Glass/Vinyl Ester System). The bars are commercially known as ISOROD<sup>®</sup> and are produced by PULTRALL. Figure 3.1 shows a photograph of the GFRP bars. A tension test was performed to determine the actual stress-strain relation of the GFRP used in the current study.

A special type of grips was prepared for the tension test specimens. FRP bars cannot be tested in the same fashion as traditional steel bars. The main problem is gripping the

specimen in the test machine. FRP bars are composed of fibres and matrix. The matrix is comparatively weaker and the FRP bar would crush within the gripping length at the time of testing. For this reason, a special type of end grips was used. The end grips were made by using two pieces of a steel pipe as shown in Fig. 3.2. Each piece of hollow steel pipe is 360 mm long with 30 mm internal diameter and 3 mm thickness. The two pieces of pipe were placed at the two ends of the FRP bar to cover the gripping length. Two hollow metal rings were placed at the ends of each to keep the FRP bar aligned at the center of the hollow pipe. The hollow steel pipe was filled with high strength epoxy produced by WEST SYSTEM<sup>®</sup>. Sufficient time was allowed for drying and hardening of the epoxy. There after, the specimen was placed in a universal testing machine. The loading jaws were then tightened on the steel pipe as shown in Fig. 3.3. In this way, the rupturing of the bar was avoided within gripping zone. Also, there was no failure of sand coating of the bar within the gripping zone. The gripping pipes were designed according to the recommendation of Benmokrane *et al.* (2001). However, a small modification in length was made to accommodate the movement of the test machine and the available space within the loading frame. The gripping lengths were 360 mm, each, and the free length in-between two gripping length was 205 mm. The specimen length was 925 mm in total. The specimen and the gripping system are shown in the sketch given in Fig. 3.4.

Two strain gauges were placed on the free length of the specimen to measure the strain. The strain and load reading were recorded and logged to a data acquisition system. The stress-strain relation obtained from the test is shown in Fig. 3.5. Note that the graph is not up to the rupture point of the specimen. The strain gauges were damaged before

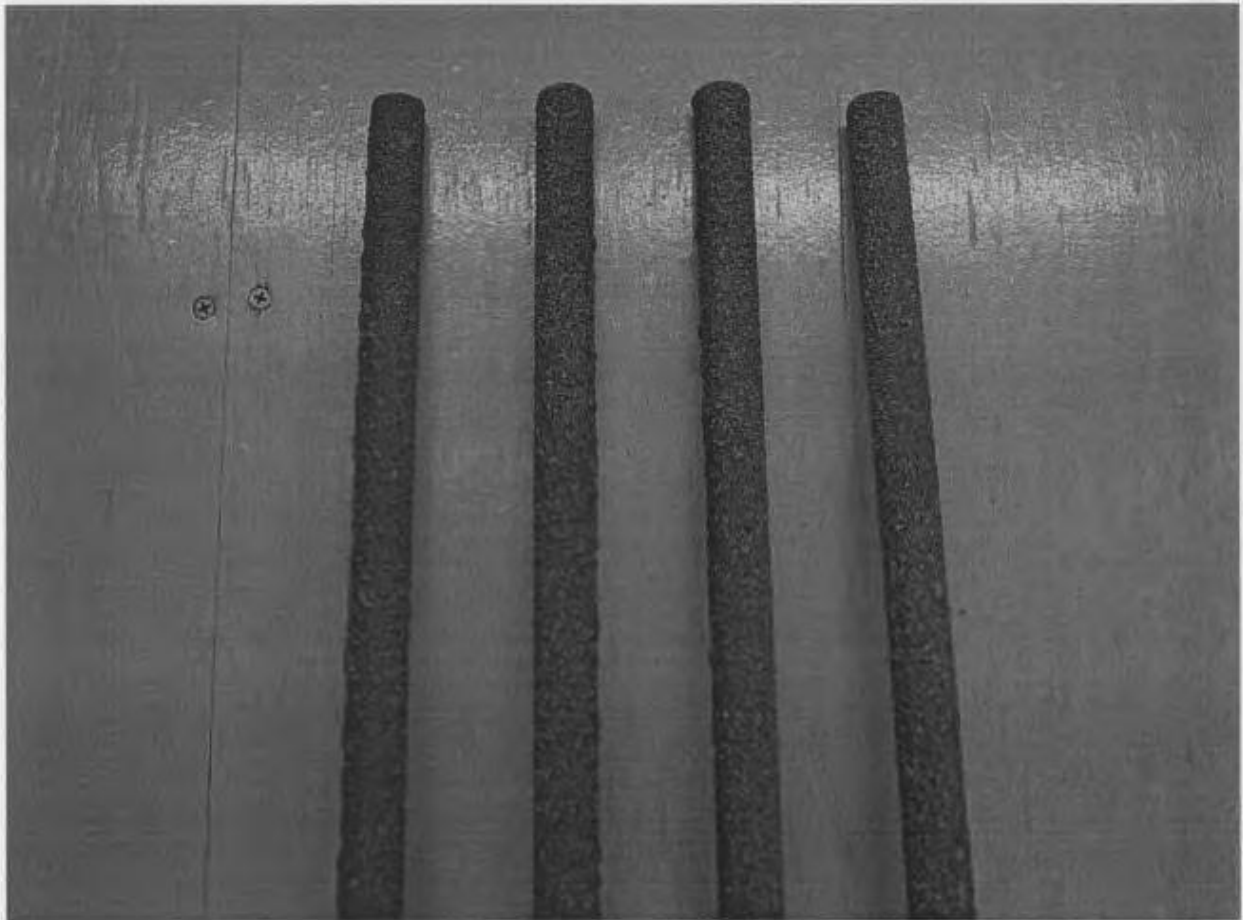


**Fig. 3.1: GFRP bars used in the test program**

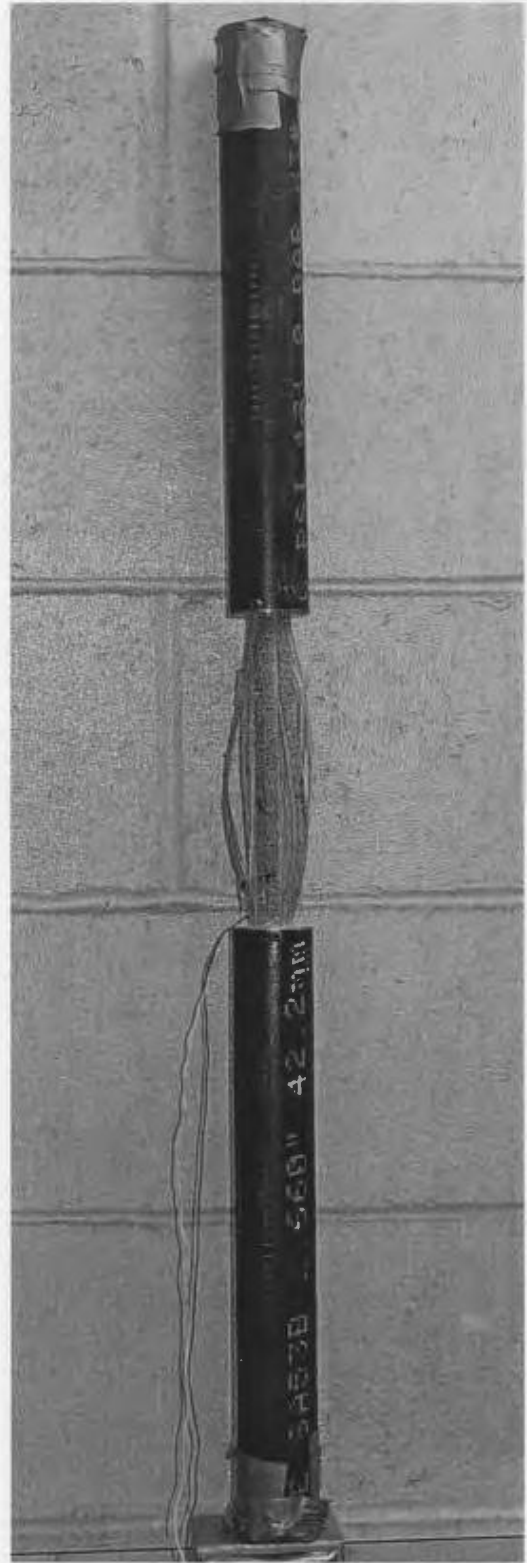


**Fig. 3.2: GFRP bar specimen before and after testing**

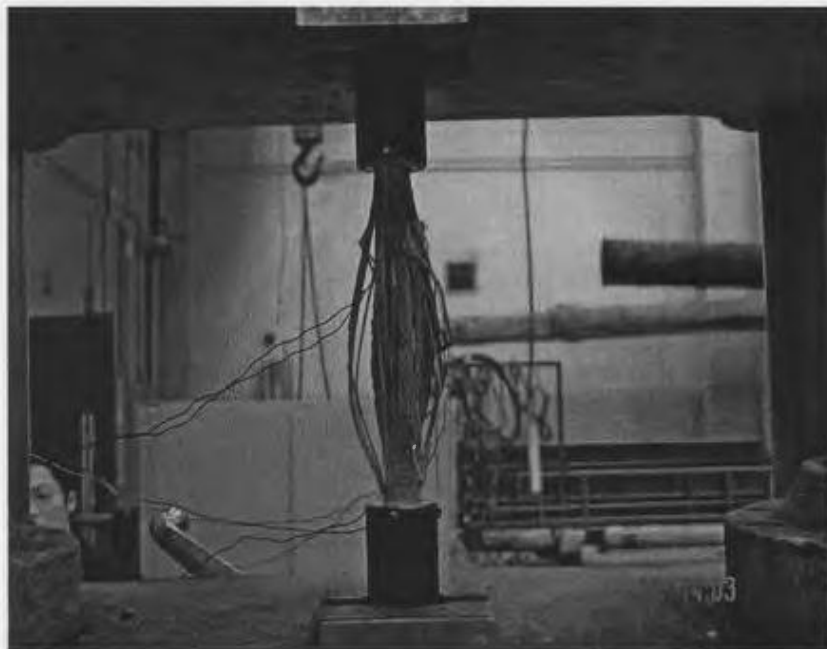


**Fig. 3.3: GFRP bar specimen in the test machine before and after testing**

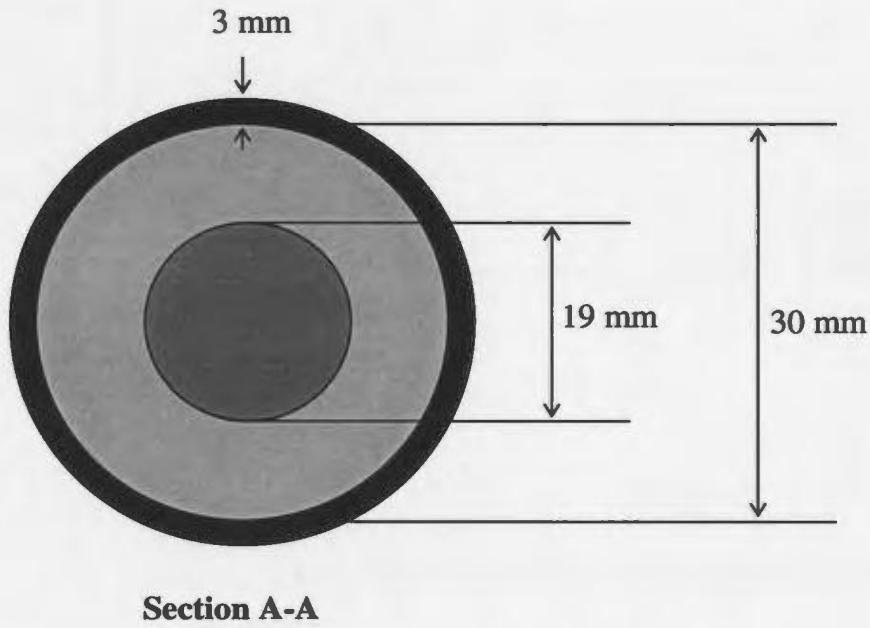
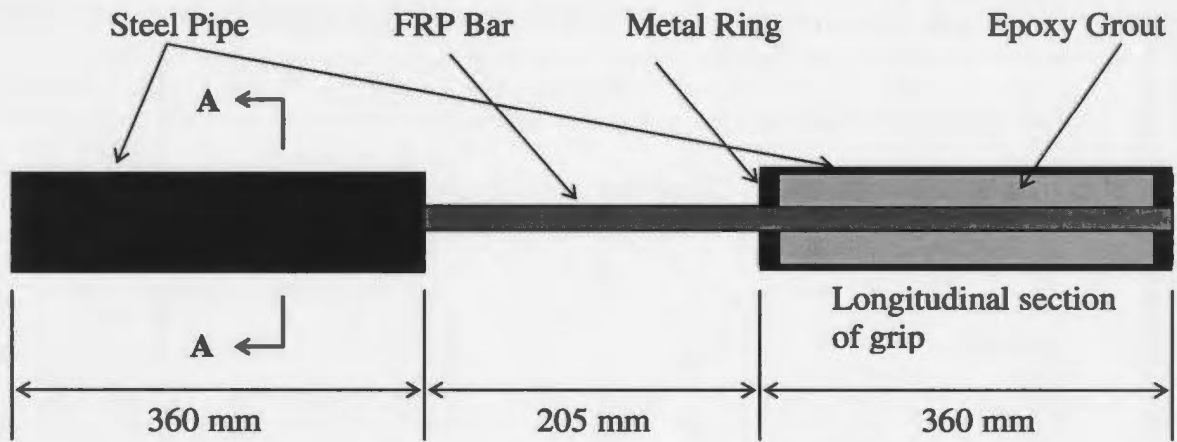


**Fig. 3.4: Sketch of the special grips for the FRP bar tension test**

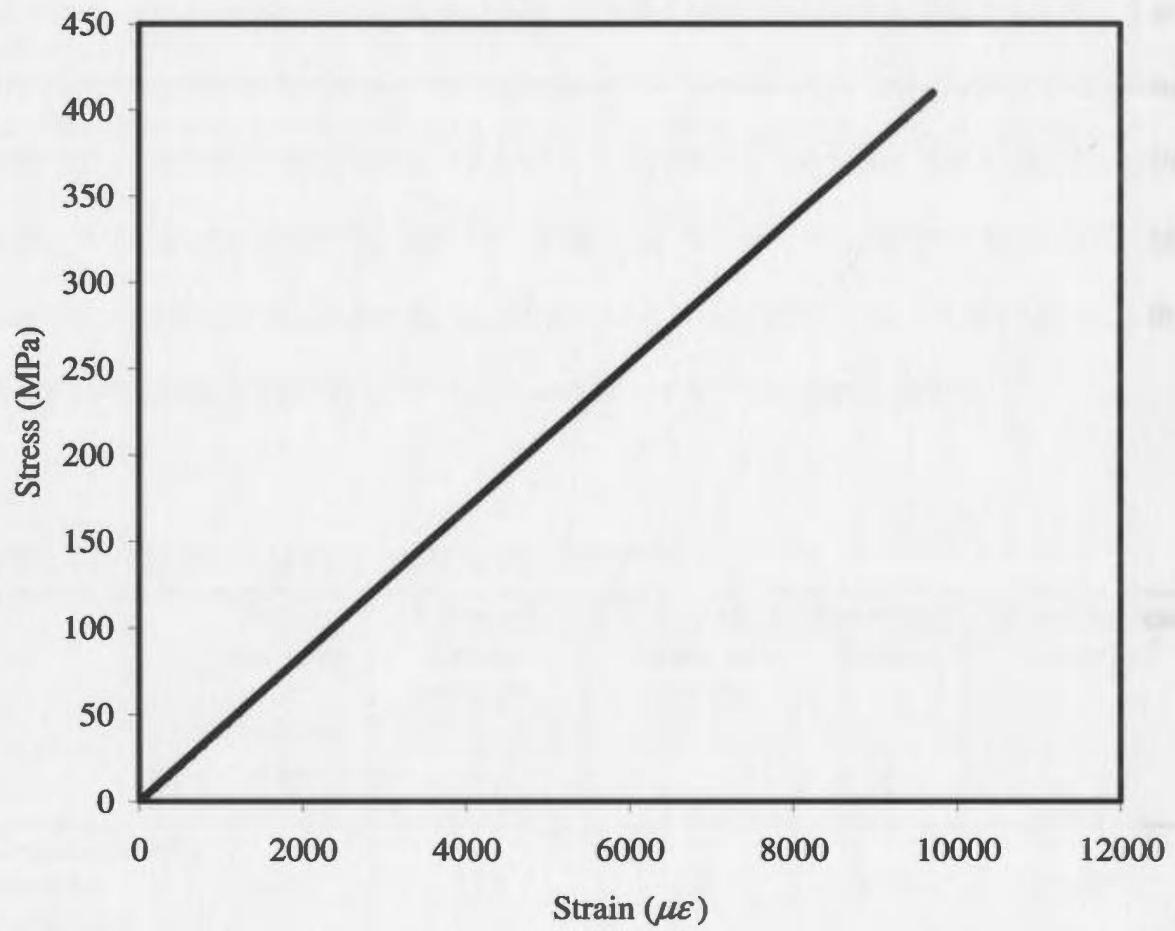


**Fig. 3.5: Recorded stress-strain relationship of GFRP bar**

reaching the ultimate strain. However, the ultimate load was measured. The modulus of elasticity was calculated from the available data. The ultimate strain was calculated using the measured ultimate load and modulus of elasticity. In total, two specimens were tested and the results presented are the average of these two specimens. The mechanical and physical properties of the bars as recommended by the fabricator and the properties found at the laboratory test are given in Table 3.1. It should be noted that due to the limitation of the existing test machine, the free length of the bar was shorter than the length recommended by Benmokrane et al (2001). As a result, the measured strength and thus the ultimate strain of the bar could have been lower than the actual values.

**Table 3.1: Mechanical properties of the GFRP bars**

	<b>Tensile modulus of elasticity</b> $E_{FRP}$ (GPa)	<b>Ultimate tensile strength</b> $f_u$ (MPa)	<b>Ultimate strain in tension</b> (%)	<b>Poisson's Ratio</b> $\nu$	<b>Development length</b> $l_d$ (mm)
<b>Recommended values by producer:</b>	42	719	1.8	0.28	400
<b>Test value:</b>	42	630	1.5 <sup>a</sup>	-	-

<sup>a</sup> strain gauges were out of order before reaching ultimate strain. It has been calculated using test value of  $E_f$  and  $f_u$ .

### 3.3 Concrete

It was mentioned before that the concrete strength is a variable of this investigation program. Therefore, two types of concrete were used. Most of the slabs were with normal

strength concrete. The specified strength was 30 MPa. Two slabs were made with high strength concrete, i.e. concrete with compressive strength more than 70 MPa.

### 3.3.1 Normal strength concrete

The normal strength concrete, used in casting the slabs, was supplied from a ready mix plant. The specified cylinder strength  $f_c'$  was 30 MPa. The normal strength concrete used in casting the short column was produced in the concrete laboratory at MUN. The mixing proportions for the normal strength concrete that was produced in the laboratory are given in Table 3.2.

**Table 3.2: Mix proportions for one batch of normal strength concrete**

<b>Ingredients</b>	<b>Normal Strength Concrete</b>
Cement (kg)	32
Coarse aggregate (kg)	107
Fine aggregate (kg)	65
Water (L)	16
<b>Target strength, <math>f_c'</math></b>	<b>30 MPa</b>

### 3.3.2 High strength concrete

The high strength concrete was made in the concrete lab at MUN. The required strength and workability are the main concerns in case of high strength concrete. To obtain the

proper mixing proportions that provides enough strength and workability, several trial mixes were made. Standard concrete cylinders were made from each trial batch to determine the strength of the concrete. A mix was finalized and used in preparing the high strength concrete specimens. The ingredients and the different chemicals used to produce the high strength concrete are described briefly in the following sections.

### **3.3.2.1 Cementitious materials**

The term 'cementitious materials' refers to the combined total weight of Portland cement and pozzolanic materials (fly ash and silica fume) for the production of high strength concrete. In the current experimental program, only silica fume is used. Fly ash is not used which is normally used to increase the workability of the mix.

#### **(a) Cement**

Commercially available Type 10 Portland cement was used to produce both normal strength and high strength concrete in the laboratory. The producer of the cement is 'St. Lawrence Cement'.

#### **(b) Silica Fume**

Silica fume is a by-product in the manufacture of ferrosilicon and silicon metal. As its fineness is extreme and glass content is high, silica fume is a very efficient pozzolanic material. Therefore, it is able to react very efficiently with the products of hydration of Portland cement to create secondary cementing materials in hydrating concrete. In a silica

fume concrete system, the calcium hydroxide produced by the hydrating Portland cement is largely consumed in the ensuing pozzolanic reactions. This results in a product with very low permeability and absorption, thus enhancing the resistance to deterioration in aggressive environments. The silica fume was supplied from the only Canadian source in Quebec. The brand name of the silica fume is 'SKW Canada'.

### 3.3.2.2 Aggregates

Locally available crushed stone was used as coarse aggregate. The maximum size of the coarse aggregate was 25 mm. the absorption capacity of the used coarse aggregate was 2.1%. Locally available well graded fine aggregates were used. The fineness modulus (FM) of the used fine aggregate was 2.91. the grading curve of the aggregates are given in Fig. 3.6.

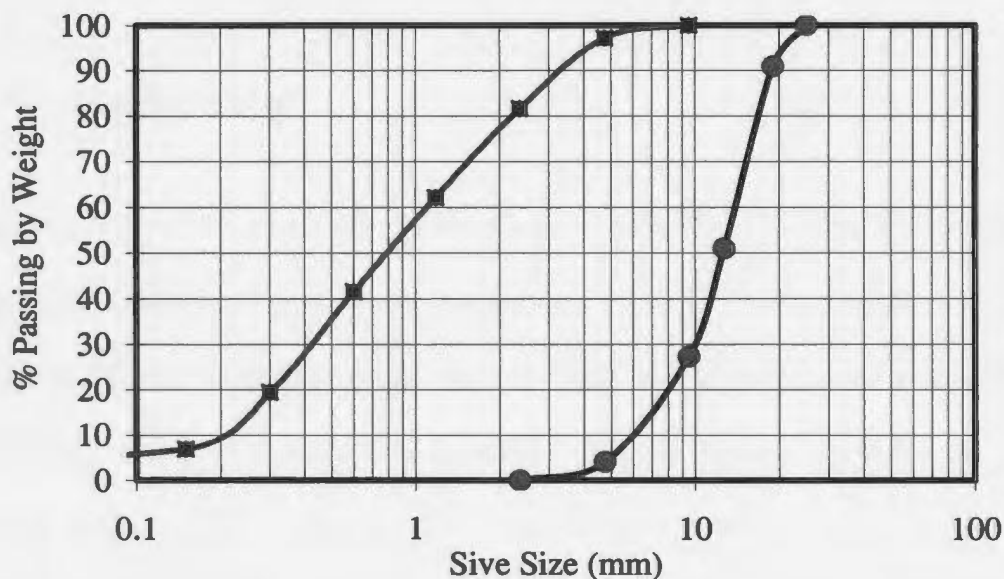


Fig. 3.6: Grading of aggregates

### **3.3.2.3 Water reducing admixture**

The water reducing admixture that was used in high strength concrete is commercially known as EUCON DX. This is a strength increasing water reducing admixture, which meets all requirements of CSA A266.2 specification for type WN and SN. It is an aqueous solution of hydroxy-carboxylic acid and catalyst that provides a better hydration of the cementitious material.

### **3.3.2.4 Retarding agent**

The set retarding agent that was used in high strength concrete is commercially known as EUCON 727 admixture. It is a water reducing, set retarding and strength increasing admixture for concrete. It contains a double metallo-organic salt derived from hydroxycarboxylic acids. It complies with CSA-A266.2 type R, RX and SR standards.

### **3.3.2.5 Superplasticizer**

A superplasticizer which meets all requirements of ASTM C494 type F was used in the mix. The superplasticizer is commonly known as EUCON 37. It is an aqueous solution of sodium salt of poly-naphthalene sulfonic acid used as a superplasticizer for concrete. A superplasticizer helps to control the hydration rate of cement to maintain optimum fluidity over time. It allows production of concrete with a much higher slump compared to a reference concrete without superplasticizer, keeping equivalent compressive strength. Unlike water addition, it does not affect mechanical strength of concrete. A

superplasticizer makes concrete easier to handle without any segregation and to placed in heavily reinforced members keeping the homogeneity of mix. It is possible to reduce the water/cementitious material ratio with the addition of superplasticizer and thus, allows the production of concrete with higher compressive strength.

**Table 3.3: Mix proportions for one batch of high strength concrete**

Ingredients	High-Strength Concrete
Cement (kg)	40
Silica fume (kg) [8.75% of Cement]	3.5
Coarse aggregate (kg)	91
Fine aggregate (kg)	65
Water (L)	11
Superplasticizer (ml)	1200
Water reducer (ml)	100
Retarding agent (ml)	50
<b>Target strength, <math>f_c'</math></b>	<b>70 MPa</b>

**3.3.2.6 Concrete mix**

After several trial mixes, the mixing proportions were determined and used to produce the high strength concrete. The different ingredients for high strength concrete are given

in Table 3.3.

### **3.3.2.7 Mixing procedure**

#### **(a) Material loading sequence**

1. Sand loading.
2. Loading of the coarse aggregate
3. Addition of 50% of the total amount of water.
4. Mixing period of 30 seconds after the addition of the water.
5. Addition of the cementitious materials after this period of mixing.

#### **(b) Initial mixing**

1. Mixing period of 30 seconds after the addition of the cementitious materials.
2. Addition of the water reducing agent (diluted in 1L max. of water) after the period of 30 seconds.
3. Addition of the retarding agent (diluted in 1L max. of water) after 1 minute and 30 seconds.
4. Addition of the superplasticizer (diluted in the remaining water) after 3 minutes.
5. Stopping the mixer after the period of 4 minutes.

#### **(c) Final mixing**

1. Restarting the mixer after 5 minutes.

2. Stopping the mixer after 8 minutes.
3. Determination of the properties of fresh concrete and starting of casting.

### **3.4 Test specimens**

Nine full scale specimens were cast, instrumented and tested. The slab specimen represents the slab portion bounded by the line of contra-flexure as shown in Fig. 3.7. Thus, the slab specimen represents the region of negative bending moment around the column and the specimen edges, which can be assumed as simply supported, to simulate the lines of contra-flexure. This type of isolated slab specimens is commonly used in laboratory testing for research purpose. Typical dimensions and reinforcement details of a typical slab specimen are shown in Fig. 3.8. Full details of the test slabs are given in Table 3.4.

The specimens were tested in a steel frame test set-up. The slabs were simply supported along the edges and the corners of the slab were free to lift. Transverse load on the slab was applied through an axially loaded stub-column.

The main variables of the experimental program were the reinforcement ratio, concrete strength and slab thickness. All of the slabs were over reinforced, except slab GSHS2, as it is recommended by the guidelines available for FRP. Balanced reinforcement ratio is calculated based on strain compatibility of concrete section under one-way flexure. That means, the slabs are over reinforced at the section capacity level. The minimum

reinforcement ratio was 0.95% which was equivalent to  $1.65\rho_b$  (GS4) and the maximum reinforcement ratio was 1.67% which correspond to  $2.65\rho_b$  (GS3) within series 1. Two slabs were made with high strength concrete (GSHS1, GSHS2) with concrete strength 92 MPa and 86 MPa respectively. All other slabs were with normal strength concrete ranging from 23 MPa to 40 MPa. Slabs GSHD1 and GSHD2 were 200 mm thick. All other test slabs had a thickness of 150 mm.

**Table 3.4: Details of the test slabs**

	Bar material	Slab desig.	Conc. comp. strength $f_c'$ (MPa)	Bar dia. $\phi$ (mm)	Bar spacing $S$ (mm)	Col. side dim. $c$ $c_1 = c_2$ (mm)	Slab thick. $h$ (mm)	Effective depth $d$ (mm)	Rein. ratio $\rho$ (%)	$\rho/\rho_b$
Series 1	GFRP	GS1	40	19	240	250	150	100	1.18	1.43
	GFRP	GS2	35	19	270	250	150	100	1.05	1.42
	GFRP	GS3	29	19	170	250	150	100	1.67	2.65
	GFRP	GS4	26	19	300	250	150	100	0.95	1.65
Series 2	GFRP	GSHD1	33	19	170	250	200	150	1.11	1.58
	GFRP	GSHD2	34	19	240	250	200	150	0.79	1.09
Series 3	GFRP	GSHS1	92	19	170	250	150	100	1.67	1.15
	GFRP	GSHS2	86	19	240	250	150	100	1.18	0.84
	Steel	R1	23	16	240	250	200	154	0.54	0.23

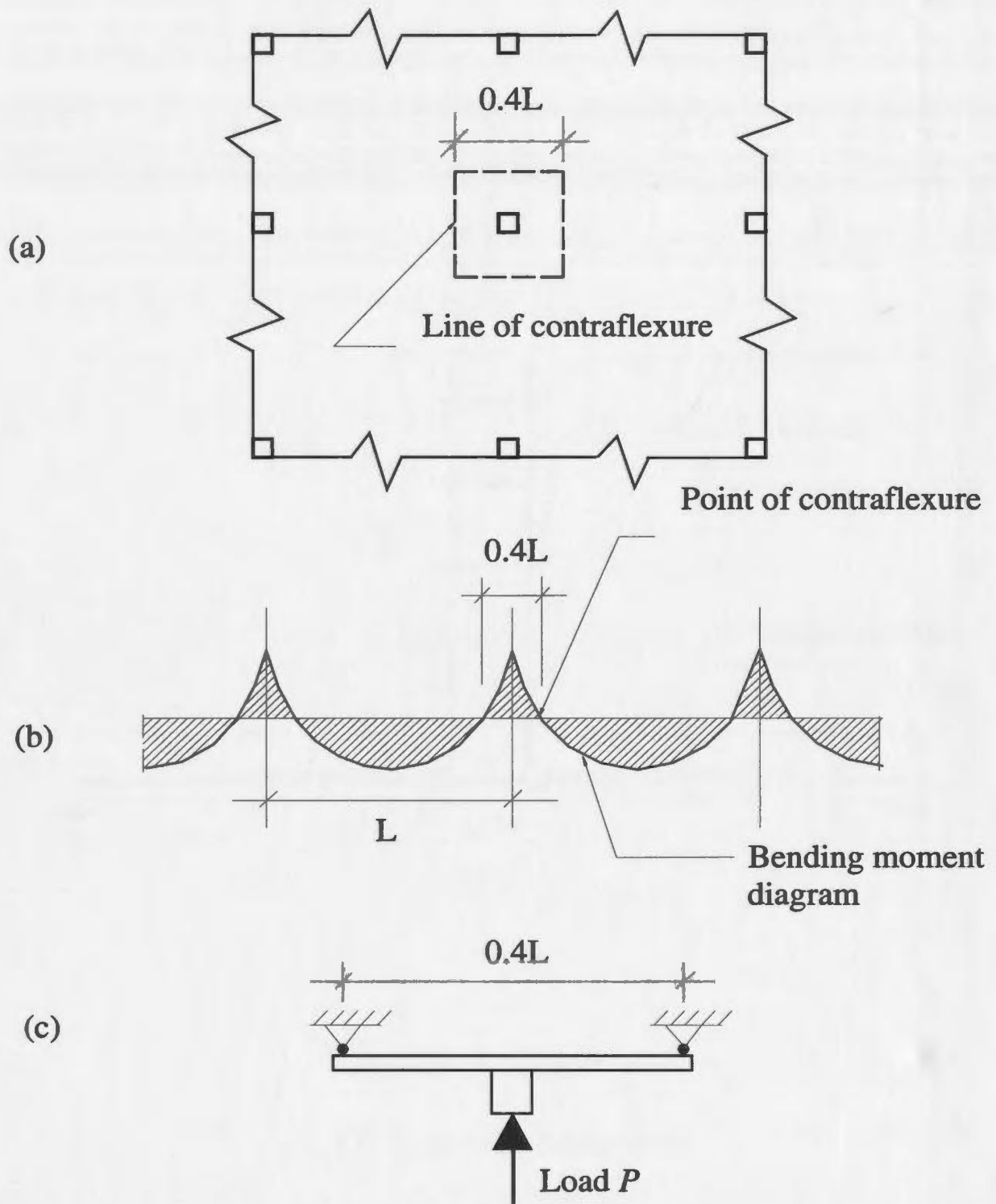


**Fig. 3.7: Conventional slab-column specimen idealization**

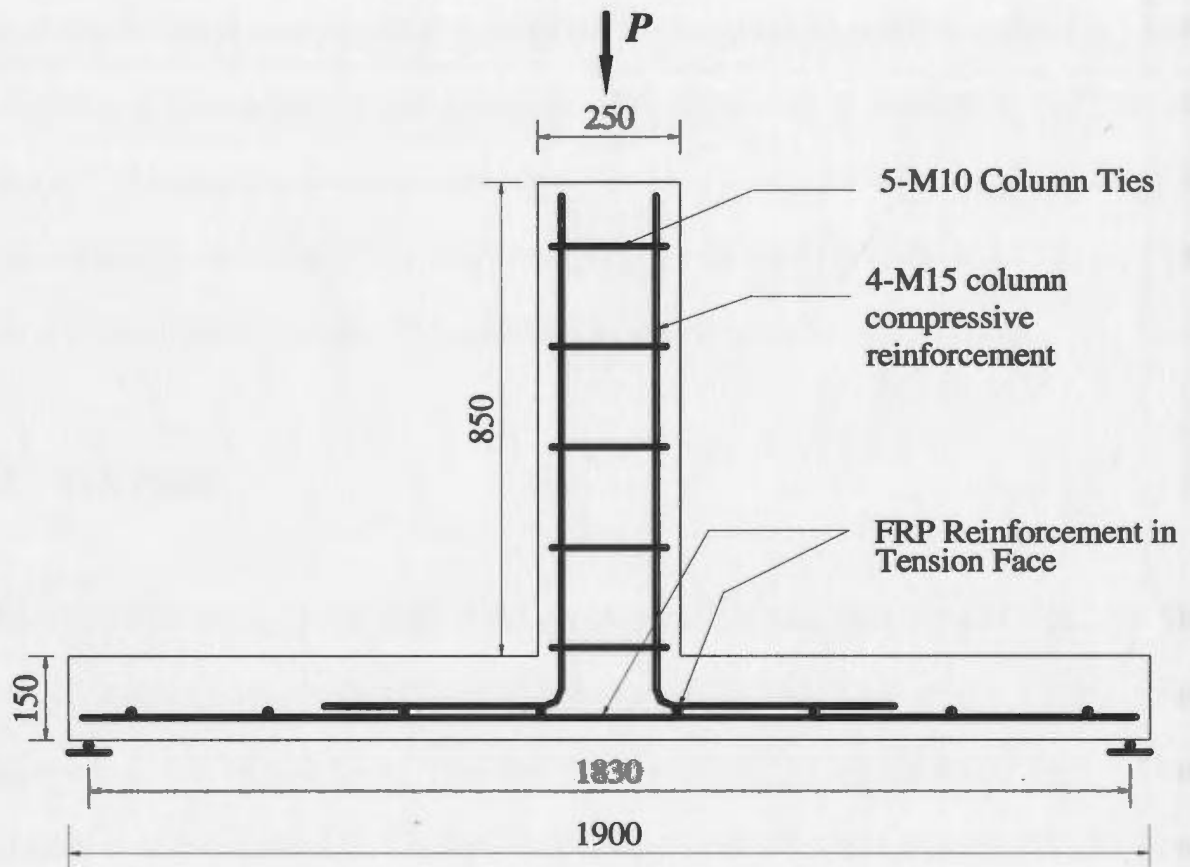


**Fig. 3.8: Typical test slab specimen**

### **3.5 Formwork**

The formwork used for casting the slabs is a permanent steel formwork in the concrete lab at MUN. The formwork had been used for several previous research programs. Figure 3.9 shows a photograph of the formwork. The formwork is supported on W-shaped columns. The columns are connected with I-beams. A 7mm thick steel plate with central hole (square shape 250x250) is supported on this I-beams. The column on top side was cast one day after the casting of slab using a steel framework.

### **3.6 Test frame**

The MUN slab testing frame used in the experimental program is shown in Fig. 3.10. The frame is a space frame made of steel W and channel section. The frame is a self-reacting space frame and is tied to the concrete floor which is 30 inches thick. Four 32 mm diameter rods are welded on the vertical W-shape sections which support the slab along the four sides. The rods act as roller supports. The slab was placed in the frame in a vertical position and the stub-column was in a horizontal position as shown in Fig. 3.11. The test set-up was designed to test the slabs in a vertical position to make it easier to place and read the various instruments and to detect the cracks, mark their propagations and measure the crack width at the time of testing in a safe way. A Neoprene strip was placed along the contact line between the supports and the test slab. The strip provided uniform support along the edges of the test slabs and avoids friction.



**Fig. 3.9: Photograph of the formwork**

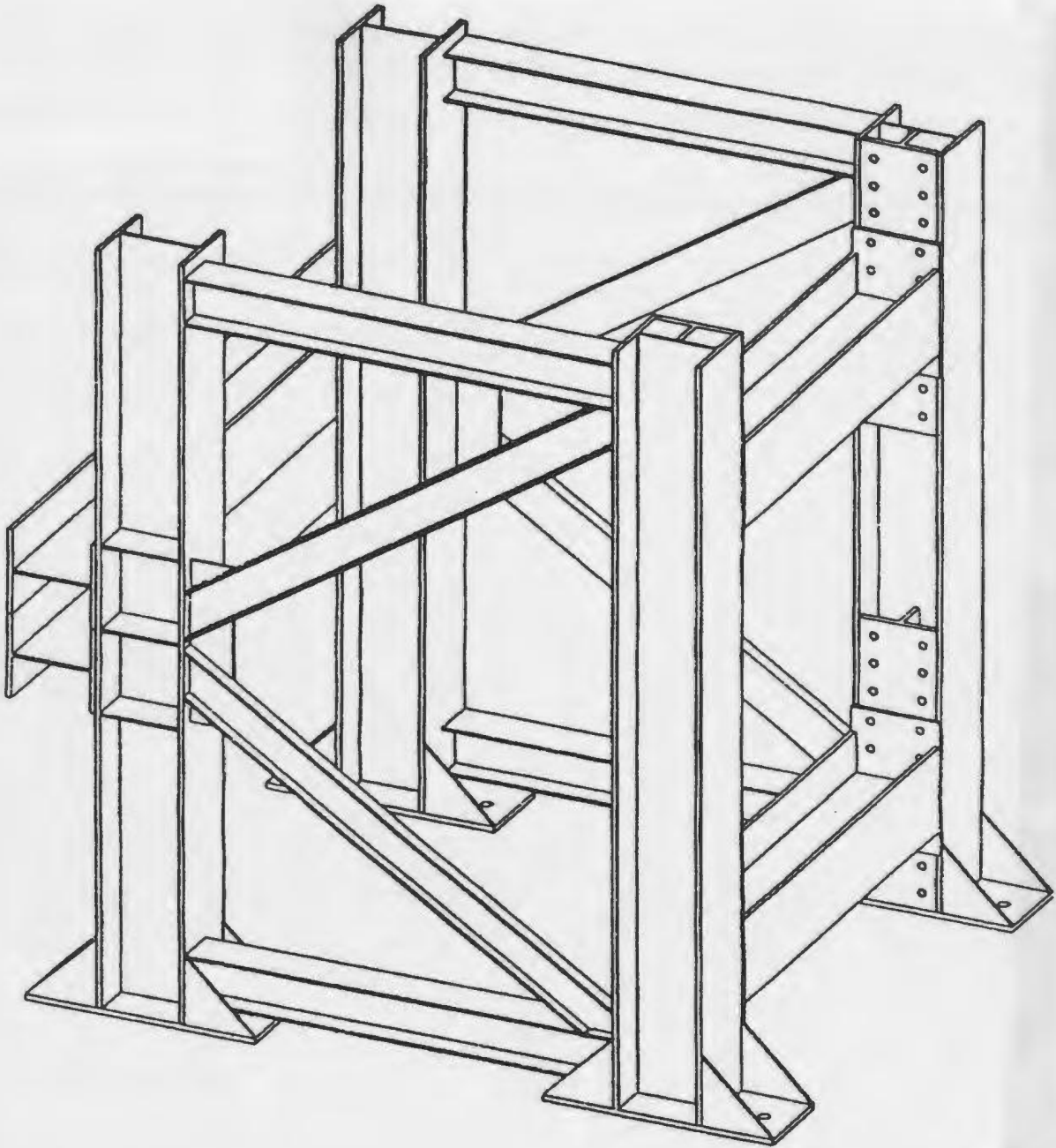


**Fig.3.10: A schematic of MUN slab testing frame [Marzouk and Perchard (1991)]**

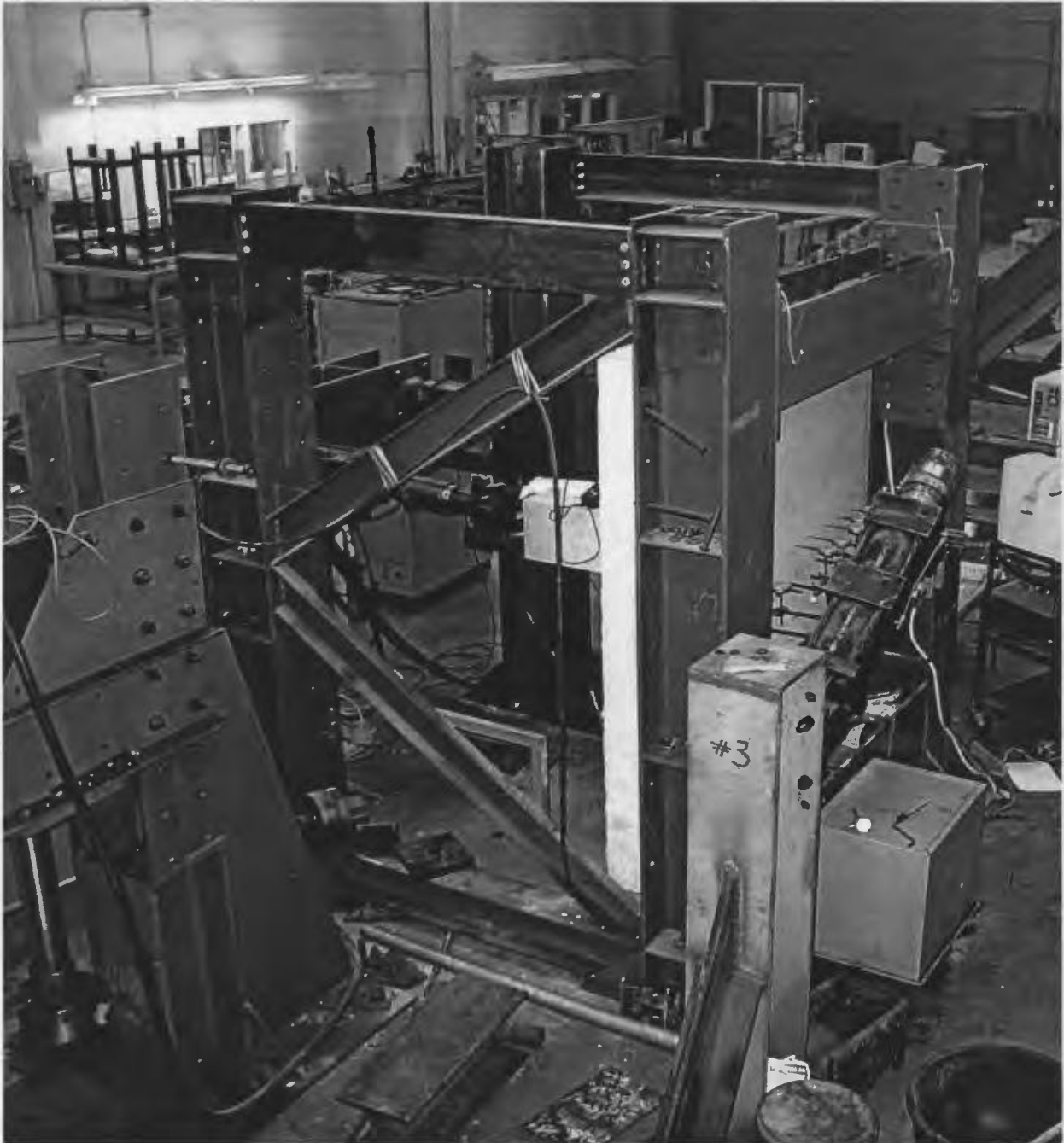


**Fig. 3.11: Photograph of the test frame with a test specimen in place**

### **3.7 Placing of a slab**

The slabs were cast in the concrete laboratory on the formwork mentioned in the previous section. An overhead crane of 2 tons capacity was used to lift the slab from the formwork. The slabs were placed on a fork-lift that was used to transfer them from the concrete laboratory to structural laboratory where the test frame is located. There is another overhead crane in structural laboratory with a capacity of 10 tons. The slabs were placed in the proper position in the test frame using that 10-tons overhead crane in the structural laboratory. To avoid any load eccentricity, special care was taken, so that, the axis of stub-column and the axis of the actuator remain in the same line. A steel plate was placed in between column-stub and actuator to fill-up the gape. The purpose of filling the gape with steel plate instead of moving actuator is to sue the maximum stroke capacity of the actuator in slab testing. To handle the test slabs two steel hooks, made with M15 bar, were set on one side of the slab at the time of casting.

### **3.8 Instrumentation and measurements**

#### **3.8.1 Loading system**

The load was applied by a servo-hydraulic actuator as shown in Fig. 3.12. The load represents the gravity load on an actual slab in a structure. The hydraulic actuator has a maximum capacity of 670 kN and a maximum displacement of 150 mm. The load and displacement are measured by means of an internal load cell and LVDT, respectively.

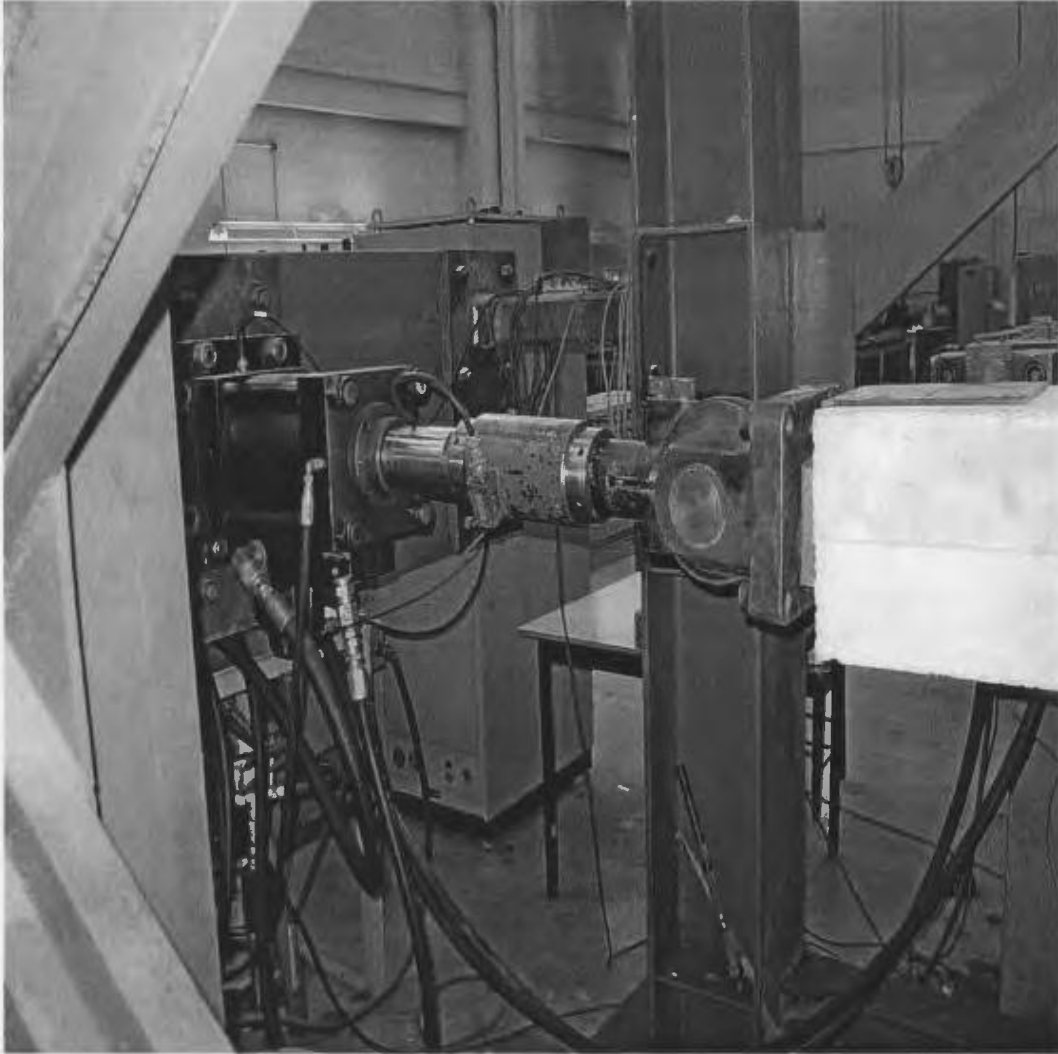


**Fig. 3.12: Actuator behind the test frame**

The actuator can operate in load control or displacement control. A Model 407 MTS Controller was used to control the actuator. A displacement control closed loop system was employed in the tests. The command signal was generated by a 410 Digital Function Generator. The internal LVDT provided the feed back signal. The closed loop control system was executed through the 407 controller. The 407 controller and 410 Digital Function Generator are shown in Fig. 3.13. The rate of displacement application was 27 mm/hr.

### **3.8.2 Deflections**

Deflections of the slab at various locations were measured in the direction of applied load. The deflections were measured by means of Linear Variable Differential Transformers (LVDTs) and by dial gauges. The dial gauges had one-hundredth of a millimetre precision. The slab's central deflection was measured by the actuator's internal AC LVDT and an external DC LVDT that was mounted at the center of the slab on the tension face. Another DC LVDT was placed at half-way from center to support. In addition, several dial gauges were used to measure the deflection profile as shown in Fig. 3.14. The dial gauge readings were taken manually and the LVDT readings were logged into the data acquisition system.

### **3.8.3 Strains in reinforcement (FRP bars)**

The strains were measured at various locations on the FRP bars. The locations of strain



**Fig. 3.13: A 410 digital function generator, 407 controller and data acquisition system**

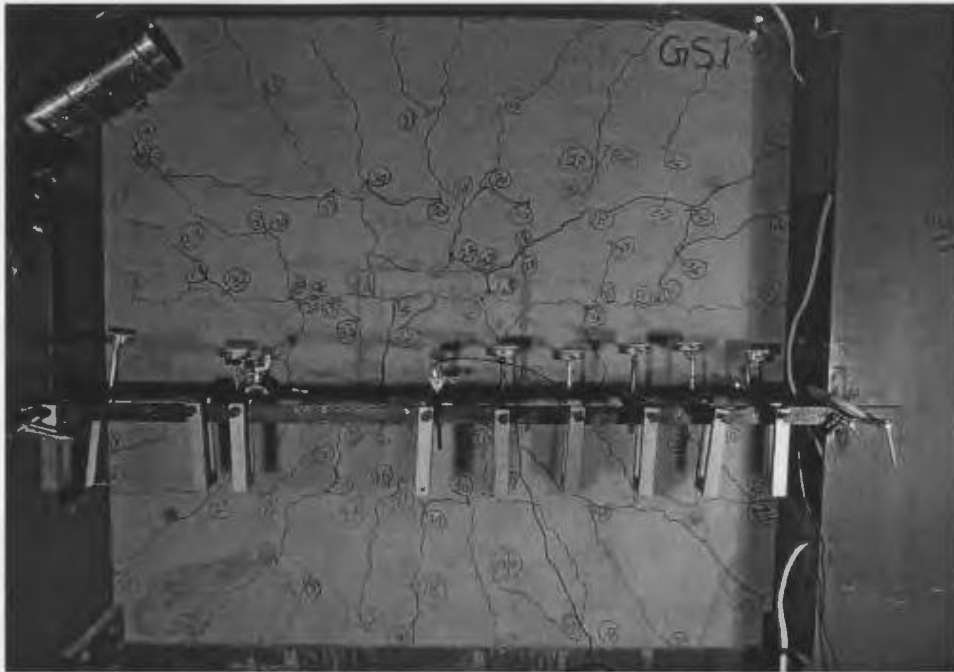


**Fig. 3.14: Location of the LVDTs and dial gauges**

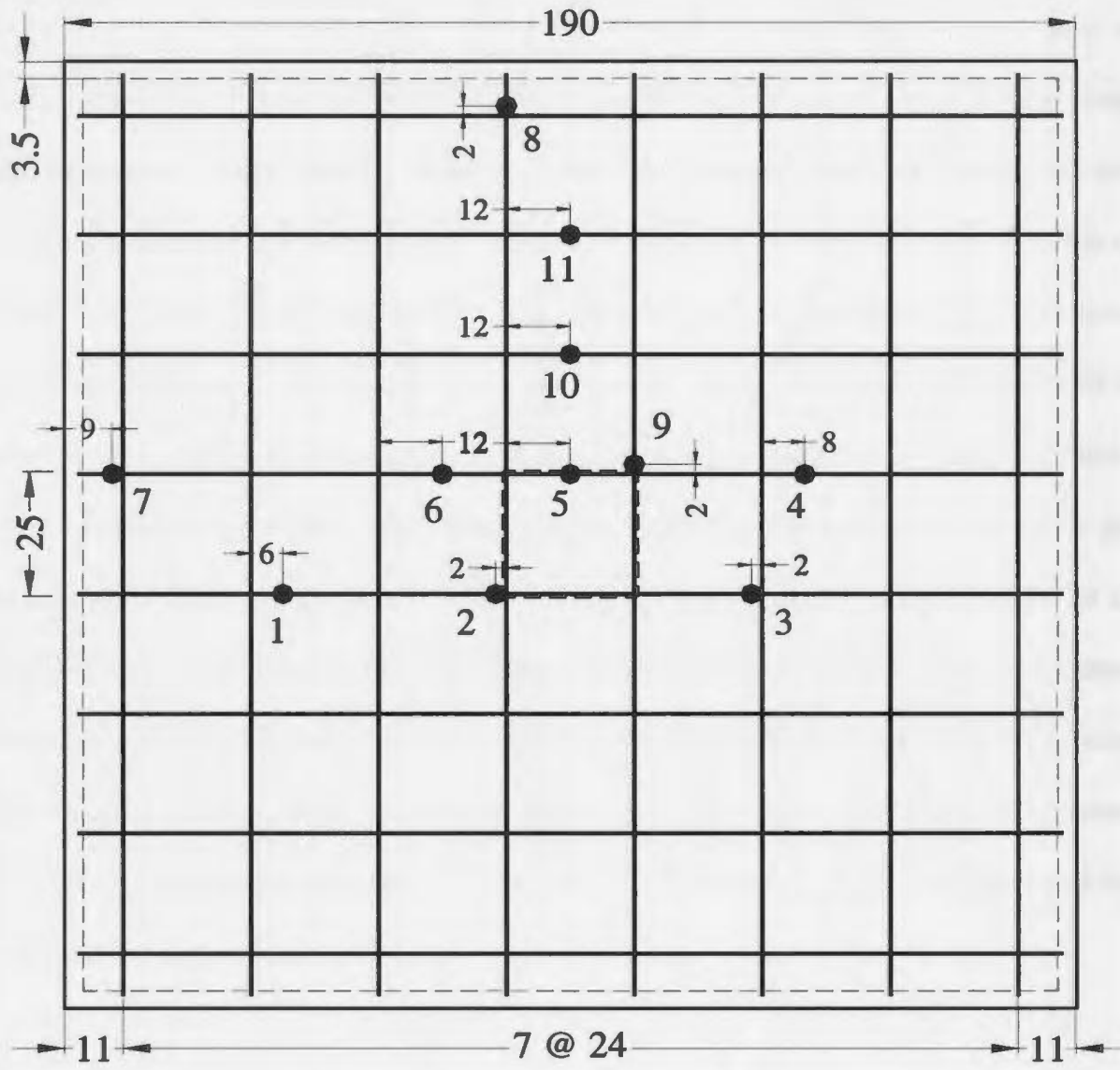


**Fig. 3.15: Strain gauge locations on the reinforcement of slab GS1**

gauges were selected to measure the maximum strain in reinforcement, variation of strain in radial direction, tangential direction and anchorage failure. Figure 3.15 shows the strain gauge locations on the FRP reinforcing bars for a typical slab. The presence of strain gauges may cause the loss of bond for the FRP bars. Therefore, placing too many strain gauges on a bar should be minimized. Also, the slabs are symmetric along the  $x$  and  $y$  axis. The locations of strain gauges were selected based on the two previous points of view. Two strain gauges were placed near the column face to measure the maximum strain. Strain gauges, 100 mm apart from one another, were placed in a radial direction to measure the variation of strain in that direction. Some strain gauges were used to measure the tangential strains in bars. Two strain gauges were placed at the end of the bar to get an indication of anchorage failure. This strain gauge arrangement was almost used for all slabs. Electric strain gauges with a resistance of  $120.0 \pm 0.3\%$  ohms at  $24^{\circ}\text{C}$  temperature were used. The gauge factor was  $2.06 \pm 0.5\%$  at the same temperature. The strain gauge was made of 0.03 mm thick flexible polyimide film. The normal use temperature range for static strain measurement was  $-75^{\circ}\text{C}$  to  $+175^{\circ}\text{C}$ . The gauge length was 6 mm and the strain limit is approximately 5%.

The strain gauges were placed on the FRP bars very carefully. At first, the sand coating on the FRP bar was removed carefully so that matrix and fibres of the bar are not affected. The strain gauge was glued on FRP bars by means of epoxy resin. The commercial name for the epoxy used is M-Bond Adhesive Type AE. Polyurethane and Acrylic coating were put on the strain gauge to protect it from water. Finally, a self

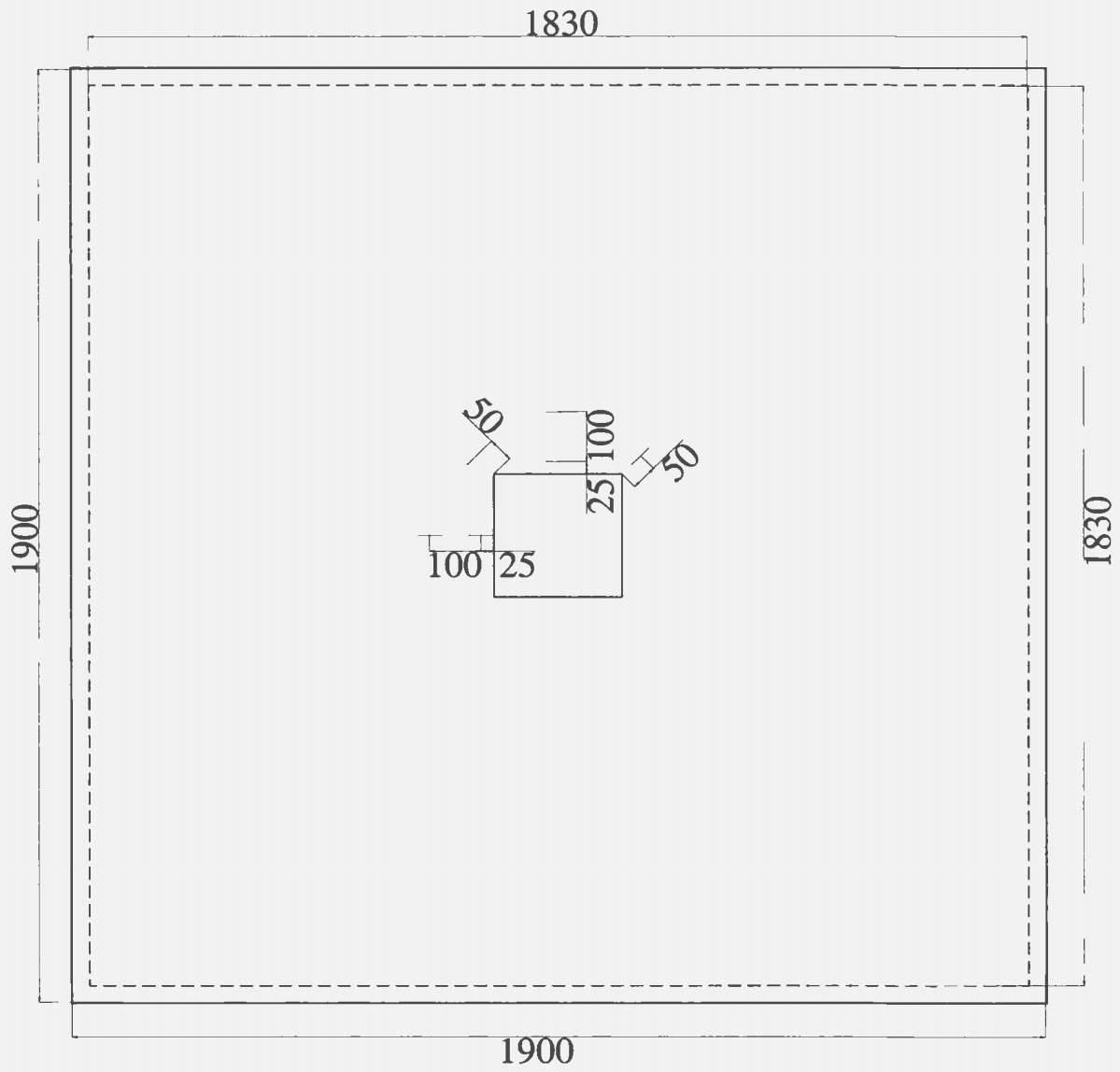


**Fig. 3.16: Concrete strain gauge locations**

vulcanizing rubber tape was used to cover the gauge to protect it from water present in the fresh concrete and any kind of physical thrust.

### **3.8.4 Concrete strains**

A number of concrete gauges were used on the compression side of the concrete slab. The locations of concrete gauges are shown in Fig. 3.16. Electric strain gauges were used. Each strain gauge is made of 0.03 mm thick flexible polyimide film. The strain gauge resistance is  $120 \pm 0.2\%$  ohms at  $24^{\circ}\text{C}$  and the gauge factor is  $2.075 \pm 0.5\%$  at the same temperature. Working temperature range is  $-75^{\circ}\text{C}$  to  $+175^{\circ}\text{C}$  for continuous use in static measurement. Strain limit is approximately 5% of gauge length. The gauge length of the strain gauge was approximately 50 mm. The locations of the strain gauges were marked on the concrete surface. The concrete surface at those locations was made smooth and plane with a hand grinder and then a very thin film of epoxy resin was placed on concrete to make the surface smooth. After drying, each strain gauge was placed in position and the wire connections were connected to the data acquisition system.

### **3.8.5 Crack detection device**

To detect and to determine the crack width an optical device was used. The device is commonly known as the Crack Detection Pocket Microscope and is produced by MASTRAD Quality and Test System. The scope is suitable for crack width measurement. A lamp facility is available with it to illuminate the field of view by

centralizing the lamp beam. There is a focusing knob to get the crack into focus field. The microscope can measure crack widths ranging between 0.02 mm to 4 mm. The microscope is calibrated by Optical Magnification 'X40' Standard.

### **3.8.6 Data acquisition system**

The electronic strain gauges, LVDT and the load readings were logged to a computerized data acquisition system. The measurements were stored in a file using LabVIEW software. The data scanning and saving rate was set on one set of readings in each five second.

### **3.9 Casting and curing**

During casting, the concrete was sufficiently vibrated with an electric rod vibrator. Once the casting was completed, the top surface of the slab was finished with a steel trowel to make it smooth as far as possible. The stub-column was cast on the following day. Details of the normal strength concrete and high strength concrete are given in Section 3.3. To determine the strength of concrete of slab and stub-column at least three 150 × 300 mm (6 × 12 in.) cylinders were taken from each batch.

When the casting and finishing were completed, the slab was covered by polythene sheet. After 48 hours, the formwork of the slab and stub-column were stripped. At the same time the cylinders were demoulded. The slab was cured by spraying water on its surface

twice in a day, for seven days. The cylinders were also cured in same manner to make them to be representative of slab and column concrete.

### **3.10 Test procedure**

The slab was placed on the testing frame very carefully so that four sides of slabs were supported on the rods that represent the roller support to obtain uniform reaction. The column axis and the loading actuator axis were aligned so that they would remain in the same line. The four corners of slab were free for rotation. Initially, approximately 4.45 kN (1 Kip) load was applied to the slab to set the slab on frame. At this stage the readings of all instruments were taken. The displacement was applied on the specimen at the rate mentioned previously. All the strain gauges on the concrete and on the FRP bars, LVDTs and load readings were logged to the data acquisition system which scanned readings with a five seconds interval. The readings were stored in a personal computer. The dial gauge readings, crack width measurement and crack pattern marking were performed manually at each 6.67 kN (1.5 Kips) intervals. After the load reached 66.7 kN (15 Kips), the interval used for manual measurements was increased to 13.3 kN (3 Kips). A photograph showing manual data collection is shown in Fig. 3.17. The crack width was measured at certain locations at each interval to determine the change in crack width with load level. One diagonal, one axial ( $x$  or  $y$  direction) and one crack at the face of column were monitored. This process was continued until the failure of slab.



**Fig. 3.17: Manual crack marking, crack width measurement and dial gauge reading collection at a load interval**

# **Chapter 4**

## **Test Results and Discussion**

### **4.1 Introduction**

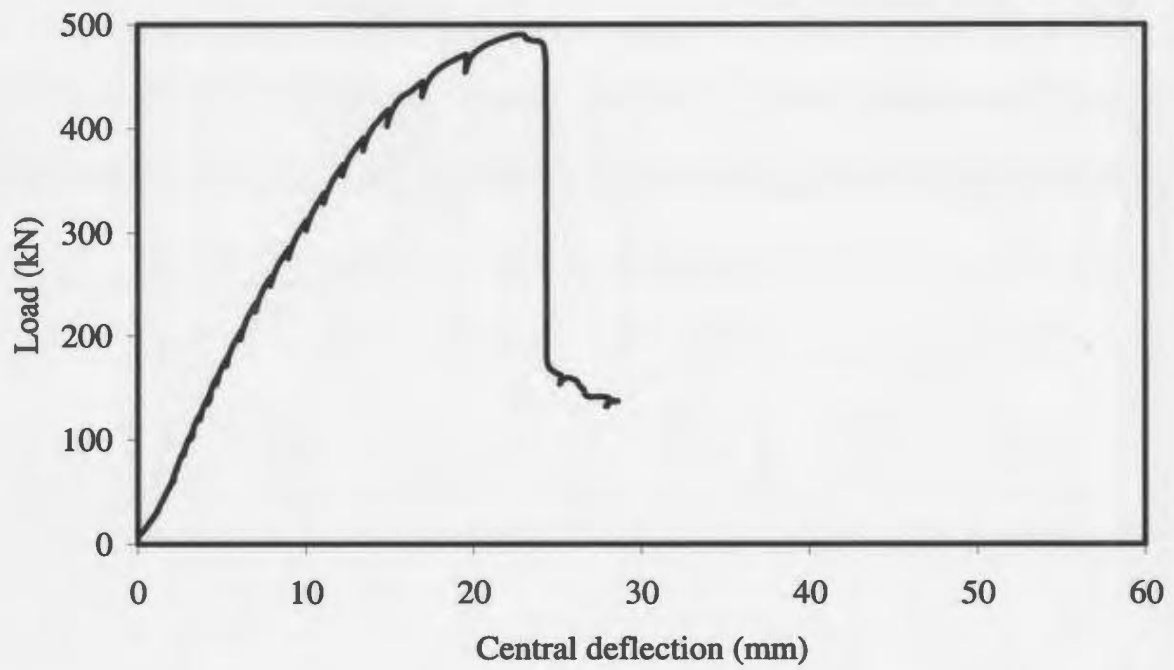
The test results obtained from the test program, described in the previous chapter, are presented in this chapter. A large amount of data was recorded and the related graphs were prepared. Few data are important for interpretation of the results, are presented here. The strains in concrete, strains of FRP bars, load deflection relationships etc. are reported. Failure mode and crack patterns are also depicted by means of photographs. In total, nine slabs were tested in the test program. All the experimental results of the nine slabs are given in this chapter.

The slabs are divided into three groups. The first group is Series 1 which is made of four slabs designated as GS1, GS2, GS3 and GS4. These slabs have normal depths (150 mm), normal strength concrete and GFRP reinforcing bars. The second group is Series 2 which contains the two slabs GSHD1 and GSHD2. The slabs of this group have higher depth (200 mm), normal strength concrete and GFRP bars. The third group is Series 3 which includes slabs GSHS1 and GSHS2. These slabs are with normal depth, high strength concrete and GFRP bars. In addition, one reference slab, R1, was tested. This slab is with higher depth, normal strength concrete and steel reinforcements. Actually, R1 is a reference slab to examine how the FRP reinforced slabs differ in behaviour than steel reinforced slabs. The reason only one reference slab was selected is that, experimental

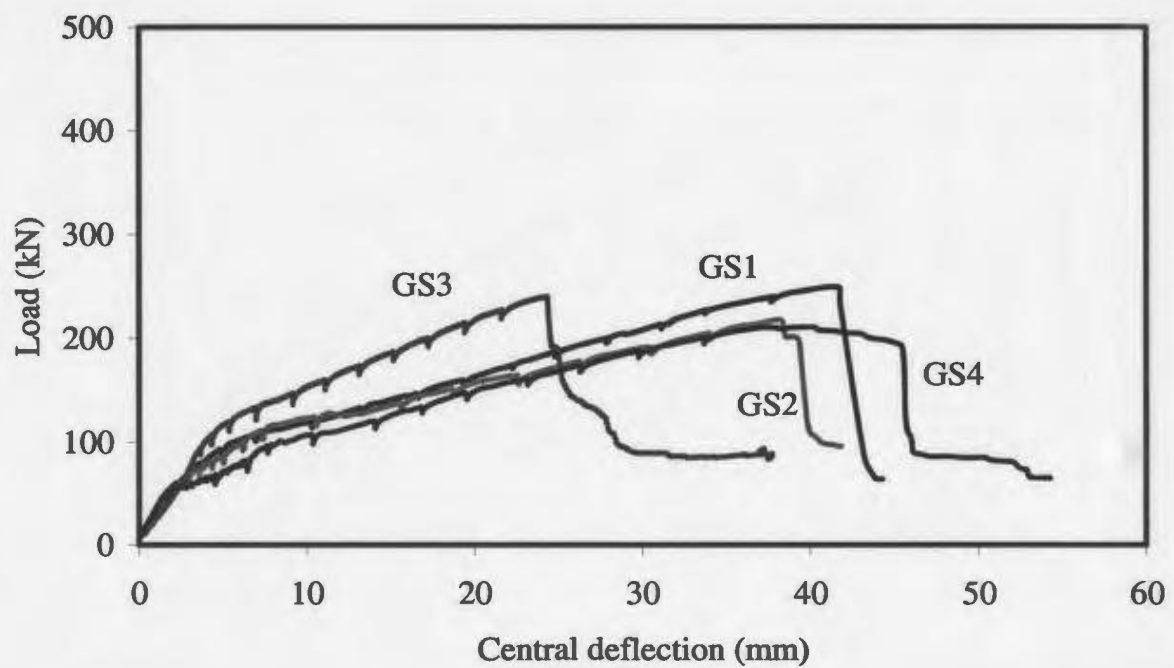
**Table 4.1: Slab details and observed ultimate loads**

	Material of bars	Slab designation.	Concrete comp. strength $f_c$ (MPa)	Bar dia. $\phi$ (mm)	Bar spacing $S$ (mm)	c $c_1 = c_2$ (mm)	Slab thickness $h$ (mm)	Effective depth $d$ (mm)	Rein. ratio $\rho$ (%)	$\rho/\rho_b$	Ultimate load
											$P_u^*$ (kN)
Series 1	GFRP	GS1	40	19	240	250	150	100	1.18	1.4	249
	GFRP	GS2	35	19	270	250	150	100	1.05	1.4	218
	GFRP	GS3	29	19	170	250	150	100	1.67	2.7	240
	GFRP	GS4	26	19	300	250	150	100	0.95	1.7	210
Series 2	GFRP	GSHD1	33	19	170	250	200	150	1.11	1.6	436
	GFRP	GSHD2	34	19	240	250	200	150	0.79	1.1	389
Series 3	GFRP	GSHS1	92	19	170	250	150	100	1.67	1.1	408
	GFRP	GSHS2	86	19	240	250	150	100	1.18	0.8	333
Ref.	Steel	R1	23	16	240	250	200	154	0.54	0.2	491

\* The ultimate load does not include the own weight of the slab.

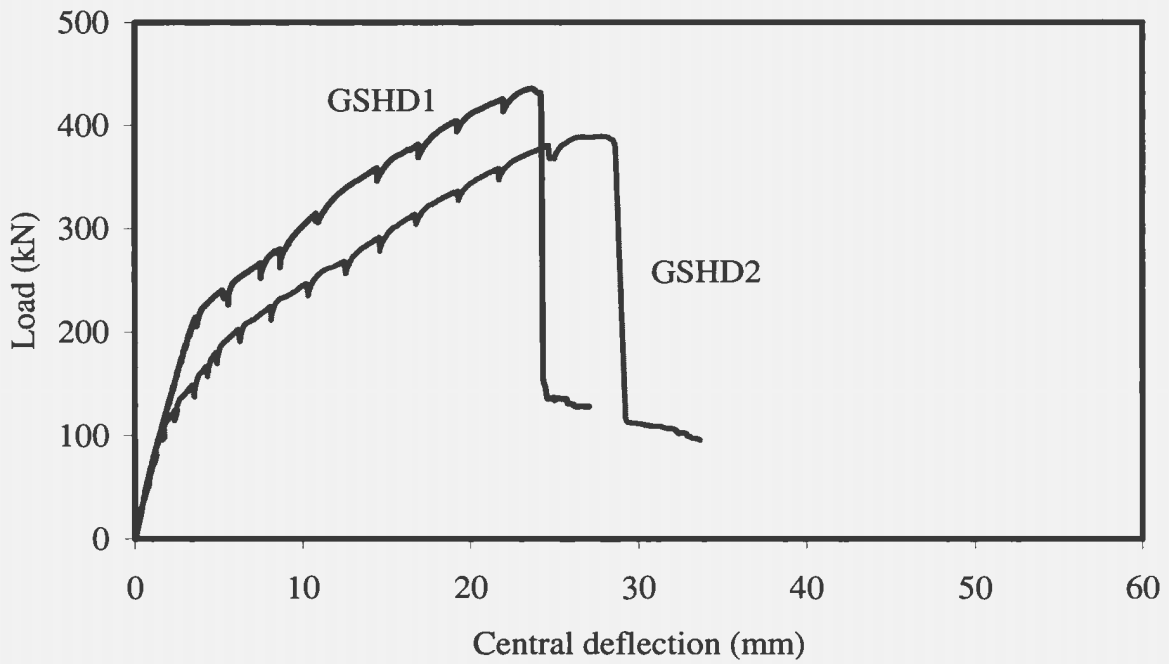


(a) Reference slab (R1)

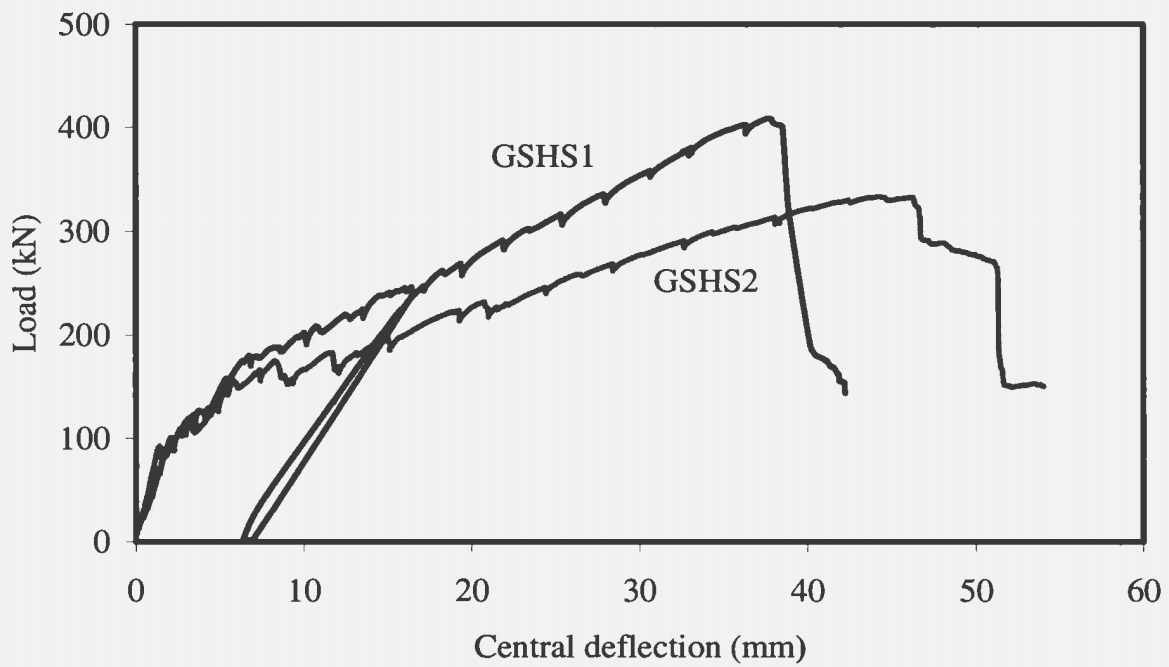


(b) Series 1 slabs

Fig. 4.1: Load-deflection history



(c) Series 2 slabs



(d) Series 3 slabs

**Fig. 4.1: Load-deflection history (contd.)**

results are available from previous tests at MUN on 150 mm thick slabs reinforced with traditional steel reinforcement [Marzouk *et al.* (1998) and Osman *et al.*(2000)]. The details of the test slabs are given in Table 4.1.

## 4.2 Load-deflection characteristics

The test program was carried out using a displacement controlled system. The process of displacement application was described in section 3.10. Real-time load and displacement readings were collected using a data acquisition system. The load-deflection graphs are shown in Fig. 4.1. At the time of testing, the load was paused at certain intervals to take the dial gauge reading and to mark and measure the cracks. When the system was put on hold, the load reading was decreased slightly due to the relaxation of the slab's internal stresses. For that reason, the load-deflection graphs are not very smooth. However, this will not affect the ultimate load and deflection.

The load deflection characteristics for the FRP slabs showed a completely different nature than steel reinforced slabs. The load-deflection graph is almost a bilinear curve. The initial part of the graph is almost a straight line with a higher slope which represents the stiffness of the un-cracked slab. After a certain load level, the graph changes to another straight line with a comparatively lower slope which represents the stiffness of the cracked slab. Stiffness represents the amount of load needed for unit displacement at the slab center. The transition between these two lines is not abrupt; it is rather a smooth transition. This indicates that the slab does not completely lose its un-cracked stiffness once the first crack is formed. When the first crack forms, the slab starts to lose its un-

cracked stiffness. When a significant number of cracks form, the slab completely loses its un-cracked stiffness. At that stage, the cracked stiffness governs, which represents the second straight line of the load-deflection curve. The obtained load-deflection graphs are similar in nature to those reported by Ospina *et al* (2003). In the case of a steel reinforced slab, the change in stiffness is gradual. The nature of the load-deflection graph nature is not bilinear like FRP reinforced slab [see Fig. 4.1(a)].

In Table 4.2, the un-cracked stiffness, cracked stiffness and ultimate deflection of the slabs are given. The results given in Table 4.2 reveals that the un-cracked stiffness of Series 1 slabs are almost the same though the slabs have different reinforcement ratios. However, the un-cracked stiffness of Series 2 and 3 slabs are significantly higher. This indicates that the slab stiffness in this un-cracked stage depends on the concrete strength and the slab depth. The reinforcement ratio has negligible effect on the slab stiffness in this stage. In general, the cracked stiffness of a slab is proportional to the reinforcement ratio. The ultimate deflection of a slab is inversely proportional to its reinforcement ratio.

The load deflection graph could give an indication of the failure mode of a slab [Hussein (1990)]. From the load deflection graphs shown in Fig. 4.1 one can notice that all slabs, except GS4, GSHD2 and GSHS2, show positive slope up to failure load and that failure appears to be a sudden one. This is a sign of punching failure. Slab GS4 showed significant negative slope before failure which could be a sign of flexural failure. Slabs GSHD2 and GSHS2 showed ductile punching failure signs with low slopes before failure.

The ultimate deflection of FRP reinforced slabs is higher than the steel reinforced slab. Various authors in the literature also reported this [Matthys and Taerwe (2000), Ospina *et al.* (2000)]. This is due to the low modulus of elasticity of FRP bars.

**Table 4.2: Slab stiffness and ultimate deflection**

Slab designation		Uncracked stiffness (kN/mm)	Cracked stiffness (kN/mm)	Ultimate deflection (mm)
Series 1	GS1	24.8	4.8	41.8
	GS2	25.5	3.5	38.4
	GS3	25.7	6.3	24.4
	GS4	21.9	3.78	45.4
Series 2	GSHD1	56.8	11.3	24.2
	GSHD2	55.0	8.6	28.6
Series 3	GSHS1	49.3	8.4	38.5
	GSHS2	60.1	4.4	46.3

### **4.3 Ductility and energy absorption**

Ductility is a term which reflects the deformation capacity of a structural member before failure. However, it is a relative measurement. For different structural members, different deformation could be used to indicate the ductility measure.

The ductility of a steel reinforced concrete slab is the ratio of the ultimate deflection to the deflection at the first yielding of flexural reinforcement. However, FRP reinforcement does not yield. The ductility for FRP reinforced slab could be defined as the ratio of the ultimate deflection to the deflection value that corresponds to the slab losing its initial stiffness. The energy absorption of a slab is defined as the area under the load deflection curve up to failure.

The results of Series 1 revealed that both the ductility and energy absorption capacity decreased as the reinforcement ratio was increased (see Table 4.3). This trend is found from the current experimental program. However, to ensure this trend, more than one laboratory should confirm the trend.

Slabs GS3, GSHD1 and GSHS1 have equal area of reinforcement. Similarly, slabs GS1, GSHD2 and GSHS2 have equal area of reinforcement. The results of the two series reveal that the change in depth and concrete strength has significant effect on the ductility and energy absorption capacity. Table 4.3 shows that 33% increase in slab depth would increase the ductility by 90% and energy absorption by 60% on average. Again, 170% increase in the concrete strength increases the ductility by 300% and energy absorption

by 125% on average. This indicates that increasing the slab depth or the concrete strength could improve the performance of the slab.

**Table 4.3: Ductility and energy absorption capacity**

Slab	Concrete strength $f'_c$ (MPa)	Reinforcement ratio $\rho$ (%)	Ductility $\Delta_c / \Delta_u$	Energy absorption capacity (kN.mm x 10 <sup>3</sup> )
GS1	40	1.18	6.3	5.8
GS2	35	1.05	4.9	5.4
GS3	29	1.67	4.2	3.7
GS4	26	0.95	20.3	6.1
GSHD1	33	1.11	6.6	7.0
GSHD2	34	0.79	14.3	7.5
GSHS1	92	1.67	10.0	9.4
GSHS2	86	1.18	35.4	11.7
R1	23	0.54	2.9*	7.4

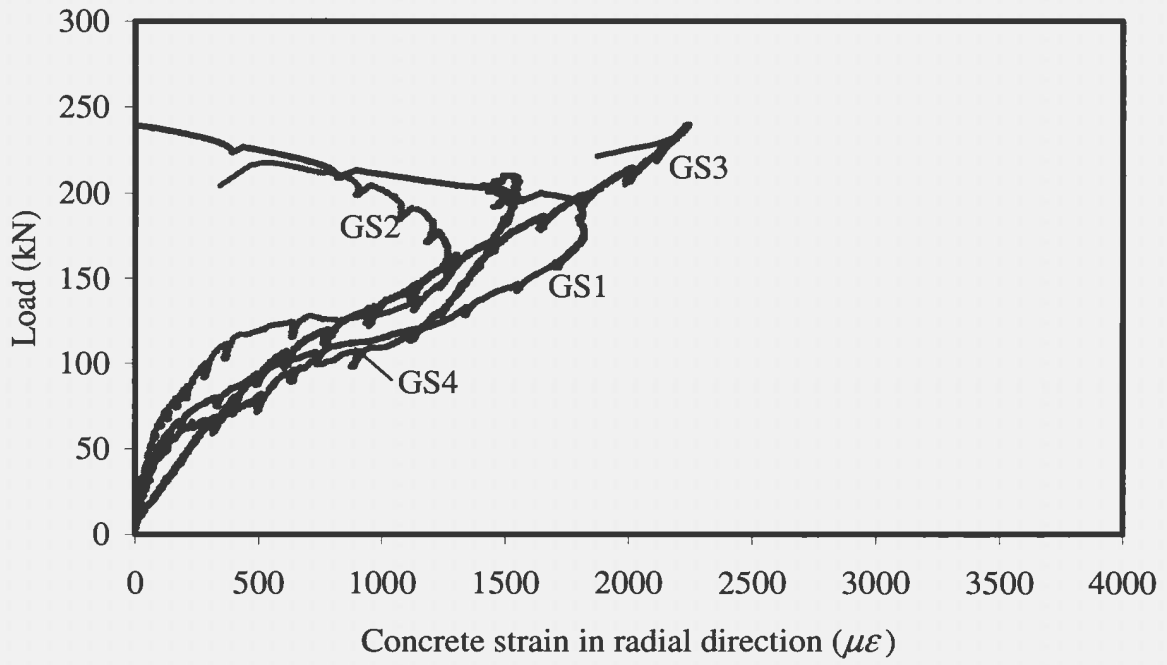
\* Ratio of ultimate deflection to first yield deflection.

## 4.4 Concrete strains

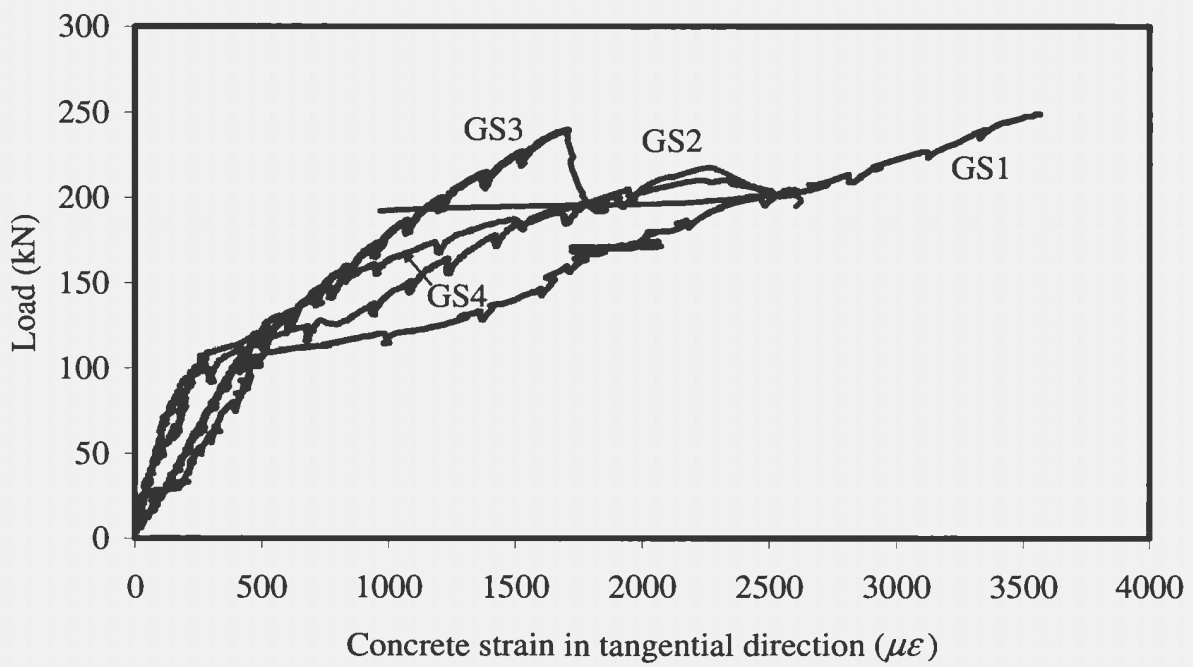
The concrete strains were measured at various locations as described in Section 3.8.4. These locations were selected to measure the radial and tangential concrete strains along a diagonal line as well as a radial line that coincides with the center line of the slab. The main objective of recording the tangential and radial concrete strain is to compare their magnitude and to calculate the ratio between them at the time of failure. Thus, concrete strain gauges were set at the critical points, as close as possible, where the radial and tangential strains are expected to be maximum.

Fig. 4.2 shows the radial and tangential concrete strains for all test slabs. The strains are for gauges 2 and 3 (shown in Fig. 3.15). The tangential strains in slabs GS1 and R1 reached  $3500 \mu\epsilon$  which is the theoretical crushing of concrete. However, there was no physical damage at these locations which could be identified by the naked eye. It seems that the theoretical crushing strain of concrete could exceed  $3500 \mu\epsilon$ .

The radial strain increased as the load was increased at the initial stages. After a certain load level, which is close to ultimate load, the strain started to decrease in most slabs. Some slabs, such as the high strength concrete slabs, the reference slab (R1), GS3 and GS4 did not follow the same exact trend. Nevertheless, this observation of the radial concrete strain is not uncommon in literature. Hallgren (1996) reported similar behaviour for high strength concrete slabs reinforced with traditional steel reinforcement.

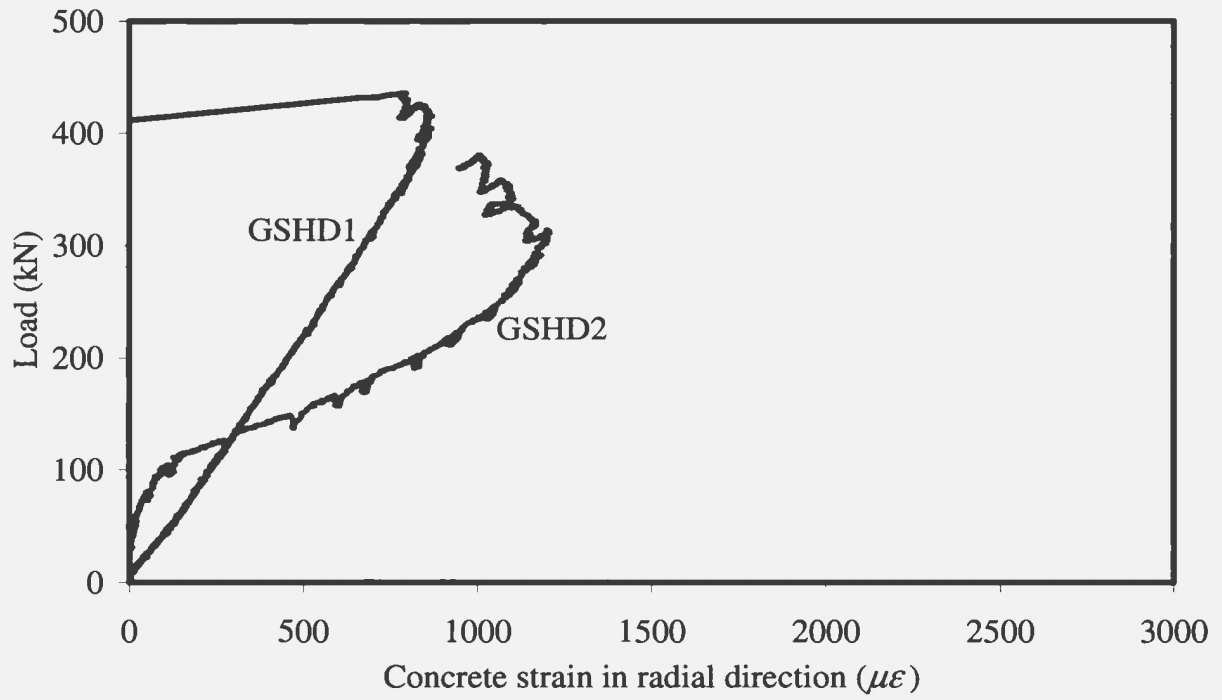


(a) Radial strains of Series 1 slabs

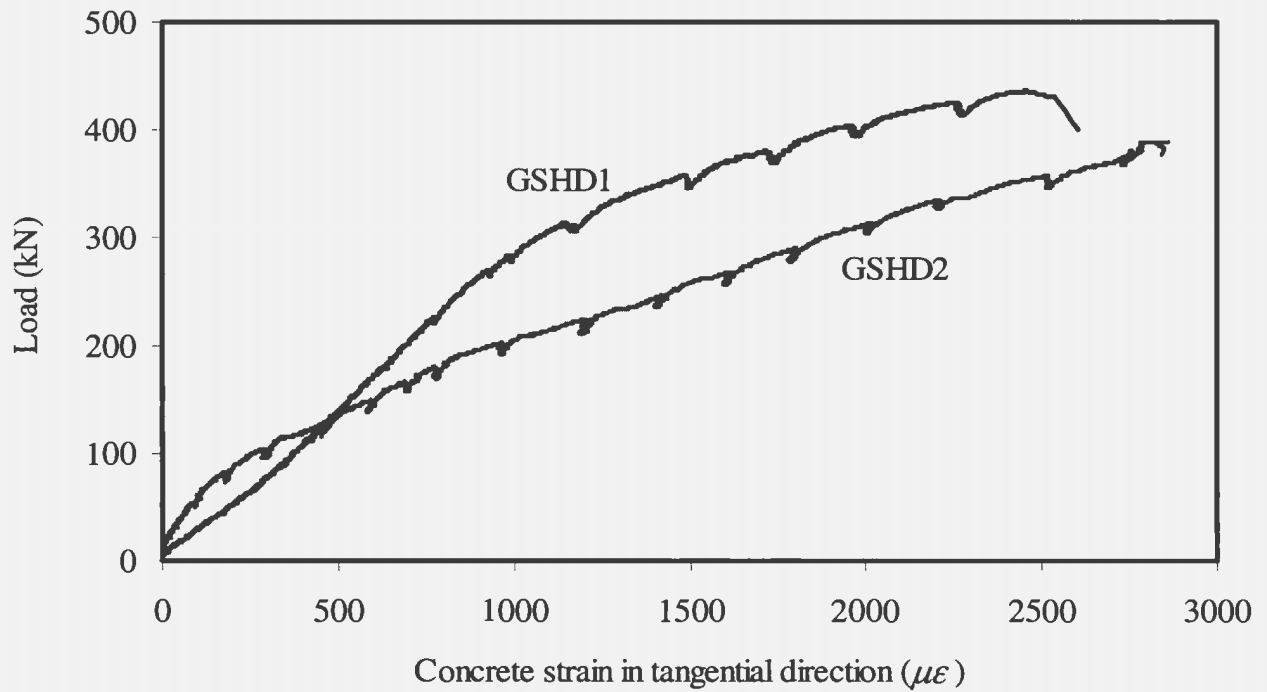


(b) Tangential strains of Series 1 slabs

Fig. 4.2: Radial and tangential concrete strains

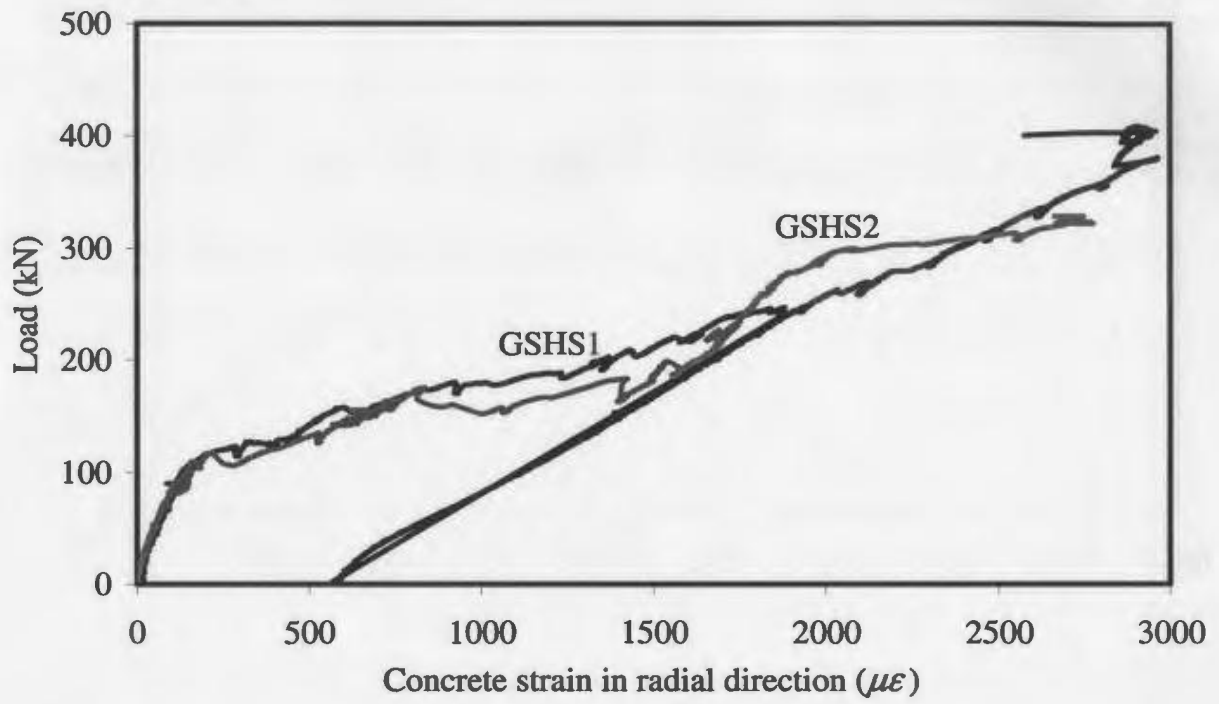


(c) Radial strains of Series 2 slabs

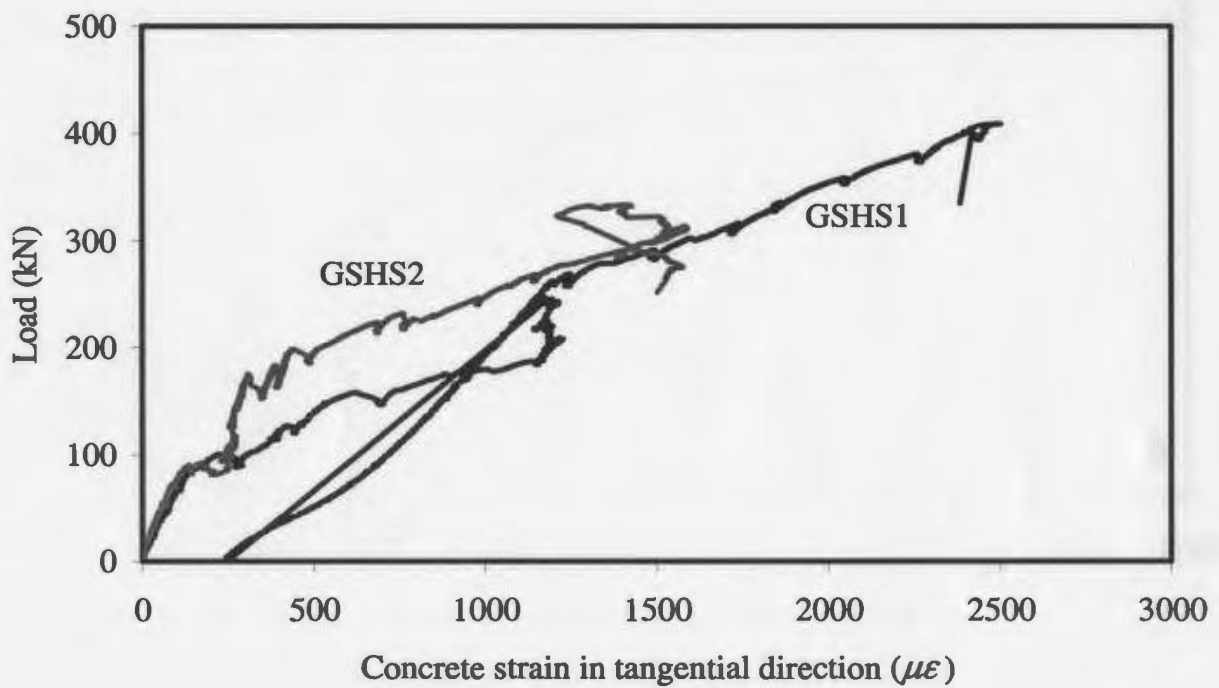


(d) Tangential strains of Series 2 slabs

Fig.4.2: Radial and tangential concrete strains (contd.)

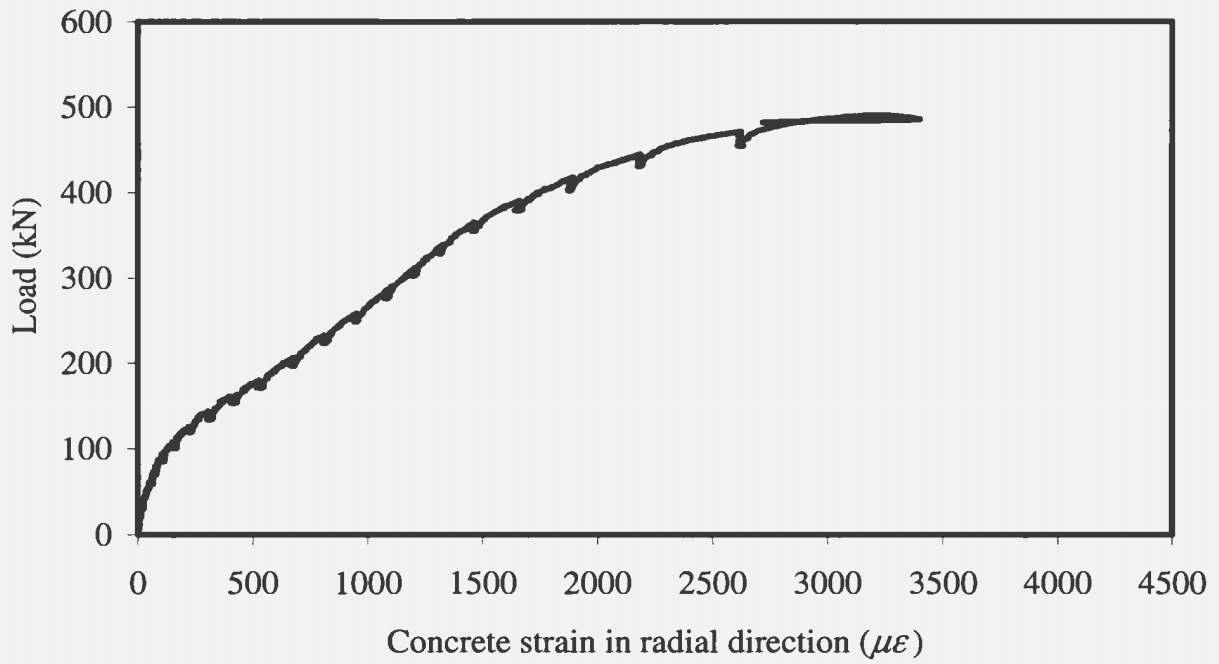


(e) Radial strains of Series 3 slabs

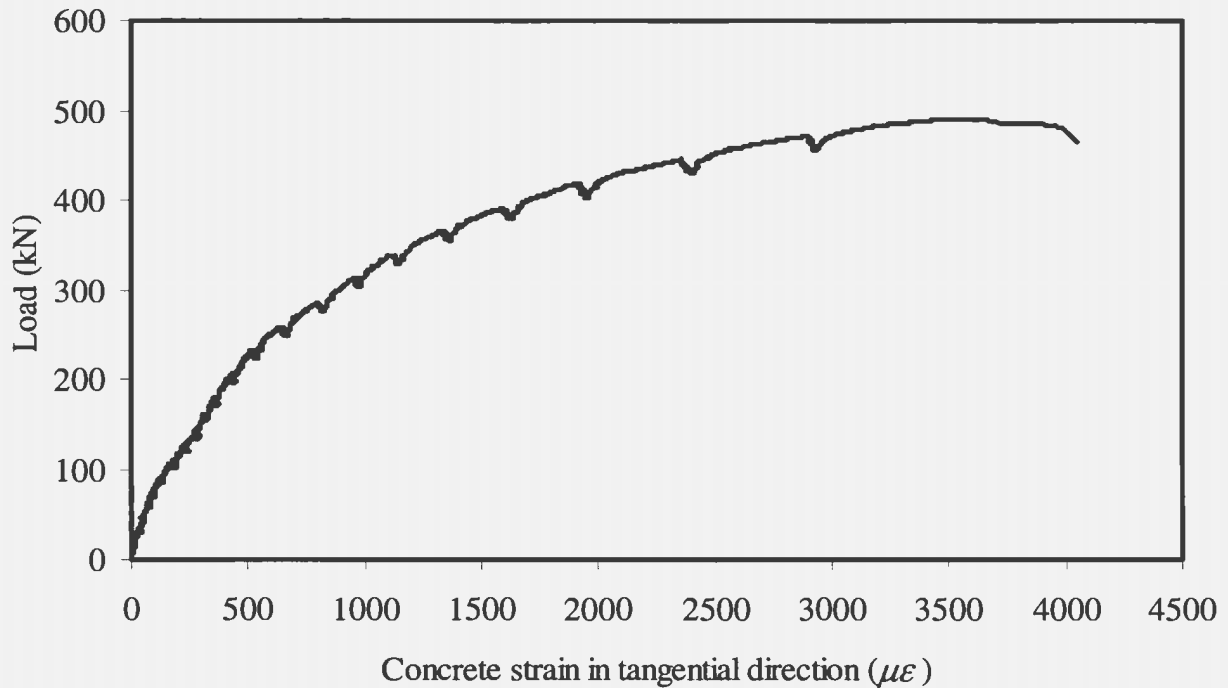


(f) Tangential strains of Series 3 slabs

Fig.4.2: Radial and tangential concrete strains (contd.)



**(g) Radial strain of reference slab R1**



**(h) Tangential strain of reference slab R1**

**Fig.4.2: Radial and tangential concrete strains (contd.)**

An explanation of this behaviour could be attributed to the strain redistribution in the concrete. If two parallel cracks develop on the tension face at a certain load level, the crack width and depth will increase gradually. On the other hand, compressive stress concentration could develop at directly opposite points of these tension cracks at the same time. Thus, stress concentration could develop along two parallel lines, on the compression side and the stress concentration could gradually rise. At the same time, the concrete between these two lines may experience gradual stress relaxation.

Figure 4.3 is used to illustrate that point. Consider a member under very low bending moment as shown in Fig. 4.3(a). No crack has developed yet and the strain in tension and compression zone is low. Accordingly, the compressive strain reading,  $S$ , in the strain gauge at this compression side is in the elastic range. As the bending moment is increased, shallow depth cracks will develop at points  $C$  and  $D$  [Fig. 4.3(b)]. The strain values at points  $C'$  and  $D'$  will be close to the strain value,  $S'$ .

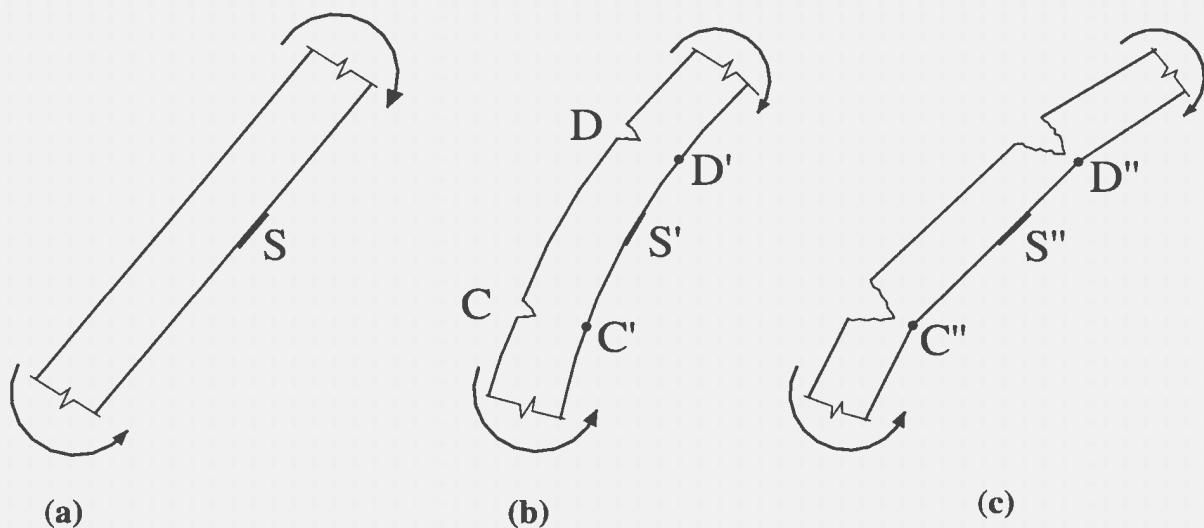


**Fig. 4.3: Strain level and the propagation of crack depth**

In the third stage [Fig. 4.3(c)], the applied bending moment is the highest. Deep cracks will develop, and thus producing stress concentrations at points C" and D". The points between C" and D" will exhibit relatively lower strain, as the curvature is lower in between C" and D". Therefore, strain gauge reading S" will be less than S' even though applied moment is higher.

The above example is for a member under one way flexure action. Nevertheless, a similar situation may occur in two way concrete slabs in particular radial direction. This could explain the strain reduction after a certain load is achieved. Slabs GS3 and GS4 of Series 1 showed slightly different behaviour. Slab GS3 is highly reinforced and the ultimate deflection is less. It seems that the previous phenomenon may occur after a certain deflection, when the circumferential tensile cracks become much deeper. The following test data could support this explanation. In slab GS1, the concrete radial strain started to decrease at a load level of 174 kN and the deflection was 24 mm. In slab GS2, the concrete radial strain started to decrease at a load level of 160 kN and the deflection was 23 mm. However, slab GS3 failed at a deflection value of 25.1 mm and slab R1 failed at 24.3 mm deflection.

Slab GS4 did not show significant strain reduction though its ultimate deflection was more than 24 mm. Most of the major cracks on the tension face of the slab were in the radial direction. There was no significant crack in the circumferential direction which is important to produce the above described phenomenon. The high strength concrete slabs did not show this kind of phenomenon for the same reason. In slab GS4, although the

radial strain is not decreasing, the strain did not increase as expected compared to the tangential strain. This could mean that the strain reduction phenomenon still occurred for this slab [see Fig. 4.4(d)].

In conclusion, it can be stated that for radial concrete strains, all slabs showed this kind of phenomenon. The corresponding deflection was approximately 24 mm. This behaviour becomes pronounced if some significant circumferential cracks, which are almost parallel, develop on the tension face.

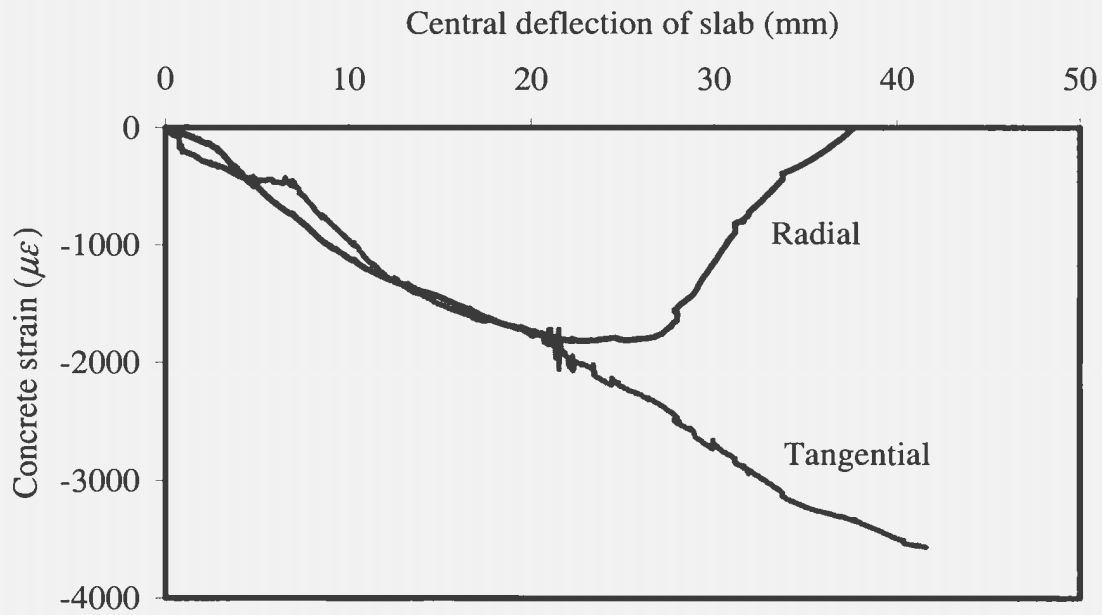
The variations of the radial and tangential concrete strains with respect to the central deflection are shown in Fig. 4.4. The tangential concrete strain increases as the deflection increases up to failure. After a certain deflection, the rate of strain increase becomes slower and after a certain deflection the rate became negative. This decrease in strain could be attributed to the stress relaxation. The stress relaxation is a function of circumferential cracks. The formation of a circumferential crack depends mainly on the deflection. In addition to deflection, it depends on the concrete strength, arrangement of reinforcement, slab depth etc. It is not possible to predict at which level of deflection the stress relaxation in the radial direction starts. Further research is needed to determine these levels. The radial concrete stress relaxation is an important phenomenon for two-way slab reinforced with GFRP. This is due to the low modulus of elasticity of the GFRP bars and the associated high deflections. From the current experimental results, it appears that the radial stress relaxation started at 20 mm deflection for the 150 mm thick normal

strength concrete slabs and at 12 mm deflection for the 200 mm thick normal strength slabs. For high strength concrete slabs, no stress relaxation was observed.

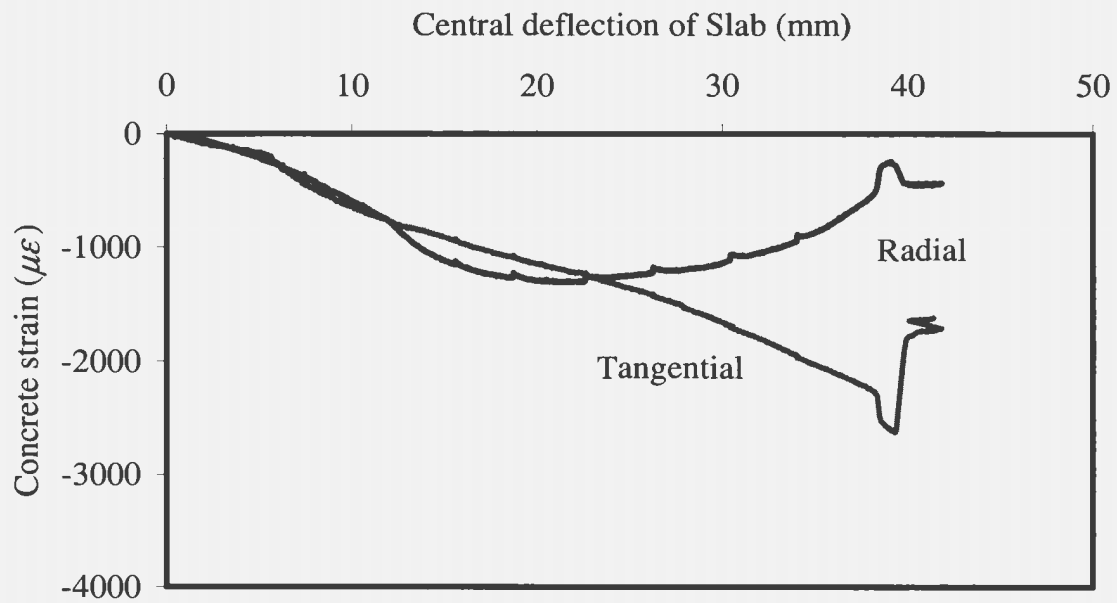
One objective of measuring the tangential and radial concrete strains was to obtain the maximum radial and tangential concrete strain at the time of failure. However, as the test results revealed, the maximum radial strain did not occur at the time of failure. Besides, radial stress relaxation occurred in some slabs. Therefore, it is not possible to calculate any ratio between the maximum radial and tangential concrete strain at failure.

**Table 4.4: Concrete strains**

Slab	Failure load (kN)	Radial		Tangential	
		Strain ( $\mu\epsilon$ )	Load level as % of failure load	Strain ( $\mu\epsilon$ )	Load level as % of failure load
GS1	249	1816	72	3566	100
GS2	218	1302	75	2289	100
GS3	240	2234	100	1707	100
GS4	210	1560	98	2513	95
GSHD1	436	860	96	2533	99
GSHD2	389	1199	80	2848	100
GSHS1	408	2950	99	2482	100
GSHS2	333	2747	98	1585	94
R1	491	3400	99	3673	100

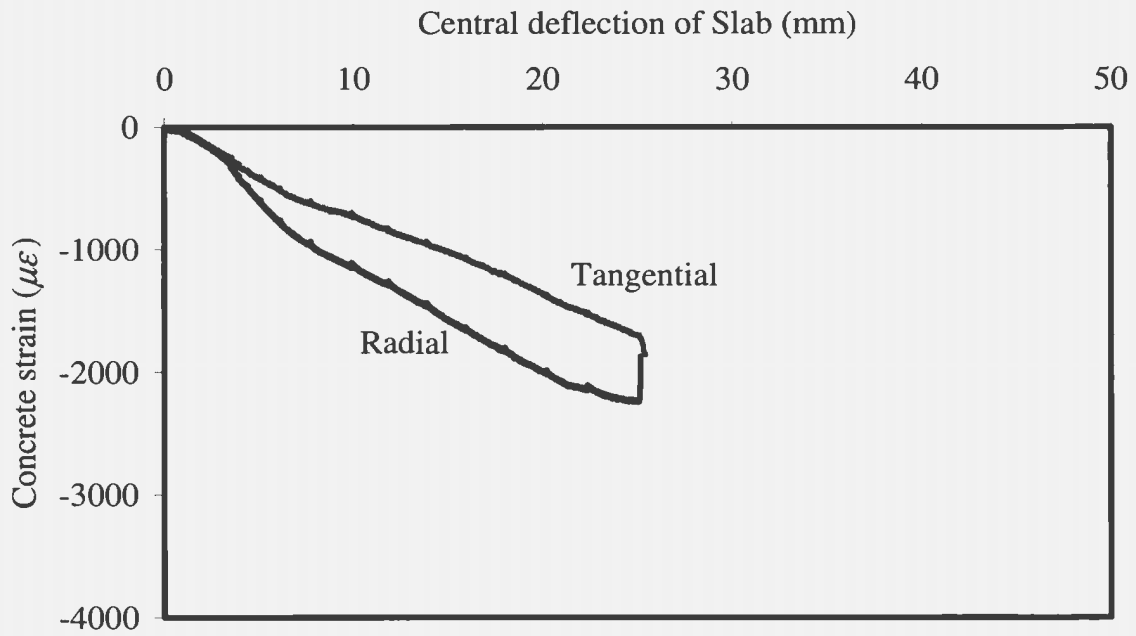


(a) Slab GS1

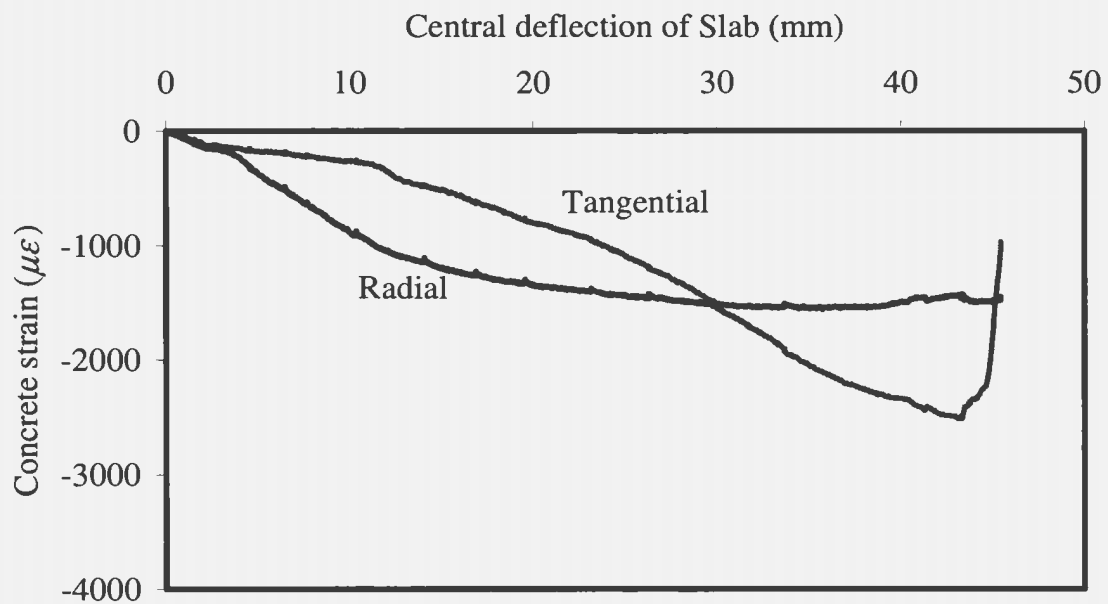


(b) Slab GS2

**Fig. 4.4: Variation of radial and tangential concrete strain w.r.t. deflection of the slab center**

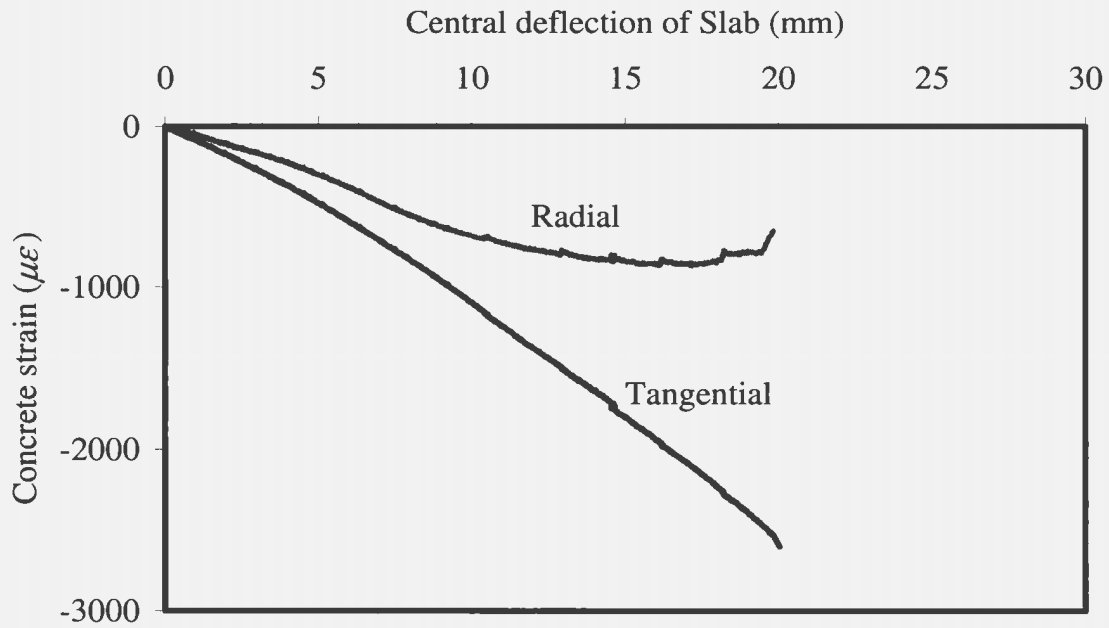


(c) Slab GS3

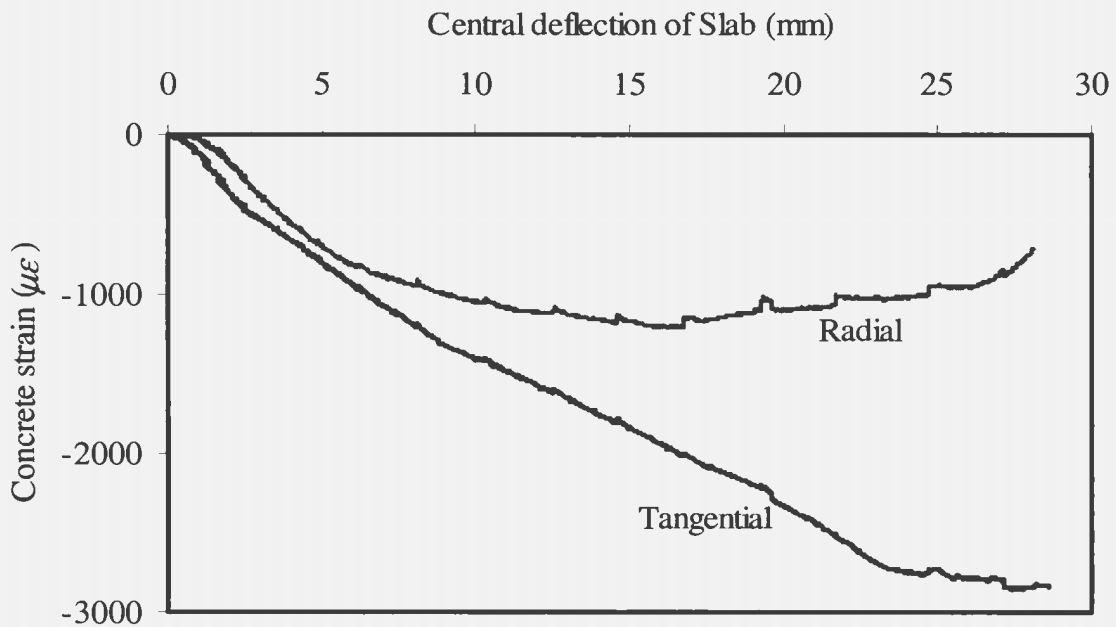


(d) Slab GS4

**Fig. 4.4: Variation of radial and tangential concrete strain w.r.t. deflection of the slab center (contd.)**



(e) Slab GSHD1



(f) Slab GSHD2

**Fig. 4.4: Variation of radial and tangential concrete strain w.r.t. deflection of the slab center (contd.)**

## 4.5 FRP strains

The strain gauge locations on the FRP reinforcement are described in Section 3.8.3. The strain gauge locations were selected to measure the maximum strains in the FRP reinforcement during the test and to obtain the strain profile in the radial and tangential directions of the slabs.

All slabs had an over reinforced section capacity, except GSHS2. The balanced reinforcement ratio was calculated considering the section under one-way flexure and strain compatibility. It was anticipated that the maximum strain of the FRP bars will not exceed their ultimate strain at the time of failure. The ultimate strain of the FRP bars is around  $15000 \mu\epsilon$ . The strain gauges used in the current study were able to measure strain values that were slightly more than  $7000 \mu\epsilon$ . Consequently it was not possible to measure the exact maximum FRP strain at the time of failure for few slabs. The load versus strain graphs are shown in Fig. 4.5. All the graphs are similar in nature. Slabs GS3 and GSHD1 showed slight inconsistencies. Initially, the slope of the load-strain graph is very high and after a certain load level the slope gradually decreased. This could be attributed to the concrete contribution at the initial stage. Most of the tensile strain was resisted by concrete. When cracks started to develop, with significant crack width and depth, the FRP bars started to take the load and the strain started to increase.

The maximum FRP strains measured in the radial and tangential direction are given in Table 4.5. The recorded strain values are presented along with the corresponding load

level as a percentage of the failure load. The maximum radial strains occurred at the face of the column.

The strain is always measured in the direction of the bar axis. The tangential FRP strain refers to the position of a strain gauge on a bar layout in such a way that the gauge axis as well as the bar axis are oriented in a direction which is perpendicular to a radial line of slab. Thus, the tangential direction term indicates the tangential direction on the slab not the tangential direction of FRP bar. For example, in Fig. 3.14 strain gauges 5, 10 and 11 measure the tangential FRP strain. The radial FRP strain refers to the gauge axis as well as the bar axis that is oriented in a radial line of the slab. For example, strain gauges 1, 2, 3, 4, 6 and 9 are used to measure the radial FRP strain.

Strain gauges were also used to check if any anchorage failure occurred in the reinforcement. It is not possible to bend the FRP bars or to make a hook at the end of bars like traditional steel bars. Hence, it is possible to have anchorage failure. Two strain gauges were set at the end of the most critical bars (which pass through the slab center) in both directions. If there is any anchorage failure, the strain at the end of the bar will decrease suddenly and a jump in the load-strain graph would be noticed. In Fig. 4.6, the load-strain graphs at the end of the critical FRP bars are plotted. The graphs show no indication of anchorage failure. That indicates that the FRP bars used in this test program had sufficient bond strength.

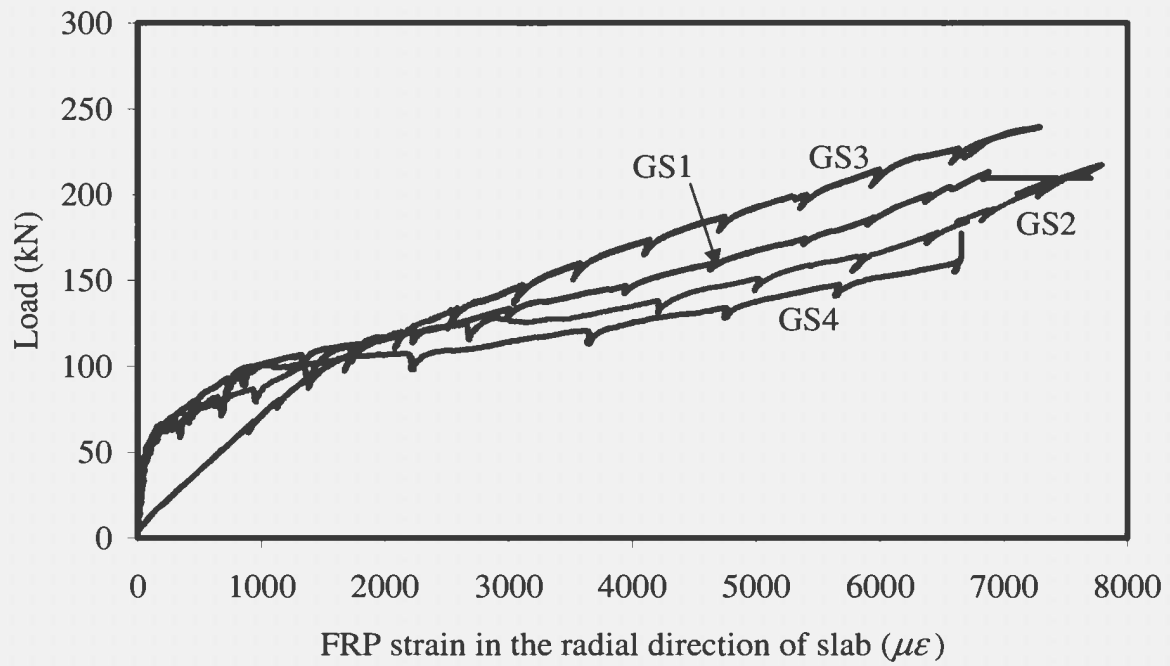
Figure 4.7 shows the typical strain profiles of FRP bars in a radial direction. The figures reveal that the strain is inversely proportional to the distance from slab center. This

behaviour is similar to that observed by Kinnunen and Nylander (1960) for steel-reinforced slabs. The strain is higher around the column up to a certain distance, and then it drops significantly. Thus, the observations support the inverse relationship of radial strain and distance from slab center.

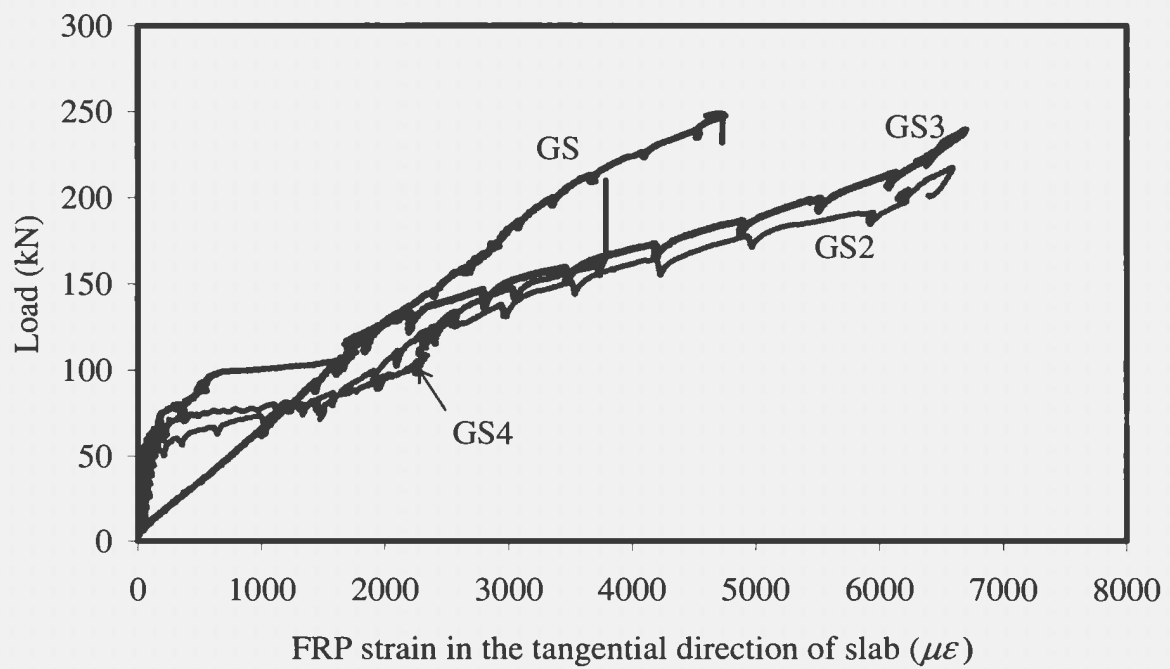
FRP strain profiles in a tangential direction are shown in Fig. 4.8. The strain profile also shows the inverse relation with distance from slab center. In the development of their mechanical model, Kinnunen and Nylander (1960) assumed that the tangential strain in the slab reinforcement (regardless whether ring or grid type) is inversely proportional to

**Table 4.5: FRP strains**

Slab	Failure load (kN)	Radial (Max.)		Tangential (Max.)	
		Strain ( $\mu\epsilon$ )	Load level as % of failure load	Strain ( $\mu\epsilon$ )	Load level as % of failure load
GS1	249	6857	85	4734	100
GS2	218	7754	100	6590	100
GS3	240	7250	100	6668	100
GS4	210	6653	77	3787	79
GSHD1	436	5877	100	5843	100
GSHD2	389	8668	100	5983	100
GSHS1	408	11520	100	9666	100
GSHS2	333	9628	90	7875	100
R1	491	7555	93	2374	100

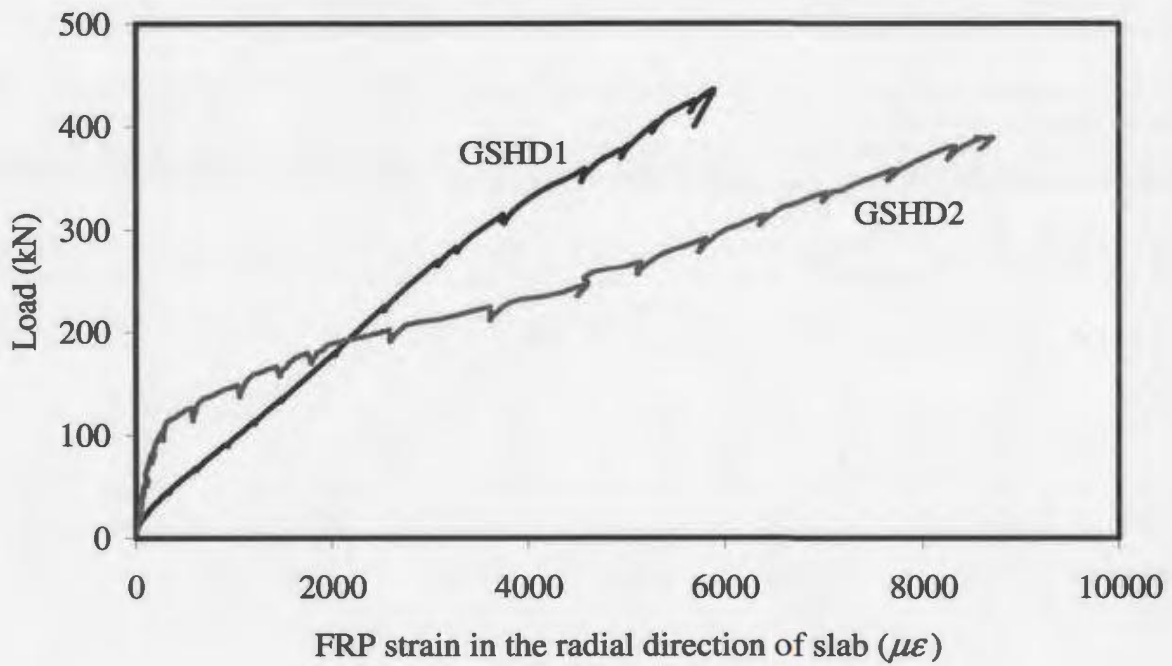


(a) Radial strains of Series 1 slabs

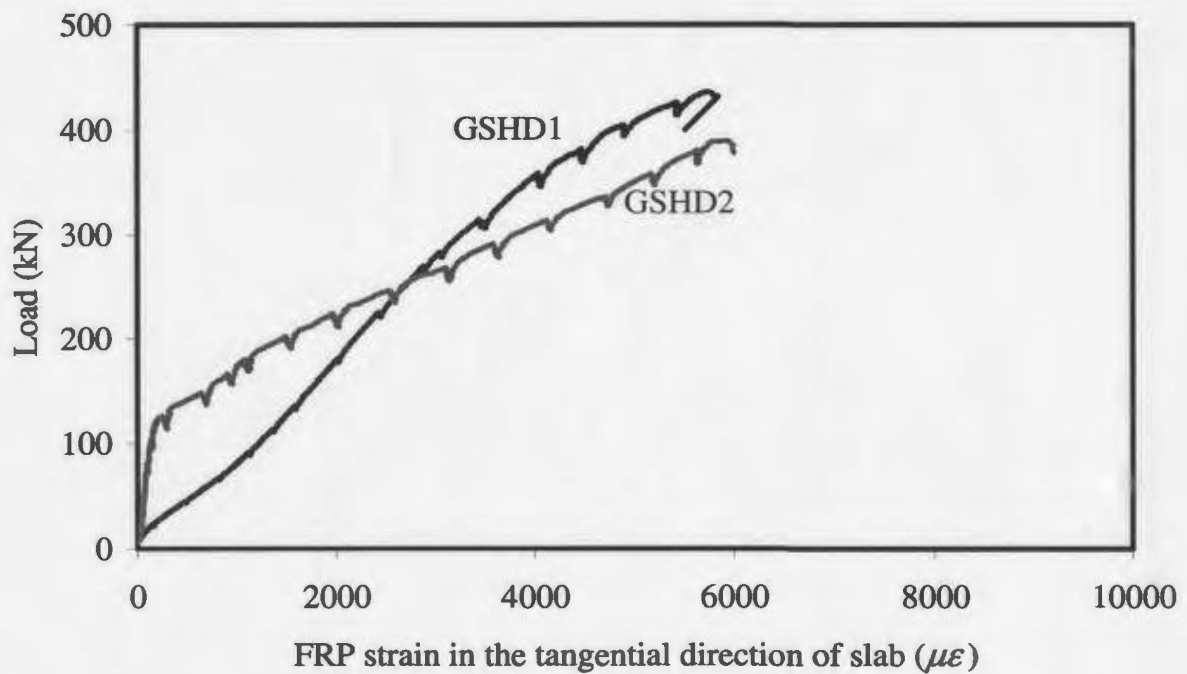


(b) Tangential strains of Series 1 slabs

Fig. 4.5: Radial and tangential FRP strains

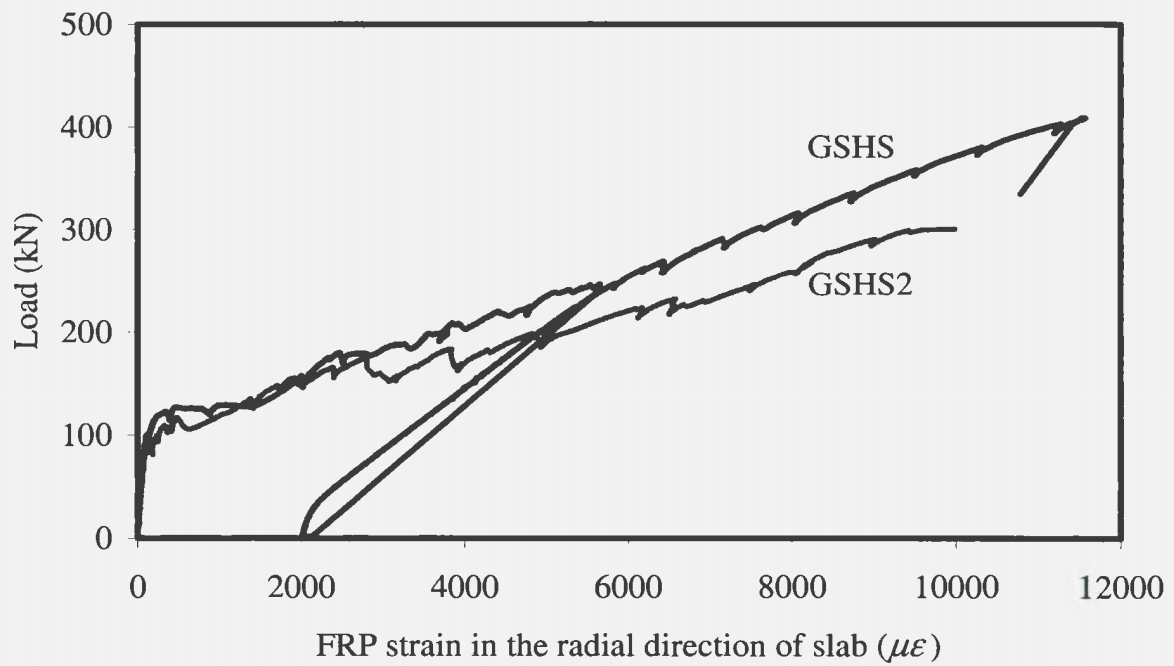


(c) Radial strains of Series 2 slabs

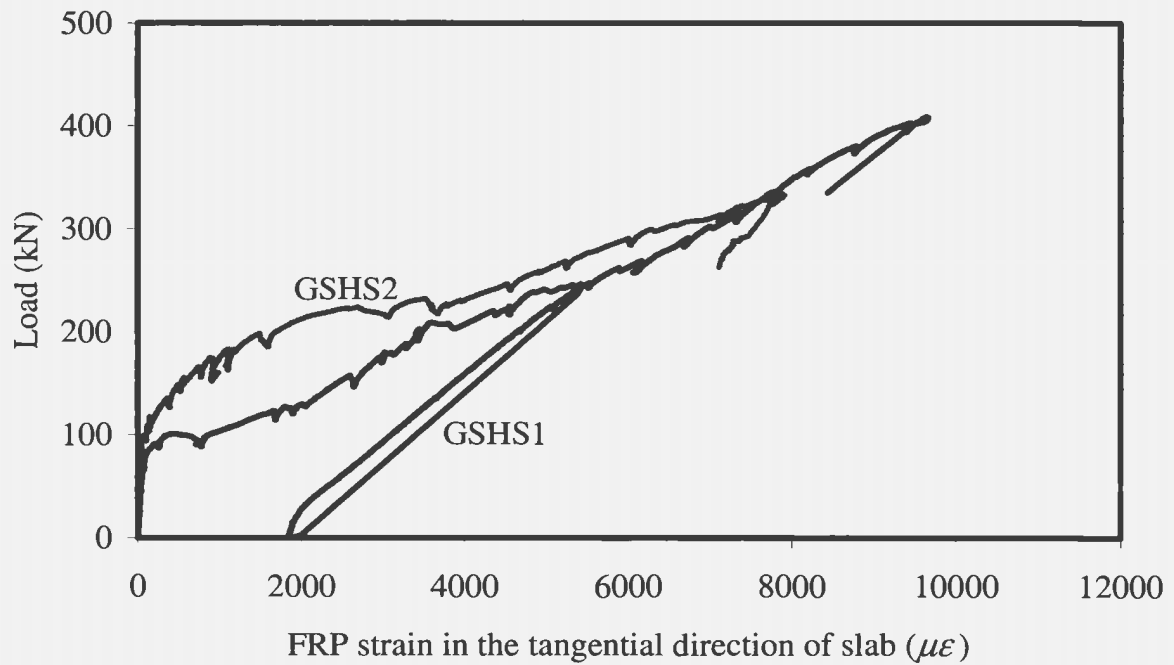


(d) Tangential strains of Series 2 slabs

Fig. 4.5: Radial and tangential FRP strains (contd.)

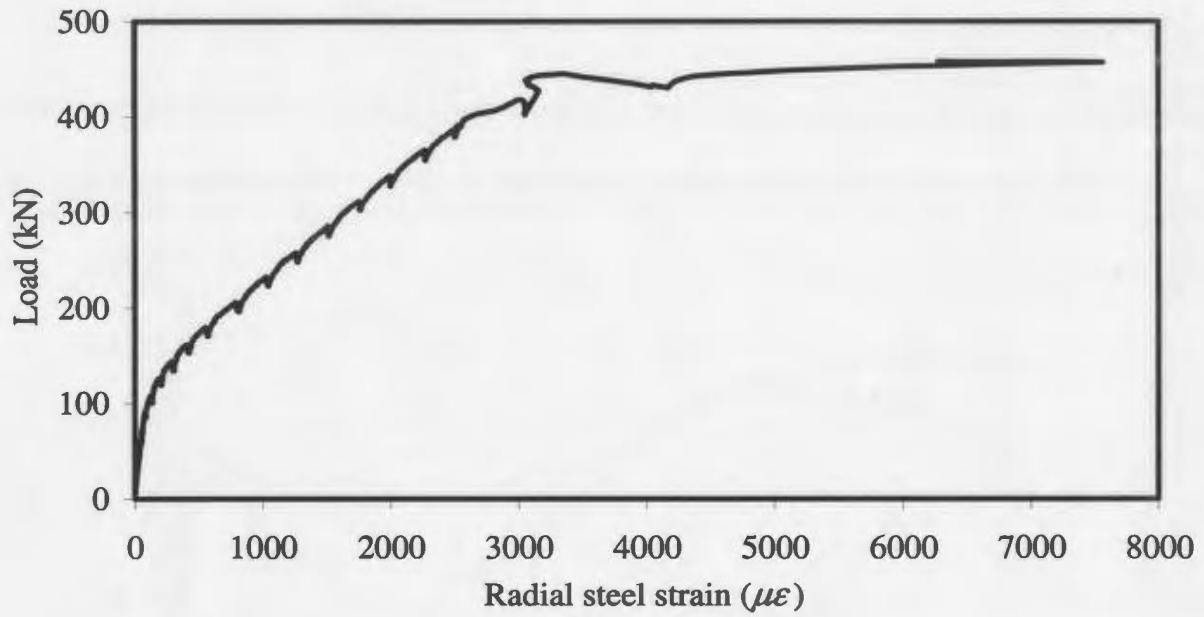


(e) Radial strains of Series 3 slabs

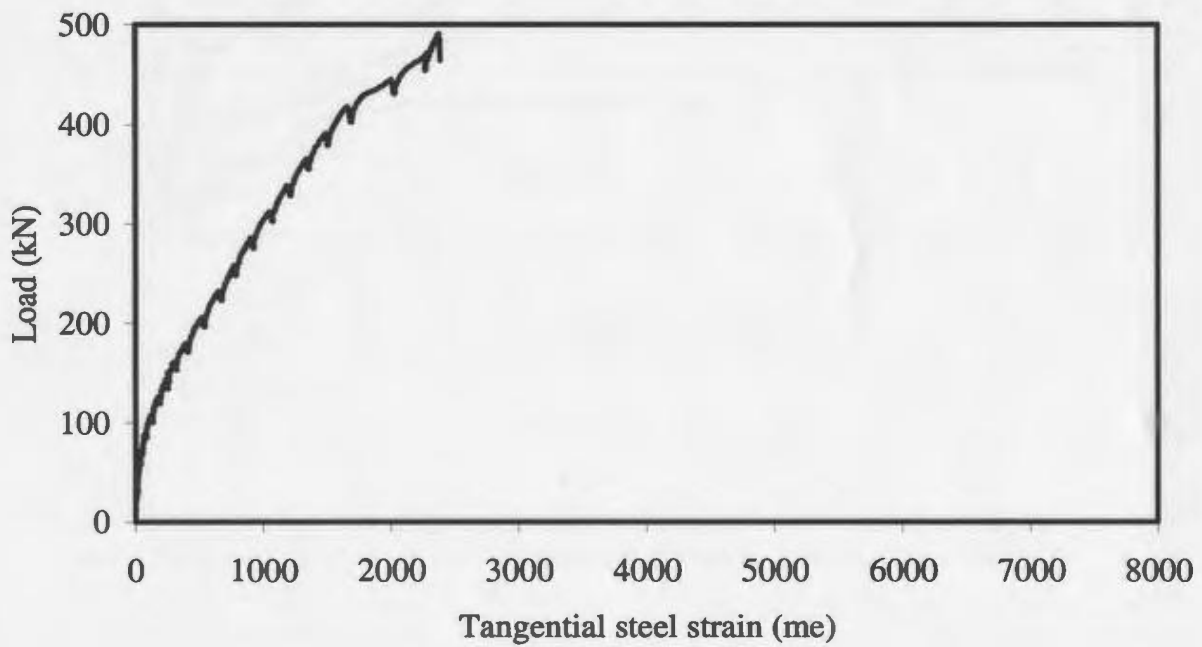


(f) Tangential strains of Series 3 slabs

Fig. 4.5: Radial and tangential FRP strains (contd.)



(g) Radial strain of Slab R1



(h) Tangential strain of Slab R1

Fig. 4.5: Radial and tangential FRP strains (contd.)

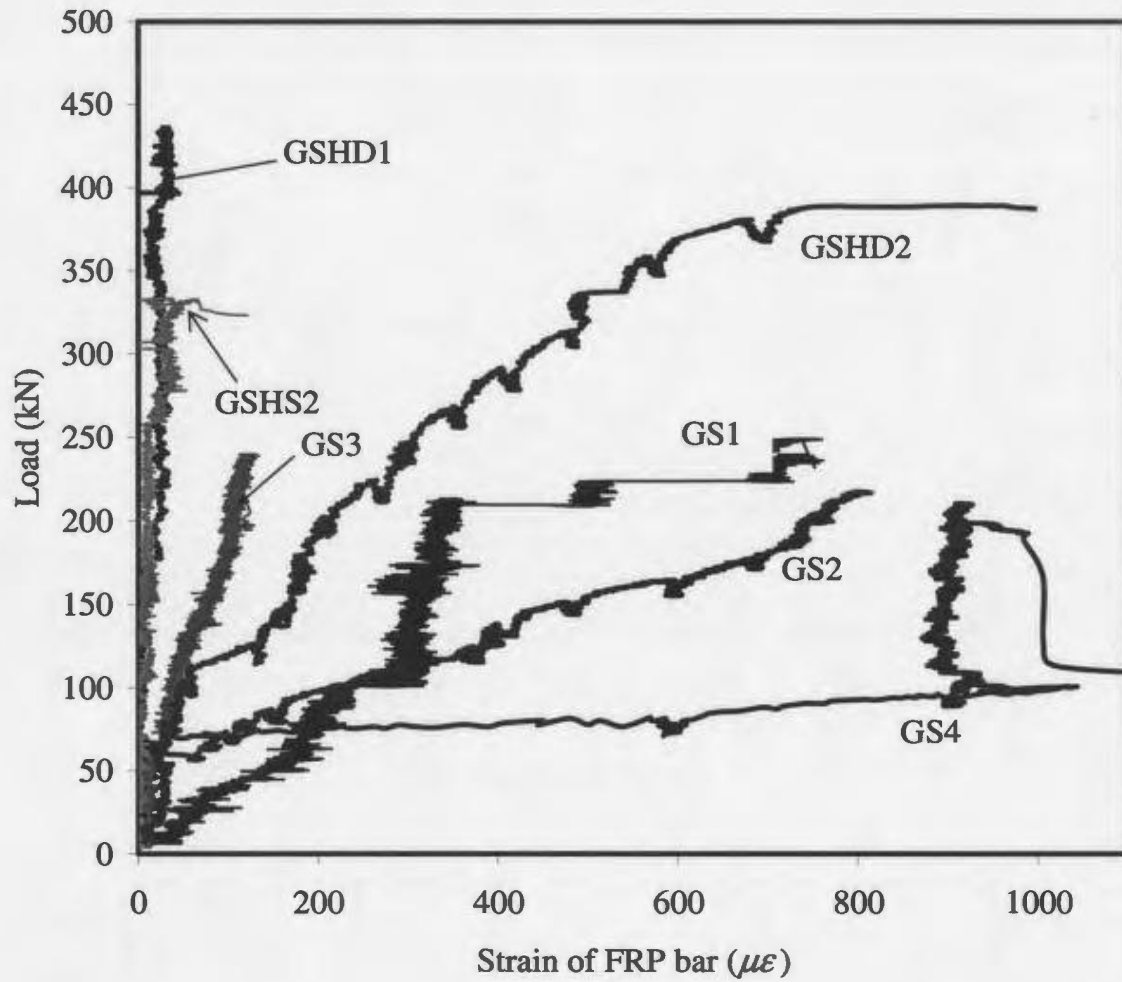


**Fig. 4.6: FRP strains at the end of the critical bars**

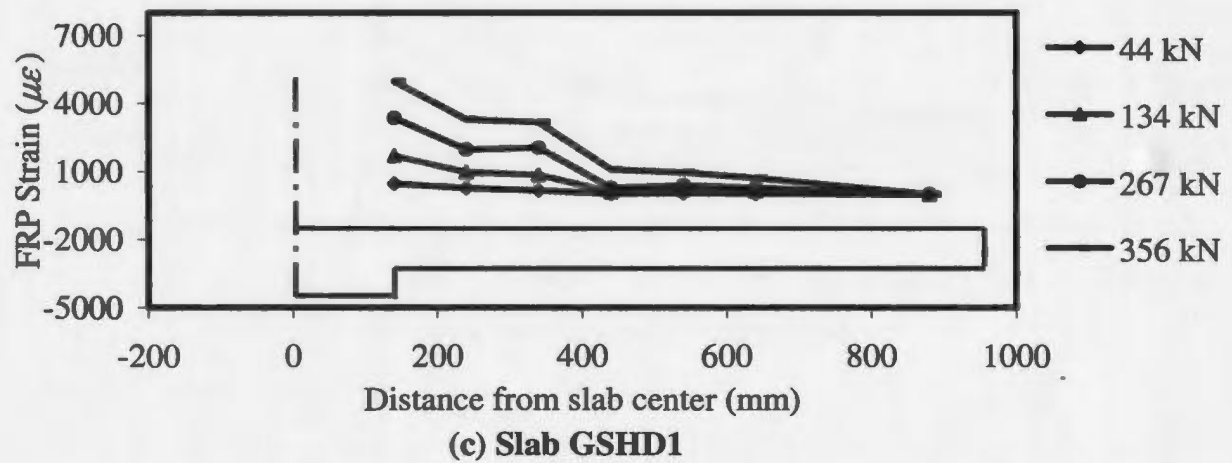
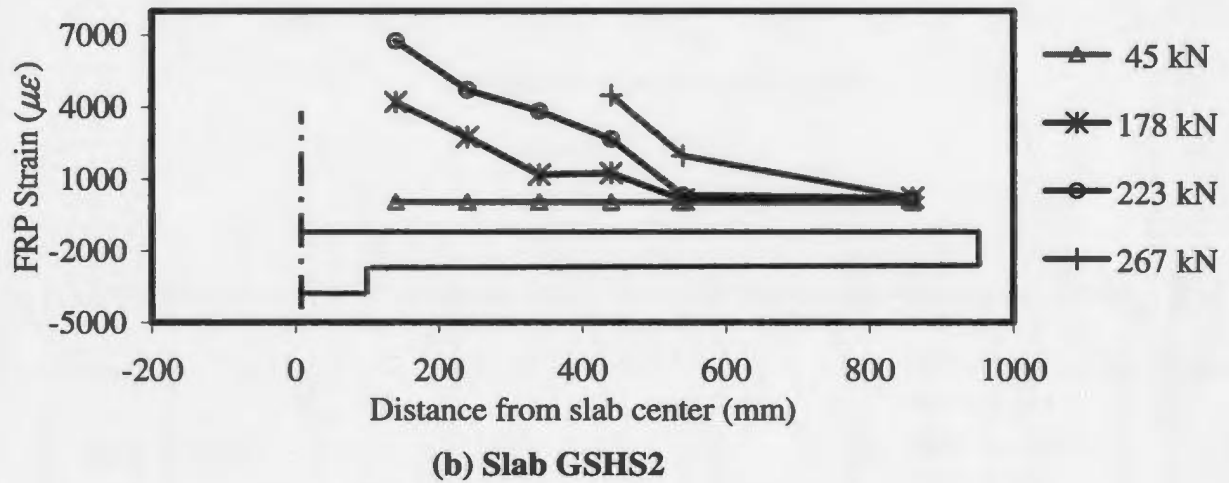
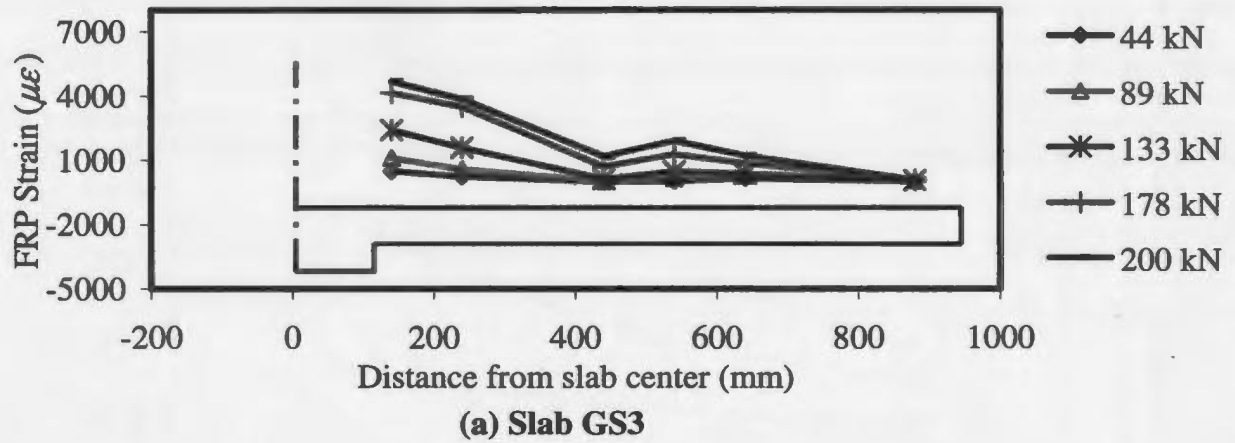
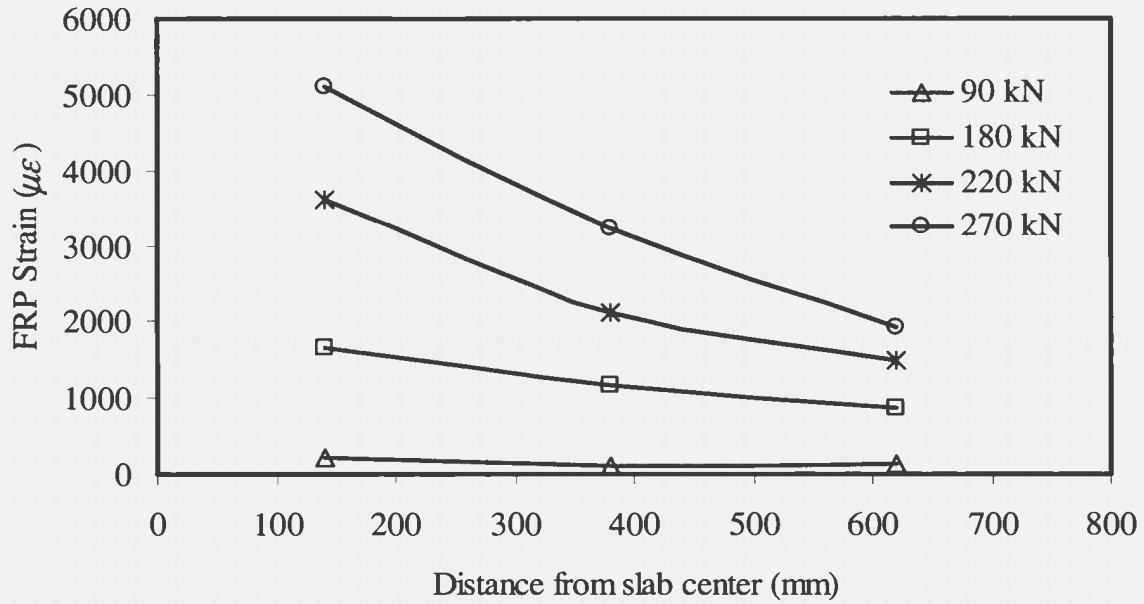
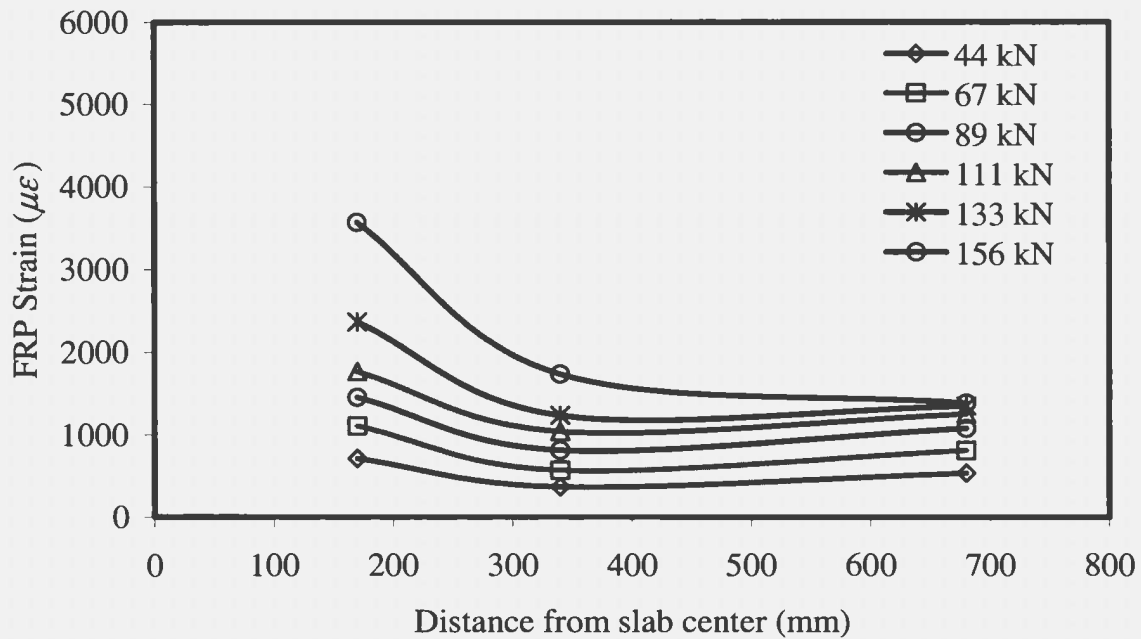


Fig. 4.7: FRP strain profile in radial direction of some typical slabs



(a) Slab GSHD2



(b) Slab GS3

Fig. 4.8: FRP strain profile in tangential direction of some typical slabs

the distance from the center of the slab. In the current research, the tangential strain profile also supports this assumption. Thus, it can be used to develop a mechanical model for punching shear of slabs with FRP bars and the same assumption is still valid.

#### **4.6 Cracking characteristics**

The first crack was formed along the reinforcement that passed through the slab center or the face of column. The crack along the reinforcement was formed in the direction of the higher depth first, followed by similar cracks in the other direction with the lower depth. After a certain load interval (described in Section 3.10), the crack width was measured and the crack pattern was checked by the naked eye. The first visible crack and the corresponding load was noted as accurately as possible. The values are reported in Table 4.6. The first cracking load primarily depends on the concrete strength and is formed in the weakest plan inside the slab. Normally, the locations of these weak planes are just above the reinforcement and along the reinforcement.

Numerous cracks developed on the tension face of slab at the time of failure. Photographs of all test slabs with the crack marks are shown Fig. 4.9. The crack pattern of steel-reinforced slabs in the literature show that either orthogonal cracks or radial flexural cracks form, depending on reinforcement ratio. If the slab has low reinforcement ratio, radial flexural cracks would form and if the slab has high reinforcement ratio, orthogonal cracks would dominate.

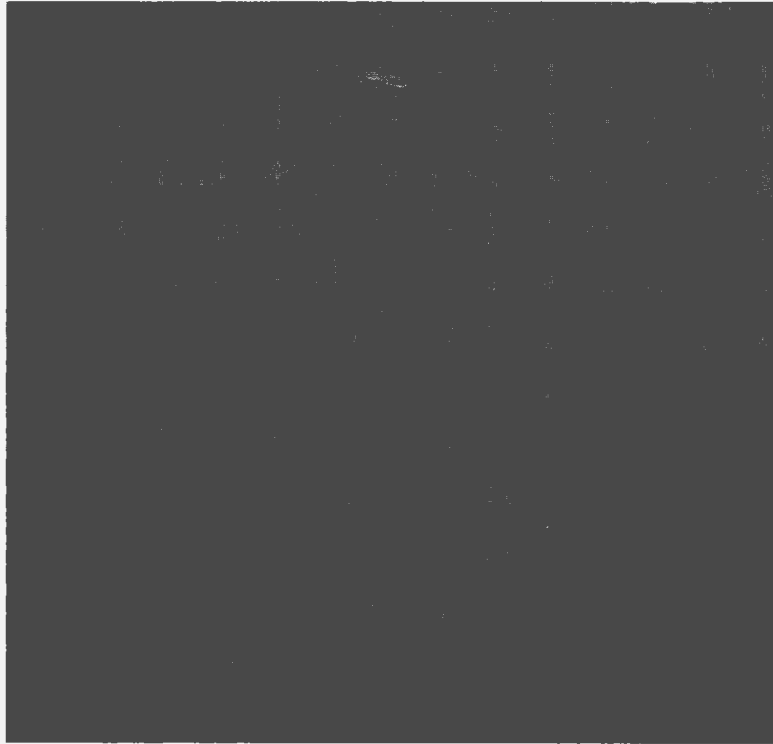
The dominating crack pattern is not only a function of the reinforcement ratio. It is also a function of the ultimate deflection and concrete strength. The orthogonal cracks that form above and along the direction of reinforcement depend on the bar force and concrete strength. Reiterating, the bar force depends on slab stiffness (i.e. amount of reinforcement, spacing, slab depth etc.) and deflection of the slab center (i.e. curvature of slab). On the other hand, the radial flexural cracks depend on the slab deflection, i.e., the curvature that the slab experiences during loading. When the slab deflection exceeds a certain deflection, radial cracks start to form. Normally, if the reinforcement ratio is low, the slab experience large deflection and shows radial flexural cracks at failure. This is the general trend of crack formation that was observed during the experiments. However, some deviations were noticed. For example, the reference slab R1 with traditional steel reinforcement had a reinforcement ratio of 0.54%. From the traditional concepts discussed above, the slab should show only radial flexural crack pattern. However, the slab showed some orthogonal crack pattern. The ultimate load is 14% higher than flexural capacity calculated by yield line analysis. It seems that the force in the bar was high enough to form a crack along the bar by splitting the clear cover. Consequently, some cracks along the reinforcement were formed. Also, slab GS3 should some splitting cracks along the lines of reinforcement.

To conclude the above discussion, it was found that, in general, the first crack forms along the rebar which passes through the slab center or close to the slab center. The second crack forms along the similar rebar in other direction. A diagonal crack developed in this stage but it has no significant influence on characteristic crack pattern. Further

increase of the applied deflection led to an increase in the curvature of slab as well as the bar force. The formation of cracks along the other bars depends on the bar force and concrete strength. At the same time, one circumferential crack formed around the column and close to the reinforcement passing near the column face. Further increase in the deflection led to the formation of radial flexural cracks and increased the width of the circumferential crack around the column. Some slabs failed before the formation of significant number of radial flexural cracks.

In the current test program, slabs GS3 of series 1, GSHD2 of series 2 and reference slab R1 exhibited orthogonal crack pattern. In the case of slab GSHD1 of series 2, orthogonal and radial flexural cracks were significant. In other slabs, radial flexural cracks were dominating. These cracks started from the circumferential crack around the column and extended toward the edges of the slab. Interestingly, this is similar to a slab with traditional steel reinforcement that is developing flexural yield lines.

It is mentioned in Chapter 2 that Nawy and Neuwerth (1976) also stated that yield line diagonal cracks formed despite the fact that there is no yielding of the FRP bars. In the absence of yielding of the FRP reinforcement, yield line mechanism should not be present. Nevertheless, the observed crack patterns appeared to be like yield line cracks. Slabs tested in that program had low reinforcement ratio compared to the slabs in the current test program. The photographs reported by Nawy and Neuwerth (1976) show that yield line diagonal cracks are dominating at failure and the reported ultimate deflections of all slabs were more than 50 mm. However, the author did not mention that the high

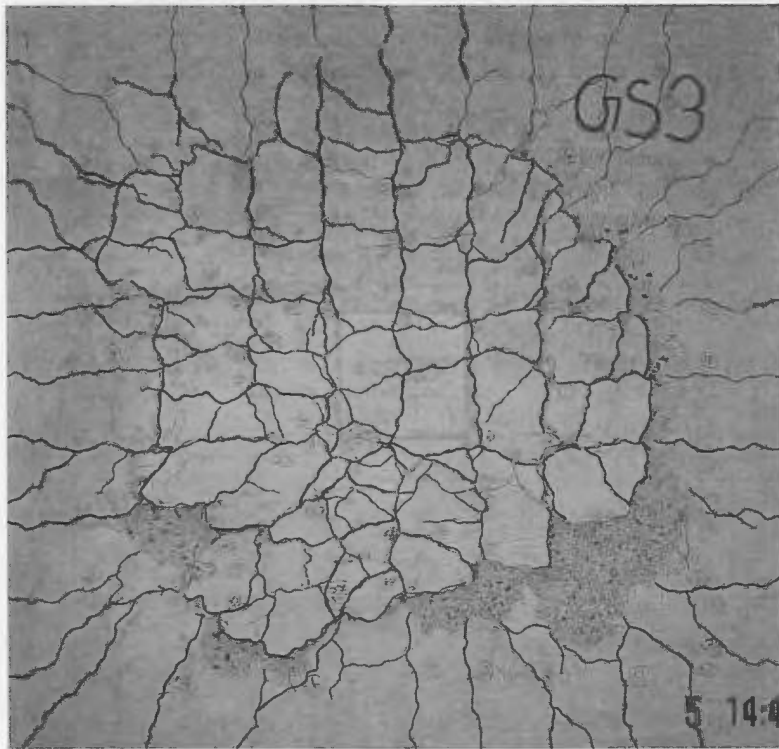


**(a) Slab GS1**

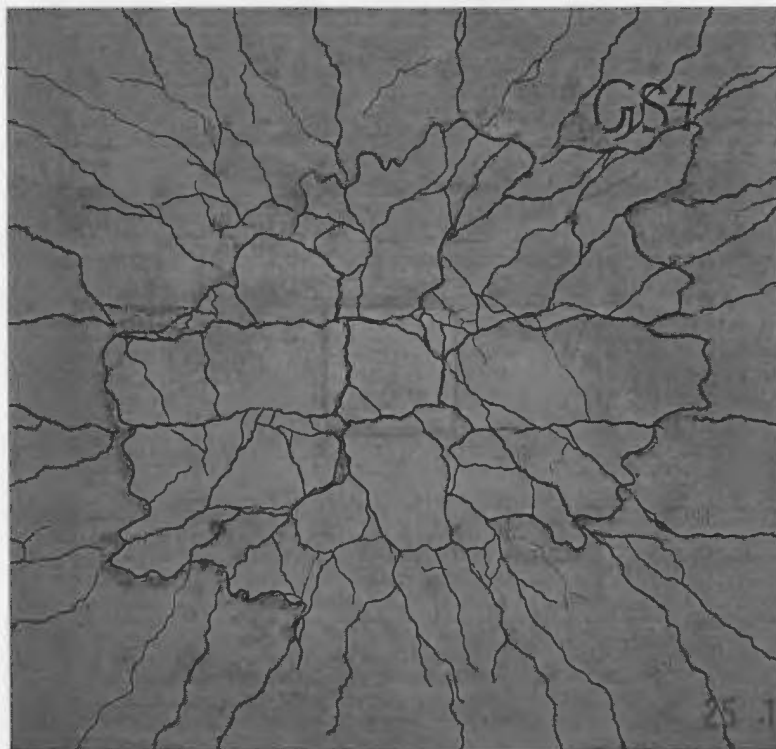


**(b) Slab GS2**

**Fig. 4.9: Crack patterns of the test slabs**

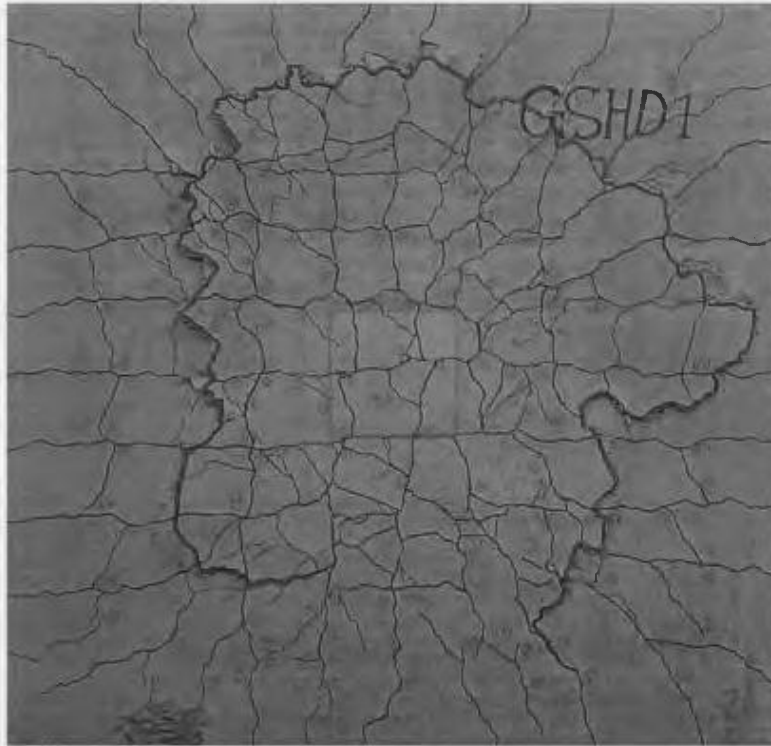


**(c) Slab GS3**



**(d) Slab GS4**

**Fig. 4.9: Crack patterns of the test slabs (contd.)**



**(e) Slab GSHD1**

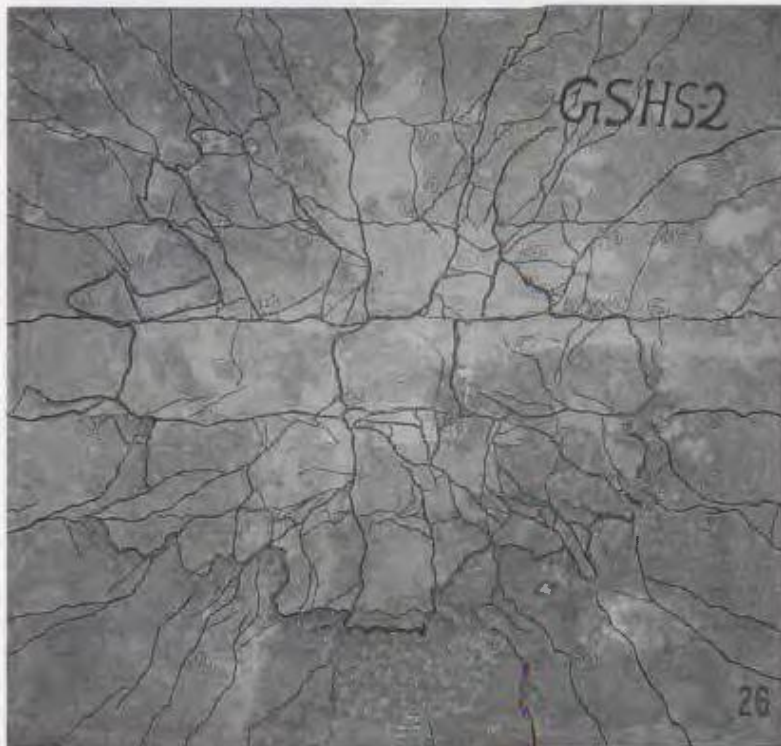


**(f) Slab GSHD2**

**Fig. 4.9: Crack patterns of the test slabs (contd.)**

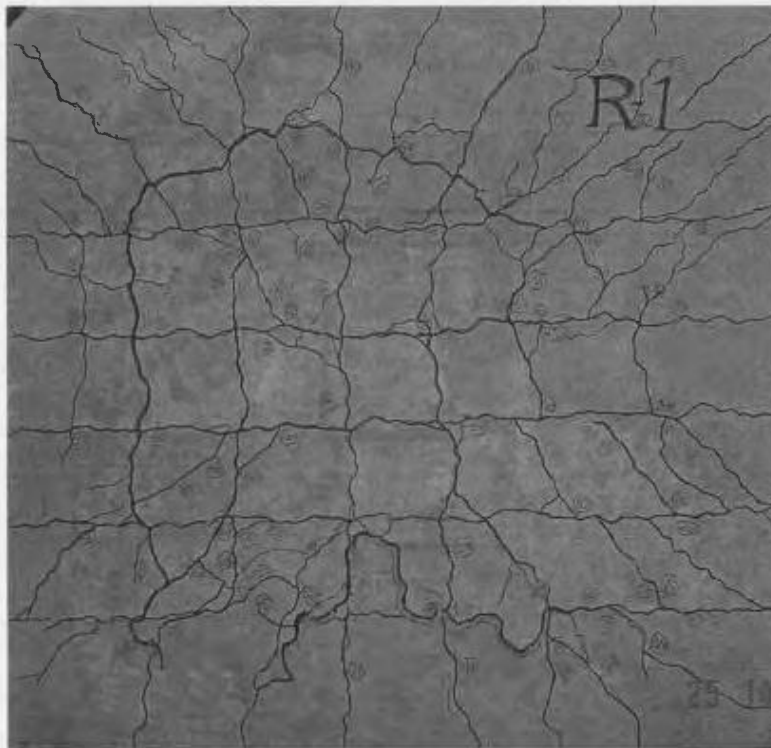


**(g) Slab GSHS1**



**(h) Slab GSHS2**

**Fig. 4.9: Crack patterns of the test slabs (contd.)**



**(i) Slab R1**

**Fig. 4.9: Crack patterns of the test slabs (contd.)**

deflection could be the reason that those types of cracks developed.

By observing the crack patterns and ultimate deflection of the slabs in the current test program, one general conclusion can be made. That is, the slabs which exhibit lower ultimate deflection, show orthogonal crack patterns and the slabs which exhibit higher ultimate deflection show radial flexural cracks at failure. The demarcation line that could separate the higher and lower ultimate deflection is approximately 25 mm. However, the small number test results from the current study may not be enough to make this kind of general conclusion. Further experiments are needed.

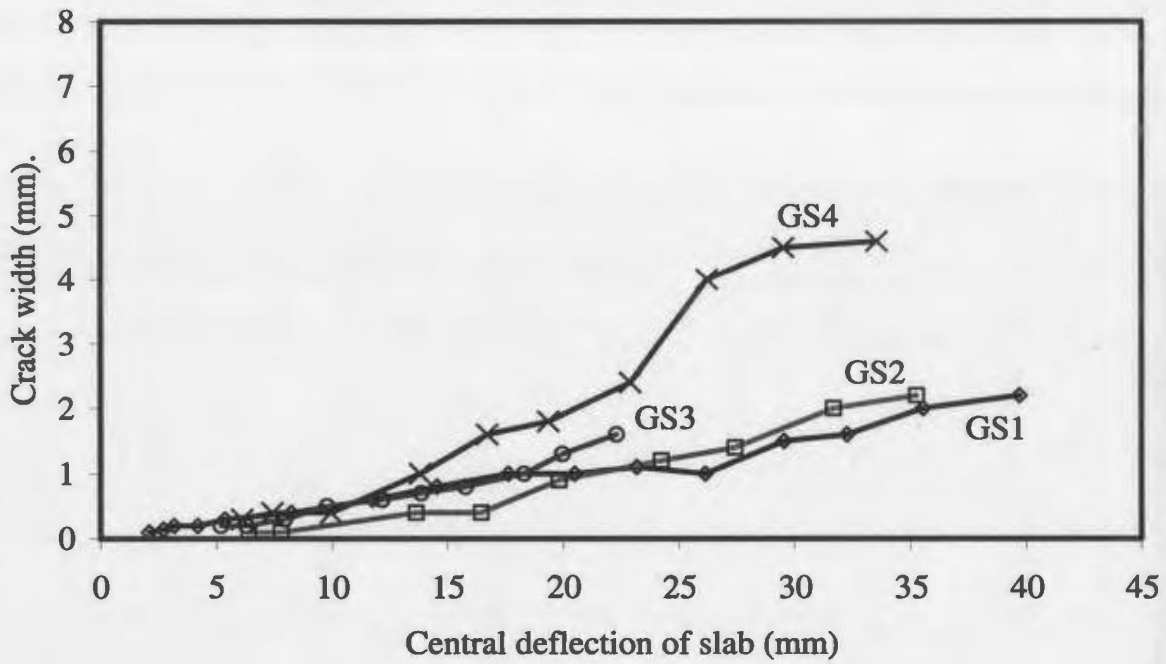
Most of the slabs failed in punching with a big radius of punching cone on the tension face of the slab. It was not possible to determine a reliable value of the shear cracking load, i.e. the load at which the shear cracks began to open up. Estimation of the shear cracking load from the crack pattern is not acceptable because there is no fundamental difference between the shear cracks and flexural cracks running in a tangential direction.

The crack width was measured at different load stages. In Fig. 4.10, the opening of the crack width is plotted versus the deflection of the slab center. The crack width increased as the deflection was increased. However, this increase was not very smooth as concrete is not a homogeneous material. The formation of a new crack affects the crack width of the previous crack located nearby the new crack. For this reason, it was sometimes common that a crack width did not increase or decrease as the deflection was increased. In the current work, the crack width of a certain crack at a certain location was considered rather than the average crack width. The results revealed an almost linear

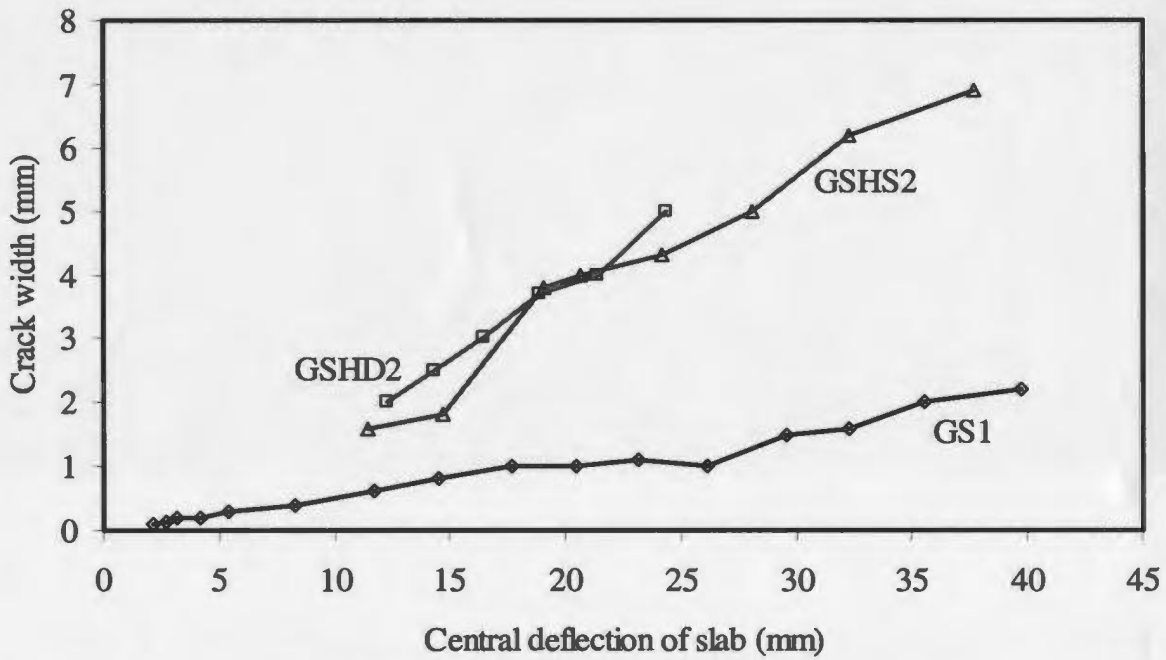
variation of the crack width with respect to slab deflection. However, slab GS4, which is lightly reinforced with high spacing, did not show such a trend. In general, the crack width varied almost linearly with the deflection. This observation is consistent with the findings of previous tests conducted by Nawy and Neuwerth (1977) and Ospina *et. al.* (2003).

**Table 4.6: Cracking load and crack width**

Slab	$f_c'$ (MPa)	$\rho$ %	First cracking		First diagonal cracking load (kN)	Max. crack width (mm)	Average diameter of punching cone on tension side (mm)
			Load (kN)	Defl. (mm)			
GS1	40	1.18	53	1.83	76	5.5	1360
GS2	35	1.05	72	3.41	-	-	930
GS3	29	1.67	67	2.89	80	2.1	1340
GS4	26	0.95	53	1.97	67	8.0	1370
GSHD1	33	1.11	53	0.74	-	2.6	1290
GSHD2	34	0.79	80	1.2	102	5.0	1140
GSHS1	92	1.67	98	2.21	156	5.0	1220
GSHS2	86	1.18	89	1.45	133	9.0	1230
R1	23	0.54	62	2.09	-	2.4	1195



(a) Slabs of Series 1



(b) Three slabs from three different series

**Fig. 4.10: Crack width expansion of certain cracks with respect to deflection of slab center**



**Fig. 4.11: Crack width of a typical FRP slab, at the time of testing, around the column periphery**



**Fig. 4.12: Crack depth at the side of a test slab**

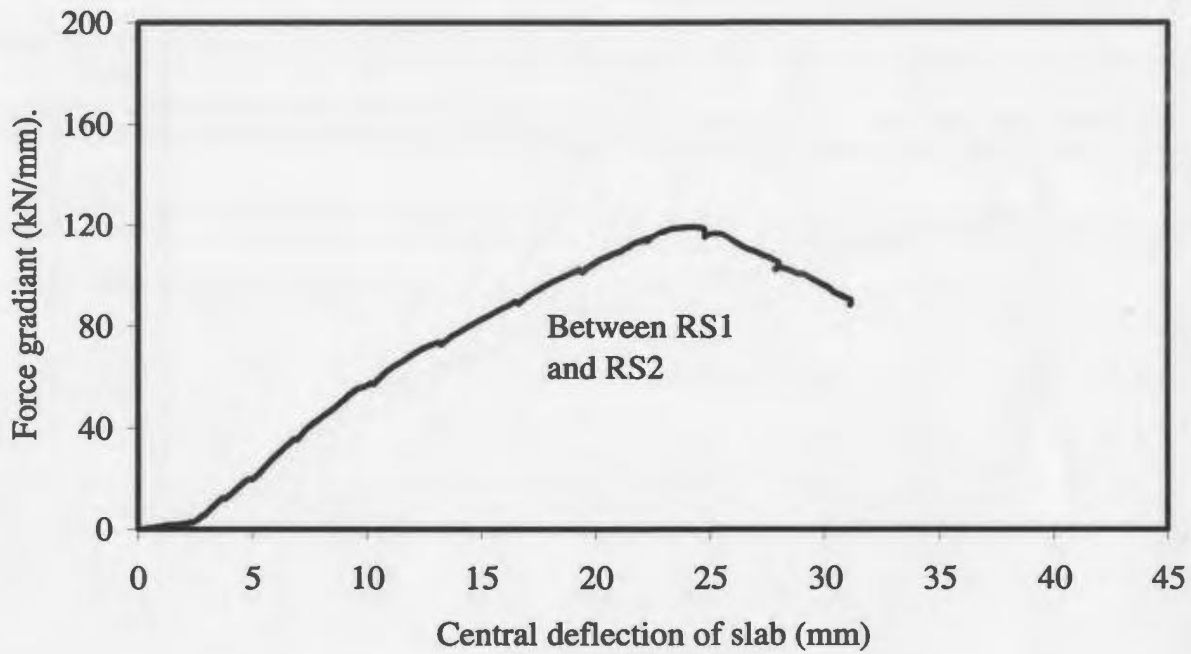
The maximum crack width was measured at the face of the column on tension side. In most slabs, a deep and wide circumferential crack was developed around the column periphery and close to the reinforcement passing near the column face. This circumferential crack started to open with the increase in deflection and exhibited the maximum crack width (see the Fig. 4.11). This observation could support the failure mechanism assumed by Shehata (1985) that was used to create a mechanical model to calculate the punching capacity. Figure 4.12 shows cracks that developed at the sides of a typical slab. These external cracks were only observed once the cracks propagated to the edges of the slab. These external cracks can provide an idea about the depth of cracks inside the slab.

The maximum crack width, at the time of failure, was measured as accurately as possible. The values are reported in Table 4.6. As expected, that maximum crack width of FRP reinforced slabs is higher than that of similar steel reinforced slabs.

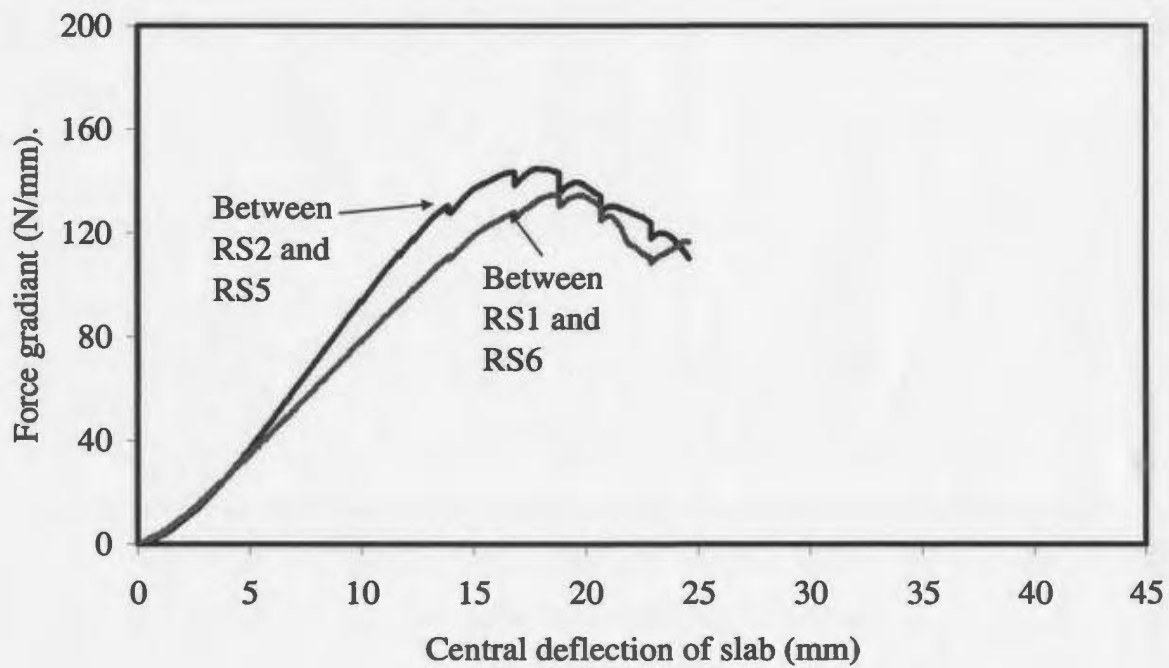
#### **4.7 Bar force gradients**

The force gradients of some critical bars are shown in Fig. 4.13. The bar force gradient was calculated using the strain gauge readings. The notations of strain gauges used to calculate the bar force gradients are given in the corresponding graphs. For example, RS1 means, strain gauge on slab reinforcement at location 1. Locations of all strain gauges and corresponding bars are given in Fig. A1 of Appendix A.

The force gradient is a qualitative measurement of the amount of shear transferred by

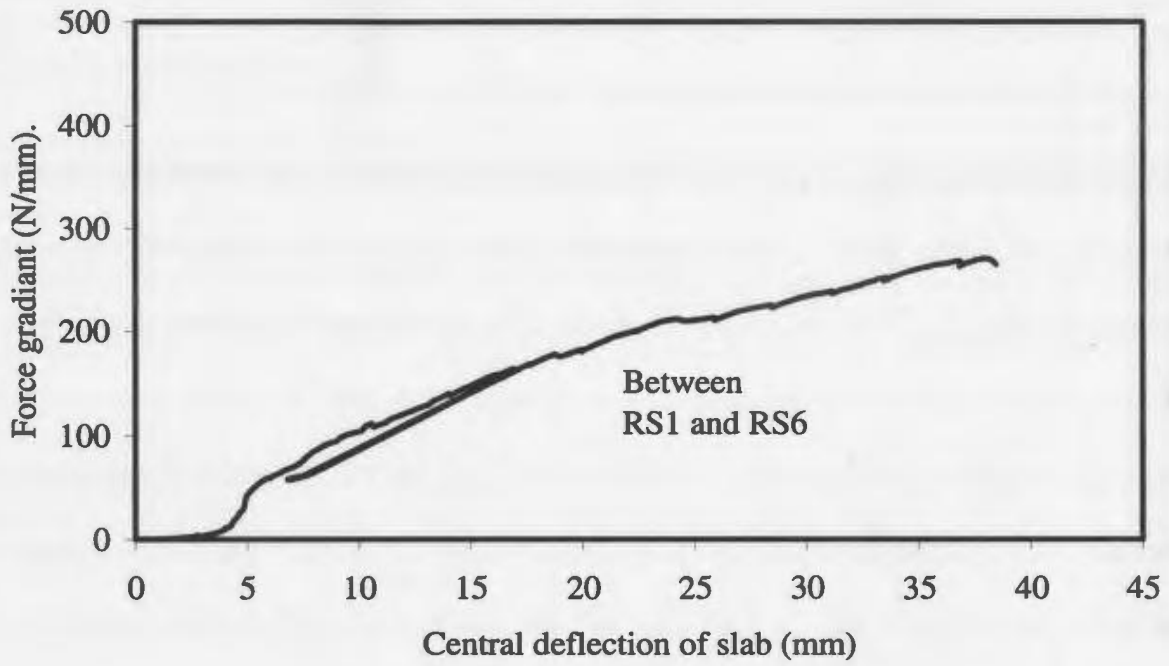


(a) Slab GS1

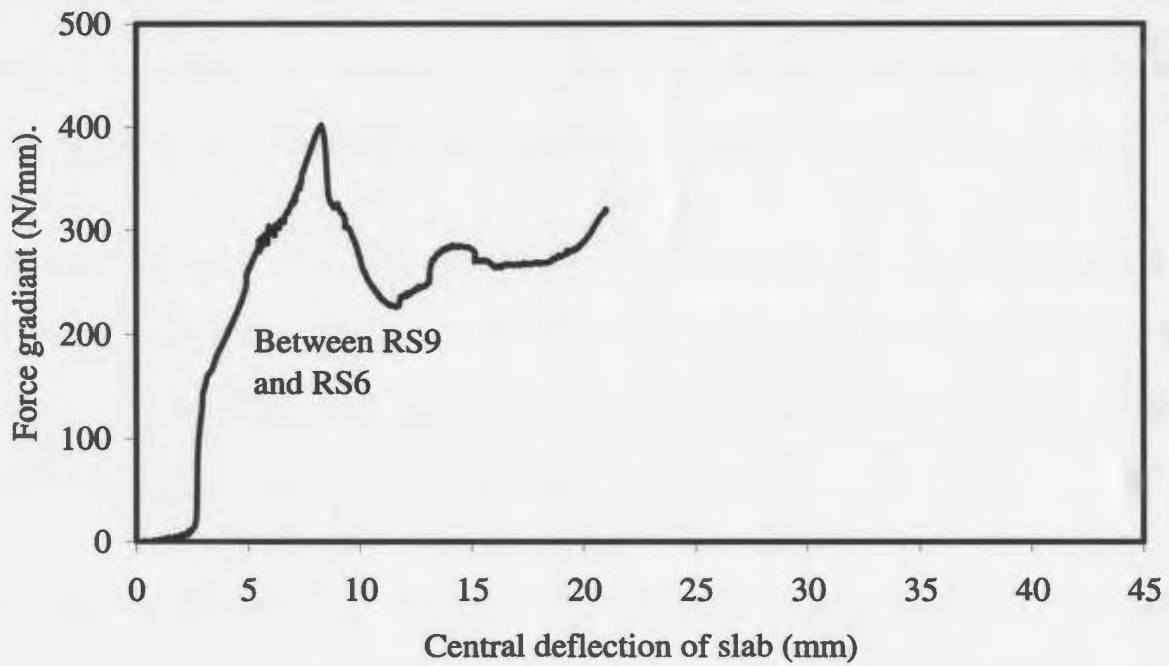


(b) Slab GSHD1

Fig. 4.13: Force gradient of some critical bars



(c) Slab GSHS1



(d) Slab GSHS2

Fig. 4.13: Force gradient of some critical bars (contd.)

beam action by the slab reinforcement. Null bar force gradient means shear is carried mainly by arching action.

If  $T$  is the bar force and  $x$  is the distance along the bar then,  $d(T)/dx$  is the mathematical expression of shear flow across any horizontal plane, inside the slab, between reinforcement and the compression zone. Shear flow can be defined as the shear force acting per unit length of horizontal plane being considered. If the shear flow exists the beam action also exists. That means, if the shear flow, on the above mentioned planes, is not zero, the concrete member is under beam action. On the other hand, if the shear flow becomes zero, the shear is transferred by the arch action. This case occurs when the reinforcement becomes unbonded i.e. when the reinforcement loses the local bond. In this case, the tensile force of reinforcement as well as compression force in concrete remains constant. The shear is transferred by changing the distance between the tensile and compressive force i.e. by changing the moment arm over the length of the shear span.

The maximum value of bar force gradient is limited by the yield stress of bar in case of slabs reinforced with traditional steel reinforcement. But in case of FRP slabs, the maximum value is limited by bond capacity of the FRP bars. The developed bar force gradient depends on the bar diameter and the bar spacing.

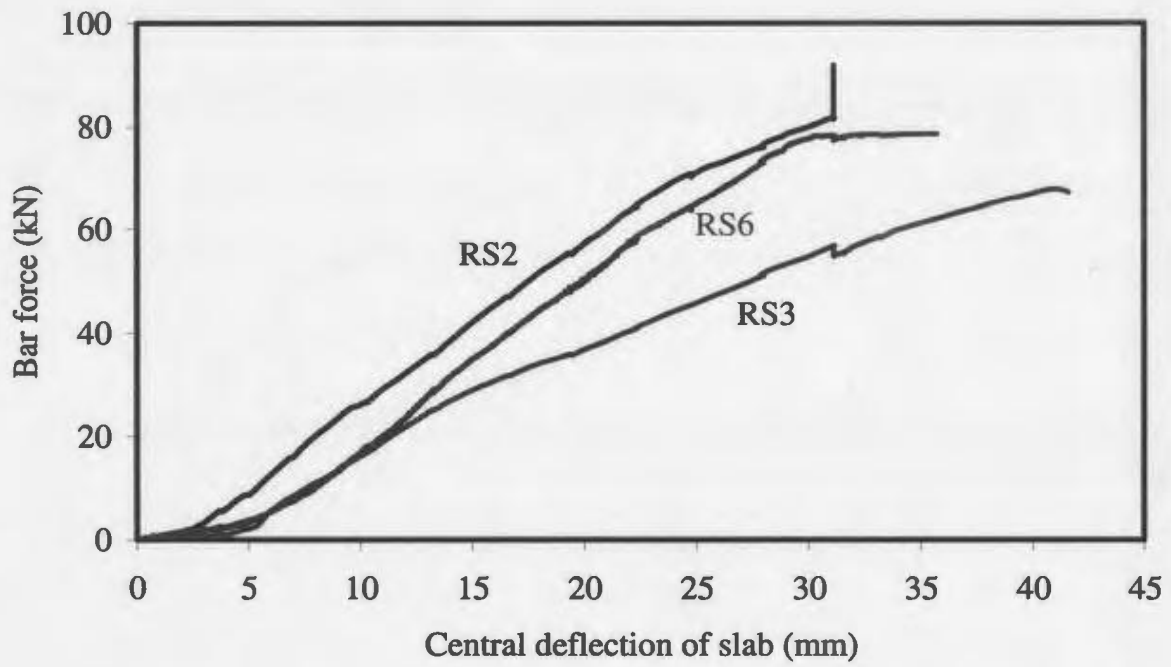
In the current test program, the maximum bar force gradient was found to be 400 N/mm. It was measured in the case of high strength concrete slabs. The bar force gradient of Series 1 slabs was always lower than 140 N/mm. The bar force gradient depends on the slab stiffness, location of the bar and length of the bar considered to calculate the force

gradient. Consequently, it is not possible to compare the test results with other available test results unless the slabs are similar regarding those factors. The high strength concrete slab showed a high force gradient during the test. Again, it could not be compared to other tests, as there are not enough results available in the literature. One interesting observation is that some bar force gradients decreases after a certain deflection which is similar to the yielding phenomenon. The force gradient graphs reported by Ospina *et al.* (2003) also showed the same trend. Nevertheless, there was no sign of bond failure showing in the graphs obtained from the current experiments.

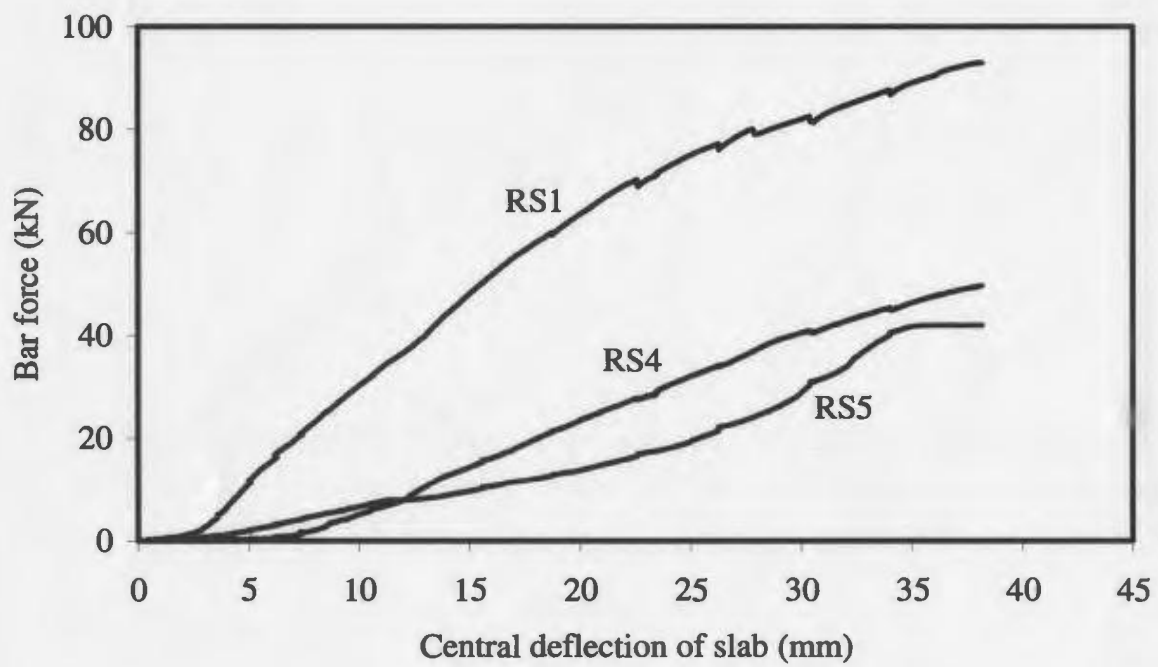
#### **4.8 Forces in the slab reinforcement**

Figures 4.14 shows the variation of the bar forces at some critical bar locations for some slabs. The bar forces were calculated from the measured strains of the bars during the test and stress-strain relationship reported in Section 3.2. The notation of the strain gauge that is used to calculate the bar force is given in the corresponding graph. The location of all strain gauges on reinforcing bars for all slabs are shown in Fig. A1 of Appendix A.

As expected, the location near the column showed the highest bar force. In all graphs, the initial bar force is almost zero up to a certain deflection. That is, the bar force was almost zero before the slab started to crack. The first crack was developed at a deflection of 1.83 mm for slab GS1. From Fig. 4.14(a), one can see that the bar force started to rise after 2 mm deflection at strain gauge location RS2. The strain gauge location RS3 was farther away from the column. The bar force started to rise at this location when the deflection

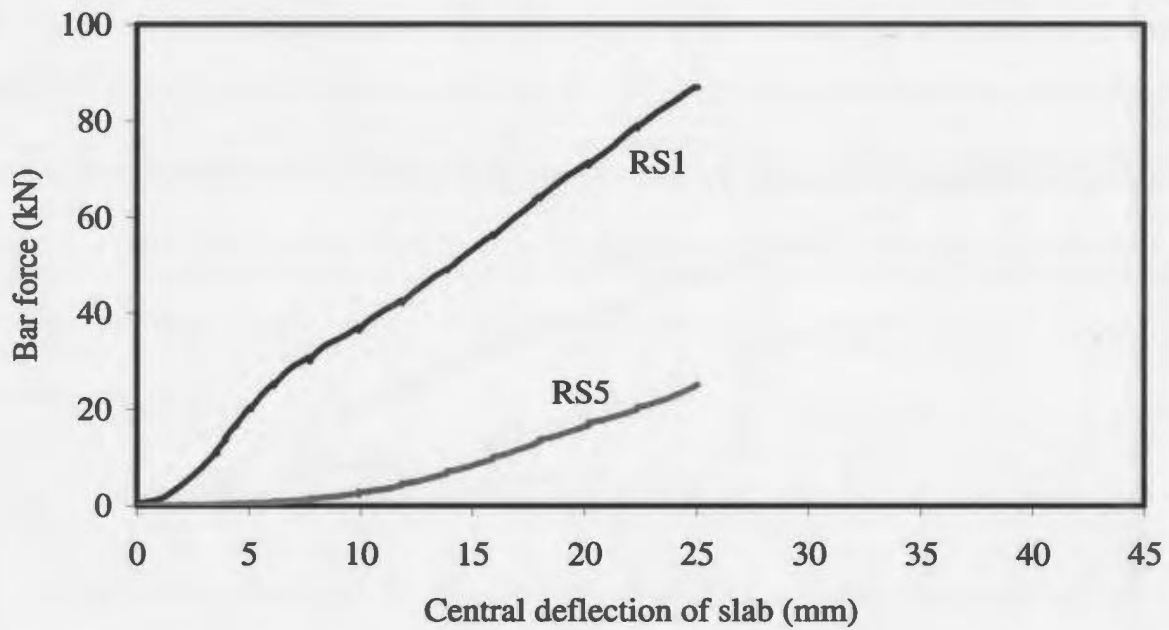


(a) Slab GS1

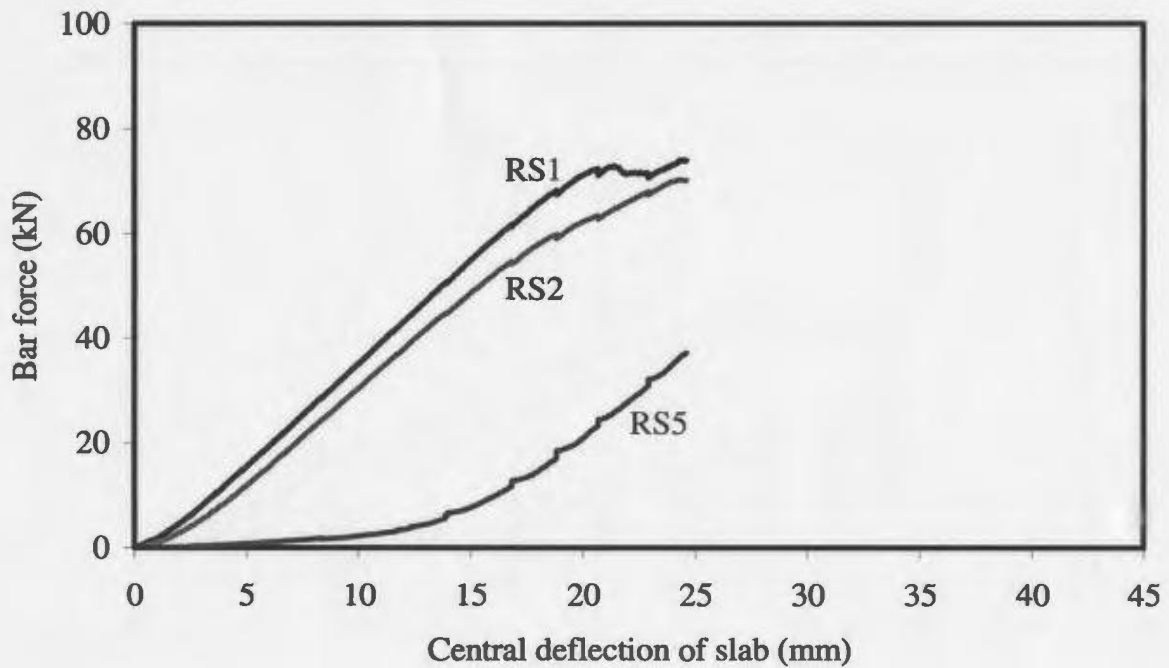


(b) Slab GS2

Fig. 4.14: Bar forces in some critical bars

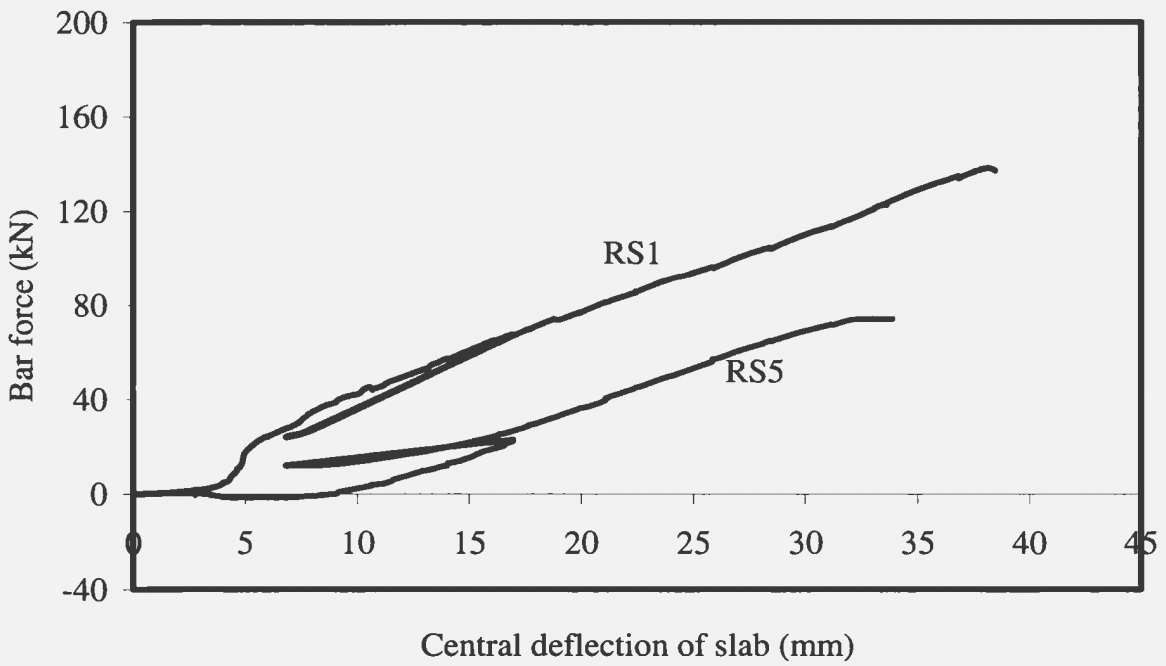


(c) Slab GS3

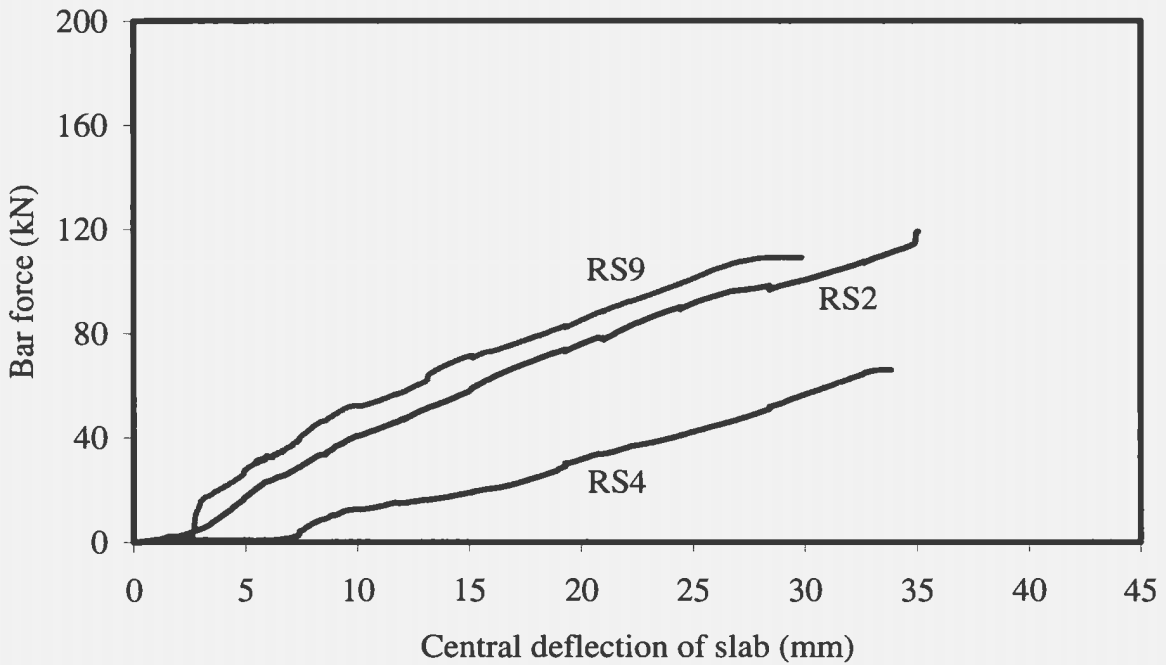


(d) Slab GSHD1

Fig. 4.14: Bar forces in some critical bars (contd.)



(e) Slab GSHS1



(f) Slab GSHS2

Fig. 4.14: Bar forces in some critical bars (contd.)

was 4 mm. The same observation applied for slab GSHD1. The first crack was formed at 0.74 mm deflection.

Fig. 4.14(d) showed that the bar force at strain gauge location RS1 and RS2 started to rise at the same deflection level. However, bar force at strain gauge location RS5, which is away from column, started to rise at 4.5 mm deflection.

The cracks started at a location near the loaded area and propagated towards the slab edges. Consequently, the strain gauge located close to column showed rising bar force just after cracking. As the cracks reached the strain gauges located away from the column, the bar force started to rise at those locations. The rate of change of bar force with respect to deflection is higher at locations close to the slab center and fairly low at the points away from the center. This character is common for all slabs. The trends observed from the graphs are consistent with the bar force graphs reported by Ospina *et al.* (2003).

## **4.9 Deflection profile**

A series of dial gauges and LVDTs were placed along the center line of the slab to measure the deflection of various points on that line as shown in Fig. 4.15. The dial gauge readings were taken manually.

In Fig. 4.16, the rotation of slab is plotted versus the deflection at the slab center. The readings from the dial gauges are used in plotting. The rotations at three different places, for each slab, were measured. One measurement zone was close to the support (dial

gauges 6 and 7), another measurement zone was close to loading column (dial gauges 4 and 5) and the last measurement zone is in between those two (dial gauges 5 and 6). Inspecting the graphs shown in Fig. 4.16, it is clear that the three lines are very close. At lower deflection, these three lines coincide on each other and at very higher deflection a little difference is noticed. Ignoring this little dispersion at higher deflection, it can be assumed that the rotation of the slab, at different points, is almost the same at different deflection levels. This observation supports the rigid body rotation assumption of slab's radial segment which was assumed and used by various authors in literature for slabs with traditional steel reinforcement. It was Kinnunen and Nylander (1960) who first observed and used the rigid body rotation to develop a mechanical model to predict punching shear capacity. The recent program on GFRP slabs by Ospina *et al.* (2003) also exhibited the same rigid body rotation property. Figure 4.17 shows the deflection profile of some typical slabs of the current test program. The graphs support the rigid body rotation assumption.

As expected, the slab depth has a significant effect on the deflection. The slab's stiffness increased dramatically with increasing the slab depth. The deflections at all points of GSHD1 slab, at 300 kN load, were lower than those of slab GSHS1 under the same load. These two slabs have the same reinforcement area. However, GSHD1 is exhibiting higher stiffness even though GSHS1's concrete strength is three times higher than GSHD1.

#### **4.10 Post punching behaviour**

The post punching behaviour of the slabs was monitored during the tests. When punching

○ = Dial Gauge

▭ = LVDT

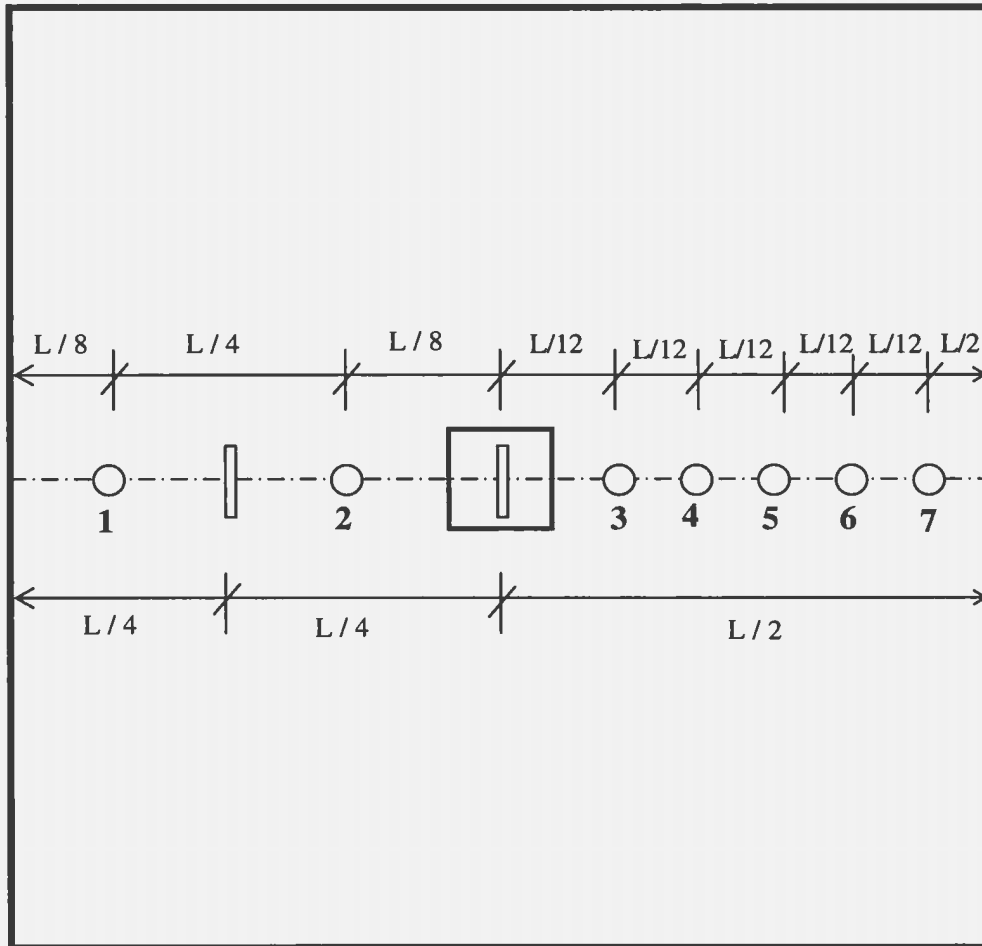


**Fig. 4.15: Schematic diagram of the dial gauges and LVDT locations along a center line of the slab on tension face**

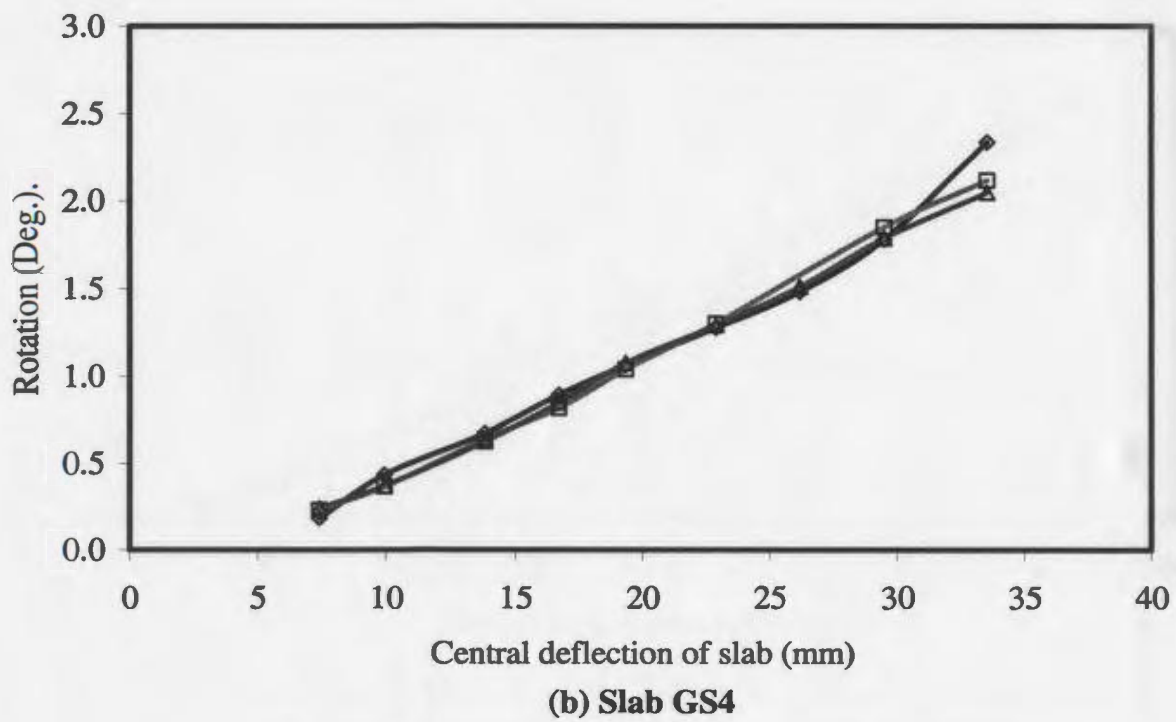
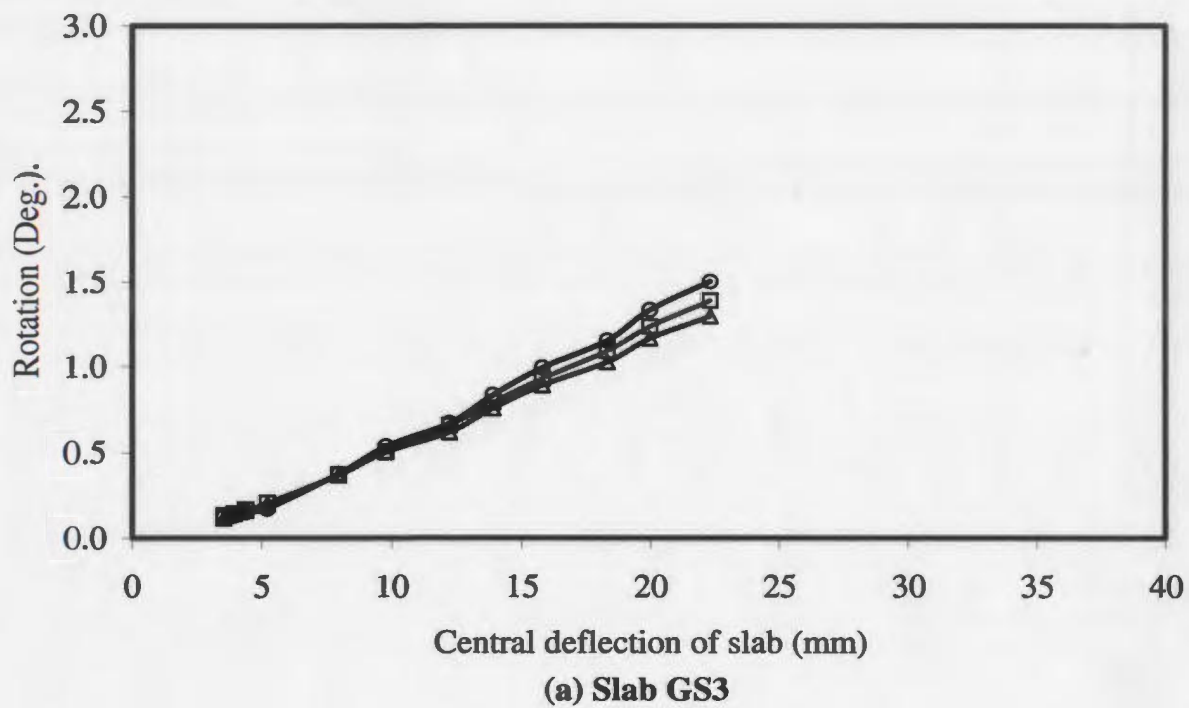
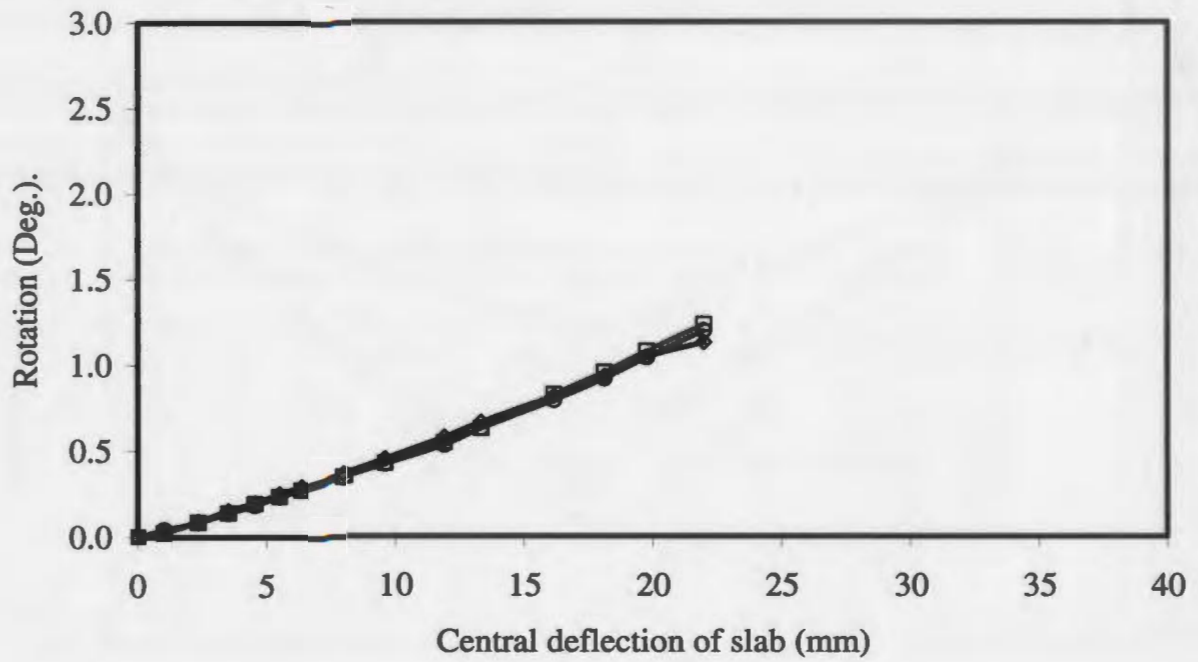
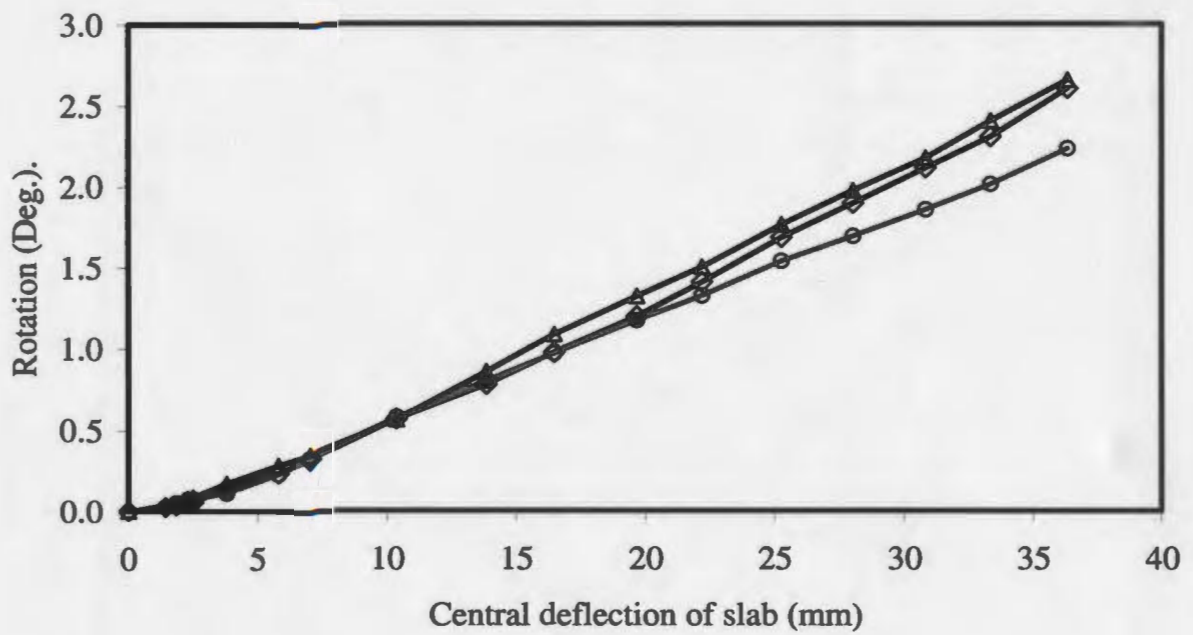


**Fig. 4.16: Slab rotation versus slab central deflection**

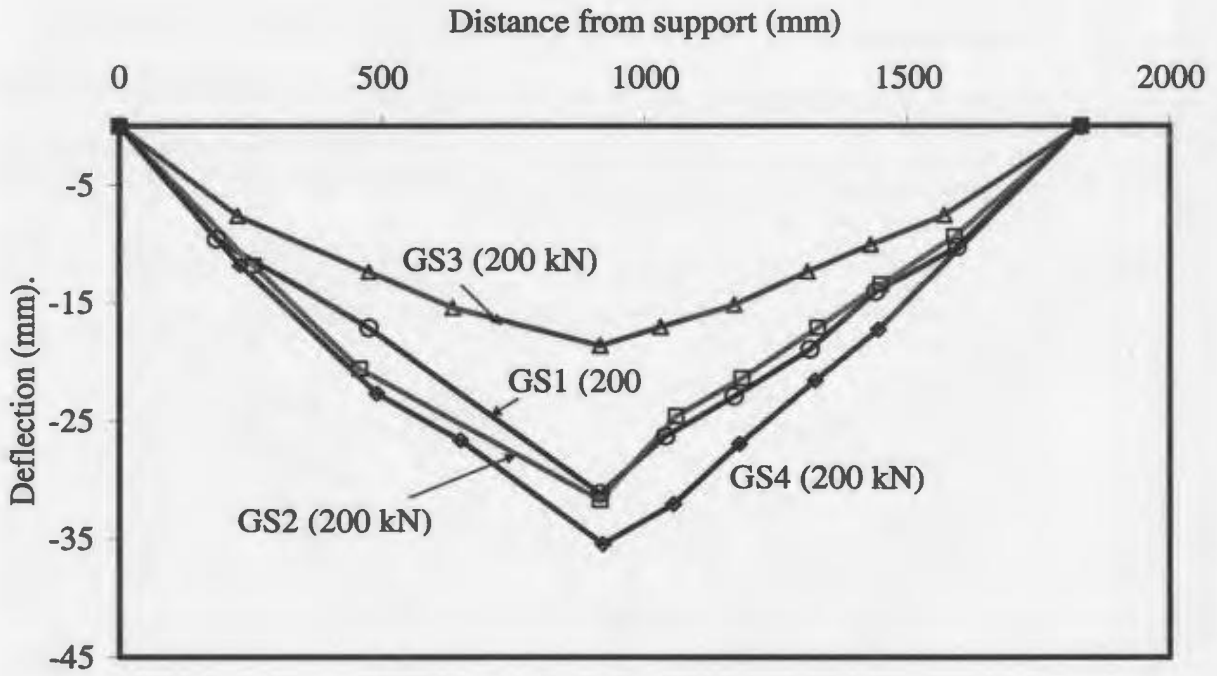


(c) GSHD1

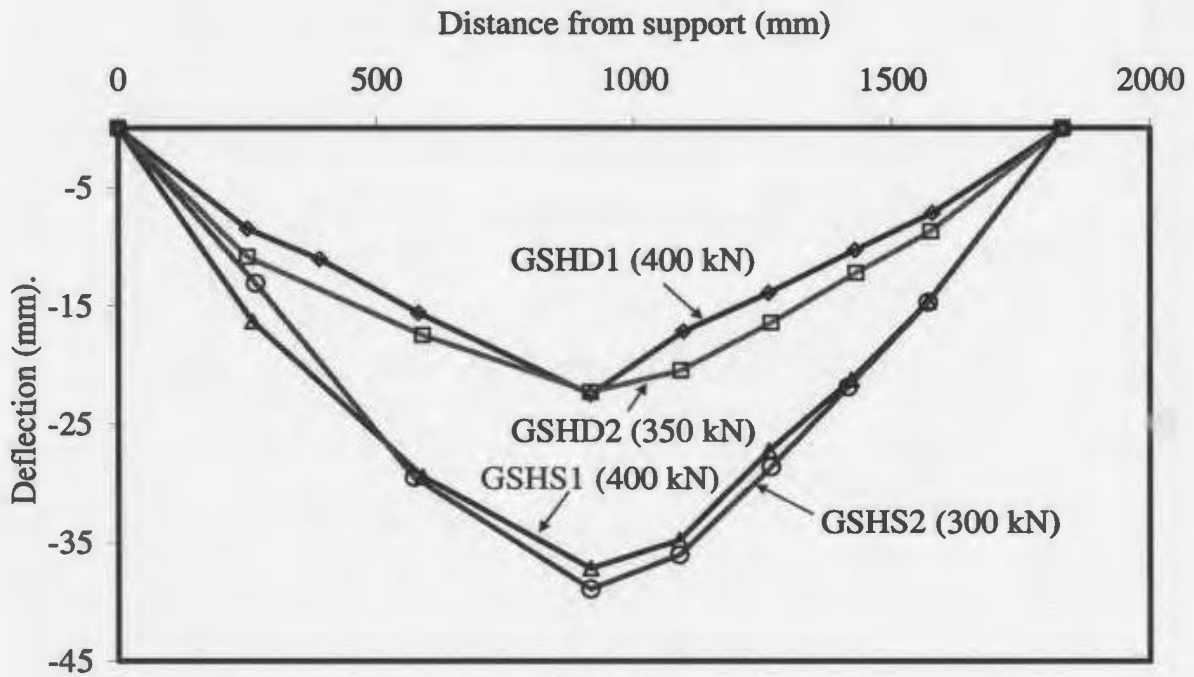


(d) GSHS1

Fig. 4.16: Slab rotation versus slab central deflection (contd.)

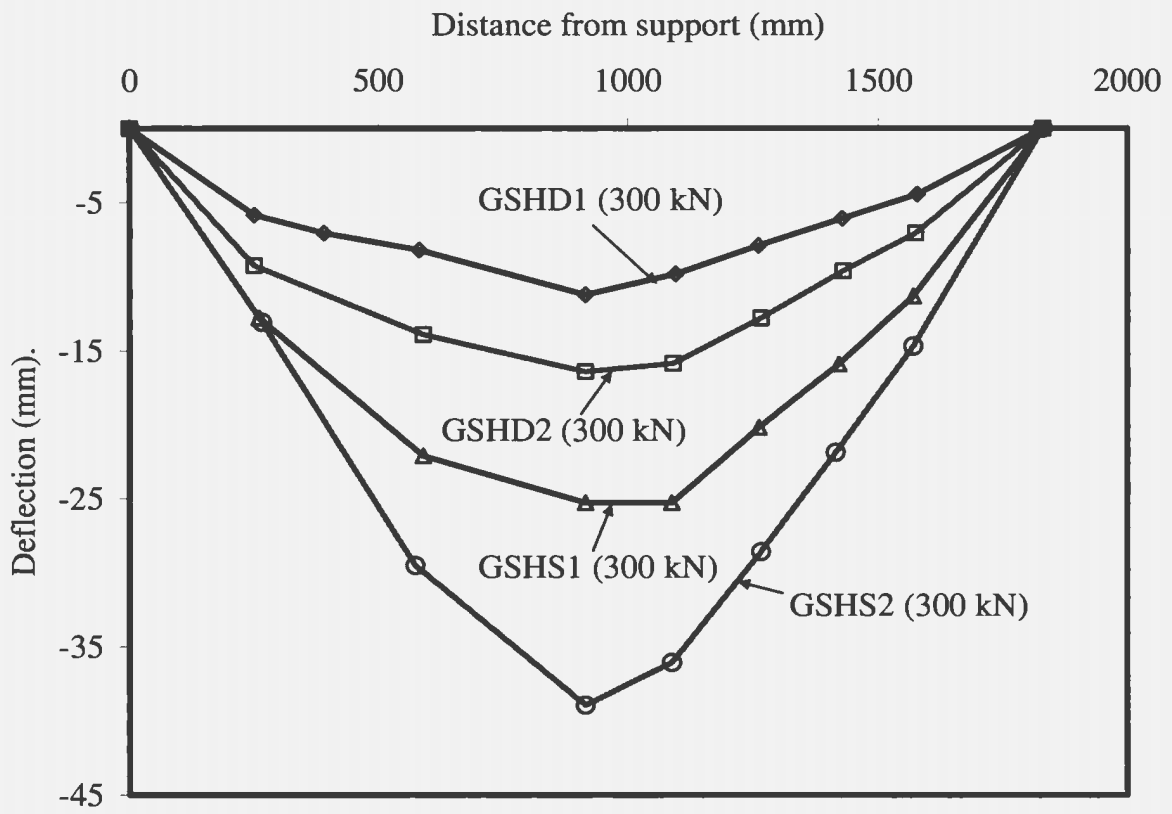


(a) Slabs of Series 1



(b) Slabs of Series 2 & 3

Fig. 4.17: Deflection profiles



(c) Slabs of Series 2 & 3

Fig. 4.17: Deflection profiles (contd.)

occurred, the load fell suddenly to a value of approximately 35% of the ultimate load. With further application of displacement, the load was almost constant. The load exhibited an almost horizontal plateau as shown in the load-deflection graphs. At this stage, the resistance was developed by the FRP bars through anchorage and bond action at the end part of bars in the intact part of the slab.

#### **4.11 Modes of failure**

Different types of failure mode are described in Section 2.3 for slabs with traditional steel reinforcement. The failure mode of the FRP slabs could be divided into two main modes. One is flexural failure mode and the other is the pure punching failure mode. The flexural failure is that kind of failure when the flexural capacity becomes exhausted at the time failure. The flexural failure mode can be subdivided into two parts. When the flexural failure occurs due to reinforcement rupture, this is referred as flexural failure in tension. On the other hand, flexural failure can occur by concrete crushing which is known as flexural failure in compression. According to code recommendations, all FRP flexural members should be over reinforced. For this reason, flexural failure in tension might not be present in FRP slabs. Pure punching failure is a pre-mature type of failure. Failure occurs due to diagonal tension cracks developing inside the concrete around the column vicinity. Another type of failure mode could be classified as ductile punching failure. It is considered as the transition between flexural and pure punching failure.

During testing, all slabs eventually failed in primary or secondary punching. The primary

punching failure occurred in the case of pure punching. Secondary punching failure occurred when a slab failed in a mode other than pure punching but eventually experienced secondary punching failure with further load application.

Hence, the current test slabs can be divided into three groups, pure punching failure (PPF), flexural failure in compression (FFC) and ductile punching failure (DPF). Classification of the failure mode of the slabs according to the load-deflection graph, the crack patterns and the concrete strains is given in Table 4.7.

Note that the different modes of failure, given in the Table 4.7, are assumed for each slab based on different points of view. In the last column, the declared mode of failure is made based on judging all the factors considered.

For slab GS1, the tangential concrete strain was close to 0.0035 which is the theoretical crushing strain. For this reason, it could be classified as FFC. However, no physical crushing of the concrete was noticed on the compression side. In addition, the strain gauges only measured the surface concrete strain. It seemed that the concrete was close to crushing. As concrete was close to crushing and the load deflection graph showed punching failure characteristic, it is more logical to assume that the failure mode of slab GS1 was DPF. For the same reason, the failure mode of slab R1 is decided as DPF.

In some slabs, flexural radial cracks and orthogonal cracks are both present in the test slab, especially for slabs with GFRP bars (see Section 4.6). It becomes difficult to decide on the mode of failure based on crack patterns only. For this reason, the failure mode

based on crack patterns is sometimes ignored as in case of slab GS4, GSHD2 and GSHS1. Also, the radial concrete strain of slab GSHS1 was close to its ultimate strain. Therefore, it is decided that the failure mode of slab GSHS1 is DPF.

**Table 4.7: Failure modes of test slabs**

Slab design.	Failure modes			
	Considering load-deflection graph	Considering crack patterns	Considering concrete strain	Final comment
GS1	PPF	DPF	FFC	DPF
GS2	PPF	PPF	PPF	PPF
GS3	PPF	PPF	PPF	PPF
GS4	DPF / FFC	FFC	DPF	DPF
GSHD1	PPF	PPF	PPF	PPF
GSHD2	DPF	PPF	DPF	DPF
GSHS1	PPF	FFC	DPF	DPF
GSHS2	DPF	DPF	DPF	DPF
R1	DPF	PPF	FFC	DPF

PPF = Pure Punching Failure, FFC = Flexural Failure by Compression, DPF = Ductile Punching Failure.

There was no sign of damage on the compression side in most of the slabs. Only one circumferential crack at the column face developed at the time of failure as shown in Fig. 4.18(a). This could be attributed to the column penetration through the compression zone of the slab at the time of punching. Some slabs showed some damage on the compression side as shown in Figs. 4.18(b) to (d). However, it is very difficult to differentiate whether that crack was formed due to flexural compression failure or due to column punching



**(a) Normal damage pattern on compression side at failure**



**(b) Slab GSHD1**

**Fig. 4.18: Compression side of slabs at failure**



**(c) Slab GS4**



**(d) Slab GSHS2**

**Fig. 4.18: Compression side of slabs at failure (contd.)**

through the slab. The measured concrete strains do not support any flexural failure. The crack patterns in slabs GSHD1 and GSHS2 may be due to punching. Crack patterns of slab GS4 do not conclusively indicate any assumption.

#### **4.12 Comparison of test results with different code predictions and some other rational approaches**

Various code equations for predicting the punching shear capacity for interior slabs are presented in Section 2.4. In this section, the mean value is designated by M and the design value is designated by D. To calculate the M value, the strength reduction factors,  $\phi$ , are ignored. Also, the specified compressive strength  $f_c'$  is replaced by the mean compressive strength ( $f_{cm}$ ) obtained from cylinder tests. The code limitations on the concrete strength are also ignored. To calculate the D values, the strength reduction factors,  $\phi$ , are considered. The compressive strength  $f_c'$  is calculated as  $f_{cm} - 8.27$  MPa. The limitations on the concrete strength are considered.

From Table 4.8, it is clear that the North American codes (ACI 318-02 and CSA A23.3-94) overestimate the punching strength of FRP reinforced slabs. The design punching strength is slightly conservative for slabs with FRP reinforcement.

The values of M, Mm and Dm are calculated according to BS 8110-97. Here, Mm is the mean strength with a modification of the reinforcement ratio for its lower modulus of elasticity as  $\rho E_{frp}/E_s$ . Similarly, Dm is the design value of the punching strength with a modification of the reinforcement ratio for its lower modulus of elasticity as  $\rho E_{frp}/E_s$ . To

obtain  $M$  and  $M_m$ , the limitations on  $\rho$ ,  $d$ ,  $f_{cu}$  ( $f_{cu} = 1.18f_c'$ ) and partial safety factor  $\gamma_m$  are ignored. To calculate  $D_m$ , all limitations and partial safety factors are considered. But in case of high strength concrete slabs, the limitation on concrete strength is ignored.

From Table 4.8, columns 10 – 12, it is clear that the mean values of BS 8110-97 predictions overestimates the strength of the FRP slabs. The modified mean value underestimates the slab strength.

For the Model Code 1990 (MC90), all necessary equations and limitations are given in Section 2.4.4. The constant 0.12 includes a partial safety factor  $\gamma_c = 1.5$ . Therefore, to calculate the mean value ( $M$  and  $M_m$ ), the constant 0.12 is multiplied by 1.5. The limitations on  $\xi$  and  $V_{max}$  are ignored. The average reinforcement ratio,  $\rho$ , is used instead of  $\rho$  specified in the code recommendation to maintain consistency in the comparison. The mean compressive strength,  $f_{cm}$ , is used. To calculate  $D_m$ , the partial safety factor,  $\gamma_c$ , is considered and  $f_{ck}$  is used instead of  $f_{cm}$  where  $f_{ck} = f_{cm} - 8$  MPa.

From Table 4.8, columns 13 – 15, it is clear that the mean strength of MC90 predictions overestimates the strength. However, the modified mean under estimates the strength.

The modifications of the empirical formula by Gardner (1990) which is proposed by Matthys and Taerwe (2000) is verified against the test results. In this formula,  $f_{cm}$  indicate the concrete cylinder strength on the day of testing and  $u_{1.5d}$  = rectangular or square control perimeter at a distance  $1.5d$  from the load patch (regardless of whether the load area is rectangular or circular in shape). From Table 4.8, columns 16 – 17, it is clear that

the mean strength is overestimated, but the modified mean strength is an acceptable underestimation of the slab strength.

The strain Approach and Modified Approach are verified against the test results. The Strain approach could be considered as a modified mean value according to BS 8110-85. The predictions of the Modified Approach, given in Table 4.9 column 4, slightly underestimate the slab strength.

The model proposed by Menétrey was applied with the angle of inclination as  $34^\circ$ . The ultimate strength of the FRP is used instead of  $f_s$ . The reinforcement ratio,  $\rho$ , is modified by multiplying it with  $E_{frp}/E_s$ . Some parts of this model are iterative. There is no consistency in the model prediction, but good agreement found with high strength slabs. The model predictions are given in column 5 of Table 4.9.

The elastic analysis method is used to estimate the flexural strength of the FRP slabs. In the elastic analysis of slabs, the moment of resistance capacity of the slab has to be calculated. To calculate the moment capacity of the slab, CSA A23.3 94 is followed. The material resistance reduction factors are ignored in calculating the moment capacity. From column 6 of Table 4.9, it can be observed that the elastic analysis overestimates the slab strength by around 20% and this overestimation is consistent for all FRP slabs. In Section 4.11, it is mentioned that all slabs failed by punching. Thus, the flexural capacity, calculated by elastic analysis, could be higher than slab's failure load for all slabs.

**Table 4.8: Comparison of test results with various code equations**

Slab (1)	$f_c'$ (MPa) (2)	$\rho$ % (3)	$d$ (mm) (4)	$P_u$ (kN) (5)	$P_u/P_{CSA}$		$P_u/P_{ACI}$		$P_u/P_{BS}$			$P_u/P_{MC90}$			$P_u/P_{MT}$	
					M (6)	D (7)	M (8)	D (9)	M (10)	Mm (11)	Dm (12)	M (13)	Mm (14)	Dm (15)	M (16)	Mm (17)
GS1	40	1.18	100	249	0.70	1.17	0.84	1.11	0.78	1.31	1.72	0.70	1.18	1.91	0.73	1.23
GS2	35	1.05	100	218	0.66	1.10	0.79	1.06	0.74	1.24	1.57	0.67	1.12	1.84	0.69	1.17
GS3	29	1.67	100	240	0.80	1.33	0.96	1.33	0.74	1.25	1.56	0.67	1.13	1.89	0.70	1.17
GS4	26	0.95	100	210	0.74	1.23	0.88	1.26	0.81	1.37	1.71	0.74	1.24	2.10	0.76	1.28
GSHD1	33	1.11	150	436	0.79	1.32	0.95	1.29	0.86	1.44	1.80	0.78	1.32	2.17	0.80	1.35
GSHD2	34	0.79	150	389	0.69	1.16	0.83	1.13	0.85	1.43	1.79	0.77	1.30	2.14	0.80	1.34
GSHS1	92	1.67	100	408	0.76	1.27	0.91	1.74	0.86	1.44	1.80	0.78	1.31	2.02	0.81	1.35
GSHS2	86	1.18	100	333	0.64	1.07	0.77	1.42	0.80	1.35	1.69	0.73	1.22	1.90	0.75	1.27
R1	23	0.54	154	491	1.03	1.71	1.23	1.81	1.33	1.33	1.67	1.22	1.22	2.11	1.25	1.25

M = Mean value, Mm = Mean value with modification for lower  $E_{tp}$ , Dm = Design value with modification for lower  $E_{tp}$ .

**Table 4.9: Comparison of test results with the prediction of some other rational models**

Slab (1)	$P_u$ (2) (kN)	Strain Approach (3)		Modified Approach (4)		Analytical model (Menétrey 1996) (5)		Elastic analysis (6)	
		$P_{cal}$ (kN)	$P_u/P_{cal}$	$P_{cal}$ (kN)	$P_u/P_{cal}$	$P_{cal}$ (kN)	$P_u/P_{cal}$	$P_{flex}$ (kN)	$P_u/P_{flex}$
GS1	249	180	1.38	220	1.13	257	0.97	299	0.83
GS2	218	166	1.31	202	1.08	270	0.81	267	0.82
GS3	240	182	1.32	221	1.08	268	0.90	291	0.82
GS4	210	145	1.44	177	1.19	181	1.16	220	0.95
GSHD1	436	286	1.52	348	1.25	363	1.20	574	0.76
GSHD2	389	258	1.51	314	1.24	317	1.23	513	0.76
GSHS1	408	267	1.53	325	1.25	436	0.94	501	0.81
GSHS2	333	233	1.43	283	1.18	350	0.95	374	0.89
R1	491	348	1.41	424	1.16	<sup>a</sup>		423 <sup>b</sup>	1.16

<sup>a</sup>Can not calculate and shows the indication of flexural failure. <sup>b</sup>From Yield Line Analysis.

## **Chapter 5**

### **Proposed Mechanical Model**

#### **5.1 Introduction**

One of the objectives of the current research program is to propose a mechanical model that is capable of predicting the punching capacity of internal slab-column connections under axial load. The mechanical models available in literature are for slabs reinforced with traditional steel bars. In this chapter, the mechanical model proposed by Hallgren (1996) is adopted and modified for slabs reinforced with FRP bars. The modifications include the difference in behaviour of FRP reinforced slabs and steel reinforced slabs. In the following sections, the Hallgren's model and the proposed modifications are described. Finally, two algorithms are proposed for the proposed model. The first one is for slabs reinforced with FRP reinforcement and the other one is for slabs with traditional steel reinforcement. The algorithm for slabs with steel reinforcement, considers the necessary modifications on model geometry and relevant changes in formulas. The other algorithm considers the modifications due to FRP's property in addition to the modification of the model geometry. The modified model, which is proposed for slabs with FRP bars as well as traditional steel reinforcement, is verified with the current test results as well as the test results available in literature.

## **5.2 Mechanical model proposed by Hallgren (1996)**

Hallgren (1996) derived a mechanical model to predict the punching capacity of slabs reinforced with traditional steel reinforcement and without shear reinforcement. The model is based on the model proposed by Kinnunen and Nylander (1960). The model is iterative in nature. It considers the equilibrium of a radial slab segment. The model geometry and the forces acting on a radial segment are briefly described in the following sections.

### **5.2.1 Model geometry**

The model considers a circular polar-symmetrical slab supported along the circumference of the slab and is loaded through a circular column at the center of the slab. The model geometry is shown in Fig. 5.1.

Inclined shear cracks around the column and radial cracks outside the inclined shear crack develop as the slab fails. The slab portions bounded by the shear crack and radial cracks, form fan like shape and rotate as a rigid body. The failure load,  $P$ , is computed from the equilibrium of forces acting on the slab segment. The load is carried by the slab portion outside the shear crack and is transferred to the column by a truncated wedge. The inclined compressive force passing through the truncated wedge is denoted by  $T$ . The

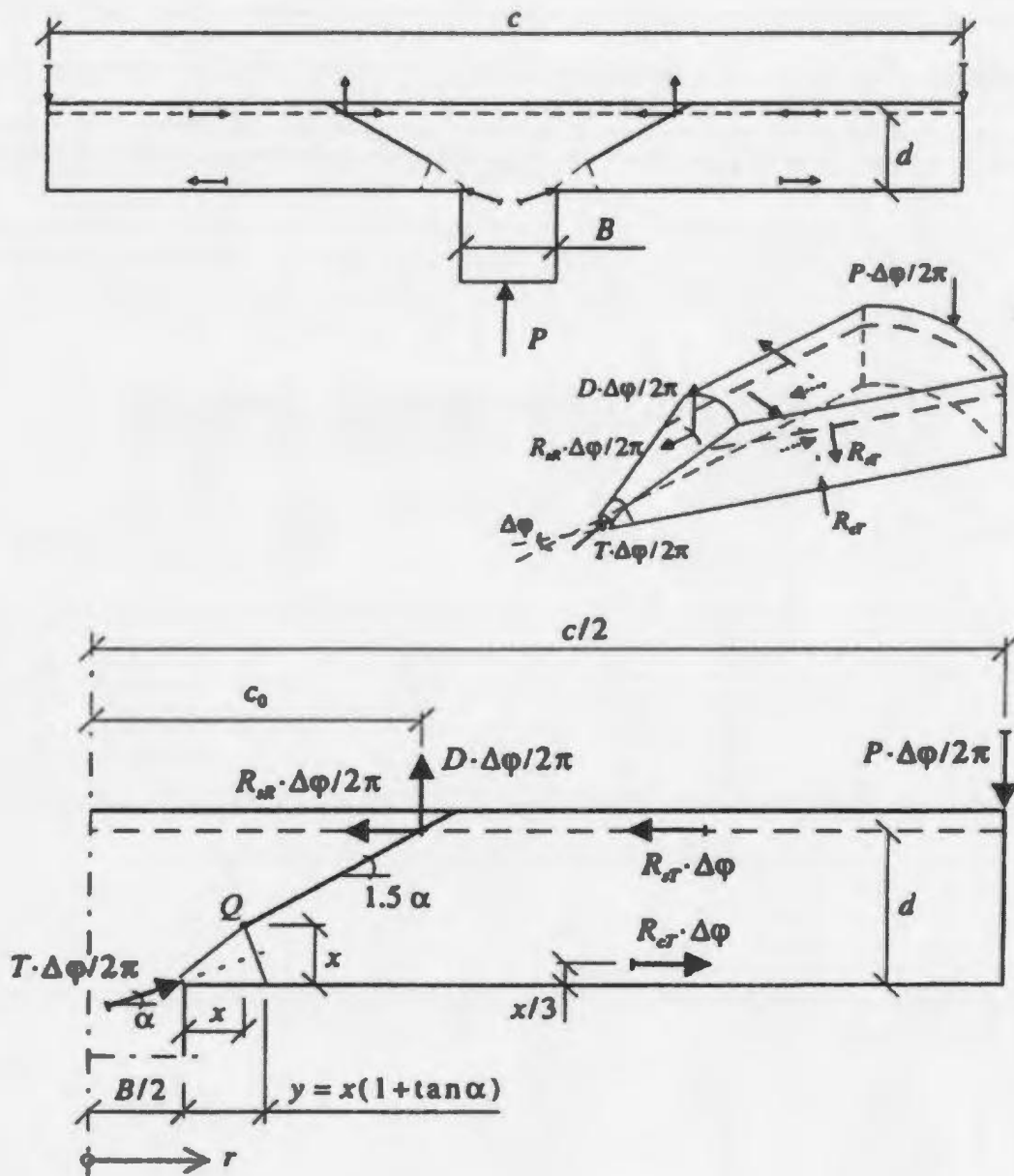
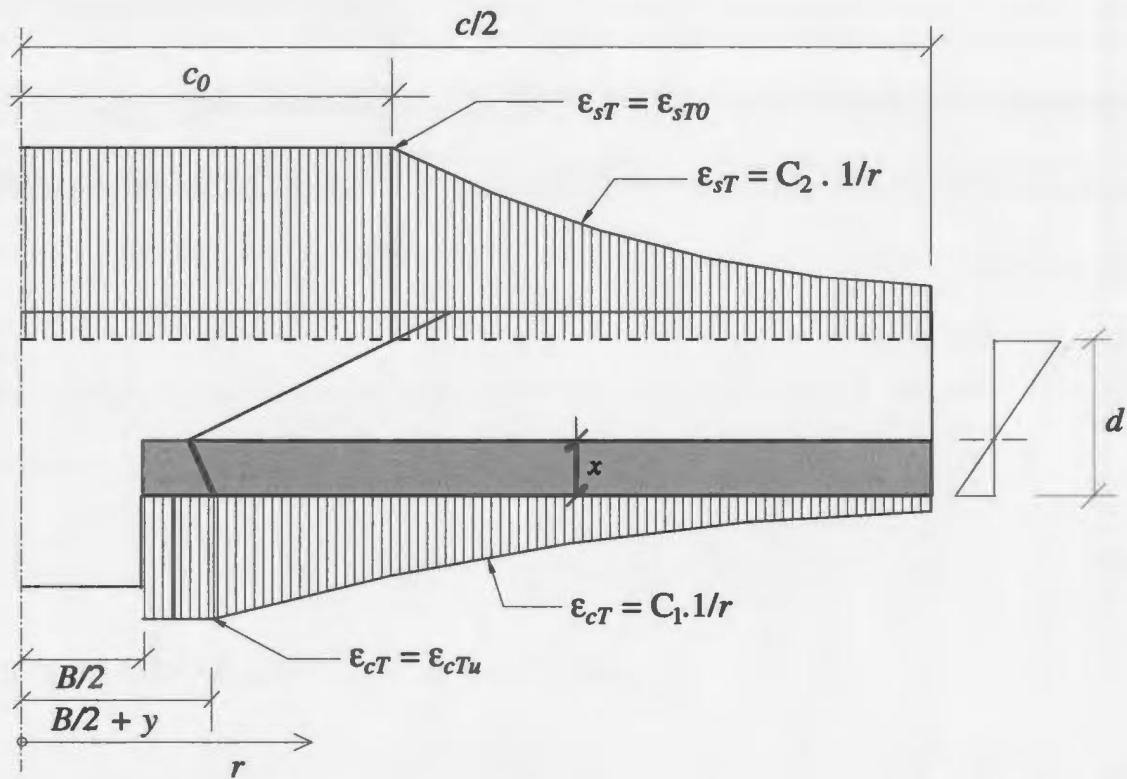


Fig. 5.1: Model geometry [Hallgren (1996)]



**Fig. 5.2: Distribution of steel and concrete tangential strains,  $\epsilon_{sT}$  and  $\epsilon_{cT}$ , respectively, along the radius  $r$  [Hallgren (1996)]**

length of the truncated wedge along the bottom surface of the slab in radial direction is given by

$$y = x (1 + \tan \alpha) \quad (5.1)$$

where  $\alpha$  is the angle of inclination of the force  $T$ . The distance  $c_o$  from the column center to the shear crack at the level of the flexural reinforcement is

$$c_o = \frac{B}{2} + x + \frac{d - x}{\tan(1.5\alpha)} \quad (5.2)$$

where  $B$  is the diameter of column and  $x$  is the depth of the compression zone.

## 5.2.2 Tangential strains

The tangential strain distribution is shown in Fig. 5.2. For  $r \geq B/2 + y$ , the tangential concrete strain is expressed as

$$\varepsilon_{cT} = C_1 \frac{1}{r} \quad (5.3)$$

where  $C_1$  is a constant. The tangential concrete strain reaches its ultimate value  $\varepsilon_{cTu}$  at  $r = B/2 + y$ . Substituting into Eq. 5.3, gives

$$\varepsilon_{cTu} = C_1 \frac{1}{B/2 + y} \quad (5.4)$$

From Eq. 5.4, the constant  $C_1$  can be evaluated as

$$C_1 = \varepsilon_{cTu} \left( \frac{B}{2} + y \right) \quad (5.5)$$

For  $r \geq c_o$

$$\varepsilon_{sT} = C_2 \frac{1}{r} \quad (5.6)$$

where  $C_2$  is a constant. The assumption of a linear strain-distribution across the section gives

$$\varepsilon_{st} = \frac{\varepsilon_{cT}(d - x)}{x} \quad (5.7)$$

Inserting Eq. 5.3 into Eq. 5.7 and combining them with Eq. 5.6 and inserting the result in Eq. 5.5, gives

$$C_2 = \left( \frac{d}{x} - 1 \right) C_1 = \left( \frac{d}{x} - 1 \right) \left( \frac{B}{2} + y \right) \varepsilon_{cTu} \quad (5.8)$$

### 5.2.3 Depth of the tangential compression zone

the depth of the compression zone,  $x$ , can be determined from the tangential strain of concrete and steel and from the stress-strain status, i.e. elastic or plastic status of concrete, and steel reinforcing bars at  $r = c_o$ . The adopted stress-strain idealization are shown in Fig. 5.3.

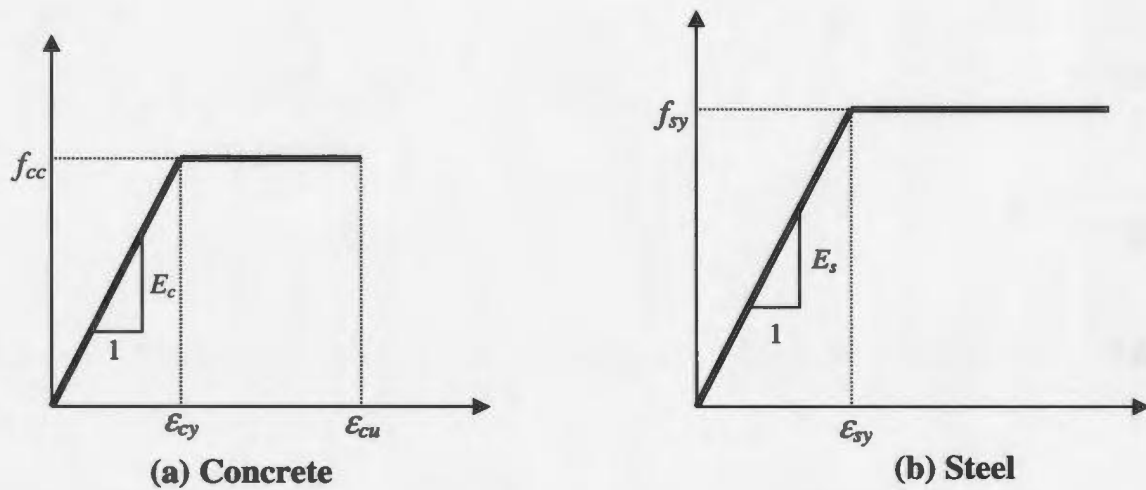


**Fig. 5.3: Adopted stress-strain curves for concrete and steel, respectively [Hallgren (1996)]**

The yield strain of the concrete is given by

$$\varepsilon_{cy} = \frac{f_{cc}}{E_c} \quad (5.9)$$

The yield strain of the steel is given by

$$\varepsilon_{sy} = \frac{f_{sy}}{E_s} \quad (5.10)$$

Therefore the resulting force of the concrete stress block can be expressed as

$$F_c = \alpha_c f_{cc} x dr \quad (5.11)$$

where the factor  $\alpha_c$  is given by

$$\alpha_c = 1 - \frac{\epsilon_{cy}}{2\epsilon_{cT}} \quad (5.12)$$

The following scenarios arise:

a) If the *steel* and *concrete* are both in the *elastic* state,  $x$  is given by

$$x = \rho \frac{E_s}{k_E E_c} \left( \sqrt{1 + \frac{2 k_E E_c}{\rho E_s}} - 1 \right) d \quad (5.13)$$

where,

$$k_E = \left( 1 - \frac{\nu + 2\nu^2}{2 + \nu} \right)^{-1} \quad (5.14)$$

where  $\nu$  is the Poisson's ratio of concrete. Assuming that  $\nu = 0.2$ , the value of the factor  $k_E$  is 1.15.

b) If the *concrete* has *yielded* at  $r = c_0$ , but *steel* is in *elastic* state, then

$$x = \frac{\rho E_s \epsilon_{cT0}}{2 \alpha_{c0} f_{cc}} \left( \sqrt{1 + \frac{4 \alpha_{c0} f_{cc}}{\rho E_s \epsilon_{cT0}}} - 1 \right) d \quad (5.15)$$

where  $\alpha_{c0}$  is obtained by inserting  $\epsilon_{cT} = \epsilon_{cT0}$  into Eq. 5.12 and  $\epsilon_{cT0}$  is obtained by inserting  $r = c_0$  into Eq. 5.3.

c) If the *steel* has *yielded* at  $r = c_0$  but *concrete* is in *elastic* state, then

$$x = \frac{2 \rho d f_{sy}}{\epsilon_{cT0} k_E E_c} \quad (5.16)$$

d) If both *steel and concrete* have yielded at  $r = c_o$  then

$$x = \frac{\rho d f_{sy}}{\alpha_{co} f_{cc}} \quad (5.17)$$

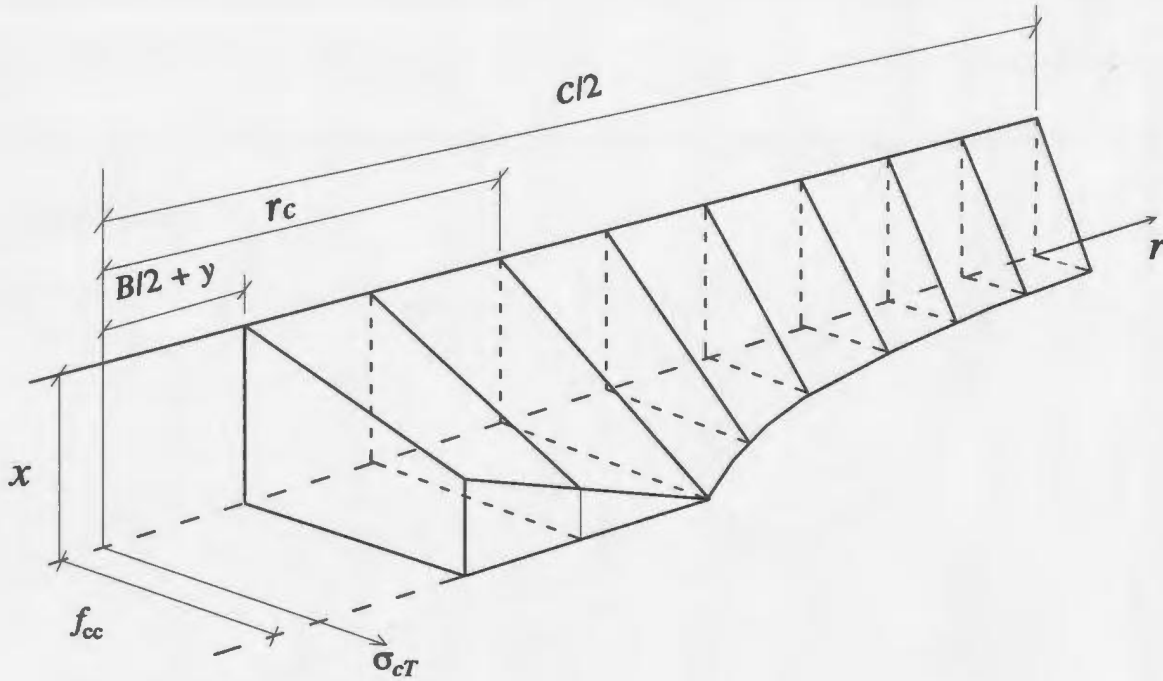


**Fig. 5.4: Distribution of tangential concrete stresses,  $\sigma_{cT}$ , in the compression zone, along the radius  $r$  of the slab, when some part the of compression zone is yielded [Hallgren (1996)]**

#### 5.2.4 Resulting forces on concrete in compression and steel in tension

If the concrete in tangential direction is in the elastic state, then by integrating from  $r = B/2 + y$  to  $r = c/2$ , the resulting tangential concrete force can be expressed as:

$$R_{cT} = \frac{1}{2} E_c \times C_1 \ln \left( \frac{c}{B+2y} \right) \quad (5.18)$$

If the tangential concrete strain reaches the yield strain,  $\epsilon_{cy}$ , at a radius from the slab center larger than  $B/2+y$ , then this yield radius can be determined from:

$$r_c = \frac{C_1}{\epsilon_{cy}} \quad (5.19)$$

If  $r_c > B/2 + y$  then by integration, the following expression results for tangential concrete force:

$$R_{cT} = f_{cc} \times \left[ r_c - \frac{B}{2} - y - \frac{\epsilon_{cy}}{4C_1} \left( r_c^2 - \left( \frac{B}{2} + y \right)^2 \right) \right] + \frac{1}{2} E_c \times C_1 \ln \left( \frac{c}{2r_c} \right) \quad (5.20)$$

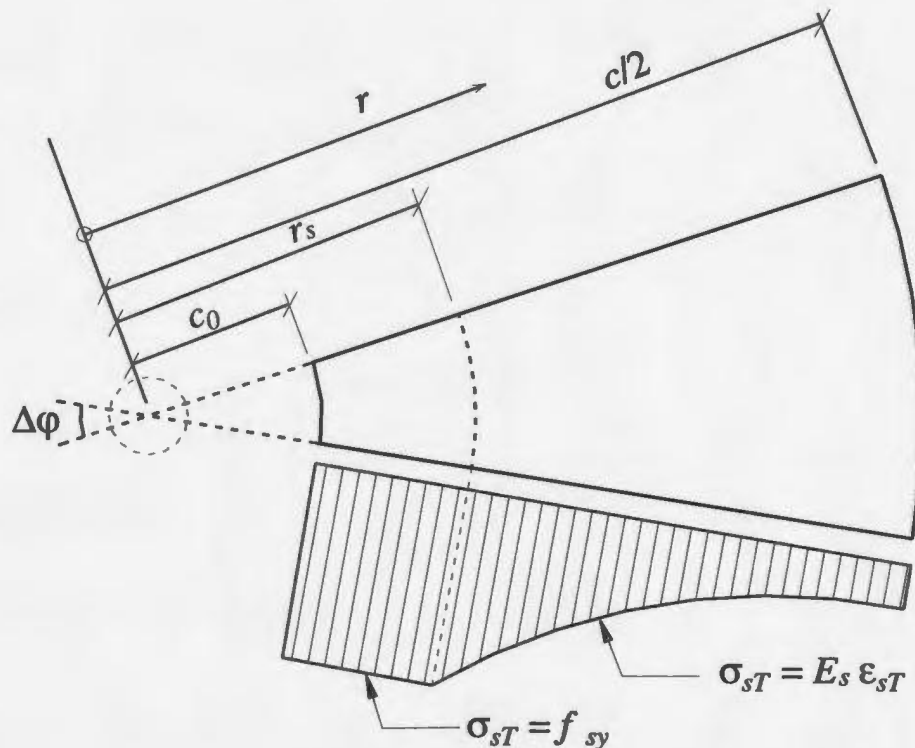


**Fig. 5.5: Tangential steel stress  $\sigma_{sT}$  in the flexural reinforcement, along the radius  $r$  of the slab, when some steel is yielded [Hallgren (1996)]**

If the steel in the tangential direction is in elastic state, then by integrating from  $r = c_o$  to  $r = c/2$ , the resulting steel force in tangential direction is:

$$R_{sT} = \rho d E_s C_2 \ln\left(\frac{c}{2c_o}\right) \quad (5.21)$$

If the tangential steel strain reaches the yield strain,  $\epsilon_{sy}$ , at a radius from the slab center larger than  $c_o$ , then this yield radius can be determined from

$$r_s = \frac{C_2}{\epsilon_{sy}} \quad (5.22)$$

If  $r_s > c_o$ , then by integrating from  $r = c_o$  to  $r = c/2$ , the resulting steel force in tangential direction is

$$R_{sT} = \rho d \left[ f_{sy} (r_s - c_o) + E_s C_2 \ln\left(\frac{c}{2r_s}\right) \right] \quad (5.23)$$

If  $r_s < c_o$ , the steel force in radial direction is

$$R_{sR} = \rho d 2\pi c_o E_s \epsilon_{sTO} \quad (5.24)$$

If  $r_s \geq c_o$  then

$$R_{sR} = \rho d 2\pi c_o f_{sy} \quad (5.25)$$

### 5.2.5 Dowel force

In Hallgren's model, the dowel force  $D$  is expressed as

$$D = 27.9 \phi^{2/3} c_o \left( 1 - 1.6 \frac{\rho d}{\phi} \right) f_{cc}^{1/3} \quad [\text{N}] \quad (5.26)$$

where  $\phi$  is the diameter of steel bars used in slab. The formula is based on modified dowel force equation proposed by Hamadi and Regan (1980). For simplicity, if the reinforcing steel bars intersecting the shear crack yields, the dowel force can be assumed as:

$$D = 0 \quad (5.27)$$

### 5.2.6 Equilibrium equations

Taking the summation of all vertical force components, the radial force components and the moments about point  $Q$  and equating them to zero, results the following equations:

$$P_v = T \sin \alpha + D \quad (5.28)$$

$$T = \frac{R_{sT} + 2\pi (R_{sT} - R_{cT})}{\cos \alpha} \quad (5.29)$$

$$P_m = \frac{(2\pi R_{sT} + R_{sR})(d - x) + D \left( c_o - \frac{B}{2} - x \right) + T \frac{x}{2 \cos \alpha} + 2\pi R_{cT} \frac{2x}{3}}{\frac{c - B}{2} - x} \quad (5.30)$$

### 5.2.7 Failure criterion

Immediately before failure, the concrete strains at  $r = B/2 + y$  is assumed as

$$\epsilon_{cT_u} = -\epsilon_{cZ_u} \quad (5.31)$$

where  $\epsilon_{cT_u}$  is the ultimate tangential concrete strain at  $r = B/2 + y$  (which is the failure strain) and  $\epsilon_{cZ_u}$  is the ultimate tensile transverse strain in the  $Z$ -direction at that location. After the ultimate stress is reached, the concrete at  $r = B/2 + y$  starts to soften and the

confining principal stress of the three-dimensional state of compressive stresses at the column-slab root decreases. The three-dimensional state of compressive stresses become unstable and the shear crack runs through the compression zone. Consequently, punching shear failure occurs.

This failure criterion is modeled based on nonlinear fracture mechanics. The concrete strain at failure which is the maximum tangential concrete strain at  $r = B/2 + y$ , is

$$\varepsilon_{cTu} = \frac{3.6 G_F^\alpha}{x f_{ct}} \left( 1 + \frac{13 d_a}{x} \right)^{-1/2} \quad (5.32)$$

where  $G_F^\alpha$  is the fracture energy,  $d_a$  is the maximum aggregate size and  $f_{ct}$  is the tensile strength of concrete.  $G_F^\alpha$  can be estimated from RILEM (1985) beam tests, where only one size is tested.

$$G_F^\alpha = G_F^R \left( 1 + \frac{13 d_a}{d^R} \right)^{1/2} \quad (5.33)$$

where  $G_F^R$  is the fracture energy, measured according to the RILEM recommendations (1985), and  $d^R$  is the depth of the RILEM test beam.

If the mechanical properties of concrete are not known such as concrete tensile strength, modulus of elasticity,  $G_F^R$  etc., some European code equations are suggested to calculate these mechanical properties of concrete. These equations are given in Appendix B and most of these equations are based on the CEB-FIP model code.



to the line  $Qd$  and  $c$  is the mid point of line  $Qd$ . The angle of inclination of force  $T$  is  $\alpha$ . Hence, the  $\angle cad = \alpha$  and the  $\angle eQd$  is also equal to  $\alpha$ . As shown in Fig. 5.6, the extension of line  $df$  and  $Qb$  intersect at point  $a$ . Nevertheless, this depends on the angle of inclination of line  $Qb$ . If the angle of inclination of line  $Qd$  is  $2\alpha$ , then both extensions will meet at point  $a$ . If the angle of inclination of line  $Qb$  is  $2\alpha$ , then the extension of line  $df$  and  $Qb$  will meet at point  $a$  and the line  $ac$  will be the bisector of  $\angle Qad$ . This implies that the force  $T$  has to pass through the center line of the truncated wedge. This appears to be more reasonable. However, Hallgren did not clarify this issue when presenting his model. In the next section, further discussion is made considering the angle of inclination of line  $Qb$  and whether it is equal to  $2\alpha$  or not.

The model is iterative in nature. First, the depth of compression zone,  $x$ , has to be determined using the strain compatibility and force equilibrium in a tangential direction. After then, the angle of inclination,  $\alpha$ , of the force  $T$  has to be determined from the equations of equilibrium. Hallgren did not place any limitation on the angle  $\alpha$ . The calculated values of the angle  $\alpha$  ranged from  $12^\circ$  to  $30.9^\circ$  for various slabs reported by him. In the next paragraphs, it will be described what happens if the angle  $\alpha$  exceeds  $22.5^\circ$ .

From Fig. 5.6, it is clear that  $eQ = x$  which is the depth of compressive zone. It is also assumed that  $fe = x$ . Therefore, the  $\angle Qfe$  will always be equal to  $45^\circ$  for any value of  $x$ .

After determining the value of  $x$  by iteration, the value of  $\alpha$  has to be changed to satisfy

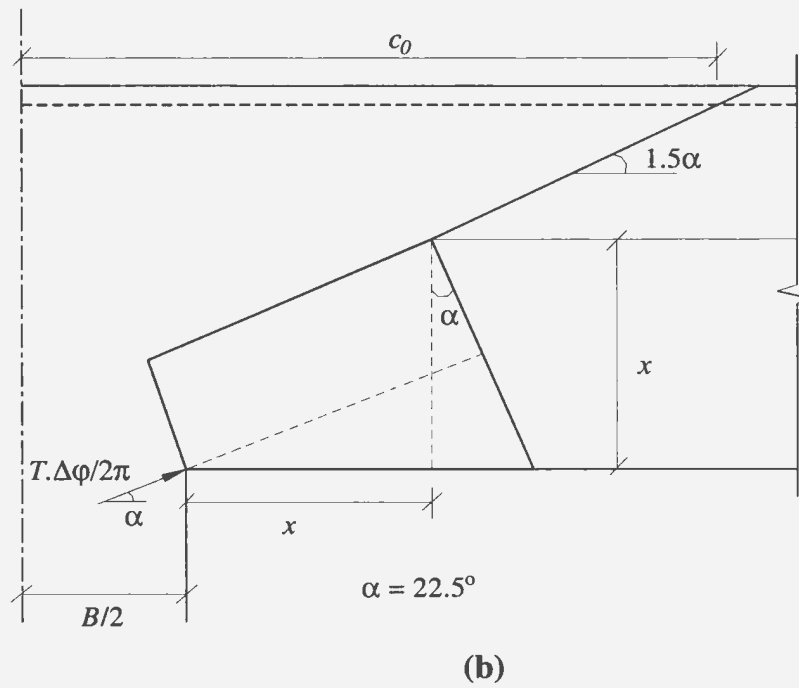
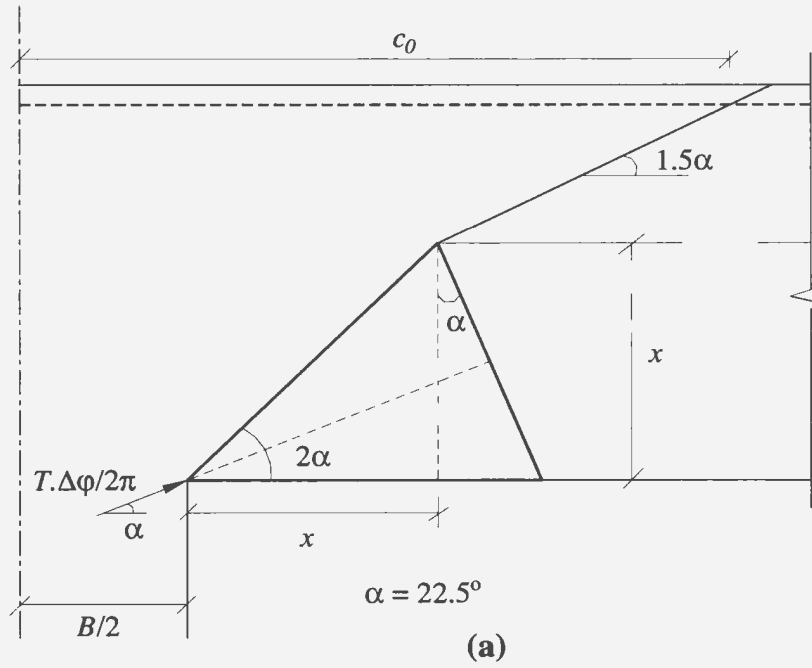
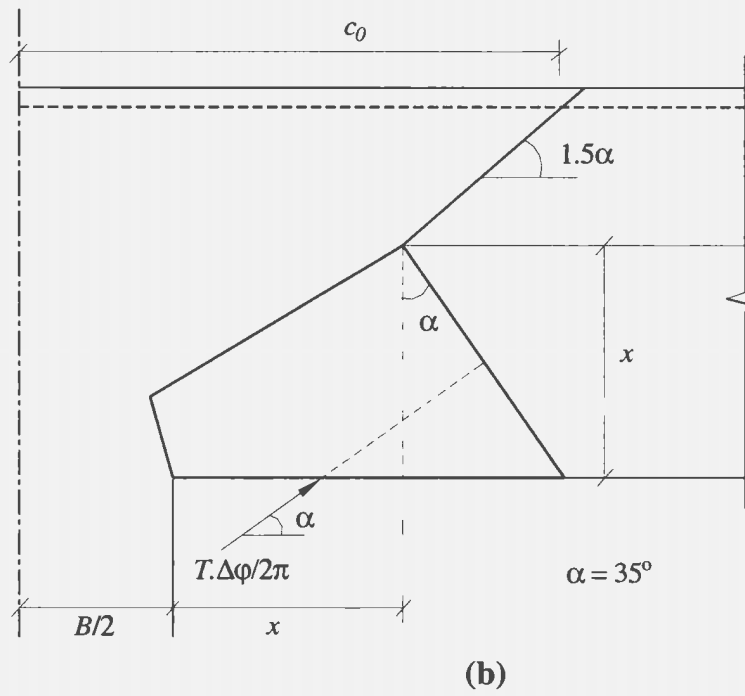
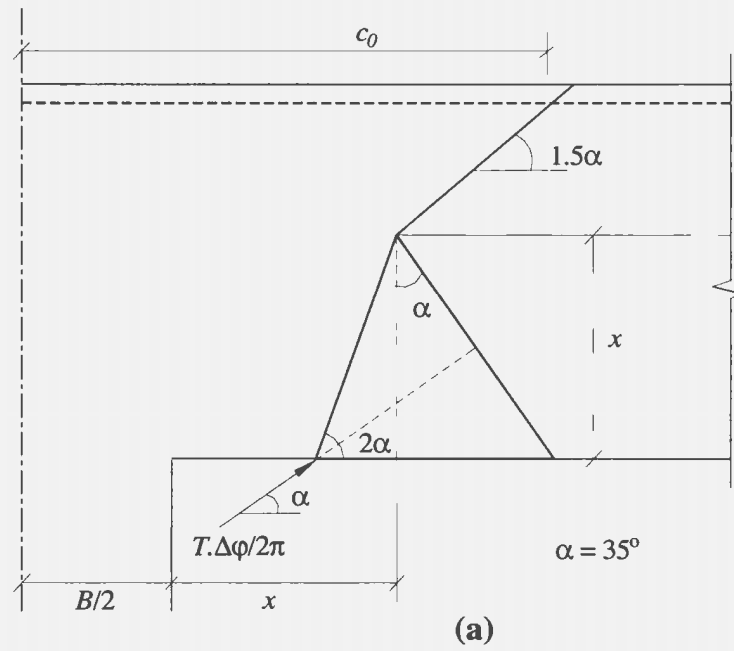


Fig. 5.7: Geometry of truncated wedge for  $\alpha = 22.5^\circ$



**Fig. 5.8: Geometry of truncated wedge for  $\alpha = 35^\circ$**

the equations of equilibrium. This implies that the line  $Qd$  has to rotate to satisfy the equations of equilibrium taking  $Q$  as the center of rotation.

If the line  $Qd$  make an angle  $22.5^\circ$  with line  $Qe$ , that is  $\alpha = 22.5^\circ$ , the shape of the truncated wedge will be as shown in Fig. 5.7. If the force  $T$  passes through the center line of the truncated wedge, the shape of the truncated wedge will be as depicted in Fig. 5.7 (a). If not, the shape of truncated wedge will be something like that shown in Fig. 5.7(b). In both cases, the force  $T$  is passing through the corner of slab-column joint may not be reasonable. Again, a truncated wedge with acute angle is not acceptable.

If the line  $Qd$  make an angle  $35^\circ$  with line  $Qe$ , that is  $\alpha = 35^\circ$ , the shape of the truncated wedge will be as shown in Fig. 5.8. If the force  $T$  pass through the center line of the truncated wedge, the shape of the truncated wedge will be as depicted in Fig. 5.8(a). If not, the shape of the truncated wedge will be something like that shown in Fig. 5.8(b). In both cases, the force  $T$  is transferred from the slab to the column through a void which is not possible.

From the above discussion, it is clear that when  $\alpha \geq 22.5^\circ$  the model becomes irrational. Therefore, modification to the model is necessary. In particular, the assumed model geometry should be revised.

## **5.4 Proposed model**

Considering the limitation of the Hallgren's model, the assumption behind the model



$0.7x_1$ . The depth of the tangential compression zone is  $x_2$ . The relation between  $x_1$  and  $x_2$  is

$$x_1 = x_2 \cot(2\alpha) \quad \text{for } \alpha > 20^\circ \quad (5.34)$$

The angle of the inclined shear crack is taken as  $\delta\alpha$  instead of  $1.5\alpha$  where  $\delta$  and  $\alpha$  both are variables. The limitation imposed is that,  $\alpha$  cannot be greater than  $45^\circ$ .

The above modification is proposed for slabs with traditional reinforcement. For the slabs reinforced with FRP reinforcement, the properties of FRP have to be incorporated in the model, along with the above mentioned modification.

Based on the proposed assumptions, the equations are:

For  $\alpha > 20^\circ$ ,

$$y = 0.7 x_1 + x_2 \tan(\alpha) \quad (5.35)$$

$$c_0 = B/2 + 0.7x_1 + (d - x_2)/\tan(\delta\alpha) \quad (5.36)$$

$$P_m = \frac{(2\pi R_{sT} + R_{sR})(d - x_2) + D \left( c_0 - \frac{B}{2} - 0.7x_1 \right) + T \frac{x_2}{2 \cos \alpha} + 2\pi R_{cT} \left( \frac{2x_2}{3} - \frac{x_2 r_c}{3c} \right)}{\frac{c - B}{2} - 0.7x_1} \quad (5.37)$$

For  $\alpha \leq 20^\circ$ ,

$$x_1 = x_2 \quad (5.38)$$

$$y = x_1 + x_2 \tan(\alpha) \quad (5.39)$$

$$c_0 = B/2 + x_1 + (d - x_2)/\tan(\delta\alpha) \quad (5.40)$$

$$P_m = \frac{(2\pi R_{sT} + R_{sR})(d - x_2) + D\left(c_0 - \frac{B}{2} - x_1\right) + T\frac{x_2}{2\cos\alpha} + 2\pi R_{cT}\left(\frac{2x_2}{3} - \frac{x_2 r_c}{3c}\right)}{\frac{c - B}{2} - x_1} \quad (5.41)$$

The values of  $y$  and  $c_0$  will be used in all equations given in Section 5.2. In addition, in all equations, the parameter  $x$  will be replaced with  $x_2$  when  $x$  indicates the depth of the tangential compression zone. The parameter  $x$  will be replaced with  $x_1$  or  $0.7x_1$  depending on the value of  $\alpha$ , where  $x$  indicates the distance from the column face to the projection of center of rotation,  $Q$ , on the slab bottom. Consequently, all equations of Section 5.2 will be changed. The changed equations are used in the proposed model. The equations for  $x$ ,  $y$ ,  $c_0$  and  $P_m$  remain the same.

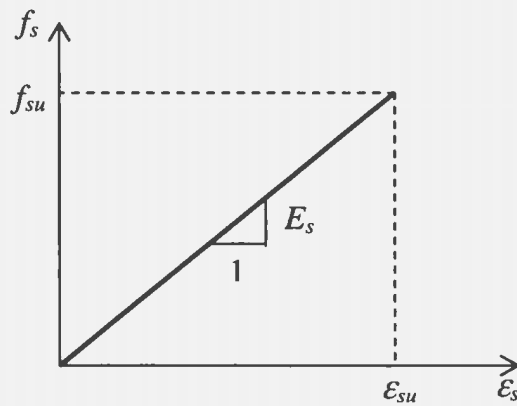


**Fig. 5.10: Stress-strain relation of FRP reinforcement**

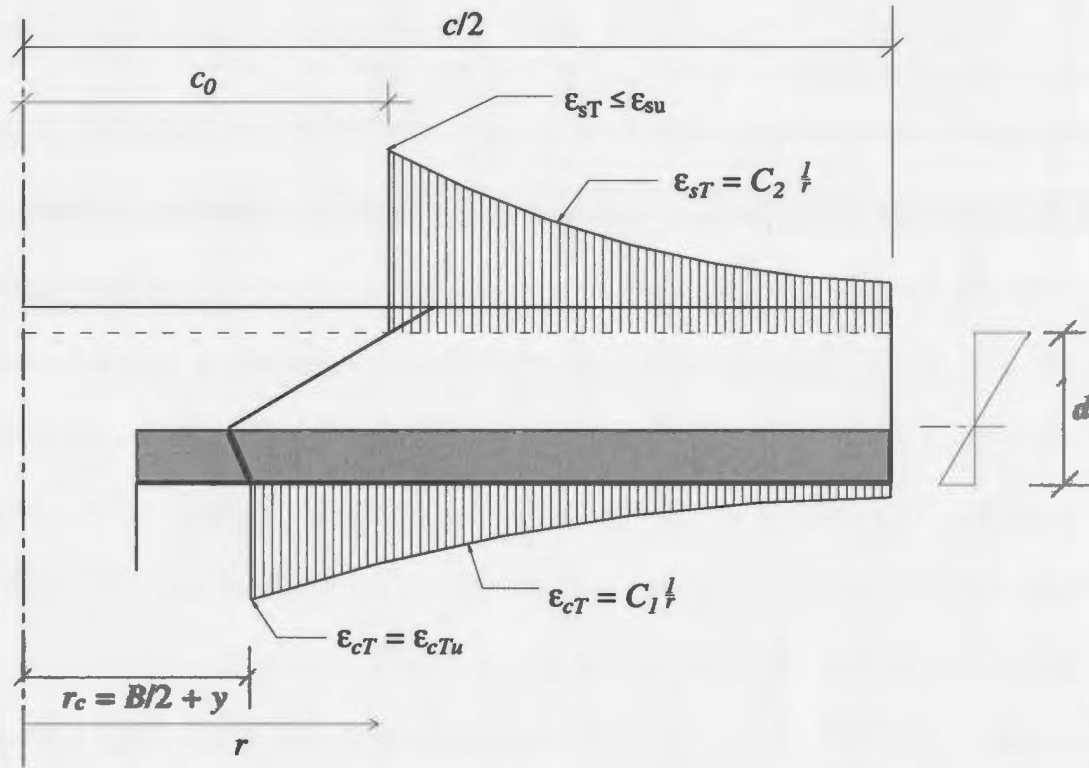


**Fig. 5.11: Tangential strain distribution of FRP reinforced slab segment outside the shear crack**

### 5.4.2 Implementation of FRP properties

For slabs reinforced with FRP bars or two-dimensional grids, the equations for calculating the depth of the tangential compression zone will change due to the different stress-strain characteristics of FRP. The linear stress-strain relation of FRP that is used in the modeling process is shown in Fig. 5.10. As some formulas are common for steel reinforced slabs and FRP reinforced slabs, the notation of the stress-strain properties are assumed in the same fashion for both steel and FRP reinforced. For example, in case of

steel reinforced slab,  $E_s$  will be used to indicate the modulus of elasticity of the steel bars. Also,  $E_s$  will be used to indicate the modulus of elasticity of FRP bars or grid ribs.

The strain distribution in the tangential direction for a slab reinforced with FRP reinforcement is shown in Fig. 5.11. As there is no yielding for FRP reinforcement, a tangential stress distribution of reinforcement, like that shown in Fig. 5.5, will not be present in case of FRP reinforced slabs. The stress distribution and strain distribution of FRP in the tangential direction are qualitatively the same. The tangential stress distribution in concrete, shown in Fig. 5.4, is still applicable for FRP reinforced slabs. The depth of the compression zone,  $x_2$ , is determined from strain compatibility of the tangential strain of the concrete and FRP and from stress-strain status i.e. elastic or plastic status of concrete at  $r = c_o$ .

a) If FRP and concrete both are in the *elastic* state at  $r = c_o$ , then

$$x_2 = \rho \frac{E_s}{k_E E_c} \left( \sqrt{1 + \frac{2k_E E_c}{\rho E_s}} - 1 \right) d \quad (5.42)$$

Where,

$$k_E = \left( 1 - \frac{\nu + 2\nu^2}{2 + \nu} \right)^{-1} \quad (5.43)$$

where  $\nu$  is the Poisson's ratio of concrete. Considering  $\nu = 0.2$ , the value of the factor  $k_E$  is 1.15. Note that, Eqs. 5.42 and 5.43 are similar to Eqs. 5.13 and 5.14.

b) If the concrete *yields* but the FRP is in the *elastic* state at  $r = c_o$ , then

$$x_2 = \frac{\rho E_s \epsilon_{cTo}}{2\alpha_{co} f_{cc}} \left( \sqrt{1 + \frac{4\alpha_{co} f_{cc}}{\rho E_s \epsilon_{cTo}}} - 1 \right) d \quad (5.44)$$

where  $\alpha_{c0}$  is obtained by inserting  $\varepsilon_{cT} = \varepsilon_{cT0}$  into Eq. 5.12 and where  $\varepsilon_{cT0}$  is obtained by inserting  $r = c_0$  into Eq. 5.3. Here Eq. 5.44 is as same as Eq. 5.15.

c) If FRP reaches *ultimate strain* and the concrete is in the *elastic state* at  $r = c_0$ , then

$$x_2 = \rho \frac{E_s}{k_E E_c} \left( \sqrt{1 + \frac{2k_E E_c}{\rho E_s}} - 1 \right) d \quad (5.45)$$

Note that Eq. 5.45 is similar to Eq. 5.42, as both equations are independent of strain.

d) If FRP reaches *ultimate strain* and the concrete is *yielded* at  $r = c_0$ , then

$$x_2 = \frac{\varepsilon_{su} E_s \rho d}{\alpha_{c0} f_{cc}} \quad (5.46)$$

The dowel force equation used in the original model by Hallgren is for steel bars. The stiffness of the FRP bars is lower than that of steel. Consequently, a dowel force reduction factor,  $\mu$ , is adopted. It is hypothesized that if the modulus of elasticity of a FRP bar is zero, then  $\mu = 0$ . If the modulus of elasticity of a FRP bar is equal to that of a steel bar,  $E_s$ , then  $\mu = 1$ . These are the boundary conditions of  $\mu$ . The variation of  $\mu$  between these two limits is not known. By analyzing all the test data available in the literature, a variation of  $\mu$  is assumed as shown in Fig. 5.12.

The value of  $\mu$  is given by the following expression:

$$\mu = -3 \xi^4 + 8.2 \xi^3 - 8.2 \xi^2 + 4 \xi \quad (5.47)$$

where  $\xi = E_{FRP} / E_s$ .

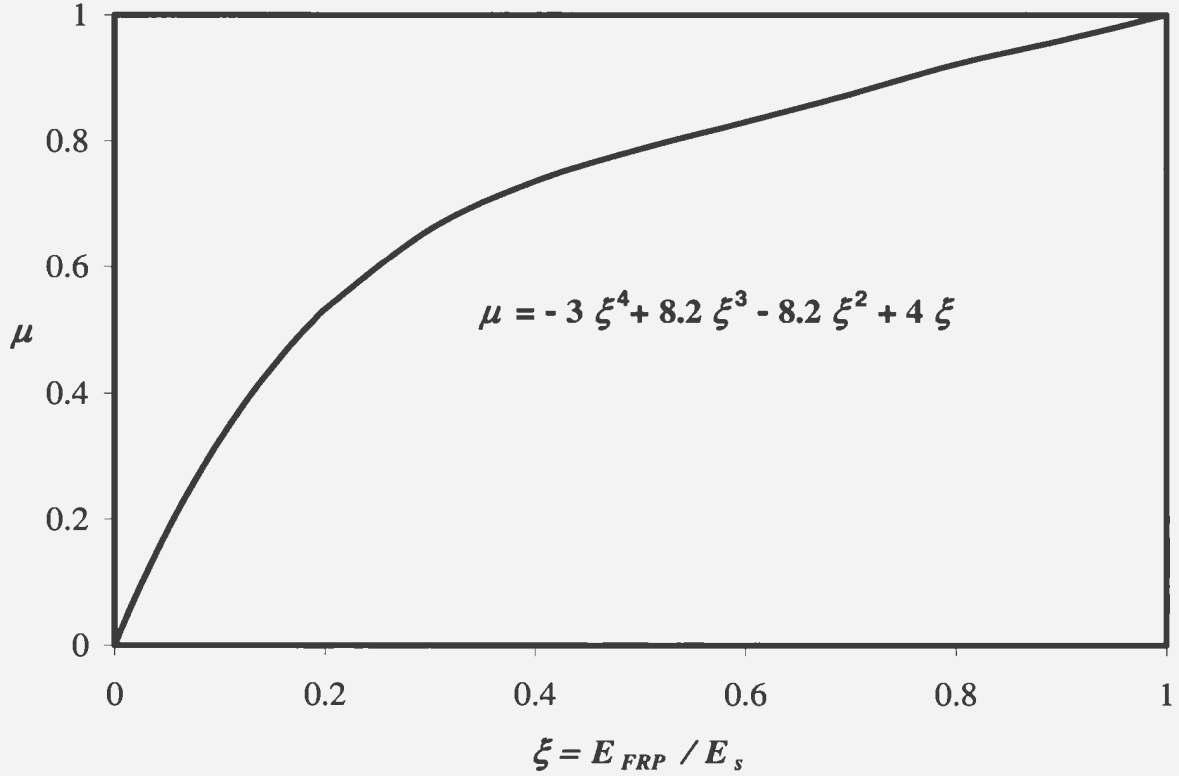


**Fig. 5.12: Variation of the dowel force reduction factor,  $\mu$**

Equation 5.48 is used to calculate the dowel force,  $D$ , for the slabs reinforced with FRP bars.

$$D = 27.9 \mu \phi^{2/3} c_0 \left( 1 - \frac{1.6 \rho d}{\phi} \right) f_{cc}^{1/3} \quad (5.48)$$

## 5.5 Solution algorithm

The equations of the proposed model are solved using an algorithm which is iterative in nature. The flow chart of the algorithm is given in Fig. 5.13 for slabs with steel reinforcement, and in Fig. 5.14 for slabs reinforced FRP bars or grids.

In the algorithm, there are several loops. The inner loop deals with the depth of the tangential compression zone of concrete. The loop converges to a solution when for an assumed depth,  $x_2$ , and the calculated depth,  $x_2$ , become equal. The outer first loop deals with the angle of inclination,  $\alpha$ , of the compressive force  $T$ . The loop converge to a solution when for an assumed  $\alpha$ , the equations of equilibrium are satisfied.

The outer second loop deals with  $\delta$ . The initial value of  $\delta$  is set to a value of 1.5 as in the original model by Hallgren. If the equations of equilibrium are not satisfied for  $\delta = 1.5$ , the value of  $\delta$  will be changed through the outer second loop to determine the value of  $\delta$  which satisfies the equations of equilibrium.

The outer third loop deals with the imposed maximum limit on  $\alpha$ . Initially, the maximum limit of  $\alpha$  is taken as  $30^\circ$ . Most of the steel reinforced slabs satisfy the equations of equilibrium within this limit and the model result agrees with the test result. However, few typical FRP slabs do not satisfy the equations of equilibrium within this limit. For these cases, the maximum limit of  $\alpha$  is slightly higher then  $30^\circ$ . In any case, it cannot exceed  $45^\circ$ . Thus, the outer third loop handles the change of the limit imposed on  $\alpha$  to satisfy the equations of equilibrium.

The computer programs of the algorithms are written in MATLAB<sup>®</sup> 6.1 (2001) code. The codes are given in Appendix C.

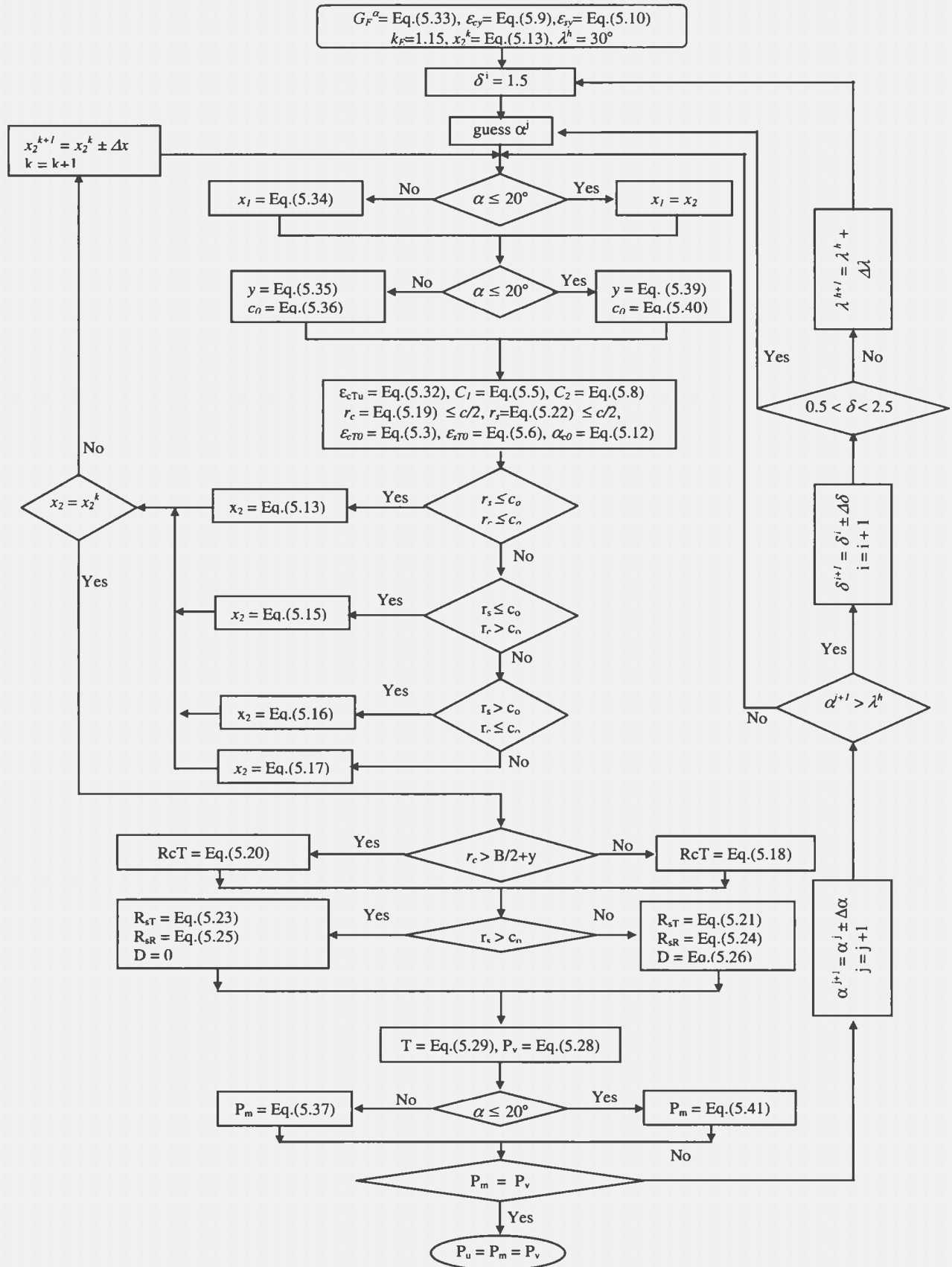


Fig. 5.13: Flow-chart of the algorithm of the proposed model for steel reinforced slabs

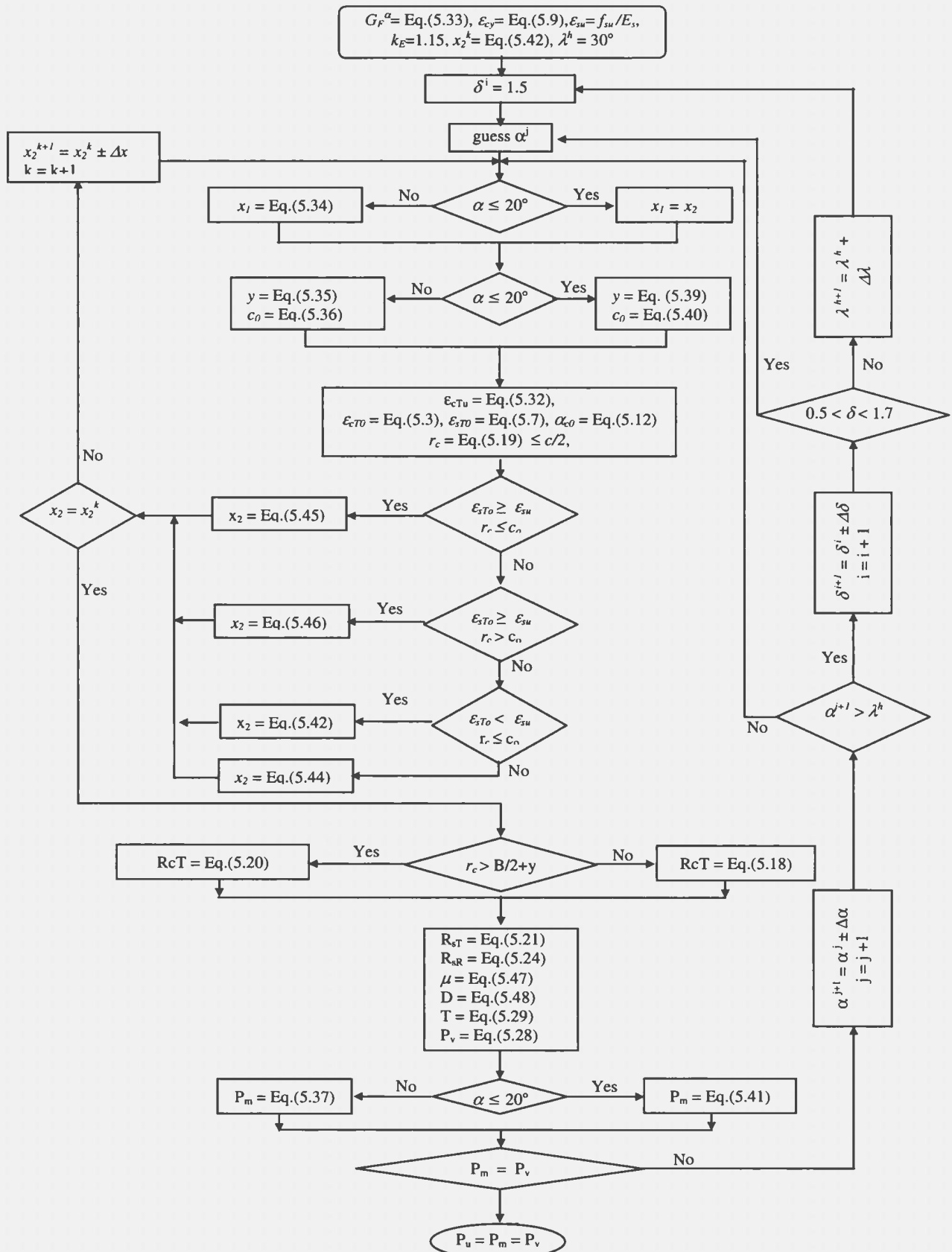


Fig. 5.14: Flow-chart of the algorithm of the proposed model for FRP reinforced slab

## 5.6 Verification of the proposed model

The prediction of the proposed model are verified using the results of the current experimental program. In addition, the test results by Ospina *et al.* (2003), El-Ghandour *et al.* (2003) and Matthys and Taerwe (2000) are also used to verify the proposed model. The ratios between the ultimate load as predicted by the proposed model, and the observed ultimate loads are given in Table 5.1.

To verify the proposed model against slabs with traditional steel reinforcement, slabs tested by Tolf (1988), Tomaszewicz (1993), Regan *et al.* (1993), Marzouk and Hussein (1991) and Hallgren (1996) are used. The model predictions, along with the test results, are given in Appendix D.

Ospina *et al.* (2003) tested three slabs with FRP reinforcement. Among these slabs, one was with FRP grid and the other two were reinforced with GFRP bar. The GFRP bars were commercially known as C-bar. Matthys *et al.* tested 11 slabs with two dimensional FRP grids and two slabs with FRP bars. El-Ghandour *et al.* (2003) tested 8 slabs in two phases. The slabs were reinforced with FRP bars. However, some slabs had shear reinforcement. The first four slabs experienced bond failure rather than punching failure. Consequently, these four slabs are not considered here. Within the last four slabs, one had shear reinforcement. The proposed model is not applicable for such slabs with shear reinforcement.

Although the slabs reinforced with FRP grids may experience different behaviour, they

are, nevertheless, used in the model verification. Actually, very few slabs are available in the literature that with FRP reinforcement. Thus, the sample population, used in verifying the model is not very large.

The model was derived considering circular slabs with circular columns, which is the ideal case for a model. However, in practice, some slabs and columns are not circular in shape. To calculate the equivalent circular column's diameter,  $B$ , the perimeter of the circular column is assumed to be equal to perimeter of non-circular column. In the case of square slabs, the diameter of the inner circle is used as the diameter,  $c$ , of an equivalent circular slab. From the experiments, it was observed that after a certain load level, the slab corners lift-up from the supports. A portion at the middle of four sides keeps in contact with the supports. As the diameter of slab,  $c$ , is used as a moment arm in the model, it is rational to use the inner circle diameter as the diameter of an equivalent circular slabs.

In Table 5.1, the slabs reinforced with FRP bars and 2-D grids are reported. The calculated values are in good agreement with the test results. The mean of the ratios is 1.05 and the standard deviation is 0.11 for the slabs reinforced with FRP bars and the mean of the ratios is 1.09 and the standard deviation is 0.19 for slabs reinforced with 2-D FRP grids. The over all mean is 1.07 and standard deviation is 0.15.

The input parameters of model for all FRP-reinforced slabs are given in Appendix D. The appendix also provides some output parameters for all slabs.

**Table 5.1: Comparison of proposed model with test results**

Author	FRP rein. type	Slab design.	$\rho$	$E_s$ (MPa)	$S$ (mm)	$d$ (mm)	$f_{cc}$ (MPa)	$P_{test}$ (kN)	$P_{cal}$ (kN)	$P_{test}/P_{cal}$
Current test program	bar	GS1	0.0118	42000	240	100	40	249	222	1.12
		GS2	0.0105	42000	270	100	35	218	204	1.07
		GS3	0.0167	42000	170	100	29	240	210	1.14
		GS4	0.0103 <sup>a</sup>	42000	300	100	26	210	177	1.19
		GSHD1	0.0111	42000	170	150	33	436	393	1.11
		GSHD2	0.0079	42000	240	150	34	389	362	1.07
		GSHS1	0.0167	42000	170	100	92	408	336	1.21
		GSHS2	0.0118	42000	240	100	86	333	306	1.09
Ospina <i>et al.</i>	bar	GFR-1	0.0073	34000	200	120	29.5	199	195	1.02
		GFR-2	0.0146	34000	100	120	28.9	249	234	1.06
	grid	NEF-1	0.0087	28400	200	120	37.5	203	216	0.94
El-Ghandor <i>et al.</i>	bar	SG2	0.0045	45000	100	142	58	271	298	0.91
		SG3	0.0045	45000	100	142	38	237	249	0.95
		SC2	0.0045	110000	100	142	37	317	328	0.97
Matthys <i>et al.</i>	bar	CS	0.0019	147600	110	95	27.2	142	145	0.98
		CS'	0.0019	147600	110	95	27.2	150	188	0.80
	grid	C1	0.0027	91800	150	96	30.4	181	130	1.39
		C1'	0.0027	91800	150	96	30.4	189	183	1.03
		C2	0.0105	95000	100	95	35.7	255	197	1.29
		C2'	0.0105	95000	100	95	36.3	273	274	1.00
		C3	0.0052	92000	100	126	33.8	347	255	1.36
		C3'	0.0052	92000	100	126	34.3	343	343	1.00
		H2	0.0376	40700	100	89	35.8	231	217	1.06
		H2'	0.0376	40700	100	89	35.9	171	146	1.17
		H3	0.0122	44800	150	122	32.1	237	271	0.87
H3'	0.0122	44800	150	122	32.2	217	190	1.14		

Note: <sup>a</sup> Average  $\rho$  around the column has been used, as the reinforcement spacing was uneven.

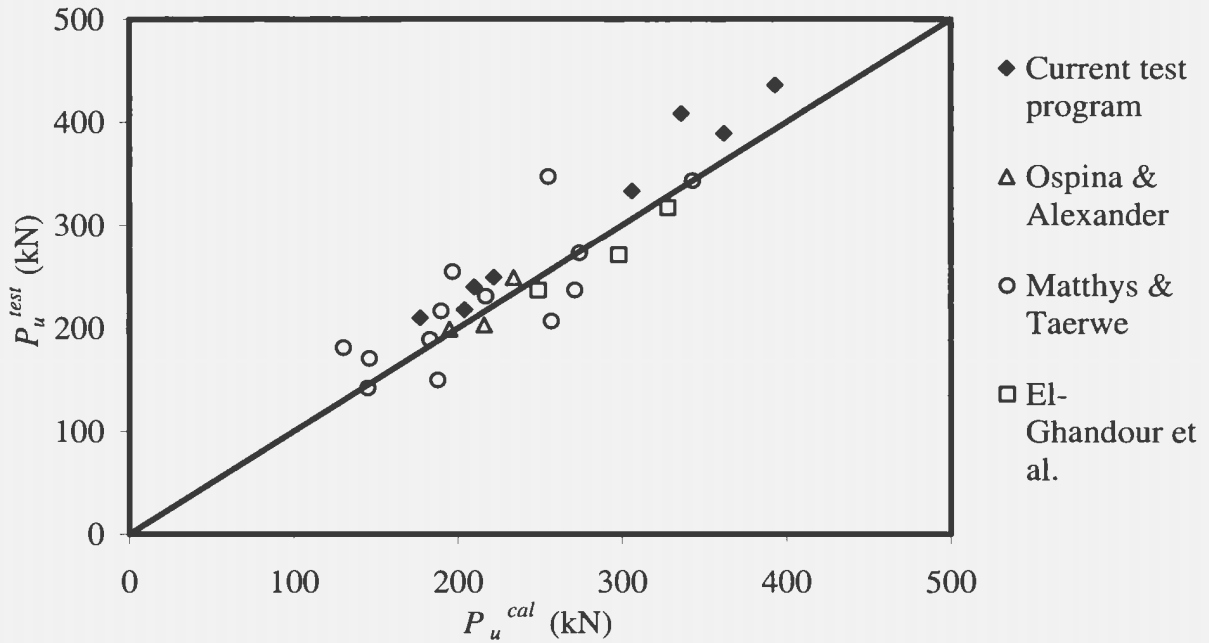


**Fig. 5.15: Observed ultimate load versus predicted ultimate load using the proposed model**

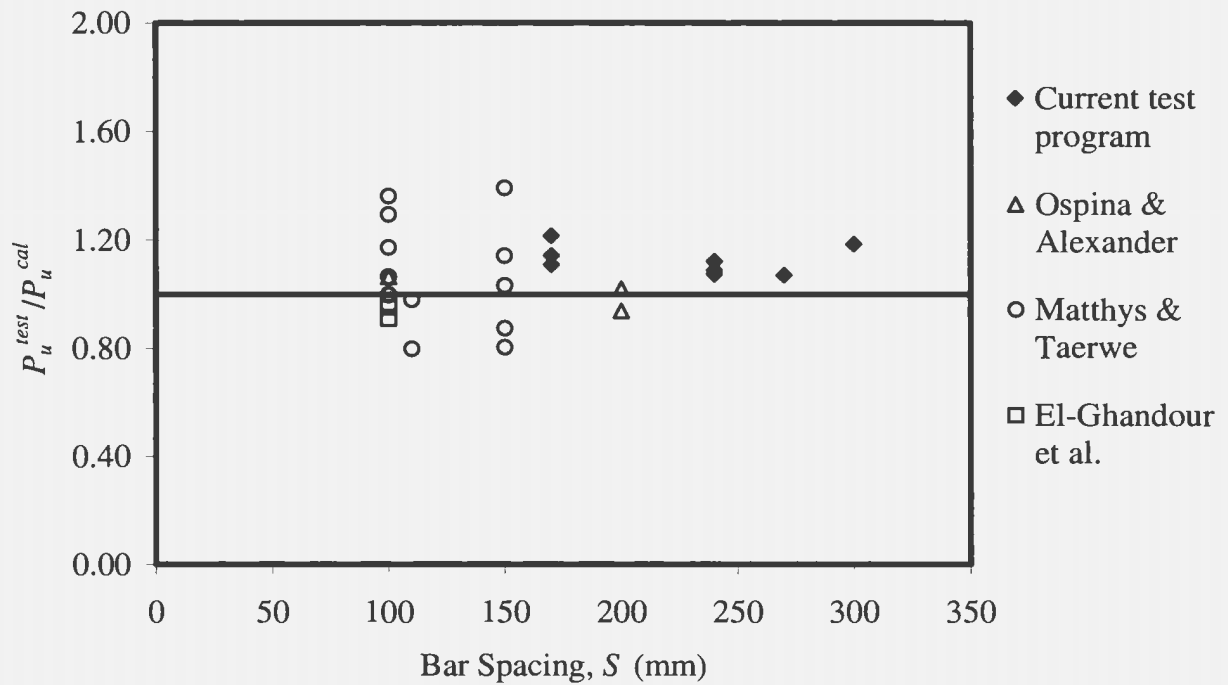


**Fig. 5.16: Ratio between the observed ultimate load and ultimate load predicted by proposed model versus bar spacing**

The calculated results of some slabs do not show good agreement with the test results. Few reasons could be identified that may have caused these inconsistencies. Most of the slabs with FRP grid were tested by Matthys *et al* (2000). Their test results have some inconsistencies. For example, it is known that, if the column diameter increases, the punching capacity will increase. Considering slabs C3 and C3', the observed capacity of C3' is lower than that of C3, although the column diameter of C3' is 53% bigger than that of C3 and the other properties are almost the same. Similar inconsistencies could be obtained in CS, CS' and C1, C1' pairs of slabs. However, the calculated results are consistent with respect to the punching diameter. The ratio between the calculated results and the test results of those pairs of slabs are not consistent. If one ratio is close to unity, the other is not.

The slabs tested by El-Ghandour *et al.* (2003) are suspected for slipping of the bars and some bond failure. The test results are lower than the calculated punching failure load which may support the existence of bar slippage at the time of testing.

In general, although observed punching capacity is showing little discrepancy with the results predicted by proposed model for few slabs, these inconsistencies can be ignored considering the reasons described above. Therefore, considering the results given in this chapter and in Appendix D, the proposed model can accurately predict the punching capacity of FRP reinforced slabs as well as steel reinforced slabs.

# Chapter 6

## Conclusion and Recommendation

### 6.1 Discussion and conclusions

The experimental results and the theoretical study discussed in the previous chapters support the following conclusions:

1. As expected, the ultimate deflection and maximum crack width of GFRP-reinforced slabs are always higher than those of similar steel reinforced slabs. Serviceability limits will be the governing factors for slabs reinforced with GFRP bars.
2. Unlike steel reinforced slabs, the load-deflection graphs of the GFRP-reinforced slabs are almost bilinear in nature. The first line has a slope corresponding to the stiffness of the un-cracked slab. The slope of the second line represents the stiffness of the cracked slab. However, the transition between these two lines is not abrupt; it is rather a smooth transition. This indicates that the slab does not completely lose its un-cracked stiffness once the first crack is formed.
3. Increasing the reinforcement ratio has no significant effect on the slab ultimate capacity. Increasing the reinforcement ratio from 0.95% to 1.67% increases the ultimate load from 210 kN to 240 kN while keeping the concrete strength very

close. That means that 75% increase of GFRP reinforcement increases ultimate strength by 15% only.

4. The use of high strength concrete with GFRP bars increases the slab ultimate strength, ductility and energy absorption. For example, slabs GS3 and GSHS1 have the same thickness of 150 mm and the same reinforcement ratio of 1.67%. The ultimate load capacity of slab GSHS1 was 70 % higher than that of slab GS3. The un-cracked stiffness of slab GSHS1 increased by 91 % and the cracked stiffness by 27%. Also, the ductility of GSHS1 increased by 138% and the energy absorption capacity by 154%.
5. Increasing the effective depth by 50% increases the ultimate strength of the slab-column connections by 50% to 80%. Ductility and energy absorption capacity also increased.
6. In general, increasing either the concrete strength or the effective depth has a beneficial effect from the serviceability point of view. To illustrate this point, by keeping every thing almost the same, using high strength concrete reduce the deflection by 43% and increasing the effective depth by 50% reduce the deflection by 77 to 81% at an arbitrary load level of 200 kN.
7. In general, no concrete splitting along the reinforcement was observed during the experiments in most of the slabs. Other investigators observed such splitting with ribbed GFRP bars. This could be attributed to the better uniform bond

performance of the sand coated bars used in the present study. In addition, the strain gauge readings showed no probable anchorage failure at the end of the bars, even though there was no mechanical anchorage used in the test specimens.

8. The mode of failure was punching for all slabs. Generally, punching starts from the column face at the compression side of the slab. On the tension side, the observed radius of punching was large. That means, the angle of inclination is small and the position of critical section from column face needs reconsideration in case of slabs with GFRP bars. The angle of inclination was not measured because it was not feasible to saw cut the slabs.
9. The governing crack patterns mainly depend on ultimate deflection of slabs. Generally, the radial flexural cracks started to open after reaching a certain amount of deflection of slab centre.
10. In general, the first crack was developed along the bar passing through the column centre and closer to the tension face of the slab. A circumferential crack formed around the column face and close to reinforcement passing around the column face. This circumferential crack started opening gradually with loading and showed the maximum crack width that was fairly large. Almost a 10 mm crack width was measured just before failure for few slabs (e.g. GS4, GSHS2).
11. Near failure, the measurements showed that the concrete strain in a radial direction decreased gradually in most of the slabs with normal strength concrete.

12. The measured radial and tangential strains in the FRP bars indicated that the strains could be assumed to be inversely proportional to the distance from the point of loading. The rotation of the radial slab segment supports the rigid body rotation assumption. Thus, the kinematic features that Kinnunen and Nylander (1960) assumed for their model for steel reinforced concrete slabs could be applicable for FRP reinforced slabs. In addition, the test observation also supports that the rigid wedge element assumed by Shehata (1985).
13. The existing codes such as CSA 23.3–94, ACI 318–02, BS 8110–97 and MC 90 overestimate the punching capacity of slabs reinforced with GFRP bars.
14. The code equations that uses a cubic root relationship for compressive strength and include the effect of the reinforcement such as BS 8110–97 and MC 90 seems to become conservative when the modular ratio correction factor is used to account for the lower modulus of elasticity of FRP bars. Nonetheless, more experimental data are needed to confirm any proposed punching shear equation for FRP reinforced slabs and to confirm that the expression covers a wide range of variables.
15. A rational model was adopted and modified to predict the capacity of FRP-reinforced slabs. The model uses strain compatibility and equilibrium equations of assumed failure criteria. The failure criteria are based on fracture mechanics. The model was verified against the results of the current test program and all the results available in the literature on FRP-reinforced slabs. The proposed model

provided good agreement with the test results of the FRP-reinforced slabs as well as the slabs reinforced with traditional steel reinforcement.

## **6.2 Recommendations for future research**

1. A wider range of parameters for FRP slabs should be investigated.
2. Further investigations should include moment transfer in addition to punching shear for slabs reinforced with FRP bars.
3. This investigation was for interior column only. Edge and corner slab-column connections should be investigated.
4. The dowel force action of FRP bars is not completely known. An experimental study is necessary to examine the dowel effects of FRP bars on concrete beams and slabs.
5. The observed reduction in concrete strain in a radial direction was discussed in Chapter 4. More experiments focusing on this issue are recommended.
6. The issue of serviceability and crack width limits, specially for the high strength concrete slabs reinforced with GFRP reinforcement needs further investigation.

## References:

ACI Committee 440 (2001). "Guide for the Design and Construction of Concrete Reinforced with FRP Bars," *ACI Committee Report-ACI 440.1R-01*, American Concrete Institute, Farmington Hills, Michigan, USA, 41 p.

ACI Committee 318. (2002). "Building Code Requirements for Structural Concrete (ACI 318-02) and Commentary (318R-02)," American Concrete Institute, Farmington Hills, Mich., 443 pp.

Ahmed, S.H., Zia, P., Yu, T.J. and Xie, Y. (1994). "Punching shear Tests of Slabs Reinforced with 3-D Carbon Fiber Fabric," *Concrete International*, V. 16, No. 6, June, pp. 36-41.

Alexander, S.D.B. and Simmonds, S.H. (1987). "Ultimate Strength of Slab-Column Connections," *ACI Structural Journal*, Vol. 84. No. 3, American Concrete Institute, Detroit, May-June, pp. 255-261.

Alexander, S.D.B. and Simmonds, S.H. (1992a). "Bond Model for Concentric Punching Shear," *ACI Structural Journal*, V. 89, No. 3, American Concrete Institute, Detroit, May-June, pp. 325-334.

Alexander, S.D.B. and Simmonds, S.H. (1992b). "Tests of Column-Flat Plate Connections," *ACI Structural Journal*, V. 89, No. 5, American Concrete Institute, Detroit, September-October, pp. 495-502.

Banthia, N. Al-Asaly, M. and Ma, S. (1995). "Behavior of Concrete Slabs Reinforced with Fiber-Reinforced Plastic Grid," *Journal of Materials in Civil Engineering*, Vol. 7, No. 4, ASCE, New York, November, pp. 252-257.

Bareš, R. (1971). *Tables for the Analysis of Plates, Slabs and Diaphragms Based on the Elastic Theory*, Second Enlarged Edition, Bauverlag GmbH., Wiesbaden und Berlin, Germany, 626 p.

Benmokrane, B., Zhang, B., Laoubi, K., Tighiouart, B. and Lord, I. (2001). "Mechanical and Bond Properties of New Generation of ISOROD CFRP Reinforcing Bars for Concrete Structures," *Technical Progress Report*, ISIS-Sherbrooke under ISIS Canada, Department of Civil Engineering, Faculty of Engineering, University of Sherbrooke, Sherbrooke, Québec, Canada, April. 23 p.

British Standards Association (1997). "Structural Use of Concrete, BS8110: Part 1," *Code of practice for design and construction*, British Standards Institution, London.172 p.

Chung, N.Y.L. (2002). "Fiber Reinforced Polymer (FRP) Composites," Queen's University, Kingston, <http://gnatchung.tripod.com/FRP/>

Clarke, J.L. (1996). "Modification of Design Rules to Incorporate Non-ferrous Reinforcement", *Report No.1*, Sir William Halcrow & Partners Ltd., UK, January, pp 13-14.

Cosenza, E., Manfredi, G. and Realfonzo, R. (1997). "Behavior and Modeling of Bond of FRP Rebars to Concrete," *Journal of Composites for Construction*, V. 1, No. 2, ASCE, New York, May, pp. 40-51.

Comité Euro-International Du Béton-Fédération de la Précontrainte (CEB-FIP) (1990). "*CEB-FIP Model Code 1990 (MC-90), Design Code*," Comité Euro-International du Béton (CEB), Thomas Telford Services Ltd., London, 1993, 437 pp.

Comité Euro-International Du Béton-Fédération de la Précontrainte (CEB-FIP) (2001). "Punching of structural concrete slabs," *Bulletin No. 12*, Technical Rep., Lausanne, Switzerland, 307 p.

CSA Standard A23.3-94 (1994). "Design of Concrete Structure with Explanatory Notes," Canadian Standards Association, Ontario, Canada, December, 220 p.

CSA Standard S806-02 (2002). "Design and Construction of Building Components with Fiber-Reinforced Polymers," Canadian Standards Association, Toronto, Canada, May, 177 p.

El-Ghandour, A.W., Pilakoutas, K. and Waldron, P. (2003). "Punching Shear Behavior of Fiber Reinforced Polymers Reinforced Concrete Flat Slabs: Experimental Study," *Journal of Composites for Construction*, V. 7, No. 3, ASCE, New York, August, pp. 258-265.

Gardner, N.J. (1990). "Relationship of the Punching Shear Capacity of Reinforced Concrete Slabs with Concrete Strength," *ACI Structural Journal*, Vol. 87, No.1, American Concrete Institute, Detroit, January-February, pp. 66-71.

Hallgren, M. (1996). "Punching Shear Capacity of Reinforced High Strength Concrete Slabs," *Doctoral Thesis*, Department of Structural Engineering, Royal Institute of Technology, S-100 44, Stockholm, Sweden, 206 p.

Hamadi Y.D., Regan P.E. (1980). "Behaviour in Shear of Beams with Flexural Cracks," *Magazine of Concrete Research*, Vol. 32, No. 111, Cement and Concrete Association, London, pp. 67-78.

Hussein A. (1990). "Behaviour of Reinforced Concrete Slabs Made with High-strength Concrete", *M. Eng. Thesis*, Faculty of Engineering and Applied Science, Memorial University of Newfoundland, St. John's, Newfoundland and Labrador, Canada, August, 145 p.

ISIS Canada Corporation (2001). "Reinforcing concrete Structures with Fiber Reinforced Polymers," *Design Manual No. 3*, Winnipeg, Manitoba, Canada, September, 16.6 p.

Kinnunen, S. and Nylander, H. (1960). "Punching of Concrete Slabs Without Shear Reinforcement," *Transactions No. 158*, Royal Institute of Technology, Stockholm, Sweden, 112 p.

Marzouk, H., Hussein A. (1991). "Experimental Investigation on the behavior of High-Strength Concrete Slabs," *ACI Structural Journal*, Vol. 88, No. 6, American Concrete Institute, Detroit, pp. 701-713.

Marzouk, H. and Perchard, R. (1991). "MUN Slab Testing Frame," Design calculation, Steel fabrication and Private correspondence, Faculty of Engineering and Applied Science, Memorial University of Newfoundland, St. John's, Canada.

Marzouk, H., Emam, M. and Hilal, S. (1998). "Effect of High-Strength Concrete Slab on the Behaviour of Slab Column Connection," *ACI-Structural Journal*, Vol.95, No.3, American Concrete Institute, Detroit, May-June, pp.227-237.

Osman, M., Marzouk, H. and Helmy, S. (2000). "Behaviour of High-Strength lightweight Concrete slabs under punching loads," *ACI Structural Journal*, Vol.97, No.3, American Concrete Institute, Detroit, May – June, pp.492- 498.

MASTRAD Limited (2003), "MASTRAD Quality and Test Systems," Douglas, UK, [www.mastrad.com/wxmicro.htm](http://www.mastrad.com/wxmicro.htm)

Matthys, S. and Taerwe, L. (2000a). "Concrete Slabs Reinforced with FRP Grids. I: One-Way Bending," *Journal of Composites for Construction*, V.4, No.3, ASCE, New York, August, pp.145-153.

Matthys, S. and Taerwe, L. (2000b). "Concrete Slabs Reinforced with FRP Grids. II: Punching Resistance," *Journal of Composites for Construction*, V.4, No.3, ASCE, New York, August, pp.154-161.

Menétrey, P. (1996). "Analytical Computation of the Punching Strength of Reinforced Concrete," *ACI Structural Journal*, Vol. 93, No. 5, American Concrete Institute, Detroit, September-October, pp. 503-511.

Nanni, A. (1993). *Fiber-Reinforced-Plastic (FRP) Reinforcement for Concrete Structures: Properties and Application*, Elsevier Science Publishers B.V., Amsterdam, Netherlands, 450 p.

Nawy, E.G. and Neuwerth, G.E. (1976). "Fiber Glass as Main Reinforcement for Concrete Two-Way Slabs, Plates and Beams," *Engineering Research Bulletin No. 56*, College of Engineering, Rutgers University, New Jersey, USA, 111 p.

Nawy, E. and Neuwerth, G.E. (1977). "Fiberglass Reinforced Concrete Slabs and Beams," *Journal of the structural Division*, V. 103, No. ST2, ASCE, New York, pp. 421-440.

Ospina, C.E.; Alexander, S.D.B. and Cheng, J.J.R. (2000). "Punching of Column-Supported Two-Way Concrete Slabs Reinforced with GFRP," *Proceedings of 3<sup>rd</sup> Int. Conf. on Advanced Composite Materials in Bridges and Structures, ACMBS III*, Ottawa, Canada, pp. 323-330.

Ospina, C.E., Alexander, S.D.B. and Cheng, J.J.R. (2003). "Punching of Two-Way Concrete Slabs with Fiber-Reinforced Polymer Reinforcing Bars or Grids," *ACI Structural Journal*, Vol. 100, No. 5, American Concrete Institute, Detroit, September-October, pp. 589-598.

Pultrall, a division of ADS Composites Group Inc., Quebec, Canada,  
[www.pultrall.com/~/isorodts.htm](http://www.pultrall.com/~/isorodts.htm)

Rankin, G.I.B. and Long, A.E. (1987). "Predicting the punching strength of conventional slab-column specimens," *Proceedings of the Institution of Civil Engineering*, Vol. 82, Part 1, Structural Engineering Group, April, pp. 327-346.

Regan, P.E. (1986). "Symmetric Punching of Reinforced Concrete Slabs," *Magazine of Concrete Research*, Vol. 38, No. 136, September, pp. 115-128.

Regan P.E., Al-Hussaini A., Ramdane K-E. and Xue H-Y. (1993). "Behaviour of High Strength Concrete Slabs," *Concrete 2000*, Proc. of Int. Conf., University of Dundee, Scotland, UK, September 7-9, Vol. 1, E & FN Spon, Cambridge, pp. 761-773.

RILEM Draft Recommendation (1985). "Determination of the Fracture Energy of Mortar and Concrete by means of Three-Point Bend Tests on Notched Beams," *Materials and Structures*, Vol. 18, No. 106, RILEM, Paris, pp. 285-290.

Rubinsky, I.A. and Rubinsky, A. (1959). "A Preliminary Investigation of the Use of Fiber-glass for Prestressed Concrete," *Magazine of Concrete Research*, Cement and Concrete Association, London, September, pp. 71-78.

Shehata, I.A.M. (1985). "Theory of Punching in Concrete Slabs," *Ph.D. thesis*, The Polytechnic of Central London, London, UK, 257 p.

Shehata, I.M. and Regan, P. (1989). "Punching in R.C. Slabs," *Journal of the Structural Division*, Vol. 115, No. 7, ASCE, New York, August, pp. 1726-1740.

Tolf P. (1988), "Plattjocklekens inverkan på betongplattors hållfasthet vid genomstansning. Försök med cikulära platter," *Bulletin 146*, Department of structural Mechanics and Engineering, Royal Institute of Technology, Stockholm, 64 p. [reported in CEB-FIP (2001), Technical report, Bulletin 12].

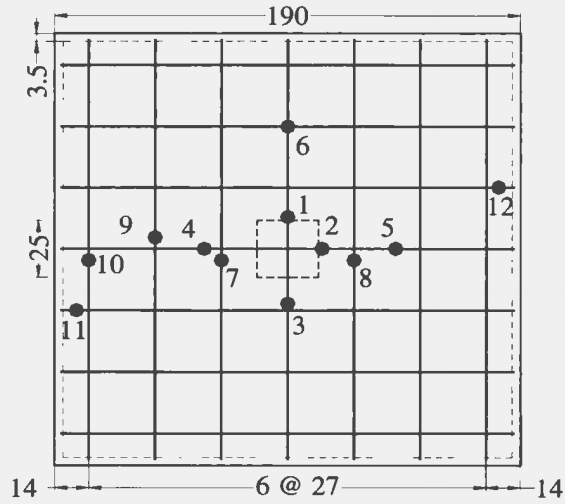
Tomaszewicz A. (1993). *High-Strength Concrete, SP2 – Plates and Shells, Report 2.3*, Punching Shear Capacity of Reinforced Concrete Slabs, Report No. STF70 A93082, SINTEF Structure and Concrete, Trondheim, 36 p. [reported in CEB-FIP (2001), Technical report, Bulletin 12].

WEST SYSTEM® User Manual & Product Guide, Gougeon Brothers, Inc., Bay City, MI, [www.westsystem.com](http://www.westsystem.com)

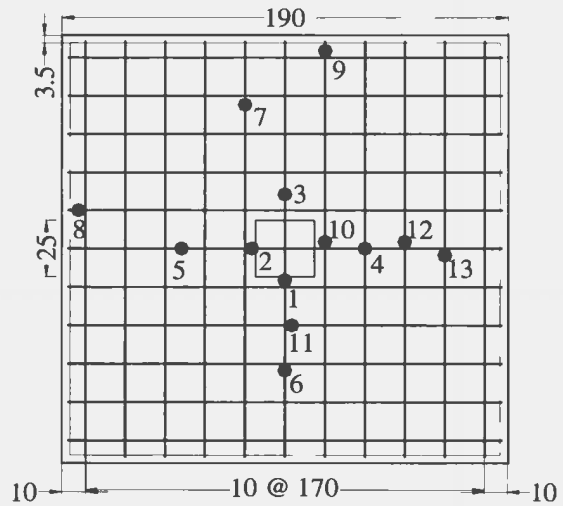
Wines, J.C. and Hoff, G.C. (1966a). "Laboratory Investigation of Plastic-Glass Fiber Reinforcement for Reinforced and Prestressed Concrete – Report 1(Plain Reinforced Concrete)," *Miscellaneous Paper No. 6-779*, U.S. Army Engineer Waterways Experiment Station, Corps of Engineers, Vicksburg, Mississippi, February, 20 p.

Wines, J.C., Dietz, R.T., and Hawley, J.L. (1966b). "Laboratory Investigation of Plastic-Glass Fiber Reinforcement for Reinforced and Prestressed Concrete – Report 2 (Prestressed Concrete)," *Miscellaneous Paper No. 6-779*, U.S. Army Engineer Waterways Experiment Station, Corps of Engineers, Vicksburg, Mississippi, July, 14 p.

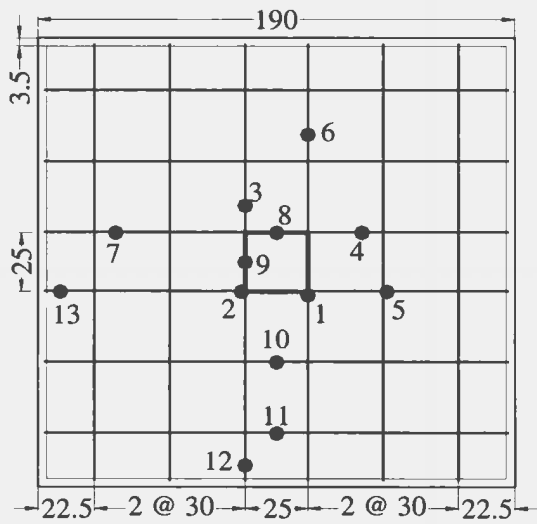
## Appendix A: Strain gauge locations on GFRP bars



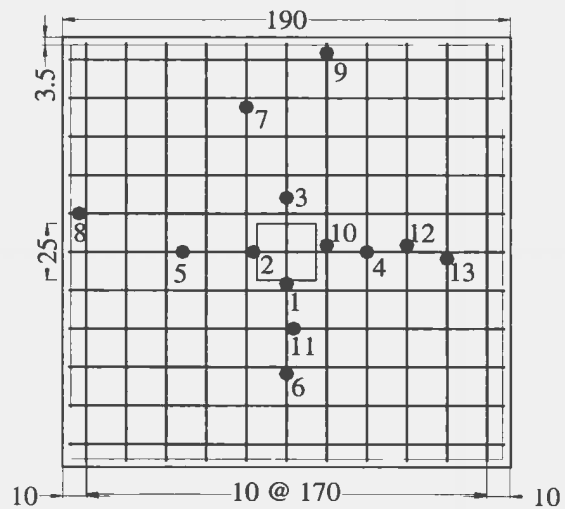
Slab GS2



Slab GS3



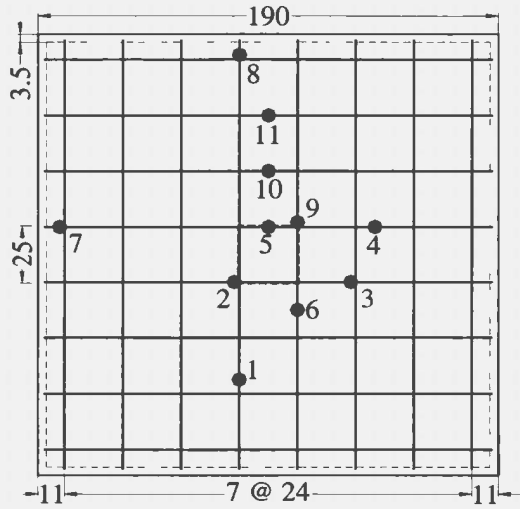
Slab GS4



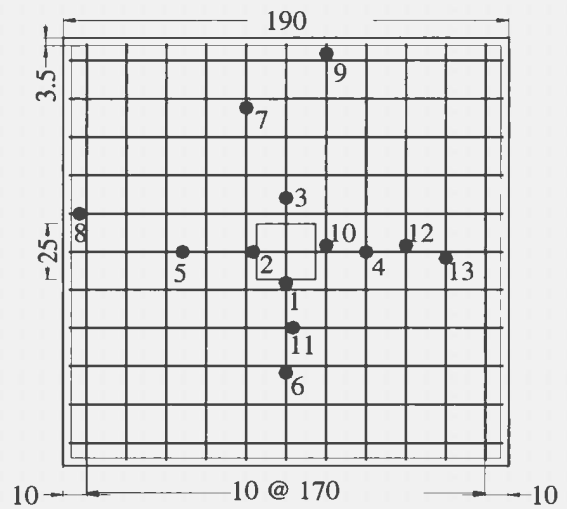
Slab GS4D1

Note: Reinforcement layout of Slab GS1 is shown in Chapter 3. Black circles are the position of 'strain gauges on the reinforcement' (RS). All dimensions are in 'cm' and the figures are to scale.

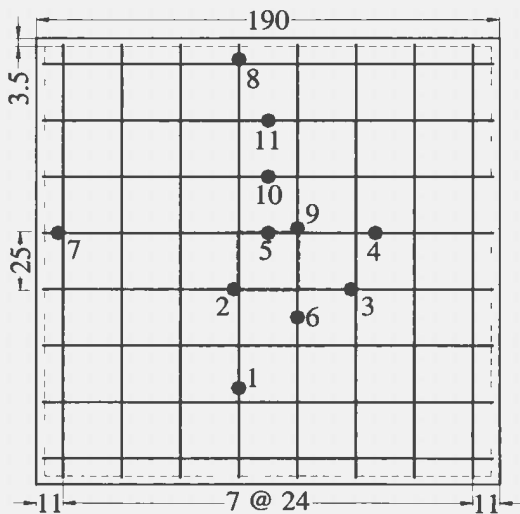
**Fig. A1: Reinforcement layout and strain gauge locations**



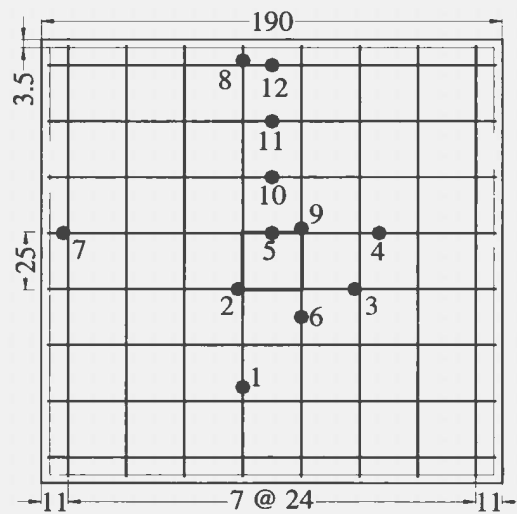
Slab GSHD2



Slab GSHS1



Slab GSHS2



Slab R1

Note: Black circles are the position of 'strain gauges on reinforcement' (RS). All dimensions are in 'cm' and figures are in scale.

**Fig. A1: Reinforcement layout and strain gauge locations (contd.)**

## Appendix B: Estimation of the mechanical properties of concrete

The following equations were used by Hallgren (1996). These equations follow the European codes. The equations are adopted for the proposed model.

If the required mechanical properties are not available, the following relations should be used. To obtain  $f_{cc}$  from cube strength:

$$f_{cc} = 0.8 f_{c,cube} \quad (B1)$$

To get  $f_{ct}$  from splitting tensile strength:

$$f_{ct} = 0.9 f_{csp} \quad (B2)$$

If the tensile strength is not available in any form, the following relation can be used to calculate the tensile strength from the compressive strength for normal density concrete.

$$f_{ct} = 1.4 \left( \frac{f_{cc}}{10} \right)^{2/3} \quad [\text{MPa}] \quad (B3)$$

For normal density concrete, the modulus of elasticity can be estimated using the following relation, if test value is not available.

$$E_c = 21.5 \left( \frac{f_{cc}}{10} \right)^{1/3} \quad [\text{GPa}] \quad (B4)$$

For light-weight aggregate concrete, the following relation can be used to obtain the concrete tensile strength and modulus of elasticity:

$$f_{ct}^{LWA} = 1.4 \left( 0.3 + 0.7 \frac{\gamma}{2400} \right) \left( \frac{f_{cc}}{10} \right)^{2/3} \quad [\text{MPa}] \quad (B5)$$

$$E_c^{LWA} = 21.5 \frac{\gamma}{2400} \left( \frac{f_{cc}}{10} \right)^{1/3} \quad [\text{GPa}] \quad (\text{B6})$$

where  $\gamma$  is the density of concrete given in  $\text{kg/m}^3$

The fracture energy, equivalent to the one obtained according to the RILEM recommendation (1985), is estimated as

$$G_F^R = G_{FO} \left( \frac{f_{cc}}{10} \right)^{0.7} \quad [\text{Nmm/mm}^2] \quad (\text{B7})$$

where,  $G_{FO} = 0.025$  for  $d_a = 8$  mm

$G_{FO} = 0.030$  for  $d_a = 16$  mm

$G_{FO} = 0.038$  for  $d_a = 32$  mm

where  $d_a$  is the maximum aggregate size and linear interpolation is acceptable if aggregate size is different. If a measured value of  $G_F^R$  is not available, and consequently no value of  $d^R$ , then  $d^R$  may be set equal to 100 mm in Eq. (5.33) for the determination of  $G_F^\alpha$ .

## Appendix C: Computer program of the proposed mechanical model

### (A) Computer program of the proposed model (Steel)

The computer program of the algorithm given in Chapter 5 for slabs with steel reinforcement is given below. The program is written in MATLAB<sup>®</sup> 6.1 (2001) code.

```
function [Pu] = mpunchs(c,B,d,ro,fi,da,fcc,fct,Ec,GFR,fsy,Es)
% c = diameter of the slab, [mm]
% B = diameter of the column, [mm]
% d = average effective depth of the slab, [mm]
% ro = ratio of the flexural reinforcement
% fi = diameter of the reinforcing bar, [mm]
% da = maximum aggregate size, [mm]
% fcc = compressive strength of concrete, [MPa]
% fct = tensile strength of concrete, [MPa]
% Ec = modulus of elasticity of concrete, [MPa]
% GFR = fracture energy of concrete, based on RILEM test, [Nmm/mm2]
% fsy = yield stress of reinforcing steel, [MPa]
% Es = modulus of elasticity of reinforcing steel, [MPa]

GFinf=GFR*sqrt(1+13*da/100);
ecy=fcc/Ec;
esy=fsy/Es;
kE=1.15

%starting assumption:

x2=ro*Es*d*(sqrt(1+2*kE*Ec/ro/Es)-1)/kE/Ec;

%outer loop 3:

h=0;
dP=1;
lam=30;

while abs(dP) > 0.5,
    dal=1.5;
    h=h+1;
    if h > 2000
        break
    end
end

%outer loop 2:

i=0;
```

```

while abs(dP) > 0.5,
    i=i+1;
    if i > 2000
        break
    end
alfa=10;

%outer loop 1:

dP=1;
j=0;

while abs(dP) > 0.5,
    j=j+1;
    if j > 200
        break
    end

    % inner loop:

    xp=0;
    k=0;
    while abs(x2-xp) > 0.1,
        k=k+1;
        if k >200
            break
        end
        if alfa <= 20
            x1=x2;
        else
            x1=x2/tan(2*alfa*pi/180);
        end

        if alfa <= 20
            y=x1+x2*tan(alfa*pi/180);
            c0=(B/2)+x1+(d-x2)/tan(dal*alfa*pi/180);
        else
            y=(0.7*x1)+x2*tan(alfa*pi/180);
            c0=B/2+(0.7*x1)+(d-x2)/tan(dal*alfa*pi/180);
        end

        ecTu=3.6*GFinf/x2/fct/sqrt(1+13*da/x2);
        C1=ecTu*(B/2+y);
        C2=C1*(d/x2-1);
        rc=C1/ecy;
        if rc >c/2
            rc=c/2
        end
        rs=C2/esy;
        if rs > c/2
            rs=c/2;
        end
    end
end

```

```

ecT0=C1/c0;
esT0=C2/c0;
alfac0=1-ecy/2/ecT0;
if rs <=c0
    if rc <= c0
        xp=ro*Es*d*(sqrt(1+2*kE*Ec/ro/Es)-1)/kE/Ec;
    else
        xp=ro*Es*ecT0*d*(sqrt(1+4*alfac0*fcc/ro/Es/ecT0)-1)/2/alfac0/fcc;
    end
else
    if rc <= c0
        xp=2*ro*d*fsy/ecT0/kE/Ec;
    else
        xp=ro*d*fsy/alfac0/fcc;
    end
end
end

x2=x2+(xp-x2)/20;

if x2 > 0.6*d
    break
end

end
%end of inner loop

if rc > B/2+y
    RcT=fcc*x2*(rc-B/2-y-ecy*(rc^2- (B/2+y)^2)/4/C1)/1000+0.5*Ec*x2*C1*log(c/2/rc)/1000;
else
    RcT=0.5*Ec*x2*C1*log(c/(B+2*y))/1000;
end

if rs > c0
    RsT=ro*d*(fsy*(rs-c0)/1000+Es*C2*log(c/2/rs)/1000);
    RsR=ro*d*2*pi*c0*fsy/1000;
    D=0;
else
    RsT=ro*d*Es*C2*log(c/2/c0)/1000;
    RsR=ro*d*2*pi*c0*Es*C2/c0/1000;
    D=27.9*fi^(2/3)*c0*(1-1.6*ro*d/fi)*fcc^(1/3)/1000;
end

T=(RsR+2*pi*(RsT-RcT))/cos(alfa*pi/180);
Pv=T*sin(alfa*pi/180)+D;

if alfa <= 20
    Pm=((2*pi*RsT+RsR)*(d-x2)+D*(c0-B/2-x1)+T*x2/2/cos(alfa*pi/180)+2*pi*RcT*(2*x2/3-
        x2*rc/3/c))/((c-B)/2-x1);
else
    Pm=((2*pi*RsT+RsR)*(d-x2)+D*(c0-B/2-0.7*x1)+T*x2/2/cos(alfa*pi/180)+2*pi*RcT*(2*x2/3-
        x2*rc/3/c))/((c-B)/2-0.7*x1);
end
end

```

```

dP=Pv-Pm

if j == 1
    fdP=dP;
end

alfa=alfa-dP/500;

if alfa > lam
    break
end
end
% end of the outer loop 1

dal=dal-(fdP)/5000;

if (dal > 2.5 | dal < 0.5)
    break
end

end
% end of the outer loop 2

lam=lam+abs(dP)/100;

if lam >= 45
    break
end

end
%end of the outer loop 3

Pu=(Pv+Pm)/2

return

```

## (B) Computer program of the proposed model (FRP)

The computer program of the algorithm given in Chapter 5 for slabs with FRP reinforcement is given below. The program is written in MATLAB® 6.1 (2001) code.

```
function [Pu] = mpunchfrp(c,B,d,ro,fi,da,fcc,fct,Ec,GFR,fsu,Es)
% c = diameter of the slab, [mm]
% B = diameter of the column, [mm]
% d = average effective depth of the slab, [mm]
% ro = ratio of the flexural reinforcement.
% fi = diameter of the reinforcing bar, [mm]
% da = maximum aggregate size, [mm]
% fcc = compressive strength of concrete, [MPa]
% fct = tensile strength of concrete, [MPa]
% Ec = modulus of elasticity of concrete, [MPa]
% GFR = fracture energy of concrete, based on RILEM test, [Nmm/mm2]
% fsu = ultimate strength of reinforcing FRP bar, [MPa]
% Es = modulus of elasticity of reinforcing FRP bar, [MPa]

GFinf=GFR*sqrt(1+13*da/100);
ecy=fcc/Ec;
esu=fsu/Es;
kE=1.15;

%starting assumption:
x2=ro*Es*d*(sqrt(1+2*kE*Ec/ro/Es)-1)/kE/Ec;

%outer loop 3:
h=0;
dP=1;
lam=30;
while abs(dP) > 0.1,
    dal=1.5;
    h=h+1;
    if h > 2000
        break
    end
end

%outer loop 2:
i=0;

while abs(dP) > 0.1,
    i=i+1;
    if i > 2000
        break
    end
end
alfa=10;

j=0;
```

```

%outer loop 1:
while abs(dP) > 0.1,
    j=j+1;
    if j > 4000
        break
    end

% inner loop:
xp=0;
k=0;
while abs(x2-xp) > 0.1,
    k=k+1;
    if k >4000
        break
    end

    if alfa <= 20
        x1=x2;
    else
        x1=x2/tan(2*alfa*pi/180);
    end

    if alfa <= 20
        y=x1+x2*tan(alfa*pi/180);
        c0=(B/2)+x1+(d-x2)/tan(dal*alfa*pi/180);
    else
        y=(0.7*x1)+x2*tan(alfa*pi/180);
        c0=B/2+(0.7*x1)+(d-x2)/tan(dal*alfa*pi/180);
    end

    ecTu=3.6*GFinf/x2/fct/sqrt(1+13*da/x2);
    ecT0=ecTu*(B/2+y)/c0;
    esT0=ecT0*(d-x2)/x2;
    alfac0=1-ecy/2/ecT0;
    rc=ecTu*(B/2+y)/ecy;
    if rc > c/2
        rc=c/2;
    end

    if esT0 >= esu
        if rc <= c0
            xp=ro*Es*d*(sqrt(1+2*kE*Ec/ro/Es)-1)/kE/Ec;
        else
            xp=esu*Es*ro*d/alfac0/fcc;
        end
    else
        if rc <= c0
            xp=ro*Es*d*(sqrt(1+2*kE*Ec/ro/Es)-1)/kE/Ec;
        else
            xp=ro*Es*ecT0*d*(sqrt(1+4*alfac0*fcc/ecT0/Es/ro)-1)/2/alfac0/fcc;
        end
    end

```

```

end

x2=x2+(xp-x2)/20;
if x2 > 0.6*d
    break
end

end
%end of the inner loop

if rc > B/2+y
    RcT=fcc*x2*(rc-B/2-y-ecy*(rc^2-
        (B/2+y)^2)/4/ecTu/(B/2+y))/1000+0.5*Ec*ecTu*(B/2+y)*x2*log(c/2/rc)/1000;
else
    RcT=0.5*Ec*x2*ecTu*(B/2+y)*log(c/(B+2*y))/1000;
end

RsT=ro*d*Es*(d/x2-1)*(B/2+y)*ecTu*log(c/2/c0)/1000;
RsR=ro*d*2*pi*c0*Es*esT0/1000;

v=(Es/200000);
mu=-3*v^4+8.2*v^3-8.2*v^2+4*v;
D=27.9*(mu)*fi^(2/3)*c0*(1-1.6*ro*d/fi)*fcc^(1/3)/1000;

T=(RsR+2*pi*(RsT-RcT))/cos(alfa*pi/180);
Pv=T*sin(alfa*pi/180)+D;

if alfa <= 20
    Pm=((2*pi*RsT+RsR)*(d-x2)+D*(c0-B/2-x1)+T*x2/2/cos(alfa*pi/180)+2*pi*RcT*(2*x2/3-
        x2*rc/3/c))/((c-B)/2-x1);
else
    Pm=((2*pi*RsT+RsR)*(d-x2)+D*(c0-B/2-0.7*x1)+T*x2/2/cos(alfa*pi/180)+2*pi*RcT*(2*x2/3-
        x2*rc/3/c))/((c-B)/2-0.7*x1);
end

dP=Pv-Pm

alfa=alfa-(dP)/500;

if alfa > lam
    break
end

end
% end of the outer loop1

dal=dal+(dP)/1000

if (dal > 1.7 | dal < 0.5)
    break
end

```

```
end
% end of the outer loop 2

lam=lam+abs(dP)/100;

if lam >= 45
    break
end

end
%end of the outer loop 3

Pu=(Pv+Pm)/2

return
```

## Appendix D: Slab details, test and calculated results for slabs tested by other investigations

**Table D-1: Slabs tested by Ospina *et al.* (University of Alberta, Canada, 2003)**

Slab	$c$ (mm)	$B$ (mm)	$d$ (mm)	$\rho$ (%)	$\phi$ (mm)	$f_{cc}$ (MPa)	$f_s$ (MPa)	$E_s$ (MPa)	$S$ (mm)
GFR-1	1830	320	120	0.73	15	30	663	34000	200
GFR-2	1830	320	120	1.46	15	29	663	34000	100
NEF-1	1830	320	120	0.87	14	38	566	28000	200

**Table D-2: Slabs tested by El-Ghandour *et al.* (University of Sheffield, UK, 2003)**

Slab	$c$ (mm)	$B$ (mm)	$d$ (mm)	$\rho$ (%)	$\phi$ (mm)	$f_{cc}$ (MPa)	$f_s$ (MPa)	$E_s$ (MPa)	$S$ (mm)
SG2	1700	255	142	0.45	8	58	533	45000	100
SG3	1700	255	142	0.45	8	38	616	110000	100
SC2	1700	255	142	0.45	8	37	800	45000	100

**Table D-3: Slabs tested by Matthys and Taerwe (Ghent University, Belgium, 2000)**

Slab	$c$ (mm)	$B$ (mm)	$d$ (mm)	$\rho$ (%)	$\phi$ (mm)	$f_{cc}$ (MPa)	$f_{ct}$ (MPa)	$f_s$ (MPa)	$E_s$ (MPa)	$S$ (mm)
C2	900	150	95	1.05	11.29	36	4.33	1340	95000	100
C2'	900	230	95	1.05	11.29	36	4.33	1340	95000	100
H3	900	150	122	1.22	16.85	32	3.28	640	44800	150
H3'	900	80	122	1.22	16.85	32	3.28	640	44800	150
H2	900	150	89	3.76	20.66	36	3.93	555	40700	100
H2'	900	80	89	3.76	20.66	36	3.93	555	40700	100
C3	900	150	126	0.52	9.1	34	4.01	1350	92000	100
C3'	900	230	126	0.52	9.1	34	4.01	1350	92000	100
C1	900	150	96	0.27	6.26	37	4.58	1690	91800	150
C1'	900	230	96	0.27	6.26	37	4.58	1690	91800	150
CS	900	150	95	0.19	5	33	3.46	2300	147600	110
CS'	900	230	95	0.19	5	33	3.46	2300	147600	110
H1	900	150	95	0.62	10.63	118	6.95	665	37300	150

**Table D-4: Comparison of proposed model predictions and test results of slabs with FRP reinforcement**

Slabs	$x_2^{cal}$ (mm)	$\alpha_F^{cal}$ Deg.	$\alpha_{cone}^{cal}$ Deg.	$P_{cal}$ (kN)	$P_{test}$ (kN)	$P_{test}/P_{cal}$
GFR-1	15	29	43	195	199	1.02
GFR-2	21	27	40	234	249	1.06
NEF-1	14	28	42	216	203	0.94
SG2	13	29	43	298	271	0.91
SG3	15	32	48	249	237	0.95
SC2	21	27	40	328	317	0.97
C2	20	29	44	197	255	1.29
C2'	19	28	38	274	273	1.00
H3	19	43	38	271	237	0.87
H3'	19	43	50	190	217	1.14
H2	22	27	41	217	231	1.06
H2'	22	30	45	146	171	1.17
C3	19	40	51	255	347	1.36
C3'	19	41	41	343	343	1.00
C1	10	34	40	130	181	1.39
C1'	10	35	30	183	189	1.03
CS	11	40	28	145	142	0.98
CS'	13	39	48	188	150	0.80
H1	8	34	51	257	207	0.81

$\alpha_F$  = inclination of force  $T$ .  $\alpha_{cone}$  = inclination of incline shear crack.  $x_2$  is the depth of compression zone in tangential direction.

**Table D-5: Circular slabs tested by Regan et al. (1993)**

Slabs	$c$ (mm)	$B$ (mm)	$d$ (mm)	$\rho$ (%)	$\phi$ (mm)	$d_a$ (mm)	$f_{cc}$ (MPa)	$f_{ct}$ (MPa)	$E_c$ (GPa)	$f_{ys}$ (MPa)
1	1372	150	98	0.58	10	10	88	5.3	48.9	550
2	1372	150	98	0.58	10	10	56	4.3	40.6	550
3	1372	150	98	0.58	10	10	27	2.6	30.8	550
4	1372	150	98	0.58	10	10	58	4.6	36.5	550
5	1372	150	98	0.58	10	12	54	3.3	20.8	550
6	1372	150	98	0.58	10	10	102	5.6	52.8	550
21	1372	150	98	1.28	10	20	42	-	-	550
22	1372	150	98	1.28	10	20	84	6.8	-	550
23	1372	150	100	0.87	10	20	56	4.5	-	550
24	1372	150	98	1.28	10	6	45	3.3	-	550
25	1372	150	100	1.27	10	10	33	-	-	550
26	1372	150	100	1.27	10	20	38	-	-	550
27	1372	150	102	1.03	10	20	34	-	-	550

**Table D-6: Rectangular slabs tested by Tomaszewicz (1993)**

Slabs	$c$ (mm)	$B$ (mm)	$d$ (mm)	$\rho$ (%)	$\phi$ (mm)	$d_a$ (mm)	$f_{cc}$ (MPa)	$f_{ct}$ (MPa)	$f_{ys}$ (MPa)	$P_{test}$ (kN)
ND65-1-1	2500	255	275	1.49	25	16	64	3.8	500	2050
ND65-2-1	2200	191	200	1.75	20	16	70	3.9	500	1200
ND95-1-1	2500	255	275	1.49	25	16	84	4.7	500	2250
ND95-1-3	2500	255	275	2.55	25	16	90	4.5	500	2400
ND95-2-1	2200	191	200	1.75	20	16	88	4.6	500	1100
ND95-2-1D	2200	191	200	1.75	20	16	87	4.6	500	1300
ND95-2-3	2200	191	200	2.62	20	16	90	4.7	500	1450
ND95-2-3D	2200	191	200	2.62	20	16	80	4.2	500	1250
ND95-2-3D+	2200	191	200	2.62	20	16	98	4.8	500	1450
ND95-3-1	1100	127	88	1.84	12	16	85	4.5	500	330
ND115-1-1	2500	255	275	1.49	25	16	112	5.3	500	2450
ND115-2-1	2200	191	200	1.75	20	16	119	5.2	500	1400
ND115-2-3	2200	191	200	2.62	20	16	108	5.2	500	1550
LWA75-1-1	2500	255	275	1.49	25	16	69	3.9	500	1600
LWA75-2-1	2200	191	200	1.75	20	16	70	3.6	500	950
LWA75-2-1D	2200	191	200	1.75	20	16	74	3.4	500	1100
LWA75-2-3	2200	191	200	2.62	20	16	74	3.6	500	1150
LWA75-2-3D	2200	191	200	2.62	20	16	74	3.7	500	1020
LWA75-3-1	1100	127	88	1.85	12	16	68	3.2	500	320

**Table D-7: Circular normal strength concrete slabs tested by Tolf (1988)**

Slabs	$c$ (mm)	$B$ (mm)	$d$ (mm)	$\rho$ (%)	$\phi$ (mm)	$d_a$ (mm)	$f_{cc}$ (MPa)	$f_{ys}$ (MPa)	$P_{test}$ (kN)
S2.1	2400	250	200	0.8	16	32	24.2	657	603
S2.2	2400	250	199	0.8	16	32	22.9	670	600
S2.3	2400	250	200	0.34	16	32	25.4	668	489
S2.4	2400	250	197	0.35	16	32	24.2	664	444

**Table D-8: Rectangular slabs tested by Marzouk and Hussein (1991)**

Slabs	$c$ (mm)	$B$ (mm)	$d$ (mm)	$\rho$ (%)	$\phi$ (mm)	$d_a$ (mm)	$f_{cc}$ (MPa)	$f_{ys}$ (MPa)	$P_{test}$ (kN)
NS1	1500	191	95	1.47	11.3	19	42	490	320
HS1	1500	191	95	0.491	11.3	19	67	490	178
HS2	1500	191	95	0.842	11.3	19	70.2	490	249
HS7	1500	191	95	1.193	11.3	19	73.8	490	356
HS3	1500	191	95	1.474	11.3	19	69.1	490	356
HS4	1500	191	90	2.37	11.3	19	65.8	490	418
NS2	1500	191	120	0.944	11.3	19	30	490	396
HS5	1500	191	120	0.64	11.3	19	68.1	420	365
HS6	1500	191	120	0.944	11.3	19	70	420	489
HS8	1500	191	120	1.111	11.3	19	69	490	436
HS9	1500	191	120	1.611	11.3	19	74	420	543
HS10	1500	191	120	2.333	11.3	19	80	420	645
HS11	1500	191	70	0.952	11.3	19	70	420	196
HS12	1500	191	70	1.524	11.3	19	75	420	258
HS13	1500	191	70	2.0	11.3	19	68	420	267
HS14	1500	280	95	1.474	11.3	19	72	420	499
HS15	1500	382	95	1.474	11.3	19	71	420	560

**Table D-9: Circular slabs tested by Hallgren (1996)**

Slabs	$c$ (mm)	$B$ (mm)	$d$ (mm)	$\rho$ (%)	$\phi$ (mm)	$d_a$ (mm)	$f_{cc}$ (MPa)	$f_{ct}$ (MPa)	$E_c$ (GPa)	$G_F^R$ (N/mm)	$f_{ys}$ (MPa)	$E_s$ (GPa)
HSC1	2400	250	200	0.8	16	18	91.3	6.2	42.9	0.179	627	200
HSC2	2400	250	200	0.8	16	18	85.7	5.1	37.2	0.168	620	200
HSC4	2400	250	200	1.2	20	18	91.6	5.9	41.3	0.154	596	195
HSC6	2400	250	200	0.6	16	18	108.9	6.8	46	0.161	633	210
HSC9	2400	250	200	0.3	16	18	84.1	6	39	0.195	634	231
N/HSC8	2400	250	200	0.8	16	18	29	2.9	29.2	0.095	631	213

**Table D-10: Comparison of proposed model predictions and test results of slabs with steel reinforcement**

Slabs	$x_2^{cal}$ (mm)	$\alpha_F^{cal}$ Deg.	$\alpha_{cone}^{cal}$ Deg.	$P_{cal}$ (kN)	$P_{test}$ (kN)	$P_{test}/P_{cal}$
<b>Slabs tested by Tolf (1988):</b>						
S2.1	53	25	39	589	603	1.02
S2.2	53	25	39	275	600	1.04
S2.3	33	29	45	451	489	1.08
S2.4	34	30	45	435	444	1.02
					Mean =	1.04
					St. Dev. =	0.03
<b>Slabs tested by Regan et al. (1993):</b>						
1	8	21	32	211	224	1.06
2	13	21	31	203	212	1.04
3	19	22	41	164	169	1.03
4	16	22	32	185	233	1.26
5	20	19	36	183	190	1.04
6	6	21	32	212	233	1.10
21	29	20	37	263	286	1.09
22	27	19	41	277	405	1.46
23	21	23	36	243	341	1.40
24	29	20	37	279	270	0.97
25	31	19	42	228	244	1.07
26	30	20	38	264	294	1.11
27	28	24	55	233	227	0.97
					Mean =	1.12
					St. Dev. =	0.16
<b>Slabs tested by Tomaszewicz (1993):</b>						
ND65-1-1	83	29	58	1640	2050	1.25
ND65-2-1	64	28	44	966	1200	1.24
ND95-1-1	80	29	59	1721	2250	1.31
ND95-1-3	98	29	58	2163	2400	1.11
ND95-2-1	62	28	45	1018	1100	1.08
ND95-2-1D	62	28	45	1007	1300	1.29
ND95-2-3	72	27	43	1130	1450	1.28
ND95-2-3D	73	27	43	1130	1250	1.11
ND95-2-3D+	71	27	45	1199	1450	1.21
ND95-3-1	24	23	36	372	330	0.89
ND115-1-1	77	30	63	2025	2450	1.21
ND115-2-1	59	29	47	1197	1400	1.17

(The table is continued on the next page)

**Table D-10 (continued)**

<b>Slabs</b>	$x_2^{cal}$ (mm)	$\alpha_F^{cal}$ Deg.	$\alpha_{cone}^{cal}$ Deg.	$P_{cal}$ (kN)	$P_{test}$ (kN)	$P_{test}/P_{cal}$
ND115-2-3	71	27	45	1214	1550	1.28
LWA75-1-1	88	29	53	1476	1600	1.08
LWA75-2-1	68	27	43	926	950	1.03
LWA75-2-1D	68	27	44	1032	1100	1.07
LWA75-2-3	79	26	42	1083	1150	1.06
LWA75-2-3D	79	26	42	1054	1020	0.97
LWA75-3-1	27	23	35	374	320	0.86
					Mean =	1.13
					St. Dev. =	0.14
<b><i>Slabs tested by Marzouk and Hussein (1991):</i></b>						
NS1	30	17	26	264	320	1.21
HS1	6	19	28	153	178	1.16
HS2	15	18	27	255	249	0.98
HS7	22	20	29	298	356	1.19
HS3	28	18	27	307	356	1.16
HS4	33	17	25	306	418	1.37
NS2	33	22	38	311	396	1.27
HS5	11	23	35	271	365	1.35
HS6	21	22	34	384	489	1.27
HS8	28	25	38	405	436	1.08
HS9	37	24	37	449	543	1.21
HS10	42	23	36	502	645	1.28
HS11	9	14	21	135	196	1.45
HS12	21	10	15	198	258	1.3
HS13	24	11	16	198	267	1.35
HS14	21	18	27	397	499	1.25
HS15	17	19	28	448	560	1.25
					Mean =	1.24
					St. Dev. =	0.11
<b><i>Slabs tested by M. Hallgren (1996):</i></b>						
HSC1	45	27	43	847	1021	1.21
HSC2	45	28	44	875	889	1.02
HSC4	54	25	39	827	1041	1.26
HSC6	36	29	44	695	960	1.38
HSC9	12	24	38	525	565	1.08
					Mean =	1.19
					St. Dev. =	0.15



